EARTHQUAKE ENGINEERING TO EXTREME EVENTS

ISSN 1520-295X

Three-Dimensional Modeling of Inelastic Buckling in Frame Structures

by

Macarena Schachter and Andrei M. Reinhorn

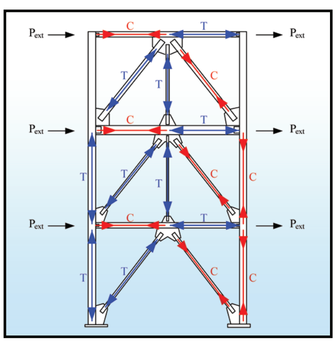

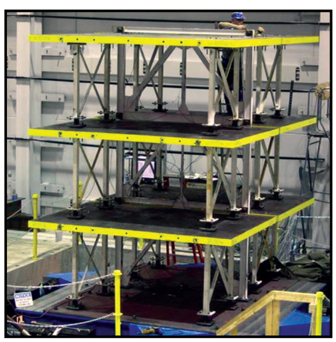

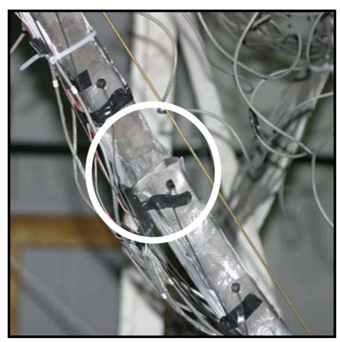

Technical Report MCEER-07-0016

September 13, 2007

This research was conducted at the University at Buffalo, State University of New York and was supported primarily by the Earthquake Engineering Research Centers Program of the National Science Foundation under award number EEC 9701471 and NSF Award CMS-0324277.

NOTICE

This report was prepared by the University at Buffalo, State University of New York as a result of research sponsored by MCEER through a grant from the Earthquake Engineering Research Centers Program of the National Science Foundation under NSF Master Contract Number EEC 9701471 and NSF Award CMS-0324277 and other sponsors. Neither MCEER, associates of MCEER, its sponsors, the University at Buffalo, State University of New York, nor any person acting on their behalf:

a. makes any warranty, express or implied, with respect to the use of any information, apparatus, method, or process disclosed in this report or that such use may not infringe upon privately owned rights; or

b. assumes any liabilities of whatsoever kind with respect to the use of, or the damage resulting from the use of, any information, apparatus, method, or process disclosed in this report.

Any opinions, findings, and conclusions or recommendations expressed in this publication are those of the author(s) and do not necessarily reflect the views of MCEER, the National Science Foundation, or other sponsors.

MCEER
EARTHQUAKE ENGINEERING TO EXTREME EVENTS

Three-Dimensional Modeling of Inelastic Buckling in Frame Structures

by

Macarena Schachter[1] and Andrei Reinhorn[2]

Publication Date: September 13, 2007
Submittal Date: August 17, 2007

Technical Report MCEER-07-0016

Task Number 9.2.4

NSF Master Contract Number EEC 9701471
and NSF Award CMS-0324277

1 Ph.D. Candidate, Department of Civil, Structural and Environmental Engineering, University at Buffalo, State University of New York
2 Clifford C. Furnas Professor, Department of Civil, Structural and Environmental Engineering, University at Buffalo, State University of New York

MCEER
University at Buffalo, The State University of New York
Red Jacket Quadrangle, Buffalo, NY 14261
Phone: (716) 645-3391; Fax (716) 645-3399
E-mail: *mceer@buffalo.edu*; WWW Site: *http://mceer.buffalo.edu*

Preface

The Multidisciplinary Center for Earthquake Engineering Research (MCEER) is a national center of excellence in advanced technology applications that is dedicated to the reduction of earthquake losses nationwide. Headquartered at the University at Buffalo, State University of New York, the Center was originally established by the National Science Foundation in 1986, as the National Center for Earthquake Engineering Research (NCEER).

Comprising a consortium of researchers from numerous disciplines and institutions throughout the United States, the Center's mission is to reduce earthquake losses through research and the application of advanced technologies that improve engineering, pre-earthquake planning and post-earthquake recovery strategies. Toward this end, the Center coordinates a nationwide program of multidisciplinary team research, education and outreach activities.

MCEER's research is conducted under the sponsorship of two major federal agencies: the National Science Foundation (NSF) and the Federal Highway Administration (FHWA), and the State of New York. Significant support is derived from the Federal Emergency Management Agency (FEMA), other state governments, academic institutions, foreign governments and private industry.

MCEER's NSF-sponsored research objectives are twofold: to increase resilience by developing seismic evaluation and rehabilitation strategies for the post-disaster facilities and systems (hospitals, electrical and water lifelines, and bridges and highways) that society expects to be operational following an earthquake; and to further enhance resilience by developing improved emergency management capabilities to ensure an effective response and recovery following the earthquake (see the figure below).

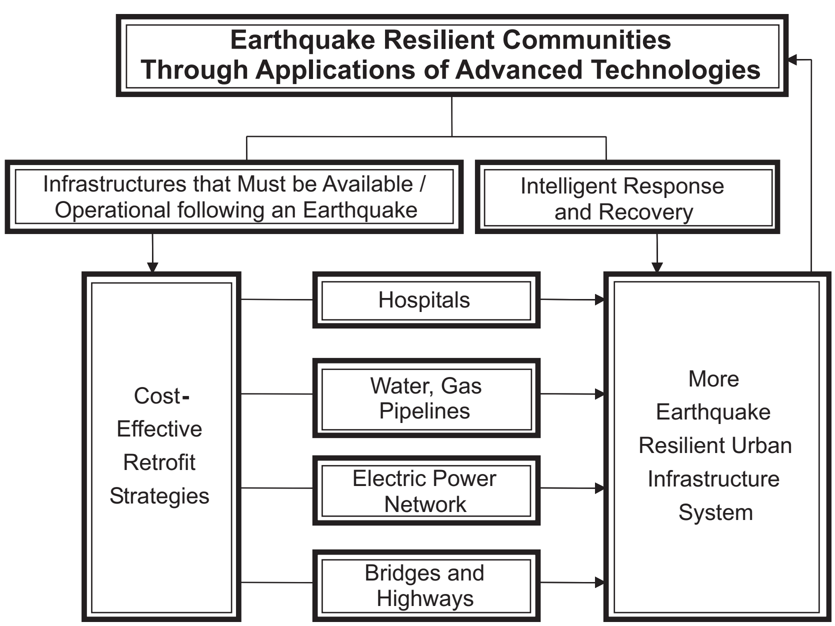

A cross-program activity focuses on the establishment of an effective experimental and analytical network to facilitate the exchange of information between researchers located in various institutions across the country. These are complemented by, and integrated with, other MCEER activities in education, outreach, technology transfer, and industry partnerships.

The main purpose of this research is to develop a formulation for three-dimensional frame structures with geometric and material nonlinearities subjected to static and dynamic loads. The first objective is to develop a corotational formulation capable of macro-modeling geometric nonlinearities that considers the plasticity of the cross sections, which facilitates understanding failures due to inelastic buckling. The second objective is to perform an experimental study, using a shake table as the base excitation, for a model where inelastic buckling is expected. The test results provide data for verification of the new formulation and computational model. The frame chosen is the "zipper frame," which is a chevron braced frame where columns link the midpoints of the beams at the brace connections. The third objective is to test the new formulation against data obtained through testing. By comparing the predictions of the new analytical model with the data obtained from the "zipper frame" experiment, the capability of the formulation to predict inelastic buckling is verified.

ABSTRACT

Inelastic buckling is the most important failure mode of a steel beam column element subjected to compression force. In order to correctly predict this phenomenon, large rotations, large displacements and the plasticity of the section along the element must be considered.

Several formulations have been proposed to model problems with three dimensional large displacements and rigid body dynamics. They are usually based in the Lagrangian or the Corotational methods and are primarily oriented to solve mechanical and aerospace problems, although some applications to structural stability do exist. Independently, several formulations have been developed to model plasticity: fiber elements, plastic flow theory and lumped plasticity are popular choices.

In this report, a novel formulation capable of solving problems with displacement and material nonlinearities in a unified way is developed. Thus, the State Space approach is selected because all the basic equations of structures: equilibrium, compatibility and plasticity are solved simultaneously and thus the global and local states are mutually and explicitly dependent. To incorporate geometric nonlinearities, the Corotational approach, where rigid body motion and deformations are described separately, is adopted. To incorporate material nonlinearities, the formulation developed by Simeonov (1999) and Sivaselvan (2003) is included.

In general, the set of equilibrium, compatibility and plasticity equations constitute a system of Differential Algebraic Equations (DAE). A procedure to solve such system exists and is implemented in the package IDA (Implicit Differential Algebraic solver) developed at the Lawrence Livermore National Laboratory (LLNL), which is used to solve the problem numerically.

An experimental study on “zipper frames” was conducted to assess the accuracy of the proposed formulation. A “zipper frame” is a chevron braced frame where the beam to brace connections are linked through columns, called “zipper columns”. The failure mode of a “zipper frame” is the successive inelastic buckling of its braces. Three shake table tests of a three stories “zipper frame” were performed at the UB-NEES laboratory.

A model of the first story of the “zipper frame” was analyzed with the new formulation and its results compared to experimental data. It is found that the new formulation can reproduce the features of the test and it is very sensitive to all the model parameters. Results are presented.

ACKNOWLEDGMENTS

This research was conducted by the University at Buffalo and was supported by National Science Foundation award CMS-0324277. Their support is gratefully acknowledged. All opinions and remarks are those of the author and do not reflect any opinion of the supporting agency.

TABLE OF CONTENTS

SECTION TITLE PAGE

TABLE OF CONTENTS (CONTINUED)

TABLE OF CONTENTS (CONTINUED)

SECTION TITLE PAGE

TABLE OF CONTENTS (CONTINUED)

TABLE OF CONTENTS (CONTINUED)

SECTION TITLE PAGE

LIST OF FIGURES

FIGURE TITLE PAGE

LIST OF FIGURES (CONTINUED)

FIGURE TITLE PAGE

LIST OF FIGURES (CONTINUED)

FIGURE TITLE PAGE

LIST OF FIGURES (CONTINUED)

FIGURE TITLE PAGE

LIST OF FIGURES (CONTINUED)

FIGURE TITLE PAGE

LIST OF FIGURES (CONTINUED)

FIGURE TITLE PAGE

LIST OF FIGURES (CONTINUED)

FIGURE TITLE PAGE

LIST OF TABLES

TABLE TITLE PAGE

SECTION 1
INTRODUCTION

1.1 Objectives

The main purpose of this report is to develop a unified formulation for three dimensional frame structures with geometric and material nonlinearities subjected to static and dynamic loads. Multiple formulations have been proposed to solve problems with large rotations and large displacements. However, in most of them, the structures were constrained to remain elastic at all levels of deformation. This is a customary idealization used to simplify the formulation, although the real behavior of large frame structures does not justify it. On the other hand, there are also several formulations capable of modeling material nonlinearities. Those models are independent of the software used to solve the structure and the user can select between many options which may be the most suitable for each particular frame element. Thus the first objective of this work is to develop a formulation capable of macro-modeling geometric nonlinearities considering the plasticity of the cross section by describing the basic section and material properties.

The second objective of this report is to perform an experimental study using a shake table as the base excitation for a model where inelastic buckling is expected. The test results provide data for verification of the new formulation and computational model. The frame chosen is the "zipper fra*me*". A "zipper frame" is a chevron braced frame where columns, called "zipper columns", link the midpoints of the beams at the brace connections. The "zipper frames" project was a collaborative study between Georgia Institute of Technology (GT), University of California at Berkeley (UCB), University of Colorado Boulder (CU) and University at Buffalo (UB). The objectives of the project were: first, to design the "zipper frame" model to be tested. Second, to test the frame under dynamic load (UB), quasi-static load (GT) and perform individual and multisite hybrid testing (UCB and CU). Third, to analyze the frame and compare the consistency of the results of each test with the team members. Finally, to develop better analytical models which might represent the behavior of the tested structure.

The third objective of the present work is to test the new formulation against data obtained through testing. In the field of instability analysis, there are several problems that are considered benchmarks. These problems are limited to a series of cases: snap through, snap-back, bifurcation and others. Most of them consist of simple structures with elastic material and have closed form solutions. The advantage of these solutions are that results from different methodologies are comparable and errors can be detected. However, the most practical case of *inelastic buckling* is not considered. By comparing the predictions of the new analytical model with the data obtained from the "zipper frame" experiment, the capability of the formulation to predict inelastic buckling is tested herein.

1.2 Motivation

1.2.1 Small displacements vs large displacements

In matrix analysis of structures with small strains/small deformations there are two main coordinate systems: "Global", which is common for all the members in the structure and "Local", which is defined in respect to the chord of the member; i.e. the straight line that connects the two end nodes of an element in its deformed configuration. The hypothesis of *small displacements* translates into the assumption that at every step the chord of the member coincides with its initial position. Thus, the deformations are calculated with respect to the initial configuration and the matrices that transform from global to local coordinates are constant throughout the analysis .

When large displacements are considered, the "Local" coordinates coincide with the chord of the member in its actual position while the "Global" coordinates remain constant. Thus, the transformation matrices are not constant, but vary with time. The global stiffness matrix, calculated as the variation of the force given a variation in displacement, is not only sensitive to the actual nodal displacements but also to the variations of the reference frame. The former is the elastic stiffness matrix, while the later is the geometric stiffness matrix.

1.2.2 The problem of large rotations

When the analysis in three dimensions (3D) assumes that the rotations are small or infinitesimal, rotations are treated as vectors, and vectorial mathematics can be used to describe them. However, large or finite rotations are manifolds and should be described with Lie algebra (Marsden 1994). Essentially, a rotation has a magnitude (the rotation angle) and a direction or rotation axis (a vector describing the normal to the plane where the rotation takes place). Finite rotations are not commutative (unless the rotation axis is fixed as in two dimensions (2D)).

There are three ways of describing rotations mathematically:

- Quaternion: The rotation value and its axis in a vector of 4 elements.
- Rotation matrix: a 3x3 orthogonal matrix.
- Pseudovector (Euler angles): the projection of the rotation into a Cartesian coordinate system.

All these representations are equivalent and the relationships between them are detailed in Chapter 2. The pseudovector representation is not unique but can be scaled by different factors. These are called parametrizations of the Euler angles (Crisfield 1991; Felippa and Haugen 2005).

1.2.3 Buckling – instability analysis

There are two main approaches to the problem of instability: The plastic hinge method and the finite element method.

In the plastic hinge method, the traditional stiffness matrix method is enhanced to automatically consider second order analysis (the effect of the geometry in the stiffness of the member) by using stability functions. These functions were first introduced by von Mises and Ratzersdorfer in 1926 (Bazant and Cedolin 1991). Derived from the differential equations of a fixed-hinged beam subjected to axial load, these functions are factors that reduce the bending stiffness of a member due to the presence of axial load. Although popular because of their simplicity, the description of instability is usually constrained to 2D and to the ideal cases the differential equations can solve (Chen 2000). Material nonlinearities are added mostly through plastic hinges or plastic zones. Other options, such as out of plane buckling and local buckling have also been incorporated (Kim and Lee 2001; Kim and Lee 2002; Kim et al. 2003; Trahair and Chan 2003; Wongkaew and Chen 2002).

This option is not discussed further since the assumptions made to derive the stability functions are very rigid. Even though modeling of buckling and instability is the purpose of the method, no consideration of large displacements is made. Rotations are always treated as infinitesimal and calculated as the first derivative of the transverse displacements, even though this is not true in any buckled member. Finally, the method is not general enough to predict local buckling because it just checks the equations provided in the AISC manual (AISC 2003), which are only mean values of data obtained empirically.

Within the finite element method, there are two main approaches: Lagrangian and Corotational. The Lagrangian method describes a beam as a continuous element. Each cross section is completely defined by a position vector and a rotation matrix, which are written with respect to a Global coordinate system. Axial strain and curvatures are written in terms of these variables. There are different ways to proceed with the calculations: the strains can be linearized first to find an admissible variation and then the virtual work principle is applied to find the equations of motion (Simo and Vu-Quoc 1986); or the virtual work principle is applied first and the resulting equations are linearized (Cardona and Geradin 1988). In a different approach, the kinematic equations are solved using a procedure similar to Lagrangian multipliers for all the unknown variables, resulting in a weak formulation of the equilibrium equations, which are afterwards discretized and linearized (Jelenic and Saje 1995).

In all the cases described above, the element cannot be integrated as a continuum, so it is discretized. Since the stiffness matrix is required, displacements and rotations of the internal nodes are approximated with interpolation functions.

The mathematical details in the above procedures depend on the chosen rotations parametrization: quaternions (Simo and Vu-Quoc 1985; Simo and Vu-Quoc 1986) and incremental pseudovectors (Cardona and Geradin 1988; Ibrahimbegovic 1997) are the most popular choices. The formulation was developed further by proposing strain invariant and path independent interpolation functions for the rotations (Jelenic and Crisfield 1999). Curvature interpolation has also been used in an approximated formulation (Schulz and Filippou 2001). Also, the kinematic equations of the beam, have been extended to include arbitrary cross sections (Gruttmann et al. 1998) and curved beam elements (Ibrahimbegovic 1995).

The Corotational method works with two coordinate systems: a Global system common for all members and a Local system for each member. The Local system is defined for every element and is updated every time step. The method is called Corotational approach because it moves and rotates following the chord of the member. Translational and rotational deformations are written with respect to the corotated system, therefore the total movement of a node can be described as the superposition of a rigid body motion (represented by the movement of the chord of the element and calculated with respect to the Global system) and a deformation (calculated with respect to the chord).

It is generally assumed that large displacements and rotations are described within the rigid body motion and that the remaining deformations are small, thus at the corotated level the hypothesis of small displacements holds and the usual stiffness matrix method can be used to calculate the local tangent stiffness matrix of the element. However, since the local stiffness matrix is written with respect to a moving frame, the stiffness matrix of the element in Global coordinates must consider the variations of the frame with time. (Crisfield 1990; Felippa and Haugen 2005; Rankin and Nour-Omid 1988). This method has been extended to incorporate plasticity by considering the von Mises yield criterion (Battini and Pacoste 2002b; Izzuddin and D.L.Smith 1996; Pi and Trahair 1994; Pi et al. 2001b), and to incorporate second and higher order terms in the Green strains definition in order to capture flexural-torsional buckling and warping distortion (Battini and Pacoste 2002a; Hsiao et al. 1999; Pi and Bradford 2001). Also a combination of Corotational and Lagrangian Methods has been proposed (Hsiao and Lin 2000).

In summary, since the kinematic description of the element in the Lagrangian Method is mathematically exact, these formulations can handle problems for very large rotations and displacements as well as for very large strains (plasticity included). In contrast, formulations based in the Corotational Method assume that the small deformations/small strains theory holds at the corotated level. On the other hand, while the Corotational concept is simple and the method can be easily incorporated into existing structural analysis software, the Lagrangian Methods are mathematically involved and are not compatible with existing software. It has been proven by various authors (Cardona and Geradin 1988; Crisfield 1990; Felippa and Haugen 2005; Simo and Vu-Quoc 1986) that both methods are successful in solving problems of stability of structures, although their scope covers mostly the areas of aerospace engineering and multibody dynamics.

Focusing on a formulation for structural instability, the Corotational Method can be a suitable choice. The physical meaning of the Corotated frame makes it easy for engineers to understand the concept behind the mathematics. The objective of the present work is to enhance the Corotational Method to handle problems of large strains, with both geometric and material nonlinearities.

1.2.4 Stiffness and flexibility base elements

In a formulation using the Corotational Method, stiffness and flexibility based elements can be used. Stiffness based elements calculate the stiffness matrix of the element by approximating the deformation field with interpolation functions. Typically, cubic polynomials are used to describe transverse deformations and linear functions describe axial deformations. This description is valid only for small displacement analysis, where rotations are calculated as derivatives of the transverse displacements. In large displacement analyses this corresponds to a first order approximation and it leads to compatibility inconsistencies (Pi et al. 2001a; Teh and Clarke 1997; Teh and Clarke 1998). Section forces are obtained through the constitutive law. Then, from the integration of the equilibrium equations (principle of virtual displacements) the global stiffness matrix is calculated. Finally, the global forces are assembled and compared to the external forces. In a nonlinear analysis, equilibrium is not satisfied and iterations must be performed.

In contrast, flexibility based elements approximate the force field. In the case where element forces are not present, bending moments vary linearly and axial force and torsion are constant, the interpolation is exact. The section deformations are then obtained through the constitutive law. By applying the principle of virtual forces, compatibility equations are obtained and after integrating them, the global flexibility matrix is found. Finally, global compatibility is not satisfied and iterations at the element level are needed. The formulation is attractive because equilibrium is always satisfied and there is no need to approximate the displacement field, even though the numerical implementation is not as simple as with stiffness based elements.

It's been proven that flexibility based elements have better performance than stiffness based elements in linear problems solved with matrix methods (Neuenhofer and Filippou 1997; Spacone et al. 1996) and in the state space (Simeonov 1999); in nonlinear problems of 2D structures solved with matrix methods (Bäcklund 1976; Neuenhofer and Filippou 1998) and in the state space (Sivaselvan 2003). It has also been implemented in the program IDARC2D (Park et al. 1987; Valles et al. 1996), where the flexibility matrix for inelastic elements with small deformations is determined and then integrated to the global system using its inverse.

The present formulation will combine the Corotational formulation, including mathematics of large rotations to create a flexibility based element capable of solving 3D nonlinear problems.

1.2.5 The plasticity problem

Most of the formulations assume that the material is elastic. They are aimed to model not only structural problems but also flying planes and mechanical systems where it is undesirable that the material becomes plastic. Therefore, most of the benchmark problems found in the literature are elastic, thus plasticity is not needed in the formulations. On the other hand, many of the instability problems in civil engineering structures involve the plastification of the cross section, thus it becomes a necessary feature. Plastic flow theories are one choice to model plasticity. A yield surface is defined along with loading, yielding and unloading rules. The result is a relationship between the rate of strains and the rate of stresses. Thus, the rate equations must first be integrated to obtain a relationship between strains and stresses (Crisfield 1991; Lubliner 1990).

It is evident that the traditional stiffness and flexibility matrix methods as well as any of the above formulations need a strain-stress relationship but it is of no consequence to the formulation itself how this matrix is calculated. Plasticity is a choice. Thus, none of the above procedures is a unified approach in the sense that plasticity analysis is treated separately from equilibrium and compatibility analyses.

Methods based in finite elements, fiber models for instance, solve the problem at a global and a local level. The global level enforces compatibility and equilibrium while the local level deals with plasticity. This is possible since the cross section is divided into small sectors where average strains and stresses are being continuously monitored. The section forces are then obtained by integrating the stresses of all sectors (Hall and Challa 1995; Izzuddin and D.L.Smith 1996; Zienkiewicz and Taylor 2005). Thus, finite element analysis is a unified approach. However, the computational costs and time required to solve a complex problem are very high.

Methods based in the state space also solve the problem at a global and a local level. At the global level the equations of motion become first order differential equations and at the local level, if plastic flow theories are used, the constitutive laws are also first order differential equations. The complete system is then solved. As a result, global and local states are mutually dependent and convergence occurs simultaneously eliminating the need for iterations within a time step (Simeonov 1999; Sivaselvan 2003). However, if static analysis is being performed, equations at the global level are algebraic, not differential. Therefore a robust procedure capable of solving Differential Algebraic Equations (DAEs) is needed. Fortunately, such a procedure exists (Brenan et al. 1989) and it is implemented in a computer software called "Implicit Differential-Algebraic solver" (IDA) developed at the Lawrence Livermore National Laboratory (Hindmarsh and Serban 2006).

It is concluded that, for the objectives of this report, the state space approach is the most suitable option for the development of a unified formulation.

1.3 Outline of the report

Flexibility based element have been combined with the state space approach to create a formulation for inelastic structures and small displacements (Simeonov 1999). The Corotational approach mixed with flexibility based elements was used by Sivaselvan (Sivaselvan 2003), to solve two dimensional (2D) inelastic buckling problems using the state space. However, as explained in 1.2.2, large rotations in 2D are not different from small rotations since the rotation axis is fixed. Thus, the challenge is to develop a formulation that mixes the Corotational approach with a flexibility based element capable of 3D large inelastic displacements and rotations, to be solved in the state space and to be tested against the results of the "zipper frame" experiments.

The organization of the work is as follows: in Chapter 2 the mathematical development of the formulation is explained. Chapter 3 details the numerical implementation of the formulation derived in Chapter 2. Chapter 4 presents the experimental study and the relevant test results from the shake table tests of the "zipper frame". Chapter 5 compares the experimental results with the analytical results obtained with the new formulation. Finally a summary of the work, conclusions and recommendations are detailed in Chapter 6.

SECTION 2
FORMULATION OF A 3D ELEMENT MODEL FOR GEOMETRIC AND MATERIAL NONLINEARITIES

2.1 Introduction

The formulation presented in this Chapter is developed for frame structures whose components are modeled as single elements, also known as macro-models. An “element” can represent a beam, column, brace or any other structural member where one of its dimensions (length) is much larger than the other two (cross section). The boundaries of the elements are represented by “nodes” which also represent connection points between different structural members. The movement of the member is described solely by the movement of its end nodes and its centerline. The element’s plasticity is incorporated by monitoring some of the cross sections along the length of the element, also known as “control sections”. The behavior of the end nodes is influenced by the integrated behavior of all the control sections.

The objective of the developed formulation is to predict the behavior of an element that undergoes inelastic buckling i.e. the correct estimation of the buckling load, post buckling displacement and residual displacements.

Although many procedures capable of analyzing elements subjected to large displacements and large rotations have been developed (Bäcklund 1976; Battini and Pacoste 2002a; Battini and Pacoste 2002b; Behdinan et al. 1998; Cardona and Geradin 1988; Crisfield 1990; Gruttmann et al. 1998; Ibrahimbegovic 1995; Jelenic and Crisfield 1999; Jelenic and Crisfield 2001; Meek and Xue 1998; Neuenhofer and Filippou 1998; Pacoste and Eriksson 1997; Rankin and Nour-Omid 1988; Simo and Vu-Quoc 1986), most of them assume elastic materials. The inclusion of the material nonlinearity is an option because the aim of such formulations is the prediction of the behavior of the elements under large rotations. Those formulations have a broad application including mechanical systems and aerospace engineering, where rigid body motion is the main source of geometric nonlinearity and where it is desirable that the material remains elastic. In civil engineering applications however, it is expected that under a strong ground motion the material will yield, therefore the inclusion of material nonlinearities is imperative in order to accurately predict element and structural instabilities.

To solve problems with large rotations and large displacements, there are two main approaches within the finite element method: Lagrangian and Corotational. In the Lagrangian approach, the displacements and forces are described with respect to a fixed coordinate system, which can be conveniently placed at the last converged configuration. Rotational increments are described as finite rotations. In a stiffness based element where the displacement field is interpolated, the most popular interpolation functions for transverse displacements are the well known Hermitian polynomials. However, this approximation is valid only when rotations are infinitesimal because they assume that the rotations can be described as the first derivative of the transverse displacements. On the other hand, this approach is very efficient handling the rotation updates from one step to the next and if shear deformations are considered, its strain description is geometrically exact.

In the Corotational approach, rigid body motion is separated from deformations. Usually deformations are assumed to be very small so that classical structural analysis is used to evaluate the element's stiffness matrix in its corotated coordinates. This is the most popular approach in Civil Engineering applications because it can be easily integrated to existing structural analysis software. In this case, the inclusion of material nonlinearity can be implemented with concentrated plasticity, as in the program DRAIN 2D (Kanaan and Powell 1973), or spread plasticity formulations, as in IDARC 2D (Valles et al. 1996), and with other finite elements like fibers, as in DRAIN 3D (Prakash et al. 1994). As long as the rotational deformations are infinitesimal, they can be treated as vectors and can be interpolated with Hermitian polynomials. Thus, most of the developed methods within the Corotational approach adopt stiffness based formulations.

The element described herein is based in the Corotational formulation, thus rigid body motion and deformations are treated separately. However, the assumption of small deformations is relaxed and deformational rotations are treated as finite rotations. To avoid compatibility and interpolation problems, a flexibility based formulation is adopted. In this case, the force field is interpolated and the resultant interpolation functions are exact. Displacements and rotations need to be interpolated in order to calculate the flexibility matrix, however these interpolations are based on compatibility relationships and not on approximated polynomials.

A unified formulation that considers both geometric and material nonlinearities is obtained by writing the equations of motion in the state space, where displacement and velocities are variables of the system such that the equations of motion – second order differential equations – become a set of first order differential equations.

When based in flow rules, plasticity equations are first order differential equations. Therefore, in a traditional matrix analysis these equations must be integrated independently and the results used in the analysis. The advantage of the state space is that all the differential equations are solved simultaneously, enforcing equilibrium, plasticity and compatibility and eliminating the need for iterations.

This chapter presents the development of the formulation. First, a brief summary of the mathematics of finite rotations is given so that latter developments would be clear. Second, the Corotational concept is introduced. Third, a summary of the adopted constitutive formulation is presented. Fourth, the state space approach is outlined. Finally, all the above elements are integrated into the formulation.

2.2 Mathematics of large rotations

2.2.1 Geometrical description of large rotations

Geometrically, a pure three dimensional (3D) rotation applied to point n in Figure 2–1, results in the movement of this point to point n+1. This rotation can be described by a rotation axis, $\widehat{\boldsymbol{\theta}}$, and a rotation angle θ. The rotation axis is normal to the rotation plane, where the angle of rotation is defined. Mathematically it is defined as:

$$\boldsymbol{\theta} = \theta \cdot \widehat{\boldsymbol{\theta}} \tag{2.1}$$

The rotation axis is a unit vector and thus its numerical description depends on the chosen coordinate system {x,y,z}. The components of $\boldsymbol{\theta} = \{\theta_x, \theta_y, \theta_z\}$ are the projections of the vector $\widehat{\boldsymbol{\theta}}$ into the given coordinate system scaled by the value of the rotation angle θ:

$$\begin{aligned} \boldsymbol{\theta} &= \left\{\theta_x \quad \theta_y \quad \theta_z\right\}^t \\ \theta &= \sqrt{\theta_x^2 + \theta_y^2 + \theta_z^2} \end{aligned} \tag{2.2}$$

$\boldsymbol{\theta}$ is called “rotational vector”, “axial vector” or “pseudovector”. Although it looks like a vector, its components cannot be interpreted as rotations about the axis {*x*,*y*,*z*}. Another important property of the axial vector is that any parametrization that preserves Equation (2.2) can be used to characterize rotations. Among them, the Rodrigues parametrization is defined as (Argyris 1982):

$$\bar{\theta} = \frac{\tan\left(\theta/2\right)}{\theta}\theta \tag{2.3}$$

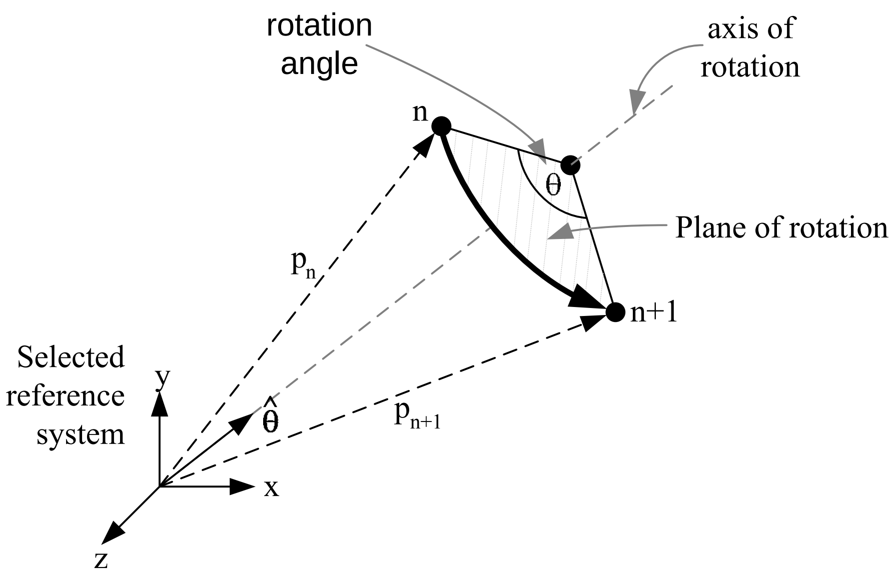

Figure 2–1: Geometrical representation of rotations.

The position of points n and n+1 (Figure 2–1) in the chosen coordinate system are $\mathbf{p}_n$ and $\mathbf{p}_{n+1}$. The movement of point n to point n+1 can then be expressed as the rotation of vector $\mathbf{p}_n$ into $\mathbf{p}_{n+1}$ through a rotation matrix $\mathbf{R}$. Geometrically, it can be demonstrated thar the rotation matrix can be written in terms of the rotational vector as (Argyris 1982):

$$\mathbf{p}_{n+1} = \mathbf{R}(\boldsymbol{\theta})\cdot\mathbf{p}_n$$

$$\mathbf{R}(\boldsymbol{\theta}) = \mathbf{I} + \frac{\sin(\theta)}{\theta}\boldsymbol{\Omega} + \frac{1}{2}\left(\frac{\sin\left(\theta/2\right)}{\theta/2}\right)^2\boldsymbol{\Omega}^2 \tag{2.4}$$

$$\boldsymbol{\Omega} = \begin{bmatrix} 0 & -\theta_z & \theta_y \\ \theta_z & 0 & -\theta_x \\ -\theta_y & \theta_x & 0 \end{bmatrix}$$

In Equation (2.4), $\boldsymbol{\Omega}$ is a 3x3 skew-symmetric matrix called Spinor. Its components are the Cartesian components of the rotational vector. Physically, $\boldsymbol{\Omega}$ represents a linearized (infinitesimal) rotation about $\mathbf{R}$. Mathematically, the spinor and the rotational vector are related by:

$$\boldsymbol{\theta} \times \mathbf{p} = \boldsymbol{\Omega} \cdot \mathbf{p} = -\mathbf{p} \times \boldsymbol{\theta} \tag{2.5}$$

for any vector **p** (**p** can represent the position of a point in space, but the definition in Equation (2.5) is very general). If Equation (2.4) is expanded into Taylor series, it is possible to demonstrate that (Argyris 1982):

$$\mathbf{R} = e^{\Omega} \tag{2.6}$$

Equation (2.6) represents the "exponential map". Although this compact format is very popular for mathematical derivations, it is very difficult to implement numerically. Instead, a parametrization of the rotational vector is used to calculate **R** (Felippa and Haugen 2005).

2.2.2 Mathematical description of large rotations

Mathematically, large (finite) rotations in three dimensions (3D) are represented by rotation matrices **R** which constitute the group of Special Orthogonal linear transformations SO(3). This is a subgroup where all matrices are orthogonal i.e. $\mathbf{R}\,\mathbf{R}^t = \mathbf{I}_3$ ($\mathbf{I}_3$ is the 3x3 identity matrix) and their determinants are 1 i.e. the rotation matrix preserves the orientation of the vectors it rotates.

The mathematical structure of the SO(3) group is a nonlinear differentiable manifold, not a linear space. In general, a differentiable manifold is defined by an open subspace where linear tangent spaces can be defined at each point and maps (or functions) relate the points in the manifold with those of the tangent space. In the finite rotations problem, each rotation matrix is a point in the manifold space. Thus, at each rotation matrix, a tangent linear space can be defined and it is composed by the set of all possible axial vectors. The relationship between the axial vector and the manifold is the "exponential map". Since it is very difficult to develop mathematics for nonlinear spaces, the existence of a tangent linear space where linear algebra is valid transforms a complex problem into a conventional problem and a space mapping.

2.2.3 Parametrization of rotations: quaternions

The most practical description of finite rotations for numerical analysis is the quaternion definition. A quaternion **q** is a rotation parametrization that uses 4 parameters: one for the rotation angle and 3 for the rotation axis with the restriction that the quaternion's modulus has to be unitary.

$$
\mathbf{q} = \begin{pmatrix} \mathbf{q}^* \\ q_0 \end{pmatrix}
$$

$$
\mathbf{q}^* = \{q_1 \quad q_2 \quad q_3\}^t \tag{2.7}
$$

$$
q_0^2 + q_1^2 + q_2^2 + q_3^2 = 1
$$

In terms of the rotational vector, the quaternion is written as (Simo and Vu-Quoc 1986):

$$
q_0 = \cos\left(\theta/2\right)
$$

$$
\{q_1 \quad q_2 \quad q_3\}^t = \frac{\sin\left(\theta/2\right)}{\theta}\boldsymbol{\theta} \tag{2.8}
$$

And the rotation matrix in terms of the quaternion components is:

$$
\mathbf{R} = 2\begin{bmatrix} q_o^2 + q_1^2 - \frac{1}{2} & q_2 q_1 + q_3 q_o & q_3 q_1 - q_2 q_o \\ q_1 q_2 - q_3 q_o & q_o^2 + q_2^2 - \frac{1}{2} & q_3 q_2 + q_1 q_o \\ q_1 q_3 + q_2 q_o & q_2 q_3 - q_1 q_o & q_o^2 + q_3^2 - \frac{1}{2} \end{bmatrix} \tag{2.9}
$$

The inverse operation: to extract the quaternions from a rotation matrix, can be done with the following formulas:

$$
q_o = \pm\tfrac{1}{2}\sqrt{1 + \mathrm{Tr}(\mathbf{R})} = \pm\tfrac{1}{2}\sqrt{1 + R_{11} + R_{22} + R_{33}}
$$

$$
q_1 = \pm\tfrac{1}{4}\frac{(R_{32} - R_{23})}{q_o}
$$

$$
q_2 = \pm\tfrac{1}{4}\frac{(R_{13} - R_{31})}{q_o} \tag{2.10}
$$

$$
q_3 = \pm\tfrac{1}{4}\frac{(R_{21} - R_{12})}{q_o}
$$

2.2.4 Compound rotations

Compound rotations are the result of successive rotations. To calculate them, it is very important to define the reference frame in which the calculation is being done. The results obtained for different coordinate systems will be numerically different but geometrically equivalent. Given two successive rotations, there are two ways of calculating the resultant rotation matrix (Argyris 1982). First, when the reference frame is constant, the final rotation is:

$$
\mathbf{R} = \mathbf{R}_1 \cdot \mathbf{R}^m \tag{2.11}
$$

where $\mathbf{R}$ is the resultant rotation matrix, $\mathbf{R}_1$ is the first rotation and $\mathbf{R}^m$ is the second rotation. This operation is called material rotation or right translation. $\mathbf{R}_1$ and $\mathbf{R}^m$ share the same reference system.

Second, when the reference frame moves and rotates with the body, the final rotation is:

$$\mathbf{R} = \mathbf{R}^s \cdot \mathbf{R}_1 \tag{2.12}$$

where $\mathbf{R}$ is the resultant rotation matrix and $\mathbf{R}^s$ is the second rotation. This operation is called spatial rotation or left translation. In this case, the reference frame rotates first with $\mathbf{R}_1$ and $\mathbf{R}^s$ is written with respect to the rotated coordinate system.

Denoting $\boldsymbol{\theta}^m$ the axial vector associated with $\mathbf{R}^m$ and $\boldsymbol{\theta}^s$ the axial vector associated with $\mathbf{R}^s$, the relationship between the axial vectors is:

$$\boldsymbol{\theta}^s = \mathbf{R}_1 \cdot \boldsymbol{\theta}^m \tag{2.13}$$

From Equation (2.12) it can be concluded that rotations are "path-sensitive" i.e. $\boldsymbol{\theta}^s$ is affected by all previous rotations. Unless the reference and rotation axes are kept fixed, finite rotations cannot be added like true vectors.

2.2.5 Derivatives of the Rotation matrix

The variations of the rotation matrix with respect to time and position are very useful during the development of the formulation. The material and spatial forms are (Cardona and Geradin 1988; Simo and Vu-Quoc 1986):

$$\begin{aligned} \frac{d\mathbf{R}}{ds} &= \boldsymbol{\Psi}^s \cdot \mathbf{R} = \mathbf{R} \cdot \boldsymbol{\Psi}^m \\ \frac{d\mathbf{R}}{dt} &= \boldsymbol{\Omega}^s \cdot \mathbf{R} = \mathbf{R} \cdot \boldsymbol{\Omega}^m \end{aligned} \tag{2.14}$$

where $\mathbf{R}$ is any rotation matrix, s is the arc-length variable and t is the time variable. $\boldsymbol{\Psi}$ and $\boldsymbol{\Omega}$ are skew-symmetric matrices representing the curvatures and instantaneous angular velocities respectively. The superscripts "s" denotes spatial and "m" denotes material forms. As explained in 2.2.4, the result of the compound rotation ($\boldsymbol{\Psi}^s$ $\mathbf{R}$) is the same as ($\mathbf{R}$ $\boldsymbol{\Psi}^m$), and the difference between the matrices $\boldsymbol{\Psi}^s$ and $\boldsymbol{\Psi}^m$ is that the reference frame in the later is fixed while the reference frame in the former rotates with $\mathbf{R}$.

Equation (2.14) is obtained after the application of the directional Fréchet derivative on the rotation matrix. Geometrically, it is equivalent to superimpose an infinitesimal rotation on to a finite rotation.

2.2.6 Incremental rotation vector: the update problem

From 2.2.4 it was concluded that finite rotations cannot be added like real numbers, nor can axial vectors be added like true vectors unless the reference frame and rotation axes remain fixed. However, this is a very desirable feature in the context of an update process in a numerical method, where the rotations at some step n (θ_n) are known, the increments ($\delta\boldsymbol{\theta}^{\mathbf{R}}$) are obtained through some type of Newton method and their values at the step $n+1$ (θ_{n+1}) have to be determined. Usually, the update procedure will be through the composition of their respective rotation matrices:

$$\mathbf{R}_{n+1} = \Delta\mathbf{R} \cdot \mathbf{R}_n \tag{2.15}$$

where $\mathbf{R}_{n+1}$ is the rotation matrix at step $n+1$, $\mathbf{R}_n$ is the rotation matrix at step n and $\Delta\mathbf{R}$ is the rotation matrix of the incremental rotation $\delta\boldsymbol{\theta}^{\mathbf{R}}$. It is very difficult to implement Equation (2.15) in the context of a Newton method, thus the incremental rotation vector (Cardona and Geradin 1988; Ibrahimbegovic 1997) was introduced. The idea is to write the incremental rotation always in respect to the same reference frame so that the axial vectors can be added like true vectors:

$$\boldsymbol{\theta}^1_{n+1} = \boldsymbol{\theta}^1_n + \delta\boldsymbol{\theta}^1 \tag{2.16}$$

Mathematically, Equation (2.16) means that the axial vector $\boldsymbol{\theta}_n{}^1$, the increment $\delta\boldsymbol{\theta}^1$ and the final axial vector $\boldsymbol{\theta}_{n+1}{}^1$ belong to the same tangent linear space, see Figure 2–2. To obtain the respective rotation matrices, the “exponential map” is used. Recalling Equation (2.6):

$$\mathbf{R}_{n+1} = e^{\boldsymbol{\Omega}^1_{n+1}} \tag{2.17}$$

where $\boldsymbol{\Omega}_{n+1}{}^1$ is the skew symmetric matrix whose components are the components of the axial vector $\boldsymbol{\theta}_{n+1}{}^1$.

It is possible to obtain a transformation between the incremental rotation vector $\delta\boldsymbol{\theta}^1$ and the axial vector of the rotation matrix $\Delta\mathbf{R}$**:** $\delta\boldsymbol{\theta}^{\mathbf{R}}$ (Cardona and Geradin 1988; Ibrahimbegovic 1997):

$$\delta\theta^{n} = T\left(\theta_{n}^{1}\right)\cdot\delta\theta^{1}$$

$$T\left(\theta_{n}^{1}\right) = \frac{\sin\left(\theta_{n}^{1}\right)}{\theta_{n}^{1}} I + \left(1 - \frac{\sin\left(\theta_{n}^{1}\right)}{\theta_{n}^{1}}\right)\cdot\left(\hat{\theta}_{n}^{1}\right)\cdot\left(\hat{\theta}_{n}^{1}\right)^{t} + \frac{1}{2}\left(\frac{\sin\left(\theta_{n}^{1}/2\right)}{\theta_{n}^{1}/2}\right)^{2} \boldsymbol{\Omega}_{n}^{1} \tag{2.18}$$

$$T^{-1}\left(\theta_{n}^{1}\right) = \frac{\theta_{n}^{1}/2}{\tan\left(\theta_{n}^{1}/2\right)} I + \left(1 - \frac{\theta_{n}^{1}/2}{\tan\left(\theta_{n}^{1}/2\right)}\right)\left(\hat{\theta}_{n}^{1}\right)\cdot\left(\hat{\theta}_{n}^{1}\right)^{t} - \frac{1}{2}\boldsymbol{\Omega}_{n}^{1}$$

Equation (2.18) is valid for spatial description of rotations. Similar relationships can be obtained for material description.

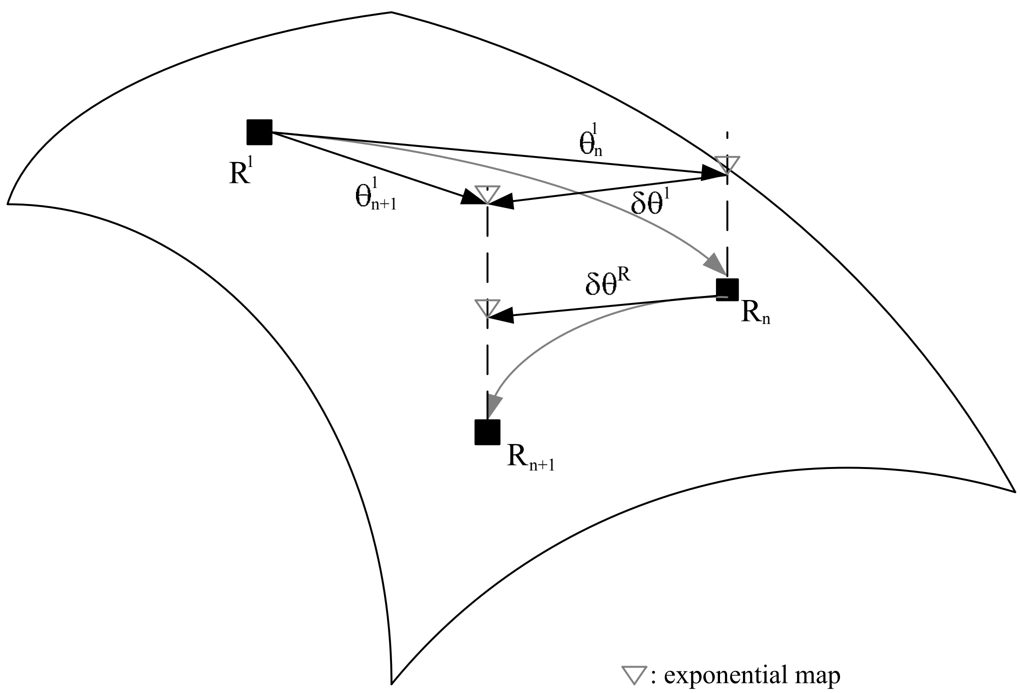

Figure 2–2: Mathematical representation of rotation updates.

2.2.7 Calculation of a rotational vector given an initial vector and its final configuration

The following procedure will be used to determine the rotation matrix that characterizes a rigid body motion (Crisfield 1997). Given two vectors, $\mathbf{t}_o$ and $\mathbf{t}_n$, the rotation that transforms $\mathbf{t}_o$ into $\mathbf{t}_n$ is described geometrically with the angle θ and the unit vector $\hat{\boldsymbol{\theta}}$:

$$\cos(\theta) = \mathbf{t}_o^t \cdot \mathbf{t}_n$$
$$\hat{\boldsymbol{\theta}} = \frac{\mathbf{t}_o \times \mathbf{t}_n}{\|\mathbf{t}_o \times \mathbf{t}_n\|} = \frac{\sin(\theta)}{\theta}\boldsymbol{\theta} \tag{2.19}$$

Thus the rotation matrix becomes:

$$\mathbf{R}(\theta) = \mathbf{I} + \boldsymbol{\Omega}(\mathbf{t}_o \times \mathbf{t}_n) + \frac{1}{1 + \mathrm{t}_o^t \cdot \mathrm{t}_n}\boldsymbol{\Omega}(\mathbf{t}_o \times \mathbf{t}_n) \cdot \boldsymbol{\Omega}(\mathbf{t}_o \times \mathbf{t}_n) \tag{2.20}$$

where $\boldsymbol{\Omega}(\mathbf{t}_0 \times \mathbf{t}_n)$ represents the Spinor of the resultant vector from the cross product $(\mathbf{t}_0 \times \mathbf{t}_n)$.

2.3 The corotational concept

The movement of an element in a body can be separated into two components: a rigid body motion (displacement and rotation) and a deformation (strains and curvatures). To describe the rigid body motion, a reference frame located outside of the element is needed. In general, the same external reference is used for all elements in the body and it is called "Global coordinate system" (**G**).

A rigid body motion is composed of (i) a rigid body translation: the displacement of the center of gravity of the element; and (ii) a rigid body rotation: the relative displacements of the nodes of the elements with respect to the center of the element. The same description can be made by considering the movement of the nodes in Global coordinates. In structural analysis, this is called the "chord of the element", see Figure 2–3.

In the Corotational approach, the element's deformations are described with respect to the chord; therefore a Local reference system has to be defined and a relationship with the Global reference system has to be found. Since the Local coordinate system describes the position of the chord in the space, moving and rotating with it, this Local system is known as Corotated (**E**). It is arbitrarily chosen that the *x* axis of the Corotated system coincides with the direction of the element's chord and that the *y* and *z* axis coincide with the principal directions of the section. The Corotated axes (**E**) are related to the global axes (**G**) through a rotation matrix.

In the context of stability analysis, a common assumption is that large displacements are described within the rigid body motion so that deformations are small. If this assumption is not valid for a particular element, it is always possible to break it into more elements until the assumption holds true. Thus, at the corotated level, the small strains theory is used to describe the deformations. The main advantage of this assumption is that existing formulation and software can be used to address the problem of large displacements, just by adding a proper transformation matrix between global and corotated coordinates and by considering the effects of the geometry in the stiffness matrix.

In the present formulation the corotational concept is adopted but the condition of small deformations is relaxed and large displacement/rotation theory is used to describe them.

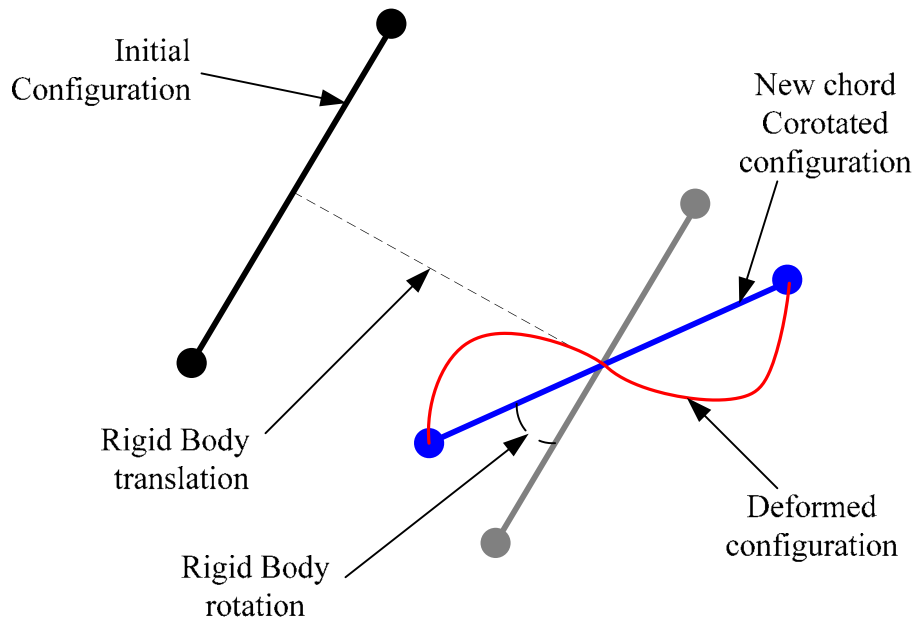

Figure 2–3: Corotational concept.

2.4 Constitutive model

Material nonlinearity is a very important aspect in stability analysis. For the present work, the constitutive model developed at the University at Buffalo (Simeonov et al. 2000; Sivaselvan and Reinhorn 2001) will be used without modifications. The following is a summary of their work.

2.4.1 Derivation of the plasticity model

The derivation of the Constitutive law is based on a parallel plasticity model. The model proposes that the total stress increments can be decomposed into elastic and hysteretic components (Figure 2–4).

$$d\sigma = d\sigma_e + d\sigma_h \tag{2.21}$$

where $d\sigma$ is the total incremental stress, $d\sigma_\varepsilon$ is the elastic portion and $d\sigma_h$ is the hysteretic portion.

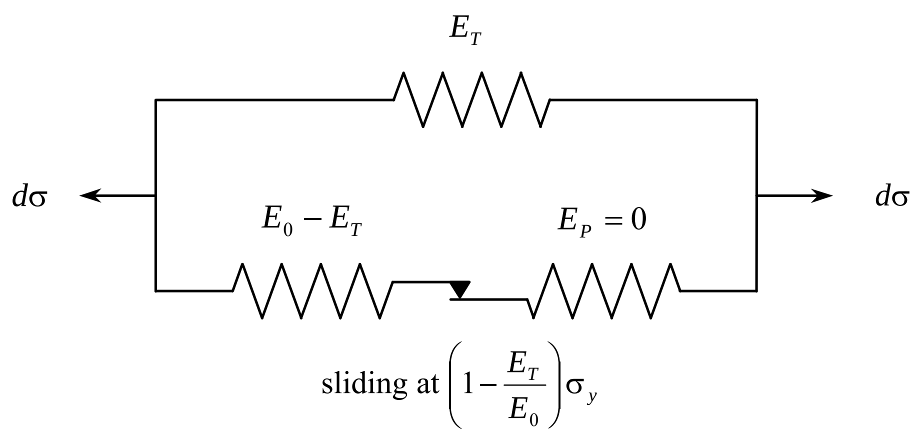

Figure 2–4: Parallel plasticity model (From Simeonov (1999) Figure 2-2 b)

The total resistance is then attributed to an elastic element of stiffness $\mathbf{K}_e$ in parallel with an elastic-ideal-plastic element. The latter is represented by a serial plasticity model of elastic stiffness $\mathbf{K}_0$-$\mathbf{K}_e$ and yield stress $(1-\mathbf{K}_e/\mathbf{K}_0)\cdot\sigma_y$. The elastic stiffness $\mathbf{K}_e$ represents the hardening after the hysteretic element has yielded and is not the total initial elastic stiffness ($\mathbf{K}_0$). The advantage of this type of model is its natural capacity of representing Bauschinger effects without the introduction of hardening rules. The relationship between stress and strain rates can then be written as:

$$\dot{\sigma} = \left(\mathrm{E}_e + \mathrm{E}_h\right)\dot{\varepsilon} \tag{2.22}$$

where σ is total stress, ε is total strains, E_e is the elastic portion of the modulus of elasticity and E_h is its hysteretic portion.

In order to define yielding, the formulation uses two yield surfaces: initial and ultimate. These surfaces describe the combination of loads under which the element is starting to yield (initial surface) or it is fully plasticized (ultimate surface). The surfaces depend on the characteristics of the section and must be smooth, continuous functions. A general mathematical representation of a yield surface is:

$$\phi = \mathrm{f}\left(\mathbf{F}_h\right) \leq 0 \tag{2.23}$$

Equation (2.23) describes the yield function ϕ as a function of $\mathbf{F}_h$, the elastic-ideal plastic component of the total force $\mathbf{F}_T$. It is always non-positive. When the yield function is equal to 0, the section is yielding.

It is also assumed that the total strains ε can be written as the sum of the elastic and hysteretic parts. In rate form:

$$\dot{\boldsymbol{\varepsilon}} = \dot{\boldsymbol{\varepsilon}}_e + \dot{\boldsymbol{\varepsilon}}_p \tag{2.24}$$

where $\boldsymbol{\varepsilon}_e$ is the elastic and $\boldsymbol{\varepsilon}_p$ is the plastic component of the total strains $\boldsymbol{\varepsilon}$.

When the element is flowing: ϕ=0, the rate of the elastic strain is zero and the rate of total strains is the rate of hysteretic strains. On the other hand, the rate of the hysteretic force can be written solely in terms of the rate of the elastic strains since after yielding the force is constant, thus its rate is zero.

$$\dot{\mathbf{F}}_h = \left(\mathbf{K}_0 - \mathbf{K}_e\right) \cdot \dot{\boldsymbol{\varepsilon}}_e \tag{2.25}$$

The plastic strain $\boldsymbol{\varepsilon}_p$ is calculated using plastic flow rules. The direction of the plastic flow is perpendicular to the yielding surface and its magnitude is proportional to the gradient of the surface at the point of yielding:

$$\dot{\boldsymbol{\varepsilon}}_p = \dot{\lambda} \frac{\partial \phi}{\partial \mathbf{F}_h} \tag{2.26}$$

where $\partial\phi/\partial\mathbf{F}_h = \{\partial\phi/\partial F_x^* \;\; \partial\phi/\partial M_y^* \;\; \partial\phi/\partial M_z^*\}^t$ is the gradient of the yield function and the rate of λ is a proportionality scalar. F_x*, M_y* and M_z* are defined in Equation (2.36) To calculate the proportionality scalar and the plastic strains, the following rules known as Kuhn-Tucker conditions must be enforced:

- The plastic flow is always directed outwards the yielding surface.
- No flow occurs for load combinations outside the yielding surface.

$$\begin{aligned} &\dot{\lambda} \geq 0 \\ &\phi \cdot \dot{\lambda} = 0 \\ &\dot{\lambda} \left(\frac{\partial \phi}{\partial \mathbf{F}_h} \right)^t \dot{\mathbf{F}}_h \geq 0 \end{aligned} \tag{2.27}$$

The plastic multiplier can be calculated from the consistency equation:

$$\left(\frac{\partial\phi}{\partial\mathbf{F}_h}\right)^t \dot{\mathbf{F}}_h = 0 \tag{2.28}$$

It expresses the fact that a force combination which has caused plastic strains, will continue to do so until unloading.

Replacing the value of the rate of $\mathbf{F}_h$ into the consistency equation:

$$\left(\frac{\partial\phi}{\partial\mathbf{F}_h}\right)^t \left(\mathbf{K}_0-\mathbf{K}_e\right)\cdot\left(\dot{\boldsymbol{\varepsilon}}-\dot{\lambda}\frac{\partial\phi}{\partial\mathbf{F}_h}\right)=0 \tag{2.29}$$

And solving for the plastic multiplier and the plastic strains:

$$\begin{aligned}
\dot{\lambda} &= \frac{\left(\frac{\partial\phi}{\partial\mathbf{F}_h}\right)^t \left(\mathbf{K}_0-\mathbf{K}_e\right)\dot{\boldsymbol{\varepsilon}}}{\left(\frac{\partial\phi}{\partial\mathbf{F}_h}\right)^t \left(\mathbf{K}_0-\mathbf{K}_e\right)\left(\frac{\partial\phi}{\partial\mathbf{F}_h}\right)}\\
\dot{\boldsymbol{\varepsilon}}_p &= \frac{\left(\frac{\partial\phi}{\partial\mathbf{F}_h}\right)^t \left(\mathbf{K}_0-\mathbf{K}_e\right)\dot{\boldsymbol{\varepsilon}}}{\left(\frac{\partial\phi}{\partial\mathbf{F}_h}\right)^t \left(\mathbf{K}_0-\mathbf{K}_e\right)\left(\frac{\partial\phi}{\partial\mathbf{F}_h}\right)}\frac{\partial\phi}{\partial\mathbf{F}_h}
\end{aligned} \tag{2.30}$$

The relationship between the force rate and the strain rate is:

$$\dot{\mathbf{F}}_h = \left(\mathbf{K}_0-\mathbf{K}_e\right)\left[\dot{\boldsymbol{\varepsilon}}-\frac{\left(\frac{\partial\phi}{\partial\mathbf{F}_h}\right)^t \left(\mathbf{K}_0-\mathbf{K}_e\right)\dot{\boldsymbol{\varepsilon}}}{\left(\frac{\partial\phi}{\partial\mathbf{F}_h}\right)^t \left(\mathbf{K}_0-\mathbf{K}_e\right)\left(\frac{\partial\phi}{\partial\mathbf{F}_h}\right)}\frac{\partial\phi}{\partial\mathbf{F}_h}\mathrm{H}_1\mathrm{H}_2\right] \tag{2.31}$$

H_1 represents the yielding condition and H_2 the unloading condition.

The yielding condition, or plastic flow, occurs only if the force combination defines a point in the yielding surface. Mathematicaly, this can be represented by a Heaviside function, that is always 0 when there is no yielding and 1 when there is yielding. Numerically, this Heaviside function can be smoothed to have a continuous function:

$$\mathrm{H}_1\left(\phi\right)=\left(\phi+1\right)^n \tag{2.32}$$

When the value of the yield function is close to zero, at the onset of yielding, the value of H_1 approaches asymptotically to 1, equaling to 1 after yielding.

The unloading criterion is modeled through another smoothed Heaviside function:

$$H_2\left(\frac{\partial\phi}{\partial \mathbf{F}_h}\dot{\mathbf{F}}_h\right) = \eta_1 + \eta_2 \operatorname{sgn}\left(\frac{\partial\phi}{\partial \mathbf{F}_h}\cdot\dot{\mathbf{F}}_h\right) \tag{2.33}$$

where $\eta_1+\eta_2=1$. η_1 and η_2 can take any value between 0 and 1. Here it will be considered $\eta_1=\eta_2=0.5$. When the section is yielding, the gradient of the yield function $\partial\phi/\partial\mathbf{F}_h$ and the rate of the forces $\dot{\mathbf{F}}_h$ have the same sign (outwards the yield surface) and therefore $\eta_1+\eta_2=1$. When the section is unloading, the flow gradient and the force rates have opposite signs, therefore $H_2=0$. This means that at the unloading stage, the total stiffness becomes the total initial elastic stiffness.

The rate of the total force is then written as:

$$\dot{\mathbf{F}} = \mathbf{K}_e\dot{\varepsilon} + \left(\mathbf{K}_0 - \mathbf{K}_e\right)\left[\dot{\varepsilon} - \frac{\left(\frac{\partial\phi}{\partial\mathbf{F}_h}\right)^t\left(\mathbf{K}_0-\mathbf{K}_e\right)\dot{\varepsilon}}{\left(\frac{\partial\phi}{\partial\mathbf{F}_h}\right)^t\left(\mathbf{K}_0-\mathbf{K}_e\right)\left(\frac{\partial\phi}{\partial\mathbf{F}_h}\right)}\frac{\partial\phi}{\partial\mathbf{F}_h}\left[\left(\phi+1\right)^n\right]\left[\eta_1+\eta_2\operatorname{sgn}\left(\frac{\partial\phi}{\partial\mathbf{F}_h}\cdot\dot{\mathbf{F}}_h\right)\right]\right] \tag{2.34}$$

Note: This can be viewed as a generalized multidimensional inelastic hysteretic model that in unidimensional form reduces to the Sivaselvan-Reinhorn model (Sivaselvan and Reinhorn 2001), which can be further reduced to Bouc-Wen model (Bouc 1967; Wen 1976). Or one can look at this model as the "generalized Bouc-Wen model" for multidimensional surfaces.

2.4.2 Elastic stiffness matrix

The elastic stiffness matrix $\mathbf{K}_e$ is the hardening slope in a force-displacement relationship. Usually, the hardening is written in terms of a percentage of the total initial elastic stiffness: $\mathbf{K}_e$ = a $\mathbf{K}_0$. Where a can be 3%, 5% or any value defined by a material coupon test.

2.4.3 Initial elastic stiffness matrix

Since the relationship above links the force rate to the strains, a typical total initial elastic stiffness matrix would look like:

$$\mathbf{K}_0 = \begin{bmatrix} EA & 0 & 0 & 0 \\ 0 & GJ & 0 & 0 \\ 0 & 0 & EI_y & 0 \\ 0 & 0 & 0 & EI_z \end{bmatrix} \tag{2.35}$$

where E: modulus of elasticity; A: area; G: shear modulus; J: torsional constant; I_y: inertia in the weak direction; I_z: inertia in the strong direction.

2.4.4 Ultimate yield function

The ultimate yield function depends on the cross section shape. However, in general it can be written as (Figure 2–5):

$$\begin{gathered} \phi = \frac{\left|m_y\right|^{\alpha_y}}{\left(1-\left|p\right|^{\beta_y}\right)^{\alpha_y}} + \frac{\left|m_z\right|^{\alpha_z}}{\left(1-\left|p\right|^{\beta_z}\right)^{\alpha_z}} - 1 \\ m_y = \frac{M_y^*}{M_{yu}^*} \qquad m_z = \frac{M_z^*}{M_{zu}^*} \qquad p = \frac{F_x^*}{F_{xu}^*} \\ M_y^* = M_y - aEI_y\phi_y \qquad M_{yu}^* = \left(1-a\right)\sigma_y Z_y \\ M_z^* = M_z - aEI_z\phi_z \qquad M_{zu}^* = \left(1-a\right)\sigma_y Z_z \\ F_x^* = F_x - aEA\varepsilon_x \qquad F_{xu}^* = \left(1-a\right)\sigma_y A \end{gathered} \tag{2.36}$$

In Equation (2.36) M_x, M_y and M_z are the moments in the x, y and z directions respectively; ϕ_y and ϕ_z are the curvatures in the y and z directions; F_x is the axial force (in x direction); ε_x is the axial strain; the exponents α and β are particular to each section and have to be determined from a finite element analysis or experimental results. All other quantities have been defined elsewhere.

The yield function depends on non-dimensional quantities p, m_y and m_z that are always less than unity. These quantities represent the proportion of the hysteretic forces, total forces minus elastic forces, with respect to the ultimate capacities.

The equation above assumes that the section is doubly-symmetric. If the section in the model is not symmetric, appropriate changes have to be made to the axial force axis representation (Sivaselvan and Reinhorn 2001).

From Equation (2.36), a general gradient of the hysteretic force can be obtained:

$$
\begin{aligned}
\frac{\partial\phi}{\partial F_x^*} &= \frac{\partial\phi}{\partial p}\frac{1}{F_{xu}^*} \\
\frac{\partial\phi}{\partial M_y^*} &= \frac{\partial\phi}{\partial m_y}\frac{1}{M_{yu}^*} \\
\frac{\partial\phi}{\partial M_z^*} &= \frac{\partial\phi}{\partial m_z}\frac{1}{M_{zu}^*}
\end{aligned}
\tag{2.37}
$$

2.4.5 Yielding criterion parameter

The parameter n in the exponent of the yielding criterion defines how smooth is the transition between the elastic and inelastic portions of the hysteretic curve. Values between 6 and 10 are normally used. A value of 10 is considered high which means that the transition is sharp or sudden. A lower exponent is better for numerical purposes. The drawback of this formulation is that it is allowing plastic deformations from the beginning of the analysis, which is not correct. An initial yield surface can be used to define incipient yielding, using an elastic stiffness matrix or a very high exponent up to that surface and switching to a lower exponent until reaching full plasticity. Numerical problems may arise when using this approach because the distance between incipient yielding and fully plastic surfaces is, in general, small.

2.4.6 Unloading criterion

Equation (2.33) depends on the yield function gradients and the hysteretic force rates. However, the hysteretic force rate is the variable that is being calculated through the above procedure. It is not desirable to have its value in the unloading function because traditional methods for solving differential equations cannot be applied. The product of the elastic stiffness matrix and the total strains vector was suggested to replace it (Simeonov et al. 2000):

$$
H_2\left(\frac{\partial\phi}{\partial \mathbf{F}_h}\dot{\mathbf{F}}_h\right) = \eta_1 + \eta_2 \operatorname{sgn}\left(\frac{\partial\phi}{\partial \mathbf{F}_h}\cdot\mathbf{K}_e\cdot\dot{\boldsymbol{\varepsilon}}\right)
\tag{2.38}
$$

The reason for the above change is that since the unloading is elastic, the force rate and the strain rate are related through the elastic stiffness matrix. The dot product ensures that the sign of the function is preserved.

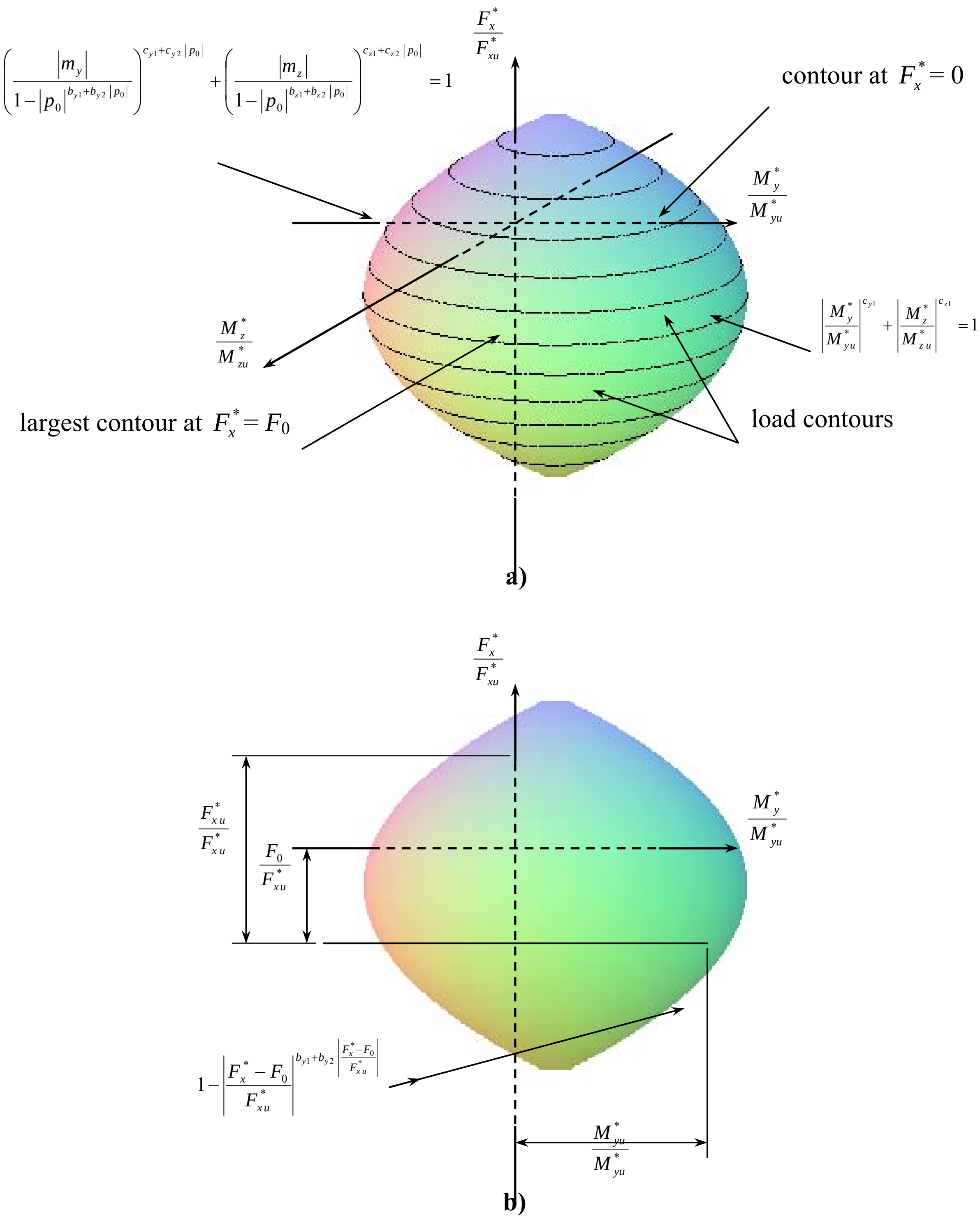

Figure 2–5: Ultimate-Yield Surface: a) General View, b) Slice in Plane $\mathbf{p}-\mathbf{m}_y$
(From Simeonov (1999) Figure 2-4)

2.5 The state space approach.

For solving a system of nonlinear equations of motion that represents a structural system, the traditional approach has been to write these equations in an incremental way, thus solving a nonlinear transient analysis as a sequence of quasi-static analyses. The system is solved in Global coordinates, therefore during a step, equilibrium, internal plasticity rules and/or compatibility between elements can be violated and iterations within a step are necessary to enforce them.

By contrast, the state space approach uses a set of variables: global nodal displacements and velocities their rates, element internal forces and their rates, total strains at pre-defined control sections along the length of the element and their rates. These variables completely define the state of each element in the structure at any time. The solution of the structural problem consists in solving a set of equations that represent the “evolution” of all these variables with time (evolution equations). Those equations are the fundamental equations of a structural system: Equilibrium, Compatibility and Plasticity. Written in rate form this set constitutes, in general, a system of Differential Algebraic Equations (DAE). The simultaneous solution of all the equations ensures that the all the basic laws (equilibrium, compatibility and plasticity) are satisfied at all times, eliminating the need for iterations within a step. The framework of this approach was developed by Simeonov (Simeonov et al. 2000).

2.5.1 State variables

First, the set of variables and their rates have to be defined.

Denoting u the displacement, m the mass, c the damping constant, k the stiffness and P the external force, the traditional equation of motion, a second order differential equation, is:

$$m \cdot \ddot{u} + c \cdot \dot{u} + k \cdot u = P \qquad (2.39)$$

Using displacements and velocities (or displacements rates) as the independent variables, Equation (2.39) is re-written as a set of two first order differential equations:

$$\begin{aligned} & y_1 = u \qquad y_2 = \dot{u} \\ & m \cdot \dot{y}_2 + c \cdot \dot{y}_1 + k \cdot y_1 = P \\ & y_2 = \dot{y}_1 \end{aligned} \qquad (2.40)$$

Two equations are needed to solve a problem of two variables. The second differential equation states that the velocity if the time derivative of the displacement.

Moreover, by introducing a new variable: the internal force $Q = k\ y_1$, Equation (2.39) becomes a set of three first order differential equations:

$$\begin{aligned} & y_1 = u \qquad y_2 = \dot{u} \qquad y_3 = Q \\ & m \cdot \dot{y}_2 + c \cdot \dot{y}_1 + y_3 = P \\ & y_2 = \dot{y}_1 \\ & \dot{Q} = k \cdot \dot{y}_1 \end{aligned} \tag{2.41}$$

where the third differential equation represents the relationship between internal forces and displacements through the stiffness matrix.

Thus displacements, velocities and internal forces are natural choices for state variables.

Finally, a variable that represents the internal state of the element (strains and stresses) at some finite number of points along the length of the element (integration points) is needed. The location and number of these points can be chosen according to the problem and can be different from one element to another. Depending on whether the formulation is stiffness or flexibility based and whether the constitutive law is derived from a strain decomposition or stress decomposition assumption, the choices for internal variables are different. Table 2-1 contains a summary of the possible choices (Simeonov 1999).

In the present formulation, the constitutive law adopted is based on a stress decomposition model and the flexibility matrix formulation is adopted. Thus according to the table, the total strains are chosen as internal variables.

Table 2-1: Selection of element state variables at the integration points (From Simeonov, (1999) Table 4-1)

	Stiffness based element	Flexibility based element
Strain decomposition law	Stresses σ	Inelastic strains ε_p
Stress decomposition law	Hysteretic stresses σ_h	Strains ε

2.5.2 Evolution equations

The evolution equations are the fundamental laws of structural analysis: Equilibrium, Compatibility and Plasticity, which are developed in the following section.

2.6 Development of an element for large displacements and large rotations

2.6.1 Objective

The objective of the present formulation is to develop a procedure capable of solving structural problems with material as well as geometrical nonlinearities.

The formulation solves the problem in the state space, using the Corotational formulation to describe each element independently. Deformations are calculated with respect to the Corotated system of coordinates and they can be large. The goal is to develop appropriate equations of Equilibrium, Compatibility and Plasticity for every element. The result is a set of Differential Algebraic Equations (DAE) equations that are being solved using the Implicit Differential Algebraic solver (IDA) from the Lawrence Livermore National Laboratory (LLNL) (Hindmarsh and Serban 2006).

The procedure can be summarized in the following steps:

1. Definition of Coordinate systems.
2. Definition of DOFs.
3. Calculation of rigid body transformation matrices.
4. Equilibrium equations.
5. Compatibility equations.
6. Plasticity equations.
7. Numerical integration methods.

2.6.2 Coordinate systems

There are 3 coordinate systems needed for understanding the present development (Figure 2–6):

- **G**: Global coordinate system. Fixed and common for all the elements, the equations of motions of the structure are solved in this system.
- **L**: Local coordinate system. Defines the position of the element in its original unstressed position. This system serves as a reference for the calculation of nodal rotations.
- **E**: Corotated coordinate system. Defines the position of the chord of the element at each time step. This system changes with each iteration.

G, **L** and **E** are 3x3 orthogonal matrices whose rows are the three axes that define the coordinate system. Each axis has 3 components: the projections in the Global system. Therefore, without any loss of generality, the Global system **G** can be defined as the Identity matrix $\mathbf{I_3}$. Matrix **L** can be calculated with the direction cosines and it is constant throughout the analysis. Matrix **E** is the rigid body transformation matrix that defines the chord of the element in its deformed configuration. Since the element moves in time, matrix **E** has to be updated every time step.

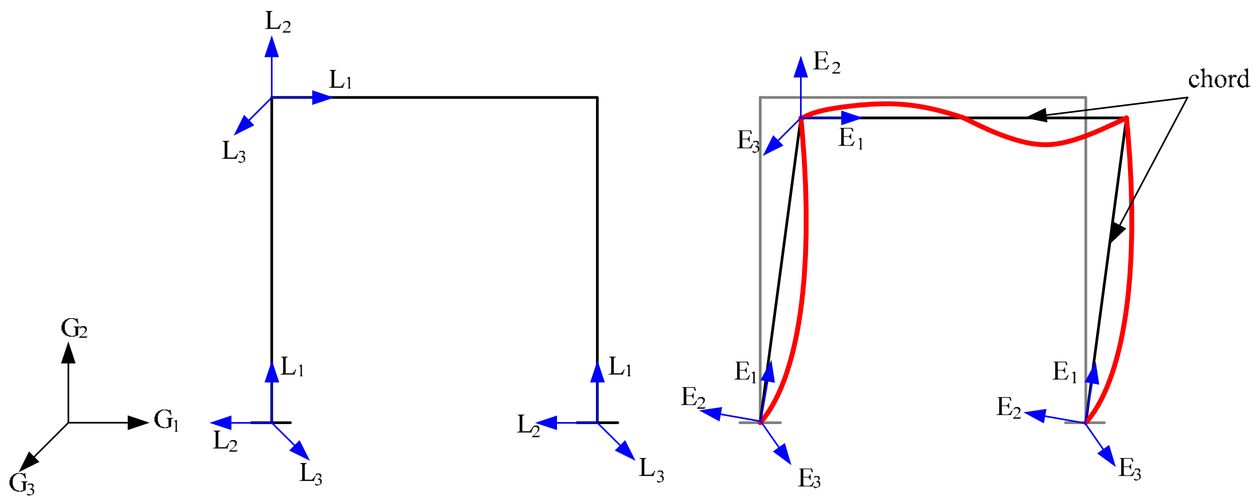

Figure 2–6: Definition of Global (G), Local (L) and Corotated (E) coordinate systems.

2.6.3 Degrees of freedom

Following the defined systems of coordinates, the DOFs can be written in Global, Local and Corotated coordinates:

An element is defined by 2 nodes (Figure 2–7). Each node has, in Global and Local coordinates, 6 DOFs: 3 displacements and 3 rotations.

$$\left\{ u_x \quad u_y \quad u_z \quad \theta_x \quad \theta_y \quad \theta_z \right\}_{node} \tag{2.42}$$

And its conjugated forces are:

$$\left\{ F_x \quad F_y \quad F_z \quad M_x \quad M_y \quad M_z \right\}_{node} \tag{2.43}$$

The meaning of the directions *x*,*y* and *z* on Equation (2.43) depend on the coordinate system used to describe the movement (Global **G** or Local **L**).

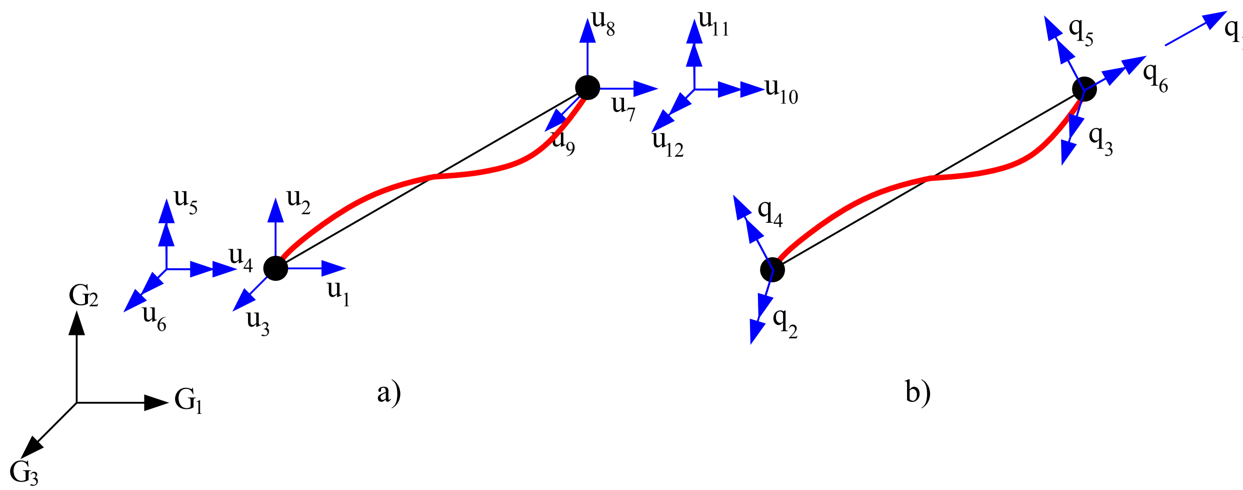

Figure 2–7: Definition of DOFs in global and local coordinates (a) and in corotated coordinates (b).

An element in its Corotated coordinates only has a total of 6 DOFs:

$$\{q_1 \quad q_2 \quad q_3 \quad q_4 \quad q_5 \quad q_6\}_{\text{element}} \tag{2.44}$$

And its conjugated forces are:

$$\{Q_1 \quad Q_2 \quad Q_3 \quad Q_4 \quad Q_5 \quad Q_6\}_{\text{element}} \tag{2.45}$$

q_1 and Q_1 refer to the axial deformation and force, respectively; q_2 and Q_2 describe the in plane rotation and moment at the initial node; q_3 and Q_3 describe the in plane rotation and moment at the end node; q_4 and Q_4 describe the out of plane rotation and moment at the initial node; q_5 and Q_5 describe the out of plane rotation and moment at the end node; q_6 and Q_6 describe the torsional rotation and torsion.

Implicit in the above equations are the following assumptions:

1. The axial force is constant throughout the element.
2. The moment diagram is linear, therefore the shear is constant and can be calculated as the sum of moments divided by the length of the element.
3. Torsion is constant along the element.

According to 2.5.1, the Global variables are the Global displacements and velocities. The Local variables are the Corotated internal forces and the total axial strains and the curvatures. Thus, the vector of variables and their rates are:

$$\mathbf{y} = \{\mathbf{u} \quad \dot{\mathbf{u}} \quad \mathbf{Q} \quad \boldsymbol{\varepsilon}\}^t \qquad \dot{\mathbf{y}} = \{\dot{\mathbf{u}} \quad \ddot{\mathbf{u}} \quad \dot{\mathbf{Q}} \quad \dot{\boldsymbol{\varepsilon}}\}^t \tag{2.46}$$

where $\mathbf{u}$ is defined in Equation (2.42), $\mathbf{Q}$ is defined in Equation (2.45) and $\boldsymbol{\varepsilon}$ is defined by:

$$\boldsymbol{\varepsilon} = \left\{ \varepsilon \quad \phi_x \quad \phi_y \quad \phi_z \right\}^t \tag{2.47}$$

$\boldsymbol{\varepsilon}$ is the set of vectors of total axial strain and curvatures of every section of the element. In Equation (2.47), ε represents axial strains and ϕ_x, ϕ_y, ϕ_z are the curvatures.

In a general structure, not all its DOFs are dynamics i.e. have an associated mass. Those DOFs are called "static" and their associated equation of motion is simply:

$$k \cdot u = P \tag{2.48}$$

For these DOFs, there are only two state variables: u and Q. Therefore, in Equation (2.46), the velocity is a state variable of dynamic DOFs only. For instance, when a static analysis is performed Equation (2.46) becomes:

$$\mathbf{y} = \left\{ \mathbf{u} \quad \mathbf{Q} \quad \boldsymbol{\varepsilon} \right\}^t \qquad \dot{\mathbf{y}} = \left\{ \dot{\mathbf{u}} \quad \dot{\mathbf{Q}} \quad \dot{\boldsymbol{\varepsilon}} \right\}^t \tag{2.49}$$

2.6.4 Calculation of rigid body transformation matrices

For each element, a matrix **E:** the rigid body transformation matrix that defines the chord and principal axes of the element in its deformed configuration, has to be calculated. At each time step, the actual position of each node of the element in Global coordinates is calculated from its original position and actual displacement:

$$\mathbf{p}_i = \mathbf{p}_0 + \mathbf{u}_i$$

where $\mathbf{p}_i$ is the vector of the actual position of node *i*, $\mathbf{p}_0$ and $\mathbf{u}_i$ are the original position and actual displacement of node *i*. The actual displacement $\mathbf{u}_i=\{u_{xi} \; u_{yi} \; u_{zi}\}^t$ at any time step is a known quantity and can be retrieved from the state variable $\mathbf{u}$. The vector describing the chord of the element can then be calculated as:

$$\mathbf{E}_1 = \frac{\mathbf{p}_i - \mathbf{p}_j}{\left\| \mathbf{p}_i - \mathbf{p}_j \right\|} \tag{2.51}$$

where the variables i and j represent the initial and end nodes of the element. The vector $\mathbf{E}_1$ is the Corotated *x* coordinate.

The next step is to obtain a rotation matrix $\mathbf{R}_{\mathbf{L\text{-}E}}$ that rotates the vector $\mathbf{L}_1$ (the Local *x* coordinate) into vector $\mathbf{E}_1$. Using Equation (2.20):

$$\mathbf{R}_{\mathbf{L\text{-}E}} = \mathbf{I} + \boldsymbol{\Omega}\left(\mathbf{L}_1 \times \mathbf{E}_1\right) + \frac{1}{1 + \mathbf{L}_1^t \cdot \mathbf{E}_1} \boldsymbol{\Omega}\left(\mathbf{L}_1 \times \mathbf{E}_1\right) \cdot \boldsymbol{\Omega}\left(\mathbf{L}_1 \times \mathbf{E}_1\right) \tag{2.52}$$

Recalling that $\boldsymbol{\Omega}(\mathbf{L}_1 \times \mathbf{E}_1)$ is the spinor of the resultant vector of the cross product $L_1 \times E_1$.

Matrix $\mathbf{R}_{\text{L-E}}$ also rotates the vectors $\mathbf{L}_2$ into $\mathbf{E}_2$ and $\mathbf{L}_3$ into $\mathbf{E}_3$. Vectors $\mathbf{L}_2$ and $\mathbf{L}_3$ represent the directions of the principal axes of the cross section in its original configuration, while $\mathbf{E}_2$ and $\mathbf{E}_3$ represent the directions of the principal axes of the cross section in its Corotated configuration.

Thus, matrix $\mathbf{E}$ is obtained by rotating matrix $\mathbf{L}$ with $\mathbf{R}_{\text{L-E}}$:

$$\mathbf{E} = \mathbf{R}_{\mathbf{L\text{-}E}} \cdot \mathbf{L} \tag{2.53}$$

Vectors $\mathbf{L}_1$, $\mathbf{L}_2$ and $\mathbf{L}_3$ are rows of the transformation matrix $\mathbf{L}$ (that rotates the Global coordinates into Local coordinates). These vectors are also known as cosine directors (Weaver, 1990 #123). Similarly, Vectors $\mathbf{E}_1$, $\mathbf{E}_2$ and $\mathbf{E}_3$ are rows of the rotation matrix $\mathbf{E}$.

Because the Global system is arbitrarily chosen as the identity matrix $\mathbf{G} = \mathbf{I}_3$, the coordinate system $\mathbf{L}$ coincides with the rotation matrix $\mathbf{L}$ i.e. $\mathbf{L} = \mathbf{L} \cdot \mathbf{G}$ and the coordinate system $\mathbf{E}$ coincides with the rotation matrix $\mathbf{E}$ i.e. $\mathbf{E} = \mathbf{E}\ \mathbf{G}$.

The origin of the Corotated coordinate system $\mathbf{E}$ can be located anywhere along the element. It is convenient to place it at one of the end nodes, say node i, for reasons that will become apparent latter in the development of the formulation.

2.6.5 Equilibrium Equations

Global equilibrium equations are the evolution equations of Global variables.

The internal forces $\mathbf{Q}$ of each element in Corotated coordinates are known variables (Equation (2.46)). Global equilibrium is calculated by transforming the internal forces into Global Coordinates, summing all the contributions from different elements in each node and comparing these values to the applied external force.

The transformation into Global variables is done through a transformation matrix $\mathbf{T}^t$. This matrix is specific to each element and is the resultant of the composition of the rigid body rotation matrix $\mathbf{T}_{\text{CG}}$ and the matrix of change of variables $\mathbf{T}_{\text{EC}}$.

$$\mathbf{T} = \mathbf{T}_{\text{EC}} \mathbf{T}_{\text{CG}} \tag{2.54}$$

$\mathbf{T}_{\text{EC}}$ is the matrix representing equilibrium at the Corotated level using the assumptions listed in part 2.6.3. $\mathbf{T}_{\text{EC}}$ transforms 12 DOFs (Local) into 6 DOFs (Corotated) (See Figure 2–7):

$$\mathbf{T}_{EC} = \begin{bmatrix} -1 & 0 & 0 & 0 & 0 & 0 & 1 & 0 & 0 & 0 & 0 & 0 \\ 0 & 1/\xi_L & 0 & 0 & 0 & 1 & 0 & -1/\xi_L & 0 & 0 & 0 & 0 \\ 0 & 1/\xi_L & 0 & 0 & 0 & 0 & 0 & -1/\xi_L & 0 & 0 & 0 & 1 \\ 0 & 0 & -1/\xi_L & 0 & 1 & 0 & 0 & 0 & 1/\xi_L & 0 & 0 & 0 \\ 0 & 0 & -1/\xi_L & 0 & 0 & 0 & 0 & 0 & 1/\xi_L & 0 & 1 & 0 \\ 0 & 0 & 0 & -1 & 0 & 0 & 0 & 0 & 0 & 1 & 0 & 0 \end{bmatrix} \tag{2.55}$$

where ξ_L is the actual length of the element.

Transformation matrix $\mathbf{T}_{CG}$ is an expanded version of matrix **E** to allow the transformation of 12 DOFs simultaneously from Global to Corotated coordinates. Matrix **E** transforms 3 DOFs (displacements **u** and rotations **θ**) from Global to Corotated coordinates:

$$\begin{aligned} \mathbf{u}^{CR} &= \mathbf{E} \cdot \mathbf{u}^{G} \\ \theta^{CR} &= \mathbf{E} \cdot \theta^{G} \end{aligned} \tag{2.56}$$

Thus, to transform all the DOFs of a node the following matrix form can be used:

$$\begin{bmatrix} \mathbf{u}^{CR} \\ \theta^{CR} \end{bmatrix} = \begin{bmatrix} \mathbf{E} & \mathbf{0} \\ \mathbf{0} & \mathbf{E} \end{bmatrix} \cdot \begin{bmatrix} \mathbf{u}^{G} \\ \theta^{G} \end{bmatrix} \tag{2.57}$$

Since an element has 2 end nodes, Equation (2.57) can be written as:

$$\begin{bmatrix} \mathbf{u}^{CR}{}_{i} \\ \theta^{CR}{}_{i} \\ \mathbf{u}^{CR}{}_{j} \\ \theta^{CR}{}_{j} \end{bmatrix} = \begin{bmatrix} \mathbf{E} & \mathbf{0} & \mathbf{0} & \mathbf{0} \\ \mathbf{0} & \mathbf{E} & \mathbf{0} & \mathbf{0} \\ \mathbf{0} & \mathbf{0} & \mathbf{E} & \mathbf{0} \\ \mathbf{0} & \mathbf{0} & \mathbf{0} & \mathbf{E} \end{bmatrix} \cdot \begin{bmatrix} \mathbf{u}^{G}{}_{i} \\ \theta^{G}{}_{i} \\ \mathbf{u}^{G}{}_{j} \\ \theta^{G}{}_{j} \end{bmatrix} \tag{2.58}$$

where the subscript i denotes node i and the subscript j denotes node j. Finally, matrix $\mathbf{T}_{CG}$ is:

$$\mathbf{T}_{CG} = \begin{bmatrix} \mathbf{E} & \mathbf{0} & \mathbf{0} & \mathbf{0} \\ \mathbf{0} & \mathbf{E} & \mathbf{0} & \mathbf{0} \\ \mathbf{0} & \mathbf{0} & \mathbf{E} & \mathbf{0} \\ \mathbf{0} & \mathbf{0} & \mathbf{0} & \mathbf{E} \end{bmatrix} \tag{2.59}$$

Matrix **T** transforms Global displacement and rotation rates into Corotated coordinates and, by virtual work, its transpose transforms Corotated forces **Q** into Global coordinates **F**:

$$\begin{aligned} \dot{\mathbf{q}} &= \mathbf{T} \cdot \dot{\mathbf{u}} \\ \mathbf{F} &= \mathbf{T}^{t} \cdot \mathbf{Q} \end{aligned} \tag{2.60}$$

Finally, Global forces at the nodes are premultiplied with a connectivity matrix **N,** specific to each element, of size {12 x total #DOFs in the structure} that identifies each DOF of each node of the element with the global numbering of DOFs of the complete structure. The contributions from all the elements are added and then compared to the externally applied forces $\mathbf{P_{ext}}$:

$$\text{Equilibrium} = \sum_{i=1}^{\#\text{elements}} \mathbf{N_i} \cdot \mathbf{F_i} - \mathbf{P_{ext}} \tag{2.61}$$

2.6.6 Compatibility equations

In this section, the element's deformations are formulated with respect to the Corotated coordinate system. It is assumed that its deformations can be large, therefore mathematics of large rotations are applied when necessary.

Consider an element and its Corotated coordinate system, **E**. Let ε be the axial deformation of the centerline and let P be any point in the centerline. P has originally coordinates $\{x,0,0\}$ with respect to the coordinate system **E**. At the deformed configuration, its new coordinates are $\{\xi,\eta,\chi\}$ with respect to the coordinate system **E** (Figure 2–8). In order to characterize the complete movement of the section, a new coordinate system $\mathbf{t}(x)$ is defined at each point P. $\mathbf{R}(x)$ is the rotation matrix that describes the rotation of the section with respect to the chord. In spatial form:

$$\mathbf{t}(x) = \mathbf{R}(x) \cdot \mathbf{E} \tag{2.62}$$

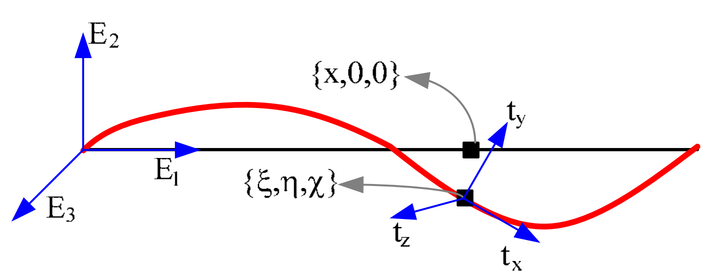

Figure 2–8: Description of the deformations in Corotated coordinates.

The variations of P's coordinate components with the x axis:

$$\frac{d\xi}{dx}(x)=\frac{d\xi}{ds}(x)\cdot\frac{ds}{dx}=\frac{d\xi}{ds}(x)\cdot(1+\varepsilon)$$
$$\frac{d\eta}{dx}(x)=\frac{d\eta}{ds}(x)\cdot\frac{ds}{dx}=\frac{d\eta}{ds}(x)\cdot(1+\varepsilon) \tag{2.63}$$
$$\frac{d\chi}{dx}(x)=\frac{d\chi}{ds}(x)\cdot\frac{ds}{dx}=\frac{d\chi}{ds}(x)\cdot(1+\varepsilon)$$

where s is the arc-length parameter tracking the deformed configuration, thus ds/dx represents the variation of the axial deformation with respect to the original length of the element and dξ/ds, dη/ds and dχ/ds represent the components of the vector $\mathbf{t_1}$ in the Corotated coordinates **E** i.e. the change in the orientation of the coordinate system along the length of the element:

$$\frac{d\xi}{dx}=\left(\mathbf{E}_1^t\cdot\mathbf{t}_1\right)(1+\varepsilon)$$
$$\frac{d\eta}{dx}=\left(\mathbf{E}_2^t\cdot\mathbf{t}_1\right)(1+\varepsilon) \tag{2.64}$$
$$\frac{d\chi}{dx}=\left(\mathbf{E}_3^t\cdot\mathbf{t}_1\right)(1+\varepsilon)$$

Considering a small variation about this deformed position, the incremental compatibility is:

$$\frac{d\dot{\xi}}{dx}=\left(\mathbf{E}_1^t\cdot\dot{\mathbf{t}}_1\right)(1+\varepsilon)+\left(\mathbf{E}_1^t\cdot\mathbf{t}_1\right)\dot{\varepsilon}$$
$$\frac{d\dot{\eta}}{dx}=\left(\mathbf{E}_2^t\cdot\dot{\mathbf{t}}_1\right)(1+\varepsilon)+\left(\mathbf{E}_2^t\cdot\mathbf{t}_1\right)\dot{\varepsilon} \tag{2.65}$$
$$\frac{d\dot{\chi}}{dx}=\left(\mathbf{E}_3^t\cdot\dot{\mathbf{t}}_1\right)(1+\varepsilon)+\left(\mathbf{E}_3^t\cdot\mathbf{t}_1\right)\dot{\varepsilon}$$

From Equation (2.14), the variations of the vector $\mathbf{t_1}$ with respect to time:

$$\dot{\mathbf{t}}_1=\dot{\mathbf{R}}\mathbf{E}_1=\boldsymbol{\Omega}\cdot\mathbf{R}\mathbf{E}_1=\boldsymbol{\Omega}\cdot\mathbf{t}_1 \tag{2.66}$$

where, **Ω** is a skew-symmetric matrix representing an instantaneous infinitesimal rotation or spin and **ω** is its correspondent rotational vector. **Ω** represents the time variation of the rotations <u>over the **t** coordinate system</u>.

It is important to note that, at the deformed level, the variations of the Corotated system **E** with time are irrelevant because the strains and stresses are not affected by rigid body motion. Also, only an observer located at the Global coordinate **G** will notice that the Corotated system **E** moves with time.

Using Equation (2.66), and after some mathematical work (see APPENDIX A, section A.1) the variations (Equations (2.65)) can be rewritten as:

$$
\begin{aligned}
&\int_0^L \frac{d\dot{\xi}}{dx}dx = -\int_0^L \left(\mathbf{E}_1^t \cdot \frac{d\mathbf{\Omega}}{dx} \cdot \mathbf{E}^t \begin{bmatrix} \xi \\ \eta \\ \chi \end{bmatrix} \right) dx + \int_0^L \mathbf{E}_1^t \cdot \mathbf{t}_1 \dot{\varepsilon} dx \\
&\int_0^L \frac{d\dot{\eta}}{dx}dx = C_2 - \int_0^L \left(\mathbf{E}_2^t \cdot \frac{d\mathbf{\Omega}}{dx} \cdot \mathbf{E}^t \begin{bmatrix} \xi \\ \eta \\ \chi \end{bmatrix} \right) dx + \int_0^L \mathbf{E}_2^t \cdot \mathbf{t}_1 \dot{\varepsilon} dx \qquad (2.67) \\
&\int_0^L \frac{d\dot{\chi}}{dx}dx = C_3 - \int_0^L \left(\mathbf{E}_3^t \cdot \frac{d\mathbf{\Omega}}{dx} \cdot \mathbf{E}^t \begin{bmatrix} \xi \\ \eta \\ \chi \end{bmatrix} \right) dx + \int_0^L \mathbf{E}_3^t \cdot \mathbf{t}_1 \dot{\varepsilon} dx
\end{aligned}
$$

where C_2 and C_3 are:

$$
\begin{aligned}
C_2 &= \left(\mathbf{E}_2^t \cdot \mathbf{\Omega}(L) \cdot \mathbf{E}_1\right)\xi(L) - \left(\mathbf{E}_2^t \cdot \mathbf{\Omega}(0) \cdot \mathbf{E}_1\right)\xi(0) = \left(\mathbf{E}_2^t \cdot \mathbf{\Omega}(L) \cdot \mathbf{E}^t\right)_1 \xi(L) \\
C_3 &= \left(\mathbf{E}_3^t \cdot \mathbf{\Omega}(L) \cdot \mathbf{E}_1\right)\xi(L) - \left(\mathbf{E}_3^t \cdot \mathbf{\Omega}(0) \cdot \mathbf{E}_1\right)\xi(0) = \left(\mathbf{E}_3^t \cdot \mathbf{\Omega}(L) \cdot \mathbf{E}^t\right)_1 \xi(L)
\end{aligned} \qquad (2.68)
$$

The compatibility equation that relates the rotations to the curvature in three dimensions (3D) is (Huddleston 1968; Simo and Vu-Quoc 1986):

$$
\frac{d\mathbf{R}}{dx} = \mathbf{\Psi}\mathbf{R}(1+\varepsilon) \qquad (2.69)
$$

where $\mathbf{\Psi}$ is a skew-symmetric matrix containing the Corotated curvatures in spatial form at any section along the length of the element. Taking variations on the Equation (2.69) and after some mathematical manipulations (see APPENDIX A, section A.2) the following relationship is found:

$$
\frac{d\omega}{dx} = \left(\dot{\phi} - \omega \times \phi\right)(1+\varepsilon) + \phi \cdot \dot{\varepsilon} = \hat{\phi}(1+\varepsilon) + \phi \cdot \dot{\varepsilon} \qquad (2.70)
$$

Where ϕ is the correspondent axial vector, in spatial form, of the curvature matrix $\mathbf{\Psi}$. The first term of the right hand side of Equation (2.70) gives the rate of change of the curvature with respect to an observer which moves with the frame $\mathbf{t}$. The material representation takes the form:

$$
\frac{d\omega^m}{dx} = \dot{\phi}^m (1+\varepsilon) + \phi^m \dot{\varepsilon} \qquad (2.71)
$$

It is found that writing the curvatures in material form i.e. in respect to the Corotated (**E**) coordinates, makes the calculations simpler. Integrating Equation (2.70):

$$\begin{aligned}\int_0^L \frac{d\boldsymbol{\omega}}{dx}dx = \boldsymbol{\omega}(L)-\boldsymbol{\omega}(0) = \begin{bmatrix}\dot{q}_6\\ \dot{q}_5-\dot{q}_4\\ \dot{q}_3-\dot{q}_2\end{bmatrix} = \int_0^L \left(\hat{\boldsymbol{\phi}}(1+\varepsilon)+\boldsymbol{\phi}^m\dot{\varepsilon}\right)dx \\ = \int_0^L \mathbf{R}\cdot\frac{d\boldsymbol{\omega}^m}{dx}dx = \int_0^L \mathbf{R}\cdot\left(\dot{\boldsymbol{\phi}}^m(1+\varepsilon)+\boldsymbol{\phi}^m\dot{\varepsilon}\right)dx = \int_0^L \begin{bmatrix}\mathbf{R}\cdot\boldsymbol{\phi}^m & \mathbf{R}(1+\varepsilon)\end{bmatrix}\begin{bmatrix}\dot{\varepsilon}\\ \dot{\boldsymbol{\phi}}^m\end{bmatrix}dx\end{aligned} \tag{2.72}$$

In Equation (2.67), the curvatures have to be expressed in terms of material coordinates. After some mathematical manipulations (see APPENDIX A, section A.3), the system can be written as follows:

$$\begin{bmatrix}\dot{q}_1\\ -C_2\\ -C_3\\ \dot{q}_6\\ \dot{q}_5-\dot{q}_4\\ \dot{q}_3-\dot{q}_2\end{bmatrix} = \int_0^L \begin{bmatrix} \mathbf{E}_1^t\cdot\mathbf{t}_1-\mathbf{E}_1^t\mathbf{R}\boldsymbol{\Psi}^m\mathbf{R}^t\mathbf{E}^t\begin{bmatrix}\xi\\ \eta\\ \chi\end{bmatrix} & \left(\mathbf{R}^t\mathbf{E}_1\times\left(\begin{bmatrix}\xi & \eta & \chi\end{bmatrix}\mathbf{E}^t\mathbf{R}\right)^t\right)(1+\varepsilon) \\ \mathbf{E}_2^t\cdot\mathbf{t}_1-\mathbf{E}_2^t\mathbf{R}\boldsymbol{\Psi}^m\mathbf{R}^t\mathbf{E}^t\begin{bmatrix}\xi\\ \eta\\ \chi\end{bmatrix} & \left(\mathbf{R}^t\mathbf{E}_2\times\left(\begin{bmatrix}\xi & \eta & \chi\end{bmatrix}\mathbf{E}^t\mathbf{R}\right)^t\right)(1+\varepsilon) \\ \mathbf{E}_3^t\cdot\mathbf{t}_1-\mathbf{E}_3^t\mathbf{R}\boldsymbol{\Psi}^m\mathbf{R}^t\mathbf{E}^t\begin{bmatrix}\xi\\ \eta\\ \chi\end{bmatrix} & \left(\mathbf{R}^t\mathbf{E}_3\times\left(\begin{bmatrix}\xi & \eta & \chi\end{bmatrix}\mathbf{E}^t\mathbf{R}\right)^t\right)(1+\varepsilon) \\ \mathbf{R}\cdot\boldsymbol{\phi}^m & \mathbf{R}(1+\varepsilon)\end{bmatrix}\begin{bmatrix}\dot{\varepsilon}\\ \dot{\boldsymbol{\phi}}^m\end{bmatrix}dx \tag{2.73}$$

Without any loss of generality it can be assumed that **E** is equivalent to $\mathbf{I}_3$, the identity matrix. And if the origin of the coordinate system **E** is located at node i, it can be demonstrated that C_2 and C_3 reduce to:

$$\begin{aligned} C_2 &= \begin{bmatrix}0 & 1\end{bmatrix}\begin{bmatrix}\dot{q}_5\\ \dot{q}_3\end{bmatrix}\xi_L \\ C_3 &= \begin{bmatrix}-1 & 0\end{bmatrix}\begin{bmatrix}\dot{q}_5\\ \dot{q}_3\end{bmatrix}\xi_L \end{aligned} \tag{2.74}$$

And that the compatibility equations can be written as (see APPENDIX A, section A.4):

$$\begin{bmatrix} \dot{q}_1 \\ \dot{q}_2 \\ \dot{q}_3 \\ \dot{q}_4 \\ \dot{q}_5 \end{bmatrix} = \int_0^L \mathbf{B} \begin{bmatrix} \dot{\varepsilon} \\ \dot{\boldsymbol{\phi}}^m \end{bmatrix} dx \tag{2.75}$$

where matrix **B** is:

$$\mathbf{B} = \begin{bmatrix} 1 & 0 & 0 & 0 & 0 & 0 \\ 0 & \frac{-1}{\xi_L} & 0 & 0 & -1 & 0 \\ 0 & \frac{-1}{\xi_L} & 0 & 0 & 0 & 0 \\ 0 & 0 & \frac{1}{\xi_L} & -1 & 0 & 0 \\ 0 & 0 & \frac{1}{\xi_L} & 0 & 0 & 0 \\ 0 & 0 & 0 & 0 & 0 & 1 \end{bmatrix} \cdot \begin{bmatrix} \mathbf{E}_1^t \cdot \mathbf{t}_1 - \mathbf{E}_1^t \mathbf{R} \boldsymbol{\Psi}^m \mathbf{R}^t \mathbf{E}^t \begin{bmatrix} \xi \\ \eta \\ \chi \end{bmatrix} & \left(\mathbf{R}^t \mathbf{E}_1 \times \left([\xi \quad \eta \quad \chi] \mathbf{R}\mathbf{E} \right)^t \right)(1+\varepsilon) \\ \mathbf{E}_2^t \cdot \mathbf{t}_1 - \mathbf{E}_2^t \mathbf{R} \boldsymbol{\Psi}^m \mathbf{R}^t \mathbf{E}^t \begin{bmatrix} \xi \\ \eta \\ \chi \end{bmatrix} & \left(\mathbf{R}^t \mathbf{E}_2 \times \left([\xi \quad \eta \quad \chi] \mathbf{R}\mathbf{E} \right)^t \right)(1+\varepsilon) \\ \mathbf{E}_3^t \cdot \mathbf{t}_1 - \mathbf{E}_3^t \mathbf{R} \boldsymbol{\Psi}^m \mathbf{R}^t \mathbf{E}^t \begin{bmatrix} \xi \\ \eta \\ \chi \end{bmatrix} & \left(\mathbf{R}^t \mathbf{E}_3 \times \left([\xi \quad \eta \quad \chi] \mathbf{R}\mathbf{E} \right)^t \right)(1+\varepsilon) \\ \mathbf{R} \cdot \boldsymbol{\phi}^m & \mathbf{R}(1+\varepsilon) \end{bmatrix} \tag{2.76}$$

Considering now the section constitutive equation and the hypothesis that plane sections remain plane, for each section S the curvature pseudovector in material form $\boldsymbol{\phi}^m(S) = \{\phi_x \ \phi_y \ \phi_z\}^t$ and the normal to the section, $\mathbf{t}_1(S)$, are defined. The deformations at every point (α,β) in the section S are described by the scalar function $\varepsilon(x,\alpha,\beta)$ for axial strains:

$$\varepsilon(x,\alpha,\beta) = \varepsilon + \left(\phi_y^m \beta - \phi_z^m \alpha \right)(1+\varepsilon) \tag{2.77}$$

where α and β are parameters describing the position of any point in the cross section with respect to its center. The curvatures, written in material form, denote an infinitesimal rotation of the section with respect to the **E** coordinate system. The factor $(1+\varepsilon)$ accounts for the difference in the chord elongation measured along the normal to the section ($\mathbf{t}_1$). Taking variations of Equation (2.77):

$$\begin{aligned} \dot{\varepsilon}(x,\alpha,\beta) &= \dot{\varepsilon} + \left(\dot{\phi}_y^m \beta - \dot{\phi}_z^m \alpha \right)(1+\varepsilon) + \left(\phi_y^m \beta - \phi_z^m \alpha \right) \dot{\varepsilon} \\ &= \dot{\varepsilon}\left(1 + \phi_y^m \beta - \phi_z^m \alpha\right) + (1+\varepsilon)\left(\dot{\phi}_y^m \beta - \dot{\phi}_z^m \alpha \right) \end{aligned} \tag{2.78}$$

Considering the normalized strain measure $\boldsymbol{\phi}_n = \boldsymbol{\phi}(1+\varepsilon)$, Equation (2.78) can be written in normalized matrix form as:

$$\begin{bmatrix} \dot{\varepsilon} \\ \dot{\phi}_x^m \\ \dot{\phi}_y^m \\ \dot{\phi}_z^m \end{bmatrix}_n = \begin{bmatrix} 1 & 0 & 0 & 0 \\ \phi_x^m & (1+\varepsilon) & 0 & 0 \\ \phi_y^m & 0 & (1+\varepsilon) & 0 \\ \phi_z^m & 0 & 0 & (1+\varepsilon) \end{bmatrix} \begin{bmatrix} \dot{\varepsilon} \\ \dot{\phi}_x^m \\ \dot{\phi}_y^m \\ \dot{\phi}_z^m \end{bmatrix} \tag{2.79}$$

The constitutive relationship in rate form can be expressed:

$$\begin{gathered} \boldsymbol{\sigma} = \mathbf{E} \cdot \boldsymbol{\varepsilon} \\ \dot{\boldsymbol{\sigma}} = \mathbf{E} \cdot \dot{\boldsymbol{\varepsilon}} + \dot{\mathbf{E}} \cdot \boldsymbol{\varepsilon} = \mathbf{E}\left(\dot{\varepsilon}\left(1+\phi_y^m\beta - \phi_z^m\alpha\right) + (1+\varepsilon)\left(\dot{\phi}_y^m\beta - \dot{\phi}_z^m\alpha\right)\right) + \dot{\mathbf{E}} \cdot \boldsymbol{\varepsilon} \end{gathered} \tag{2.80}$$

From Equation (2.80) it is evident that the constitutive equation depends on the normalized strains rather than the actual strains. Integrating Equation (2.80) over the section area, the relationship between section forces and normalized strains is obtained:

$$\begin{bmatrix} \dot{\varepsilon} \\ \dot{\phi}_x^m \\ \dot{\phi}_y^m \\ \dot{\phi}_z^m \end{bmatrix}_n = \mathbf{f} \cdot \begin{bmatrix} \dot{P} \\ \dot{M}_x \\ \dot{M}_y \\ \dot{M}_z \end{bmatrix} \tag{2.81}$$

In Equation (2.81), **f** represents the flexibility matrix; P is the axial force oriented in the direction of $\mathbf{t}_1$; M_x, M_y and M_z are the moments at the section S in the directions $\mathbf{t}_1$, $\mathbf{t}_2$ and $\mathbf{t}_3$ respectively. Replacing Equation (2.81) in Equation (2.79):

$$\begin{bmatrix} \dot{\varepsilon} \\ \dot{\phi}_x^m \\ \dot{\phi}_y^m \\ \dot{\phi}_z^m \end{bmatrix} = \begin{bmatrix} 1 & 0 & 0 & 0 \\ \phi_x^m & (1+\varepsilon) & 0 & 0 \\ \phi_y^m & 0 & (1+\varepsilon) & 0 \\ \phi_z^m & 0 & 0 & (1+\varepsilon) \end{bmatrix}^{-1} \cdot \mathbf{f} \cdot \begin{bmatrix} \dot{P} \\ \dot{M}_x \\ \dot{M}_y \\ \dot{M}_z \end{bmatrix} = \begin{bmatrix} 1 & 0 & 0 & 0 \\ -\frac{\phi_x^m}{1+\varepsilon} & \frac{1}{1+\varepsilon} & 0 & 0 \\ -\frac{\phi_y^m}{1+\varepsilon} & 0 & \frac{1}{1+\varepsilon} & 0 \\ -\frac{\phi_z^m}{1+\varepsilon} & 0 & 0 & \frac{1}{1+\varepsilon} \end{bmatrix} \cdot \mathbf{f} \cdot \begin{bmatrix} \dot{P} \\ \dot{M}_x \\ \dot{M}_y \\ \dot{M}_z \end{bmatrix} \tag{2.82}$$

And introducing Equation (2.82) in Equation (2.75):

$$\begin{bmatrix} \dot{q}_1 \\ \dot{q}_2 \\ \dot{q}_3 \\ \dot{q}_4 \\ \dot{q}_5 \\ \dot{q}_6 \end{bmatrix} = \int_0^L \mathbf{B} \begin{bmatrix} 1 & 0 & 0 & 0 \\ -\dfrac{\phi_x^m}{1+\varepsilon} & \dfrac{1}{1+\varepsilon} & 0 & 0 \\ -\dfrac{\phi_y^m}{1+\varepsilon} & 0 & \dfrac{1}{1+\varepsilon} & 0 \\ -\dfrac{\phi_z^m}{1+\varepsilon} & 0 & 0 & \dfrac{1}{1+\varepsilon} \end{bmatrix} \cdot \mathbf{f} \cdot \begin{bmatrix} \dot{P} \\ \dot{M}_x \\ \dot{M}_y \\ \dot{M}_z \end{bmatrix} dx = \int_0^L \mathbf{B}^* \cdot \mathbf{f} \cdot \begin{bmatrix} \dot{P} \\ \dot{M}_x \\ \dot{M}_y \\ \dot{M}_z \end{bmatrix} dx \tag{2.83}$$

where matrix $\mathbf{B}^*$ reduces to:

$$\mathbf{B}^* = \begin{bmatrix} t_{11} & R_{31}\eta - R_{21}\chi & R_{32}\eta - R_{22}\chi & R_{33}\eta - R_{23}\chi \\ \dfrac{-R_{12}}{\xi_L} & \dfrac{-1}{\xi_L}\left(-R_{31}\xi + R_{11}\chi\right) - R_{31} & \dfrac{-1}{\xi_L}\left(-R_{32}\xi + R_{12}\chi\right) - R_{32} & \dfrac{-1}{\xi_L}\left(-R_{33}\xi + R_{13}\chi\right) - R_{33} \\ \dfrac{-R_{12}}{\xi_L} & \dfrac{-1}{\xi_L}\left(-R_{31}\xi + R_{11}\chi\right) & \dfrac{-1}{\xi_L}\left(-R_{32}\xi + R_{12}\chi\right) & \dfrac{-1}{\xi_L}\left(-R_{33}\xi + R_{13}\chi\right) \\ \dfrac{R_{13}}{\xi_L} & \dfrac{1}{\xi_L}\left(R_{21}\xi - R_{11}\eta\right) - R_{21} & \dfrac{1}{\xi_L}\left(R_{22}\xi - R_{12}\eta\right) - R_{22} & \dfrac{1}{\xi_L}\left(R_{23}\xi - R_{13}\eta\right) - R_{23} \\ \dfrac{R_{13}}{\xi_L} & \dfrac{1}{\xi_L}\left(R_{21}\xi - R_{11}\eta\right) & \dfrac{1}{\xi_L}\left(R_{22}\xi - R_{12}\eta\right) & \dfrac{1}{\xi_L}\left(R_{23}\xi - R_{13}\eta\right) \\ 0 & R_{11} & R_{12} & R_{13} \end{bmatrix} \tag{2.84}$$

and Equation (2.75) becomes:

$$\begin{bmatrix} \dot{q}_1 \\ \dot{q}_2 \\ \dot{q}_3 \\ \dot{q}_4 \\ \dot{q}_5 \end{bmatrix} = \int_0^L \mathbf{B}^* \begin{bmatrix} \dot{\varepsilon} \\ \dot{\phi}^m \end{bmatrix}_n dx \tag{2.85}$$

Equation (2.85) is the compatibility equation for an element with large deformations. Physically, it means that the nodal deformations can be calculated from the integration of strains and curvatures along the element, with some weight factor. This weight factor is matrix $\mathbf{B}^*$.

2.6.7 Relationship between matrix $\mathbf{B}^*$ and forces

Considering the assumptions listed in 2.6.3 for load distribution, the forces at any section S can be written, in Corotated coordinates, as a function of nodal forces as (See Figure 2–9 a):

$$
\begin{aligned}
&M_y^E(x)=Q_4\left(\frac{\xi}{\xi_L}-1\right)+Q_5\left(\frac{\xi}{\xi_L}\right)+Q_1(E_1\times x)E_2=(Q_4+Q_5)\frac{\xi}{\xi_L}-Q_4-\chi Q_1\\
&M_z^E(x)=Q_2\left(\frac{\xi}{\xi_L}-1\right)+Q_3\left(\frac{\xi}{\xi_L}\right)+Q_1(E_1\times x)E_3=(Q_2+Q_3)\frac{\xi}{\xi_L}-Q_2+\eta Q_1\\
&M_x{}^E(x)=Q_6-V_y\chi-V_z\eta=Q_6-V_y\chi-V_z\eta\\
&P^E(x)=Q_1
\end{aligned}
\tag{2.86}
$$

Equation (2.86) must be transformed into local deformed coordinates $\mathbf{t}(x)$ (See Figure 2–9 b). This transformation is done through matrix $\mathbf{R}^t(x)$ (see APPENDIX A, section A.5):

$$
M_x(x)=Q_1R_{11}-\frac{Q_2+Q_3}{\xi_L}R_{12}+\frac{Q_4+Q_5}{\xi_L}R_{13} \tag{2.87}
$$

$$
\begin{aligned}
M_y(x)=&\left(Q_6-\frac{Q_2+Q_3}{\xi_L}\chi-\frac{Q_4+Q_5}{\xi_L}\eta\right)R_{12}+\\
&\left((Q_4+Q_5)\frac{\xi}{\xi_L}-Q_4-\chi Q_1\right)R_{22}+\left((Q_2+Q_3)\frac{\xi}{\xi_L}-Q_2+\eta Q_1\right)R_{32}
\end{aligned}
\tag{2.88}
$$

$$
\begin{aligned}
M_z(x)=&\left(Q_6-\frac{Q_2+Q_3}{\xi_L}\chi-\frac{Q_4+Q_5}{\xi_L}\eta\right)R_{13}+\\
&\left((Q_4+Q_5)\frac{\xi}{\xi_L}-Q_4-\chi Q_1\right)R_{23}+\left((Q_2+Q_3)\frac{\xi}{\xi_L}-Q_2+\eta Q_1\right)R_{33}
\end{aligned}
\tag{2.89}
$$

$$
P(x)=Q_1R_{11}-\frac{Q_2+Q_3}{\xi_L}R_{12}+\frac{Q_4+Q_5}{\xi_L}R_{13} \tag{2.90}
$$

The above equations can be written in matrix form:

$$
\begin{bmatrix} P \\ M_x \\ M_y \\ M_z \end{bmatrix}(x)=\mathbf{B}^{*t}\begin{bmatrix} Q_1 \\ Q_2 \\ Q_3 \\ Q_4 \\ Q_5 \\ Q_6 \end{bmatrix} \quad (2.91)
$$

Therefore, the reciprocal of matrix $\mathbf{B}^*$ is the interpolation matrix for the section forces.

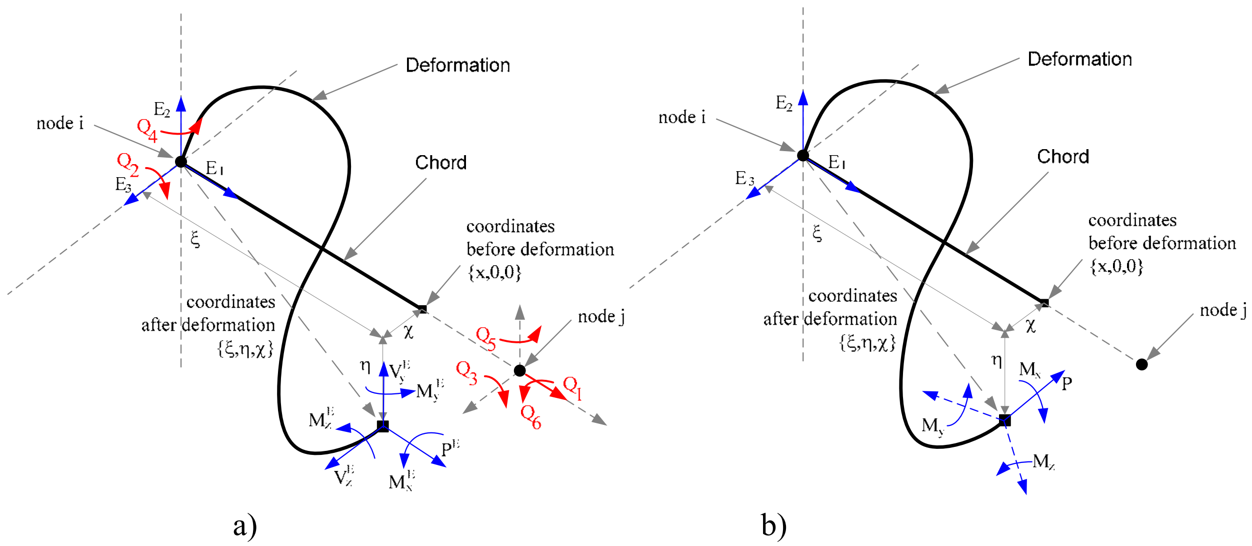

Figure 2–9: Diagrams to calculate the interpolation of forces in Local deformed coordinates. Left: interpolation of forces in Corotated coordinates, Right: transformation to Local deformed coordinates.

2.6.8 Compatibility equations as functions of state space variables

Finally, the compatibility equations can be written in terms of matrix $\mathbf{B}^*$ and the variables of the DAE system:

$$\dot{\mathbf{q}} = \int_0^L \mathbf{B}^* \begin{bmatrix} \dot{\varepsilon} \\ \dot{\phi}^m \end{bmatrix}_n \mathrm{dx} = \int_0^L \mathbf{B}^* \mathbf{f}(\mathrm{x}) \dot{\mathbf{P}}(\mathrm{x}) \mathrm{dx} \tag{2.92}$$

$$\dot{\mathbf{q}} = \int_0^L \mathbf{B}^* \mathbf{f}(\mathrm{x}) \left(\dot{\mathbf{B}}^{*t} \mathbf{Q} + \mathbf{B}^{*t} \dot{\mathbf{Q}} \right) \mathrm{dx} = \int_0^L \left(\mathbf{B}^* \mathbf{f}(\mathrm{x}) \dot{\mathbf{B}}^{*t} \right) \mathbf{Q} \mathrm{dx} + \int_0^L \left(\mathbf{B}^* \mathbf{f}(\mathrm{x}) \mathbf{B}^{*t} \right) \dot{\mathbf{Q}} \mathrm{dx} \tag{2.93}$$

Transforming the displacements to global coordinates:

$$\mathbf{T}\dot{\mathbf{u}} = \int_0^L \left(\mathbf{B}^* \mathbf{f}(\mathrm{x}) \dot{\mathbf{B}}^{*t} \right) \mathbf{Q} \mathrm{dx} + \int_0^L \left(\mathbf{B}^* \mathbf{f}(\mathrm{x}) \mathbf{B}^{*t} \right) \dot{\mathbf{Q}} \mathrm{dx} \tag{2.94}$$

2.6.9 Plasticity Equations.

Equation (2.81) represents the evolution equation of section S. These equations can be written in terms of the variables of the DAE system:

$$\begin{bmatrix} \dot{\varepsilon} \\ \dot{\phi}^m \end{bmatrix}_n = f(x)\dot{\mathbf{P}}(x) = f(x)\left(\mathbf{B}^{*t}\dot{\mathbf{Q}} + \dot{\mathbf{B}}^{*t}\mathbf{Q}\right)$$

$$\begin{bmatrix} \dot{\varepsilon} \\ \dot{\phi}^m \end{bmatrix} = \begin{bmatrix} 1 & 0 & 0 & 0 \\ \phi_x^m & (1+\varepsilon) & 0 & 0 \\ \phi_y^m & 0 & (1+\varepsilon) & 0 \\ \phi_z^m & 0 & 0 & (1+\varepsilon) \end{bmatrix}^{-1} \cdot f(x)\cdot\left(\mathbf{B}^{*t}\dot{\mathbf{Q}} + \dot{\mathbf{B}}^{*t}\mathbf{Q}\right) \tag{2.95}$$

2.7 Summary of the formulation

In Section 2.6, a formulation for solving inelastic systems with large displacements in the state space was presented. In summary, the formulation works with a set of variables (Global and Local); Equation (2.46):

$$\mathbf{y} = \{\mathbf{u} \quad \dot{\mathbf{u}} \quad \mathbf{Q} \quad \boldsymbol{\varepsilon}\}^t \qquad \dot{\mathbf{y}} = \{\dot{\mathbf{u}} \quad \ddot{\mathbf{u}} \quad \dot{\mathbf{Q}} \quad \dot{\boldsymbol{\varepsilon}}\}^t \tag{2.96}$$

which must satisfy the basic equations of structures. Equilibrium equations (2.61):

$$\text{Equilibrium} = \sum_{i=1}^{\#\text{nodes}} \mathbf{N_i} \cdot \mathbf{T}_i^t \cdot \mathbf{Q}_i - \mathbf{P_{ext}} \tag{2.97}$$

Compatibility equations (2.94) (one per element):

$$\text{Compatibility} = \mathbf{T}\dot{\mathbf{u}} - \int_0^L \left(\mathbf{B}^*\mathbf{f}(x)\dot{\mathbf{B}}^{*t}\right)\mathbf{Q}dx + \int_0^L \left(\mathbf{B}^*\mathbf{f}(x)\mathbf{B}^{*t}\right)\dot{\mathbf{Q}}\cdot dx \tag{2.98}$$

Plasticity equations (2.95) (one per sections S):

$$\text{Plasticity} = \begin{bmatrix} \dot{\varepsilon} \\ \dot{\phi}^m \end{bmatrix}_n - \begin{bmatrix} 1 & 0 & 0 & 0 \\ \phi_y^m & (1+\varepsilon) & 0 & 0 \\ \phi_y^m & 0 & (1+\varepsilon) & 0 \\ \phi_y^m & 0 & 0 & (1+\varepsilon) \end{bmatrix}^{-1} \cdot f(x)\cdot\left(\mathbf{B}^{*t}\dot{\mathbf{Q}} + \dot{\mathbf{B}}^{*t}\mathbf{Q}\right) \tag{2.99}$$

Equations (2.98) and (2.99) are always in rate form. Equations (2.97) are algebraic in a static analysis (for dynamic analysis, the inertia and damping terms have to be included in Equation (2.97)). Therefore, the problem to be solved is a system of Differential Algebraic Equations (DAE). The mathematical solution of this type of systems is described in Chapter 3.

Equation (2.98) is written in integral form, therefore it has to be discretized before a numerical analysis can be performed. A numerical integration with a Gauss-Lobatto scheme is adopted because it makes use of the values at the nodes, which are known state variables. Thus, a number of points, "Integration Points" are defined along the length of the member. At these Integration Points the total strains are known at each time step (because they are local state variables) and the plasticity equations are evaluated. Thus, matrix **B*** and its rate are evaluated at each Integration Point and therefore the following variables need to be interpolated along the length of the element: coordinates and coordinate rates; rotations and rotation rates (or spins). These values are only known at the nodes. Details of the implemented interpolation scheme are presented in Chapter 3.

Once all the variables are known, the equations are evaluated and the residuals are compared to the pre-defined error tolerance. If the residuals are smaller than the tolerance, the values for the step are accepted and a new step is attempted. When the errors are large, the step size is reduced and the step is recalculated.

SECTION 3
NUMERICAL IMPLEMENTATION OF THE FORMULATION

3.1 Introduction.

The formulation developed in Chapter 2 results in a set of Differential Algebraic Equations (DAE). The unknown variables the system is solved for are: displacements and velocities at the nodes, local Corotated forces of all elements and strains and curvatures along the length of each element. The set of equations are: global equilibrium at all nodes, compatibility conditions at each element and plasticity equations along the length of the member. From this set of equations, in a dynamic analysis, only the equilibrium equations for all DOFs with no associated mass are algebraic or, in a static analysis, all the equilibrium equations are algebraic. The compatibility and plasticity equations are always differential. This set of equations can be solved with a DAE solver. Based on recent research on DAE solutions (Brenan et al. 1989), researchers at the Lawrence Livermore National Laboratory (LLNL) have developed a mathematical software called "Implicit Differential Algebraic" (IDA) capable of solving such systems (Hindmarsh and Serban 2006). The present chapter summarizes the procedure implemented in IDA.

This Chapter also includes a step by step summary of the numerical implementation of the procedure presented in Chapter 2 along with the assumption, approximations and interpolation functions used.

3.2 Solution of DAE equations

As explained in Chapter 2, the equations of equilibrium, compatibility and plasticity form a DAE system. In general such system can be written as:

$$\mathbf{f}\left(t, \mathbf{y}, \dot{\mathbf{y}}\right) = 0 \tag{3.1}$$

where $\mathbf{f}(\cdot)$ represents a function where the set of equations are evaluated, t is an independent variable (time), $\mathbf{y}$ is the vector of variables. In a DAE system, the rates of the variables are also variables in the system and thus their values are known at every time step.

In order to solve this problem, a set of initial conditions must be known:

$$\begin{aligned} \mathbf{y}\left(t_0\right) &= \mathbf{y}_0 \\ \dot{\mathbf{y}}\left(t_0\right) &= \dot{\mathbf{y}}_0 \end{aligned} \tag{3.2}$$

where t_0 is the initial time and y_0 is the vector of the variables evaluated at time t_0. This set must be consistent i.e. it has to satisfy Equation (3.1):

$$\mathbf{f}\left(t_0,\mathbf{y}_0,\dot{\mathbf{y}}_0\right)=\mathbf{0} \tag{3.3}$$

The system in Equation (3.1) is coupled and singular due to the algebraic components. A measure of the singularity of the problem is the index, which counts the number of times the system must be differentiated with respect to t in order to determine the rate of **y** explicitly as a function of **y** and t. In other words, to obtain a set of Ordinary Differential Equations (ODE) of the form:

$$\dot{\mathbf{y}}=g\left(t,\mathbf{y}\right) \tag{3.4}$$

Algorithms exist to solve systems like Equation (3.1) of index 1, however problems of higher index don't have a simple numerical solution yet. In a structural problem, the equations of static equilibrium are algebraic:

$$k\cdot u=P \tag{3.5}$$

Writing Equation (3.5) in the state space with $y_1 = u$ and $y_2 = Q$:

$$\begin{aligned} y_2 &= P \\ k\cdot\dot{y}_1 &= \dot{y}_2 \end{aligned} \tag{3.6}$$

The algebraic equation in the set of Equations (3.6) needs to be differentiated only once to become an explicit ODE:

$$\begin{aligned} \dot{y}_2 &= \dot{P} \\ k\cdot\dot{y}_1 &= \dot{y}_2 \end{aligned} \tag{3.7}$$

Therefore, the structural problem is a DAE of order 1.

As in any numerical analysis, the values for the variables are approximated:

$$\begin{aligned} \mathbf{y}_n &\approx \mathbf{y}\left(t_n\right) \\ \dot{\mathbf{y}}_n &\approx \dot{\mathbf{y}}\left(t_n\right) \end{aligned} \tag{3.8}$$

where $\mathbf{y}_n$ is the approximated value for the exact evaluation $\mathbf{y}(t_n)$. DAEs of index 1 are solved using the Backward Differentiation Formula (BDF), where the rate of **y** is calculated in terms of the values for the variable **y** at t_n and at previous times:

$$h_n\cdot\dot{\mathbf{y}}_n=\sum_{i=0}^{k}\alpha_{n,i}\cdot\mathbf{y}_{n-i} \tag{3.9}$$

where h_n is the time step, $\alpha_{n,i}$ are coefficients of the method and k is the order of the method. Then, replacing Equation (3.9) into Equation (3.1):

$$\mathbf{f}\left(\mathbf{y}_n\right) = \left(t_n, \mathbf{y}_n, \frac{1}{h_n}\sum_{i=0}^{k}\alpha_{n,i}\cdot\mathbf{y}_{n-i} \right) \neq \mathbf{0} \tag{3.10}$$

Equation (3.10) is, in general, not identically zero because the variables $\mathbf{y}_n$ are approximations. Therefore, iterations are needed and the Newton method is used. A Jacobian matrix (**J**) is formed and a new approximation of $\mathbf{y}(t_n)$ is found based on the errors of the previous approximation. The objective is to find $\mathbf{y}_n$ such that $\mathbf{f}(\mathbf{y}_n)\cong\mathbf{0}$ within a tolerance:

$$\mathbf{J}\cdot\left[\mathbf{y}_{n(m+1)} - \mathbf{y}_{n(m)}\right] = -\mathbf{f}\left(\mathbf{y}_{n(m)}\right) \tag{3.11}$$

where $\mathbf{y}_{n(m)}$ represents the m^{th} iteration of the set of variables **y** at time t_n and **J** is the jacobian matrix. Analytically **J** is calculated as:

$$\mathbf{J} = \frac{\partial \mathbf{f}}{\partial \mathbf{y}} + \alpha\frac{\partial \mathbf{f}}{\partial \dot{\mathbf{y}}} \qquad \alpha = \frac{\alpha_{n,0}}{h_n} \tag{3.12}$$

The Jacobian depends both on the variables and their rates and the parameter α is an accelerator of the Newton method that allows the update of the Jacobian without having to calculate it explicitly.

Numerically, the i^{th} column of the Jacobian is obtained as the difference between the values of the function **f** evaluated with a small increment in the variable i and its original value:

$$\begin{gathered} J_i = \frac{\mathbf{f}\left(t_h, \mathbf{y}+\delta\mathbf{y}_i, \dot{\mathbf{y}}+\delta\dot{\mathbf{y}}_i\right) - \mathbf{f}\left(t_h, \mathbf{y}, \dot{\mathbf{y}}\right)}{\Delta} \\ \left(\delta\mathbf{y}_i\right)_j = \begin{cases} \Delta & i = j \\ 0 & i \neq j \end{cases} \qquad \left(\delta\dot{\mathbf{y}}_i\right)_j = \begin{cases} \alpha\Delta/h_n & i = j \\ 0 & i \neq j \end{cases} \end{gathered} \tag{3.13}$$

where Δ is the calculated increment, t_h is the actual time when the iteration is taking place and h_n is the actual step size. Once the Jacobian matrix is calculated, Equation (3.11) is solved as a linear system and the value of $\mathbf{y}_{n(m+1)}$ is:

$$\mathbf{y}_{n(m+1)} = -\mathbf{J}^{-1}\cdot\mathbf{f}\left(\mathbf{y}_{n(m)}\right) + \mathbf{y}_{n(m)} \tag{3.14}$$

The program IDA from the LLNL implements the procedure described in Equations (3.1) - (3.14). The program is compiled into a library compatible with the languages C and FORTRAN. Some features of the program are:

8. It is able to adapt the order of the method as needed, depending of convergence.

9. It calculates the Jacobian matrix if not provided and automatically calculates the necessary increment Δ based on the actual step size, the actual value of the variable and the tolerance of the variable.
10. The actual step size is increased or decreased depending on convergence. The user can define a maximum step size to ensure the accuracy of the integration.

The tolerances of the variables (allowable errors) are defined as follows:

$$\mathrm{ewt}_i = \frac{1}{\mathrm{rtol} \cdot |y_i| + \mathrm{atol}_i} \tag{3.15}$$

where, rtol is a relative tolerance valid for all variables and atol is an absolute tolerance specified for each variable y_i. It is recommended to define different absolute tolerances depending on the nature of the variable. It is also possible to implement a different error definition.

Along with the function **f**, initial conditions specific to each problem must be provided, i.e. the values of each variable and its rate for a given time. The values of the variables can be, for example, the static solution of the structure under a simple loading. It is difficult, however, to calculate the values for the rates. IDA has an internal function that modifies a given set of initial conditions to render them consistent. Thus, the rates of the variables can be initialized with a zero value and the solver will calculate their consistent values.

3.3 Numerical Integration of the formulation

In Chapter 2, the three key equations: Equilibrium (2.93), Compatibility (2.94) and Plasticity (2.95) that constitute the basis of the formulation have been derived assuming that the member is continuous. In this section, the required steps to calculate the residual vector **f** are outlined along with the implemented discretization and integration methods.

Step #1. Update of node coordinates.

Knowing the original coordinates ($\mathbf{p}_0$) and their movement at step n+1 ($\mathbf{u}_{n+1}$), the updated coordinates can be obtained:

$$\mathbf{p}_{n+1} = \mathbf{p}_0 + \mathbf{u}_{n+1} \tag{3.16}$$

Due to the nature of the Newton method (Equation (3.11)), the incremental rotation vector (see section 2.2.6) is the only possible rotation parametrization because the rotation and the increment must belong to the same tangent space so they can be added like true vectors. This method is easy to implement in a formulation where displacements and forces are calculated in respect to the last converged configuration. However, the formulation presented in Chapter 2 has a constant global reference thus, the update of rotations is cumbersome.

To update the rotations, the value of the increment is needed, however after every time step, IDA returns the values of the variable $\mathbf{y}_{n+1}$ and not the increment $\mathbf{y}_{n+1}$-$\mathbf{y}_n$; therefore the value of the rotation at the last converged iteration must be stored. Then, the increment can be retrieved:

$$\delta\theta^1 = \bar{\theta}_{n+1} - \bar{\theta}_n \tag{3.17}$$

where $\delta\boldsymbol{\theta}^1$ is the incremental rotation vector, $\bar{\theta}_n$ is the value of the rotation saved from last iteration and $\bar{\theta}_{n+1}$ is the value for the rotation at the actual iteration. $\bar{\theta}_{n+1}$ and $\bar{\theta}_n$ are the results of the Newton iteration, but do not correspond with the definition of axial vector employed in the derivation of the formulation of Chapter 2. The increment $\delta\boldsymbol{\theta}^1$ has to be converted to the rotational vector parametrization $\delta\boldsymbol{\theta}^R$ using Equation (2.18):

$$\begin{gathered}\delta\boldsymbol{\theta}^R = T\left(\bar{\theta}_n\right)\cdot\delta\theta^1 \\ T\left(\bar{\theta}_n\right) = \frac{\sin\left(\bar{\theta}_n\right)}{\bar{\theta}_n} I + \left(1 - \frac{\sin\left(\bar{\theta}_n\right)}{\bar{\theta}_n}\right)\cdot\hat{\bar{\theta}}_n\cdot\hat{\bar{\theta}}_n^t + \frac{1}{2}\left(\frac{\sin\left(\bar{\theta}_n/2\right)}{\bar{\theta}_n/2}\right)^2\boldsymbol{\Omega}_n\end{gathered} \tag{3.18}$$

where $\boldsymbol{\Omega}_n$ is the skew –symmetric matrix whose components are the cartesian components of the axial vector $\bar{\theta}_n$

Finally, the exponential map of the skew-symmetric matrix $\boldsymbol{\Omega}(\delta\boldsymbol{\theta}^R)$ (whose components are the cartesian components of the axial vector $\delta\boldsymbol{\theta}^R$) is calculated and the result composed with the rotation matrix of the previous step $\mathbf{R}_n$ to obtain the rotation matrix at the actual step $\mathbf{R}_{n+1}$:

$$\mathbf{R}_{n+1} = \exp(\boldsymbol{\Omega}\left(\delta\boldsymbol{\theta}^R\right))\cdot\mathbf{R}_n \tag{3.19}$$

The actual axial vector $\boldsymbol{\theta}_{n+1}$ is extracted from $\mathbf{R}_{n+1}$ using the quaternion procedure (section 2.2.3).

It is important to note that curvatures are infinitesimal incremental rotations pertaining to a linear vector space, therefore the update procedure is through a normal vectorial sum and no modifications are needed.

*Step #2. Calculation of matrices **E** and **T** for each element at step n+1.*

Matrix **E** defines the rigid body movement of an element and is necessary for the calculation of equilibrium and compatibility. Matrix **T** transforms Global DOFs into Corotated DOFs and is used to calculate equilibrium (*step 3*).

Using Equations (2.51) and (2.52):

$$\begin{aligned}&\mathbf{E}_{n+1}=\left(\mathbf{R}_{\mathbf{L\text{-}E}}\right)_{n+1}\cdot\mathbf{L}\\&\left(\mathbf{R}_{\mathbf{L\text{-}E}}\right)_{n+1}=\mathbf{I}+\mathbf{\Omega}\left(\mathbf{L}_1\times\left(\mathbf{E}_1\right)_{n+1}\right)+\frac{1}{1+\mathbf{L}_1^t\cdot\left(\mathbf{E}_1\right)_{n+1}}\mathbf{\Omega}\left(\mathbf{L}_1\times\left(\mathbf{E}_1\right)_{n+1}\right)\cdot\mathbf{\Omega}\left(\mathbf{L}_1\times\left(\mathbf{E}_1\right)_{n+1}\right)\end{aligned}\tag{3.20}$$

Matrix **L** is the rotation matrix that transforms Global coordinates into Local coordinates and is calculated using the same procedure (Equation (3.20)), replacing **L** by **G** and **E** by **L**. Recalling that matrix **G** is arbitrarily assumed to be the identity matrix $\mathbf{I}_3$:

$$\begin{aligned}&\mathbf{L}=\mathbf{L}\cdot\mathbf{G}\\&\mathbf{L}=\mathbf{I}+\mathbf{\Omega}\left(\mathbf{G}_1\times\mathbf{L}_1\right)+\frac{1}{1+\mathbf{G}_1^t\cdot\mathbf{L}_1}\mathbf{\Omega}\left(\mathbf{G}_1\times\mathbf{L}_1\right)\cdot\mathbf{\Omega}\left(\mathbf{G}_1\times\mathbf{L}_1\right)\end{aligned}\tag{3.21}$$

Matrix **L** is constant throughout the analysis, thus this operation just needs to be performed once, at the beginning of the calculations.

Matrix T_{n+1} is calculated as follows:

$$\mathbf{T}_{n+1}=\left(\mathbf{T}_{EC}\right)_{n+1}\left(\mathbf{T}_{CG}\right)_{n+1}\tag{3.22}$$

$$\left(\mathbf{T}_{EC}\right)_{n+1}=\begin{bmatrix}-1&0&0&0&0&0&1&0&0&0&0&0\\0&1/\left(\xi_L\right)_{n+1}&0&0&0&1&0&-1/\left(\xi_L\right)_{n+1}&0&0&0&0\\0&1/\left(\xi_L\right)_{n+1}&0&0&0&0&0&-1/\left(\xi_L\right)_{n+1}&0&0&0&1\\0&0&-1/\left(\xi_L\right)_{n+1}&0&1&0&0&0&1/\left(\xi_L\right)_{n+1}&0&0&0\\0&0&-1/\left(\xi_L\right)_{n+1}&0&0&0&0&0&1/\left(\xi_L\right)_{n+1}&0&1&0\\0&0&0&-1&0&0&0&0&0&1&0&0\end{bmatrix}\tag{3.23}$$

$$\left(\xi_L\right)_{n+1}=\left(\sqrt{\left(p_{ix}-p_{jx}\right)^2+\left(p_{iy}-p_{jy}\right)^2+\left(p_{iz}-p_{jz}\right)^2}\right)_{n+1}$$

$$\left(\mathbf{T}_{CG}\right)_{n+1}=\begin{bmatrix}\mathbf{E}_{n+1} & \mathbf{0} & \mathbf{0} & \mathbf{0}\\ \mathbf{0} & \mathbf{E}_{n+1} & \mathbf{0} & \mathbf{0}\\ \mathbf{0} & \mathbf{0} & \mathbf{E}_{n+1} & \mathbf{0}\\ \mathbf{0} & \mathbf{0} & \mathbf{0} & \mathbf{E}_{n+1}\end{bmatrix} \tag{3.24}$$

In Equations (3.23) $(\xi_L)_{n+1}$ is the actual length of the element, calculated as the norm of the vectorial difference between the actual positions of its end nodes $\mathbf{p}_i$ and $\mathbf{p}_j$.

Step #3. Calculate Equilibrium.

Using Equation (2.58), the forces in global coordinates are found:

$$\mathbf{F}_{n+1}=\mathbf{T}_{n+1}^{t}\cdot\mathbf{Q}_{n+1} \tag{3.25}$$

In Equation (3.25), the local Corotated forces $\mathbf{Q}_{n+1}$ of each element (extracted from the known vector $\mathbf{y}_{n+1}$) are transformed into Global Coordinates with the correspondent matrix $\mathbf{T}_{n+1}$ (calculated in *Step #2*).

Using Equation (2.59):

$$\text{Equilibrium}_{n+1}=\sum_{i=1}^{\#\text{elements}}\mathbf{N}_{\mathbf{i}}\cdot\left(\mathbf{F}_{\mathbf{i}}\right)_{n+1}-\left(\mathbf{P}_{\mathbf{ext}}\right)_{n+1} \tag{3.26}$$

Step #4. Calculation of deformational rotation matrices at nodes.

In the formulation, the rigid body motion is calculated with matrix **E** (*step #2*). To calculate the compatibility equations, the deformational part of the total rotation is needed because the equations were deduced with respect to the Corotated system of coordinates.

The directions of the rotational DOFs coincide with the Global reference frame. However, rotations are measured with respect to the initial configuration. Therefore, the updated rotations obtained in *Step 1* will be rigidly rotated into Local coordinates:

$$\boldsymbol{\theta}_{n+1}^{L}=\mathbf{L}\cdot\boldsymbol{\theta}_{n+1} \tag{3.27}$$

where $\boldsymbol{\theta}_{n+1}{}^{L}$ is the axial vector of the total rotations at any node with respect to the Local coordinate system and matrix **L** was calculated in *Step #2*. Then, the correspondent rotation matrix $\mathbf{R}(\boldsymbol{\theta}_{n+1}{}^{L})$ is found using the quaternion procedure (section 2.2.3). Finally, the deformational part of the rotations is obtained using compound rotations:

$$\left(\mathbf{R}_d\right)_{n+1}=\mathbf{R}\left(\boldsymbol{\theta}_{n+1}^{L}\right)\cdot\mathbf{L}\cdot\mathbf{E}_{n+1}^{t} \tag{3.28}$$

where the product (**R L**) represents the total rotations in Global coordinates. The product (**$\mathbf{R_d}$ E**) also represents the total rotations in Global coordinates, but in this case, the rigid body motion is completely represented by **E**, thus $\mathbf{R_d}$ contains only the deformational part of the rotations. Equation (3.28) is written in spatial form so that $\mathbf{R_d}$ is described with respect to the **E** system of coordinates.

Step #5. Calculate the rotational vector associated with the deformational rotation matrix.

The rotational vectors will be needed to interpolate the deformational rotations along the length of the element.

Using the quaternion procedure (section 2.2.3), the quaternion $\mathbf{q}_d$ that corresponds to each deformational rotation matrix found in *Step #4* is found:

$$\begin{aligned} &(q_d)_0 = \pm\tfrac{1}{2}\sqrt{1+\mathrm{Tr}(\mathbf{R}_d)} \quad ; \quad (q_d)_1 = \pm\tfrac{1}{4}\frac{\left((R_d)_{32}-(R_d)_{23}\right)}{q_o} \\ &(q_d)_2 = \pm\tfrac{1}{4}\frac{\left((R_d)_{13}-(R_d)_{31}\right)}{q_o} \quad ; \quad (q_d)_3 = \pm\tfrac{1}{4}\frac{\left((R_d)_{21}-(R_d)_{12}\right)}{q_o} \end{aligned} \tag{3.29}$$

Using the inverse of Equation (2.8), the axial vector $\boldsymbol{\theta}_d$ is found:

$$\begin{aligned} &\theta_d = 2\times\cos^{-1}(q_0) \\ &\boldsymbol{\theta}_d = \frac{\theta_d}{\sin\left(\theta_d/2\right)}\{q_1 \quad q_2 \quad q_3\}^t \end{aligned} \tag{3.30}$$

To evaluate the compatibility equations, a discretization procedure is needed to perform a numerical integration. Thus, a number of “Integration Points” (IP) are selected along the length of the member according to the Gauss-Lobatto rule (given the number of IPs, it provides the position and weight of each IP). Matrix **B*** (Equation (2.82)) and its rate (derived below) are needed for the calculation of compatibility and plasticity equations. Matrix **B*** depends on:

- The actual deformed position in respect to the Corotated coordinates at each IP.
- The actual deformational rotation matrix at each IP.

The rate of matrix **B*** depends on the above quantities plus:

- The rates of the positions at each IP.
- The rates of the deformational rotation matrices (or spins) at each IP.

Thus, an interpolation scheme must be implemented for the above 4 quantities. Step 6 to Step 12 detail the procedure to evaluate both matrix **B*** and its rate.

Step #6. Interpolate the nodal deformational rotations to obtain rotations at the integration points.

The undeformed coordinates of the IPs are constant and determined by the number of points considered in the interpolation. With respect to the **E** coordinate system, located at one of the nodes, the original coordinates of each integration point (IP) can be described as:

$$\mathbf{x}_{ip} = \left\{ x_{ip} \quad 0 \quad 0 \right\}^t \tag{3.31}$$

The rotational vectors at the nodes $(\boldsymbol{\theta}_d)_i$ and $(\boldsymbol{\theta}_d)_j$ have been obtained in *Step #5*. To calculate the values of the rotational vectors along the length of the member, a simplified procedure is adopted. The interpolation is done independently for each coordinate (r) and the curvatures are assumed to be constant between two consecutive IPs:

$$\begin{aligned}
&\frac{d\theta_r}{ds} = \phi_r^m(s) \\
&\frac{d\theta_r}{dx} = \frac{d\theta_r}{ds} \cdot \frac{ds}{dx} = \phi_r(s) \cdot \frac{ds}{dx} = \phi_r^m(s)(1+\varepsilon) \\
&\theta_r(x_i) = \int_{x=0}^{x=x_i} \phi_r^m(s) \cdot (1+\varepsilon) \cdot dx \approx \theta_r(x_{ip-1}) + (x_{ip} - x_{ip-1}) \cdot \phi_r^m(x_{ip})\left(1+\varepsilon(x_{ip})\right)
\end{aligned} \tag{3.32}$$

Because the deformational axial vectors are known at both nodes, two integrations are performed: the first starts at node i and the second starts at node j. The final value adopted is the average of both integration procedures:

$$\begin{aligned}
&\theta_{dx}^1(x_{ip}) = \theta_{dx}^1(x_{i-1}) + (x_{ip} - x_{ip-1})\phi_{dx}^m(x_{ip})\left(1+\varepsilon(x_{ip})\right) \\
&\theta_{dx}^2(x_{ip}) = \theta_{dx}^2(x_{i+1}) + (x_{ip} - x_{ip+1})\phi_{dx}^m(x_{ip})\left(1+\varepsilon(x_{ip})\right) \\
&\theta_{dx}(x_{ip}) = \frac{\theta_{dx}^1(x_{ip}) + \theta_{dx}^2(x_{ip})}{2}
\end{aligned} \tag{3.33}$$

$$\begin{aligned}
&\theta_{dy}^1(x_{ip}) = \theta_{dy}^1(x_{i-1}) + (x_{ip} - x_{ip-1})\phi_{dy}^m(x_{ip})\left(1+\varepsilon(x_{ip})\right) \\
&\theta_{dy}^2(x_{ip}) = \theta_{dy}^2(x_{i+1}) + (x_{ip} - x_{ip+1})\phi_{dy}^m(x_{ip})\left(1+\varepsilon(x_{ip})\right) \\
&\theta_{dy}(x_{ip}) = \frac{\theta_{dy}^1(x_{ip}) + \theta_{dy}^2(x_{ip})}{2}
\end{aligned} \tag{3.34}$$

$$\begin{aligned}
&\theta_{dz}^{1}\left(x_{ip}\right)=\theta_{dz}^{1}\left(x_{i-1}\right)+\left(x_{ip}-x_{ip-1}\right)\phi_{dz}^{m}\left(x_{ip}\right)\left(1+\varepsilon\left(x_{ip}\right)\right)\\
&\theta_{dz}^{2}\left(x_{ip}\right)=\theta_{dz}^{2}\left(x_{i+1}\right)+\left(x_{ip}-x_{ip+1}\right)\phi_{dz}^{m}\left(x_{ip}\right)\left(1+\varepsilon\left(x_{ip}\right)\right)\\
&\theta_{dz}\left(x_{ip}\right)=\frac{\theta_{dz}^{1}\left(x_{ip}\right)+\theta_{dz}^{2}\left(x_{ip}\right)}{2}
\end{aligned}\tag{3.35}$$

In Equation (3.33), $\boldsymbol{\phi}^{m}(x_{ip})=\{\phi_x^{m}(x_{ip})\ \ \phi_y^{m}(x_{ip})\ \ \phi_z^{m}(x_{ip})\}^t$ is the axial vector of material curvatures at the IP x_{ip}. These values are known quantities because they are the local state variables of the system and can be extracted from the complete vector of variables $\mathbf{y}_n$ at each step.

Having found the rotational vectors at each IP, the rotation matrices $\mathbf{R}_d(x_{ip})$ are obtained, for each IP, with the quaternion procedure.

Step #7. Calculate the deformed coordinates of the Integration Points.

Upon deformation, the coordinates of the IPs are:

$$\mathbf{x}_{ip}^{new}=\left\{\xi_{ip}\quad \eta_{ip}\quad \chi_{ip}\right\}^{t}\tag{3.36}$$

The chord of the element links the deformed positions of its 2 end nodes. Therefore the nodal coordinates are:

$$\begin{aligned}
&\mathbf{x}_{i}=\left\{0\quad 0\quad 0\right\}^{t}\\
&\mathbf{x}_{j}=\left\{\xi_{L}\quad 0\quad 0\right\}^{t}
\end{aligned}\tag{3.37}$$

where ξ_L is the actual length of the chord obtained in *Step #2*. The coordinates of the IPs are interpolated using Equation (2.62):

$$\begin{aligned}
&\xi^{1}\left(x_{ip}\right)=\xi^{1}\left(x_{ip-1}\right)+\left(x_{ip}-x_{ip-1}\right)t_{11}\left(x_{ip}\right)\left(1+\varepsilon\left(x_{ip}\right)\right)\\
&\xi^{2}\left(x_{ip}\right)=\xi^{2}\left(x_{ip+1}\right)+\left(x_{ip}-x_{ip+1}\right)t_{11}\left(x_{ip}\right)\left(1+\varepsilon\left(x_{ip}\right)\right)\\
&\xi\left(x_{ip}\right)=\frac{\xi^{1}\left(x_{ip}\right)+\xi^{2}\left(x_{ip}\right)}{2}
\end{aligned}\tag{3.38}$$

$$\begin{aligned}
&\eta^{1}\left(x_{ip}\right)=\eta^{1}\left(x_{ip-1}\right)+\left(x_{ip}-x_{ip-1}\right)t_{12}\left(x_{ip}\right)\left(1+\varepsilon\left(x_{ip}\right)\right)\\
&\eta^{2}\left(x_{ip}\right)=\eta^{2}\left(x_{ip+1}\right)+\left(x_{ip}-x_{ip+1}\right)t_{12}\left(x_{ip}\right)\left(1+\varepsilon\left(x_{ip}\right)\right)\\
&\eta\left(x_{ip}\right)=\frac{\eta^{1}\left(x_{ip}\right)+\eta^{2}\left(x_{ip}\right)}{2}
\end{aligned}\tag{3.39}$$

$$
\begin{aligned}
&\chi^1\left(x_{ip}\right)=\chi^1\left(x_{ip-1}\right)+\left(x_{ip}-x_{ip-1}\right)t_{13}\left(x_{ip}\right)\left(1+\varepsilon\left(x_{ip}\right)\right)\\
&\chi^2\left(x_{ip}\right)=\chi^2\left(x_{ip+1}\right)+\left(x_{ip}-x_{ip+1}\right)t_{13}\left(x_{ip}\right)\left(1+\varepsilon\left(x_{ip}\right)\right)\\
&\chi\left(x_{ip}\right)=\frac{\chi^1\left(x_{ip}\right)+\chi^2\left(x_{ip}\right)}{2}
\end{aligned}
\tag{3.40}
$$

Since the values at both end nodes are known, an initial value integration is done starting from nodes i and j. The final value is the average from both integration schemes. In Equations (3.38), (3.39) and (3.40) the components of $\mathbf{t}_1(x_{ip})$ are needed. However, since the Corotated coordinate system $\mathbf{E}$ is the identity matrix, then $\mathbf{R}_1(x_{ip}) = \mathbf{t}_1(x_{ip})$. This assumption is made, without any loss of generality, because the compatibility conditions depend only on the deformations along the length of the element not on its rigid body motion.

Step #8. Calculate matrix ***B*** for each Integration Point.*

Evaluating Equation (2.75) for each IP:

$$
\mathbf{B}^*\left(x_{ip}\right)=\left[\begin{array}{cc}
R_{11}(x_{ip}) & R_{31}(x_{ip})\eta(x_{ip})-R_{21}(x_{ip})\chi(x_{ip})\\
\frac{-R_{12}(x_{ip})}{\xi_L} & \frac{-1}{\xi_L}\left(-R_{31}(x_{ip})\xi(x_{ip})+R_{11}(x_{ip})\chi(x_{ip})\right)-R_{31}(x_{ip})\\
\frac{-R_{12}(x_{ip})}{\xi_L} & \frac{-1}{\xi_L}\left(-R_{31}(x_{ip})\xi(x_{ip})+R_{11}(x_{ip})\chi(x_{ip})\right)\\
\frac{R_{13}(x_{ip})}{\xi_L} & \frac{1}{\xi_L}\left(R_{21}(x_{ip})\xi(x_{ip})-R_{11}(x_{ip})\eta(x_{ip})\right)-R_{21}(x_{ip})\\
\frac{R_{13}(x_{ip})}{\xi_L} & \frac{1}{\xi_L}\left(R_{21}(x_{ip})\xi(x_{ip})-R_{11}(x_{ip})\eta(x_{ip})\right)\\
0 & R_{11}(x_{ip})
\end{array}\right.\quad\cdots\cdots
$$

$$
\left.\begin{array}{cc}
R_{32}(x_{ip})\eta(x_{ip})-R_{22}(x_{ip})\chi(x_{ip}) & R_{33}(x_{ip})\eta(x_{ip})-R_{23}(x_{ip})\chi(x_{ip})\\
\frac{-1}{\xi_L}\left(-R_{32}(x_{ip})\xi(x_{ip})+R_{12}(x_{ip})\chi(x_{ip})\right)-R_{32}(x_{ip}) & \frac{-1}{\xi_L}\left(-R_{33}(x_{ip})\xi(x_{ip})+R_{13}(x_{ip})\chi(x_{ip})\right)-R_{33}(x_{ip})\\
\frac{-1}{\xi_L}\left(-R_{32}(x_{ip})\xi(x_{ip})+R_{12}(x_{ip})\chi(x_{ip})\right) & \frac{-1}{\xi_L}\left(-R_{33}(x_{ip})\xi(x_{ip})+R_{13}(x_{ip})\chi(x_{ip})\right)\\
\frac{1}{\xi_L}\left(R_{22}(x_{ip})\xi(x_{ip})-R_{12}(x_{ip})\eta(x_{ip})\right)-R_{22}(x_{ip}) & \frac{1}{\xi_L}\left(R_{23}(x_{ip})\xi(x_{ip})-R_{13}(x_{ip})\eta(x_{ip})\right)-R_{23}(x_{ip})\\
\frac{1}{\xi_L}\left(R_{22}(x_{ip})\xi(x_{ip})-R_{12}(x_{ip})\eta(x_{ip})\right) & \frac{1}{\xi_L}\left(R_{23}(x_{ip})\xi(x_{ip})-R_{13}(x_{ip})\eta(x_{ip})\right)\\
R_{12}(x_{ip}) & R_{13}(x_{ip})
\end{array}\right]
\tag{1.41}
$$

Step #9.   Calculate the rate of rotational deformations or Spins at IP.

The displacement rates are state variables and thus their values are known at each time step. Using matrix **T** (obtained in *step #2*) the rates of the displacements in Corotated coordinates can be obtained:

$$\dot{\mathbf{q}} = \mathbf{T} \cdot \dot{\mathbf{u}} \tag{3.42}$$

And the "spins" $\boldsymbol{\omega}^{m}$ are defined as the variation of rotations with time, therefore:

$$\begin{aligned} \boldsymbol{\omega}^{m}(0) &= \left\{ -\dot{q}_6/2 \quad \dot{q}_4 \quad \dot{q}_2 \right\} \\ \boldsymbol{\omega}^{m}(\xi_L) &= \left\{ \dot{q}_6/2 \quad \dot{q}_5 \quad \dot{q}_3 \right\} \end{aligned} \tag{3.43}$$

Recalling the relationship between material spins and curvatures (Equation (2.69)):

$$\frac{d\boldsymbol{\omega}^{m}}{dx} = \dot{\boldsymbol{\phi}}^{m}(1+\varepsilon) + \boldsymbol{\phi}^{m}\dot{\varepsilon} \tag{3.44}$$

The material measure of the instantaneous spins can be interpolated as follows:

$$\begin{aligned} \omega^{m1}(x_{ip}) &= \omega^{m1}(x_{ip-1}) + (x_{ip} - x_{ip-1}) \cdot \left(\dot{\boldsymbol{\phi}}^{\mathbf{m}}(x_{ip})\left(1+\varepsilon(x_{ip})\right) + \boldsymbol{\phi}^{\mathbf{m}}(x_{ip})\dot{\varepsilon}(x_i p) \right) \\ \omega^{m2}(x_{ip}) &= \omega^{m2}(x_{ip-1}) + (x_{ip} - x_{ip+1}) \cdot \left(\dot{\boldsymbol{\phi}}^{\mathbf{m}}(x_{ip})\left(1+\varepsilon(x_{ip})\right) + \boldsymbol{\phi}^{\mathbf{m}}(x_{ip})\dot{\varepsilon}(x_{ip}) \right) \\ \omega^{m}(x_{ip}) &= \frac{\omega^{m1}(x_{ip}) + \omega^{m2}(x_{ip})}{2} \end{aligned} \tag{3.45}$$

*Step #10.   Calculate the rate of **R**.*

The rate of **R** at any IP is **R** times the skew symmetric matrix of the spin:

$$\begin{aligned} \dot{\mathbf{R}}(x_{ip}) &= \mathbf{R}(x_{ip})\boldsymbol{\Omega}^{m}(x_{ip}) \\ \boldsymbol{\Omega}^{m}(x_{ip}) &= \begin{bmatrix} 0 & -\omega_3^m & \omega_2^m \\ \omega_3^m & 0 & -\omega_1^m \\ -\omega_2^m & \omega_1^m & 0 \end{bmatrix}(x_{ip}) \end{aligned} \tag{3.46}$$

Step #11.   Calculate the rate of the coordinates.

The rate of the coordinate is an important quantity for evaluating the rate of matrix $\mathbf{B}^{*}$. The interpolation procedure is the same as in previous cases and the boundary conditions are:

$$\begin{aligned} \dot{x}_i &= \{0 \quad 0 \quad 0\}^t \\ \dot{x}_j &= \{\dot{\xi}_L \quad 0 \quad 0\}^t \end{aligned} \tag{3.47}$$

The rate of ξ_L is equal to the rate of q_1, also obtained through **T**. All the other quantities are null because by construction, the chord always links the node in its deformed position, therefore their coordinates with respect to the **E** coordinate system never move. The interpolation is done using Equation (2.63):

$$\begin{aligned}
&\dot{\xi}^1\left(x_{ip}\right)=\dot{\xi}^1\left(x_{ip-1}\right)+\left(x_{ip}-x_{ip-1}\right)\left[\dot{R}_{11}\left(x_{ip}\right)\left(1+\varepsilon\left(x_{ip}\right)\right)+R_{11}\left(x_{ip}\right)\dot{\varepsilon}\left(x_{ip}\right)\right]\\
&\dot{\xi}^2\left(x_{ip}\right)=\dot{\xi}^2\left(x_{ip+1}\right)+\left(x_{ip}-x_{ip+1}\right)\left[\dot{R}_{11}\left(x_{ip}\right)\left(1+\varepsilon\left(x_{ip}\right)\right)+R_{11}\left(x_{ip}\right)\dot{\varepsilon}\left(x_{ip}\right)\right]\\
&\dot{\xi}\left(x_{ip}\right)=\frac{\dot{\xi}^1\left(x_{ip}\right)+\dot{\xi}^2\left(x_{ip}\right)}{2}
\end{aligned}\tag{3.48}$$

$$\begin{aligned}
&\dot{\eta}^1\left(x_{ip}\right)=\dot{\eta}^1\left(x_{ip-1}\right)+\left(x_{ip}-x_{ip-1}\right)\left[\dot{R}_{12}\left(x_{ip}\right)\left(1+\varepsilon\left(x_{ip}\right)\right)+R_{12}\left(x_{ip}\right)\dot{\varepsilon}\left(x_{ip}\right)\right]\\
&\dot{\eta}^2\left(x_{ip}\right)=\dot{\eta}^2\left(x_{ip+1}\right)+\left(x_{ip}-x_{ip+1}\right)\left[\dot{R}_{12}\left(x_{ip}\right)\left(1+\varepsilon\left(x_{ip}\right)\right)+R_{12}\left(x_{ip}\right)\dot{\varepsilon}\left(x_{ip}\right)\right]\\
&\dot{\eta}\left(x_{ip}\right)=\frac{\dot{\eta}^1\left(x_{ip}\right)+\dot{\eta}^2\left(x_{ip}\right)}{2}
\end{aligned}\tag{3.49}$$

$$\begin{aligned}
&\dot{\chi}^1\left(x_{ip}\right)=\dot{\chi}^1\left(x_{ip-1}\right)+\left(x_{ip}-x_{ip-1}\right)\left[\dot{R}_{13}\left(x_{ip}\right)\left(1+\varepsilon\left(x_{ip}\right)\right)+R_{13}\left(x_{ip}\right)\dot{\varepsilon}\left(x_{ip}\right)\right]\\
&\dot{\chi}^2\left(x_{ip}\right)=\dot{\chi}^2\left(x_{ip+1}\right)+\left(x_{ip}-x_{ip+1}\right)\left[\dot{R}_{13}\left(x_{ip}\right)\left(1+\varepsilon\left(x_{ip}\right)\right)+R_{13}\left(x_{ip}\right)\dot{\varepsilon}\left(x_{ip}\right)\right]\\
&\dot{\chi}\left(x_{ip}\right)=\frac{\dot{\chi}^1\left(x_{ip}\right)+\dot{\chi}^2\left(x_{ip}\right)}{2}
\end{aligned}\tag{3.50}$$

Step #12. Calculate the rate of matrix $\boldsymbol{B}^*$.

The rate of matrix $\mathbf{B}^*$ is a very important component for the evaluation of the rate of the internal forces. Its rate is:

$$
\dot{\mathbf{B}}^{*} = \begin{bmatrix}
\dot{R}_{11} & \dot{R}_{31}\eta - \dot{R}_{21}\chi & \dot{R}_{32}\eta - \dot{R}_{22}\chi & \dot{R}_{33}\eta - \dot{R}_{23}\chi \\
\frac{-\dot{R}_{12}}{\xi_L} & \left(\frac{\xi}{\xi_L}-1\right)\dot{R}_{31} - \dot{R}_{11}\frac{\chi}{\xi_L} & \left(\frac{\xi}{\xi_L}-1\right)\dot{R}_{32} - \dot{R}_{12}\frac{\chi}{\xi_L} & \left(\frac{\xi}{\xi_L}-1\right)\dot{R}_{33} - \dot{R}_{13}\frac{\chi}{\xi_L} \\
\frac{-\dot{R}_{12}}{\xi_L} & \frac{\xi\dot{R}_{31} - \dot{R}_{11}\chi}{\xi_L} & \frac{\xi\dot{R}_{32} - \dot{R}_{12}\chi}{\xi_L} & \frac{\xi\dot{R}_{33} - \dot{R}_{13}\chi}{\xi_L} \\
\frac{\dot{R}_{13}}{\xi_L} & \left(\frac{\xi}{\xi_L}-1\right)\dot{R}_{21} - \dot{R}_{11}\frac{\eta}{\xi_L} & \left(\frac{\xi}{\xi_L}-1\right)\dot{R}_{22} - \dot{R}_{12}\frac{\eta}{\xi_L} & \left(\frac{\xi}{\xi_L}-1\right)\dot{R}_{23} - \dot{R}_{13}\frac{\eta}{\xi_L} \\
\frac{\dot{R}_{13}}{\xi_L} & \frac{\xi\dot{R}_{21} - \dot{R}_{11}\eta}{\xi_L} & \frac{\xi\dot{R}_{22} - \dot{R}_{12}\eta}{\xi_L} & \frac{\xi\dot{R}_{23} - \dot{R}_{13}\eta}{\xi_L} \\
0 & \dot{R}_{11} & \dot{R}_{12} & \dot{R}_{13}
\end{bmatrix} +
$$

$$
\begin{bmatrix}
0 & R_{31}\dot{\eta} - R_{21}\dot{\chi} & R_{32}\dot{\eta} - R_{22}\dot{\chi} & R_{33}\dot{\eta} - R_{23}\dot{\chi} \\
0 & \frac{\dot{\xi}R_{31} - R_{11}\dot{\chi}}{\xi_L} & \frac{\dot{\xi}R_{32} - R_{12}\dot{\chi}}{\xi_L} & \frac{\dot{\xi}R_{33} - R_{13}\chi}{\xi_L} \\
0 & \frac{\dot{\xi}R_{31} - R_{11}\dot{\chi}}{\xi_L} & \frac{\dot{\xi}R_{32} - R_{12}\dot{\chi}}{\xi_L} & \frac{\dot{\xi}R_{33} - R_{13}\chi}{\xi_L} \\
0 & \frac{\dot{\xi}R_{21} - R_{11}\dot{\eta}}{\xi_L} & \frac{\dot{\xi}R_{22} - R_{12}\dot{\eta}}{\xi_L} & \frac{\dot{\xi}R_{23} - R_{13}\dot{\eta}}{\xi_L} \\
0 & \frac{\dot{\xi}R_{21} - R_{11}\dot{\eta}}{\xi_L} & \frac{\dot{\xi}R_{22} - R_{12}\dot{\eta}}{\xi_L} & \frac{\dot{\xi}R_{23} - R_{13}\dot{\eta}}{\xi_L} \\
0 & 0 & 0 & 0
\end{bmatrix} - \frac{\dot{\xi}_L}{\xi_L^2}
\begin{bmatrix}
0 & 0 & 0 & 0 \\
-R_{12} & \xi R_{31} - R_{11}\chi & \xi R_{32} - R_{12}\chi & \xi R_{33} - R_{13}\chi \\
-R_{12} & \xi R_{31} - R_{11}\chi & \xi R_{32} - R_{12}\chi & \xi R_{33} - R_{13}\chi \\
R_{13} & \xi R_{21} - R_{11}\eta & \xi R_{22} - R_{12}\eta & \xi R_{23} - R_{13}\eta \\
R_{13} & \xi R_{21} - R_{11}\eta & \xi R_{22} - R_{12}\eta & \xi R_{23} - R_{13}\eta \\
0 & 0 & 0 & 0
\end{bmatrix} \tag{3.51}
$$

The above matrix is evaluated at each IP.

At this step, the evaluation of matrix **B*** and its rate for each IP is completed. The only matrix that still needs to be evaluated is the flexibility matrix at each control section (or IP). This is done in *step #13.*

Step #13. Evaluate the flexibility matrix.

To evaluate the flexibility matrix, a proper ultimate yield function has to be defined such that it properly represents the section capacity.

For a square HSS section (used in the experimental studies, see Chapter 4), the proposed function is (Duan and Chen 1990):

$$
\begin{aligned}
& m_y^{\alpha}\left(1-p^{\beta}\right)^{\alpha} + m_z^{\alpha}\left(1-p^{\beta}\right)^{\alpha} - \left(1-p^{\beta}\right)^{2\alpha} = 0 \\
& \alpha = 1.7 + 1.5 \cdot p \\
& \beta = 1.5
\end{aligned} \tag{3.52}
$$

With this function and the procedure described in the Section 2.4, the flexibility matrix **f** is found for every integration point.

Finally, all the information required for the evaluation of the equations of compatibility (2.94) and plasticity (2.95). is available for each IP of every element of the complete structure. This is done in *step #14*.

Step #14. Evaluate the compatibility equation for each element.

The compatibility equation in integral form reproduced below:

$$\dot{\mathbf{q}} = \int_0^L \left(\mathbf{B}^*\mathbf{f}\dot{\mathbf{B}}^{*t}\right)\mathbf{Q}dx + \int_0^L \left(\mathbf{B}^*\mathbf{f}\mathbf{B}^{*t}\right)\dot{\mathbf{Q}}dx \tag{3.53}$$

Is discretized as follows:

$$\begin{aligned}\text{compatibility} = \mathbf{T}_{n+1}\cdot\dot{\mathbf{u}}_{n+1} - \sum_1^{NIP}\left(\mathbf{B}^*\left(x_{ip}\right)\right)_{n+1}\left(\mathbf{f}\left(x_{ip}\right)\right)_{n+1}\left(\dot{\mathbf{B}}^{*t}\left(x_{ip}\right)\right)_{n+1}\left(\mathbf{Q}\left(x_{ip}\right)\right)_{n+1}\mathbf{W}\left(x_{ip}\right)+ \\ \sum_1^{NIP}\left(\mathbf{B}^*\left(x_{ip}\right)\right)_{n+1}\left(\mathbf{f}\left(x_{ip}\right)\right)_{n+1}\left(\mathbf{B}^{*t}\left(x_{ip}\right)\right)_{n+1}\left(\dot{\mathbf{Q}}\left(x_{ip}\right)\right)_{n+1}\mathbf{W}\left(x_{ip}\right)\end{aligned} \tag{3.54}$$

Where x_{ip} represents the integration point and $W(x_{ip})$ is the weight of that particular point into the integral according to the Gauss-Lobatto rule. All the other components have been found in previous steps.

Step #15. Evaluate the plasticity equations at each Integration Point.

Recalling the local evolution equations:

$$\begin{bmatrix}\dot{\varepsilon} \\ \dot{\phi}^m\end{bmatrix}_n = \mathbf{f}\left(x\right)\dot{\mathbf{P}}\left(x\right) = \mathbf{f}\left(x\right)\left(\mathbf{B}^{*t}\dot{\mathbf{Q}} + \dot{\mathbf{B}}^{*t}\mathbf{Q}\right) \tag{3.55}$$

The discretization is:

$$\text{plasticity} = \left(\dot{\boldsymbol{\varepsilon}}_n\left(x_{ip}\right)\right)_{n+1} - \left(\mathbf{f}\left(x_{ip}\right)\right)_{n+1}\left(\left(\dot{\mathbf{B}}^{*t}\left(x_{ip}\right)\right)_{n+1}\left(\mathbf{Q}\left(x_{ip}\right)\right)_{n+1} + \left(\mathbf{B}^{*t}\left(x_{ip}\right)\right)_{n+1}\left(\dot{\mathbf{Q}}\left(x_{ip}\right)\right)_{n+1}\right) \tag{3.56}$$

Step #16. Solve the problem.

Once all the equations have been formulated, a call to IDA solver will use the numerical procedure of section 3.2 to determine the values of the variables $\mathbf{y} = \{\mathbf{u}\ \mathbf{Q}\ \boldsymbol{\varepsilon}\}$ and their rates for a given time.

3.4 Brief description of "element.exe"

The procedure described in Section 3.3 has been implemented in a computer program called "Element.exe". The program is written in C language. The library IDA is already built in the executable file, therefore the user does not need to install it unless a modification to the code is done.

The program reads an input file of name “InputFile.dat” where the user describes the problem to be solved, the forcing functions and the initial conditions. The input file’s name cannot be changed; otherwise the program will not work.

To describe the structural problem, a description of the nodes’ location, the elements’ connectivity and the materials’ parameters are needed. The restraints are assigned to the nodal DOFs with a 1 or 0 entry (1=restrained, 0=not restrained). A restrained DOF is equivalent to a fixed support in that DOF. It is not possible to define hinges.

The loading can be a force, a prescribed displacement or a base acceleration. In all the cases, an independent file must be provided with the time history of the loading (even if the loading is a single number).

Finally, the Initial Conditions of each node, element and integration point must be provided.

A complete user’s manual is described in APPENDIX B.

SECTION 4
EXPERIMENTAL STUDY ON "ZIPPER FRAMES"

4.1 Introduction

An experimental study was needed to generate data for validation of the analytical model presented in Chapter 2 and Chapter 3. The experimental study on "zipper frames" was an ideal project because the main failure mode of this type of frame is the inelastic buckling of its braces. The experimental study on "zipper frames" was part of a multi-site NEES collaborative project between Georgia Institute of Technology (GT), University of California at Berkeley (UCB), University of Colorado Boulder (CU) and the University at Buffalo (UB).

The global objectives of the experimental study were to test for the first time the "zipper frames" concept and to demonstrate that a multi-site experimental study is advantageous and useful. In addition, the specific objective of the tests at UB was to obtain detailed data about the three dimensional inelastic behavior of the structure under dynamic loading. This data is compared to analytical predictions obtained from an analytical "zipper frames" model using the formulation described in previous Chapters.

The experiments were performed at all the NEES Equipment Sites according to the capacities of each laboratory, thus at Georgia Institute of Technology quasi-static tests were performed (Yang et al. 2006a; Yang et al. 2007a), at University of California at Berkeley (Yang et al. 2006b) and University of Colorado Boulder (Stavridis and Shing 2006), hybrid simulations were carried out and at the University at Buffalo shake table tests were conducted. This chapter includes only the experimental study done at the University at Buffalo.

4.2 Description of "zipper frames"

Concentrically Braced Frames (CBF) are frames where diagonal elements resist lateral loads through the development of high axial forces and small moments. The Inverted V-braced frame or Chevron is the most popular configuration, however it has an important design problem. When subjected to lateral force, the braces resist in tension and compression. For steel structures, the capacity in compression is, in general, smaller than the capacity in tension and its value depends both on the properties of the cross section and the boundary conditions. When the compression capacity is attained, the brace buckles and a plastic hinge develops at midheight. At this stage, the midpoint of the brace undergoes large displacements, generating even larger moments. Since the section is fully plastic, the axial capacity of the member reduces to accommodate a larger moment capacity. On the other hand, the brace in tension attracts even more load to compensate for the loss in capacity of the compression brace. This generates an unbalanced vertical force that is transmitted to the beam at its midpoint. Thus, the capacity design of the beam becomes very costly due to the big section size required to resist such a force. As a solution for this problem, the idea to link every beam to brace intersection point with columns, called "zipper columns", was proposed (Khatib et al. 1988). In this case, when a brace buckles, the unbalanced vertical force is transmitted to the "zipper column" as tension force. The column re-distributes the force to the upper story braces as an extra compression force, forcing the upper story compression brace to buckle. A new unbalanced vertical force is then generated and transmitted to the next level through another "zipper column". This mechanism, called the "zipper mechanism", will repeat itself at all levels forcing all the compression braces to buckle almost simultaneously, resulting in a better energy dissipation distribution over the height of the building and avoiding concentration of damage in just one story. Plastic hinges also develop at the base of the columns and at the midspan of the beams (Figure 4–1, left). This is the plastic collapse mechanism of the "zipper frame". To improve the performance of the frame, the "suspended zipper frame" concept was proposed (Leon and Yang 2003; Yang 2006). In this configuration, the last story braces are purposely designed to remain elastic at all times. The "zipper columns" are designed to yield shortly after the yielding of the brace in tension. This is achieved by considering only P_y (nominal yield force) instead of R_yP_y (expected yield force) in the capacity design. The yielding of the "zipper columns" delays the development of plastic hinges in the beams, which will develop at the beam to column connections instead (Figure 4–1, right). The objective of the design procedure developed by Yang (Yang 2006; Yang et al. 2007b) is to ensure that the desired plastic mechanism develops.

On occasions, the "zipper columns" could be loaded in compression, thus the compression capacity of the selected section must be checked to meet the load requirements. However, in a properly designed frame, the "zipper columns" are expected to be loaded primarily in tension. A drawing with the expected distribution of forces in all the elements of the "suspended zipper frame" is presented in Figure 4–2.

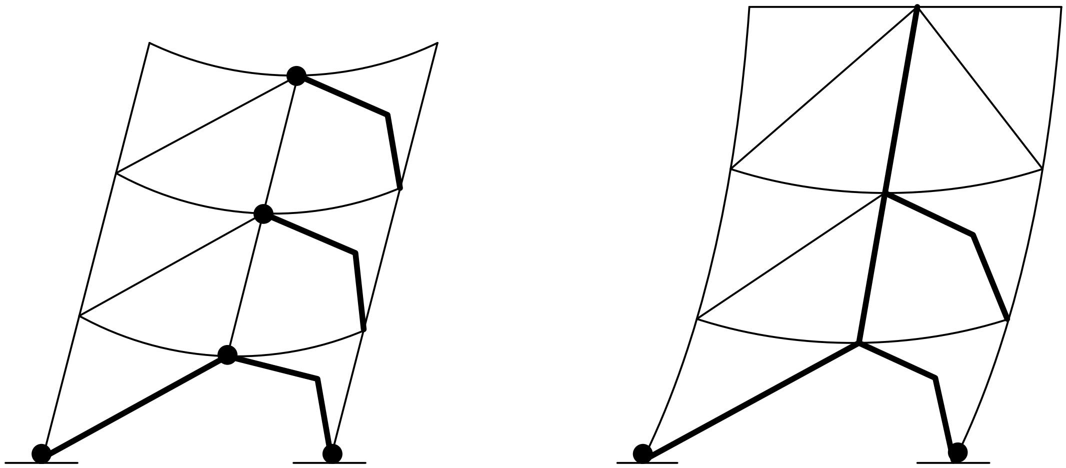

Figure 4–1: Plastic mechanism of "zipper frame" (left) and "suspended zipper frame" (right).

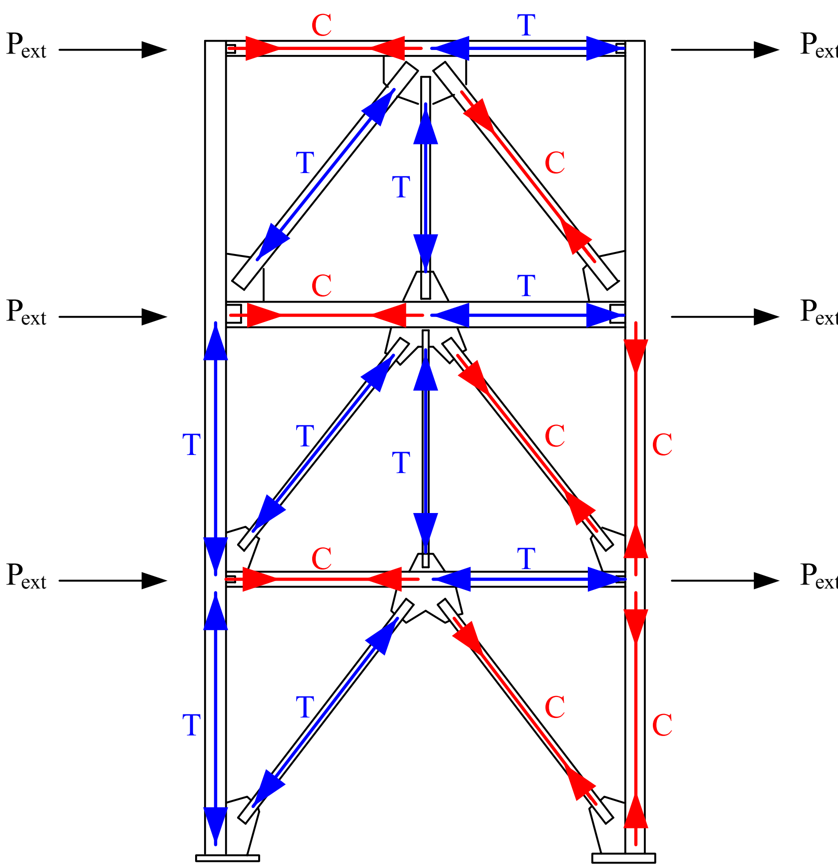

Figure 4–2: Instantaneous flow of forces in the "zipper frame".

4.3 Definition of model

The building used for the prototype design is the 3 stories steel SAC building (Figure 4–3 and Table 4–1). The building has 2 resisting frames per direction and each frame has 6 braces. The resisting frames were designed at Georgia Tech (Leon and Yang 2003) for the joint collaboration project between UB, UCB, CU and GT, considering the dimensional restrictions of the building and the real seismic masses (see APPENDIX C). The final sizes of the components of a typical 1 bay frame (chosen prototype) are listed in Table 4–1. A summary of the prototype design, extracted from (Yang 2006), can be found in APPENDIX C.

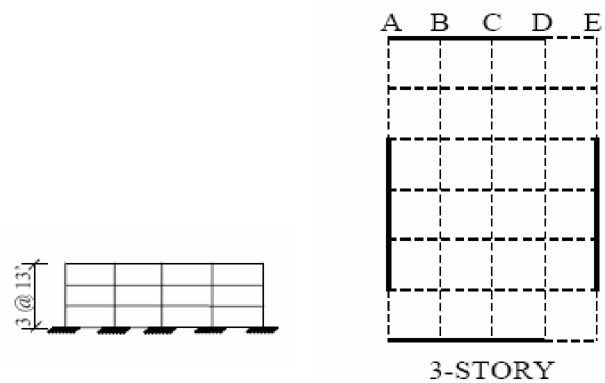

Figure 4–3: Elevation and plan view of the 3 stories SAC building.

Table 4–1: Summary of components for prototype

Story	Braces	Columns	Beams	Zipper columns
3	HSS10x10x5/8	W10x77	W8x21	W8x48
2	HSS7x7x3/8	W10x77	W14x82	W8x24
1	HSS7x7x3/8	W10x77	W12x50	

The prototype was scaled down to meet the capacities of the shake table. The dimensional scale was set to 3. If the acceleration scale factor is set to 1, the calculated scale factor for the mass is 9 and the total weight of the model would be approximately 120 kips, 2 times larger than the vertical capacity of a single shake table at UB-SEESL. Therefore it was decided to set the mass scale factor to 18, reducing the total mass in the model by half. In this case, the required acceleration scale factor is 0.5 (see Table 4–1 and Table 4–3).

Table 4–2: Scale factors for linear dimensions

Quantity	Floor	Prototype (in)	Model (in)	Scale ratio
Total height		468	154.25	3.03
Floor height	Third	156	50.75	3.07
	Second	156	50.75	3.07
	First	156	52.75	2.96
Beam bay	All	120	40	3.00

Table 4–3: Scale factors for weight per floor.

Quantity	Prototype weight (kip)	Ideal weight (kip)	Scale factor	Provided weight (kip)	Scale factor
Total	1080	60.21	18	51	21.17
3rd Floor	380.5	21.14	18	17	22.38
2nd Floor	351.67	13.53	18	17	20.68
1st Floor	351.67	13.53	18	17	20.68

In general, an acceleration scale factor applies to horizontal accelerations as well as gravity. Since gravity cannot be scaled, the usual acceleration scale factor is 1 and the resulting mass scale is 9. However, in this case, the test setup allows for a complete independence of the lateral resisting system from the gravity resisting system, therefore an independent scale factor for horizontal accelerations is possible.

The scale factor for the modulus of elasticity of the material is the last independent factor chosen. Since steel is used in both the prototype and the model, a factor of 1 is selected. Thus the scales factors for all other variables can be determined. Among them, the resultant scale factor for time is 2.45. Table 4–4 presents a complete list of all scale factors.

It is important to emphasize the meaning of a scale factor. In the case of linear dimensions, it is simply the ratio between the dimensions of the prototype versus the ones of the model. In the case of forces, velocities and accelerations, the scale factor can be used to extrapolate the results from the experiment to a full size prototype. Therefore the extrapolated accelerations in the prototype are be only half the amount obtained for the model during testing. This is also true for the input file ground motion. In practice, the above procedure is valid only in case of linear structures. In the present model, geometric and material nonlinearities are expected; therefore a direct extrapolation of test results to a full size structure is not entirely meaningful.

Table 4–4: List of scale factors of "zipper frame" model.

Quantity	Scale Factor
Geometric length*	$\lambda_L = 3.00$
Elastic modulus*	$\lambda_E = 1.00$
Acceleration	$\lambda_a = 0.50$
Density	$\lambda_\rho = 0.67$
Velocity	$\lambda_v = 0.67$
Forces	$\lambda_F = 9.00$
Strain	$\lambda_\varepsilon = 1.00$
Stress	$\lambda_\sigma = 1.00$
Area	$\lambda_A = 9.00$
Volume	$\lambda_V = 27.00$
Second moment of area	$\lambda_I = 81.00$
Mass*	$\lambda_M = 18.00$
Impulse	$\lambda_i = 22.05$
Energy	$\lambda_e = 27.00$
Frequency	$\lambda_\omega = 0.41$
Time	$\lambda_T = 2.45$
Gravitational acceleration	$\lambda_g = 1.00$
Gravitational force	$\lambda_{Fg} = 18.00$
Critical damping	$\lambda_\xi = 1.00$

* Indicates independent scale quantities.

The components of the model were selected considering the scale factors for section properties and the available AISC sections. A list of the model components is presented in Table 4–5 and Figure 4–4. The only significant difference is that the "zipper column" section changed from a type W to a type HSS. The "zipper column" is expected to behave primarily in tension with little or no moment. Therefore, despite the fact that the selected HSS sections have much more moment capacity than required by the scaling process, their area scale factors (10.55 for second floor and 11.85 for third floor) are very close to the desired quantity (9.0).

Table 4–5: Summary of components of the model

Story	Braces	Columns	Beams	Zipper columns
3	HSS3x3x3/16	S4x9.5	S3x5.7	HSS2x2x3/16
2	HSS2x2x1/8	S4x9.5	S5x10	HSS1.25x1.25x3/16
1	HSS2x2x1/8	S4x9.5	S3x7.5	

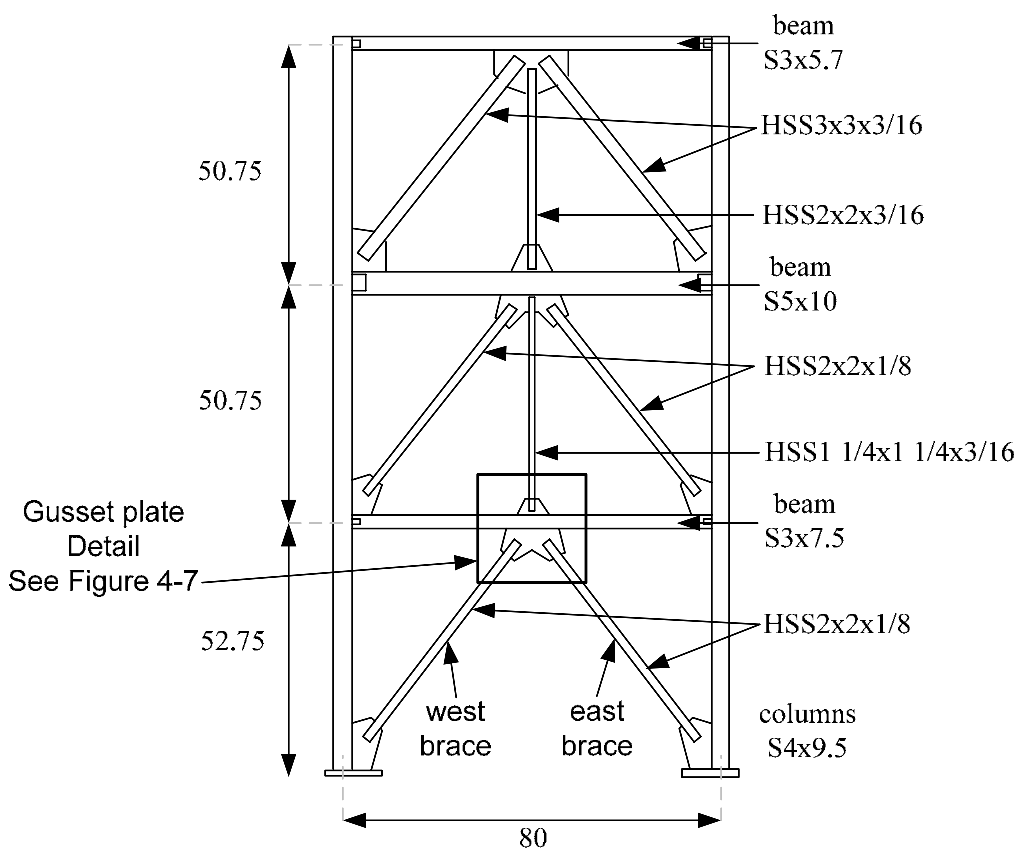

Figure 4–4: Scaled model, dimension (in) and members.

All sections meet the seismic limitations on compactness and slenderness. The detail of these verifications can be found in APPENDIX C. The gusset plates were designed according to the actual seismic provisions (AISC 2005a; AISC 2005b).

It is important to emphasize that the axial behavior of braces and “zipper columns” are the most important sources of data for this study.

Complete drawings of the model, including connection details can be found in APPENDIX D.

4.4 Test setup

For the shake table test three planar “zipper frames” were built. They were assembled between a dual “gravity frame” system. These two additional structures were designed at the University at Buffalo (Kusumastuti 2005) as a versatile construction for testing planar and spatial structures. The “gravity frame” is composed of a set of individual members: columns, beams and plates, that can be easily combined to build any desired configuration. In the present test, columns and plates were used to build 2 identical structures of 1 bay and 3 stories high (Figure 4–5) which were placed at each side of the “zipper frame”.

Figure 4–5: “Zipper frame” alone (left) and with gravity frame (right)

Each floor of the “gravity frame” is composed of 4 columns and a steel plate of 3.5 in of thickness and 8.5 kips of weight. Each column sits on a special “dish” that has been machined to provide a rotation free movement, a real hinge in two directions. Thus none of these columns can resist any lateral force. The columns of a same floor are independent in the in plane direction and braced in the out of plane direction to ensure unidirectional motion. The columns of two consecutive floors are connected through rods that ensure that individual columns work together with a common centerline (Figure 4–6). Due to the hinged columns, the gravity frames have a real lateral mechanism and cannot stand without being connected to the "zipper frame" for lateral stability.

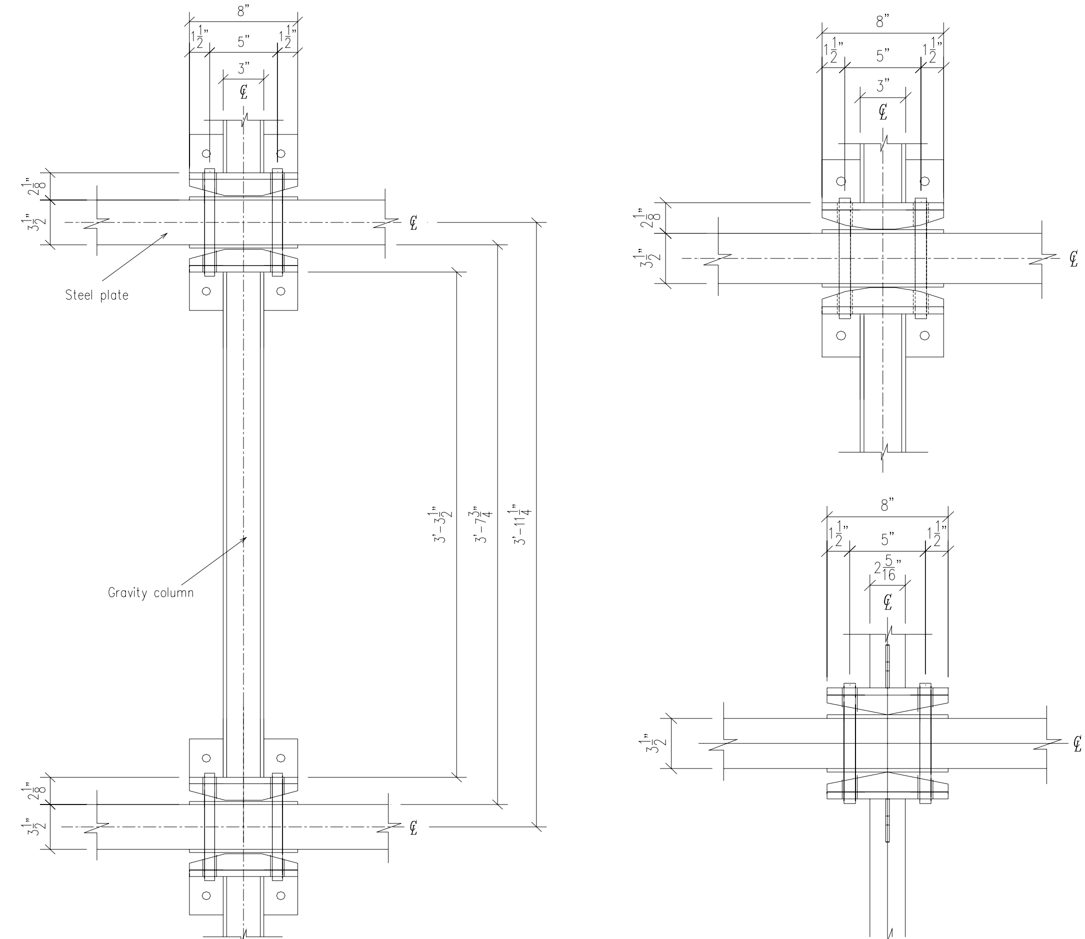

Figure 4–6: Gravity column layout (left) and connection details (right).

The columns of the "zipper frame" are continuous elements. The webs of the beams are connected to the flanges of the columns though welded angles. There is no connection between the flanges of the beams and the columns. The objective of this configuration is to reproduce a hinged beam to column connection.

To connect the gravity frame to the "zipper frame", a slotted hole of 1⅛ in diameter is made in every column to beam joint. The connection is strengthened by welding in the joint a steel filler block. For the gravity system, angles are welded at the top of each plate. A pin, running thought both angles and the slotted hole connects the "zipper frame" with the "gravity frames".

When the system moves laterally, the gravity columns rock and the columns deform. If the lateral movement is large, then the vertical projection of the gravity column’ length is smaller than its actual length. The slotted hole allows the plate to follow the movement of the gravity columns without disconnecting from the “zipper frame” or imposing new stresses on the connection.

Complete drawings of the test setup can be found in APPENDIX D.

4.5 Test #1

4.5.1 Description of frame details in test #1

The beams to brace connections are designed to be very flexible, with a notch in the gusset plate, as can be seen in the detailed drawings in APPENDIX D. However, the frame tested in Test #1 has a full gusset at the beam to brace connection of the 1st floor (Figure 4–7, right). The designed gusset plate (Figure 4–7, left) had an inverted V shape which was ignored in the construction. This detail was not considered very important at the moment of testing. However data from the test suggested the opposite. The same gusset error was present in the frame of Test #2. The gusset was corrected in the frame of Test #3.

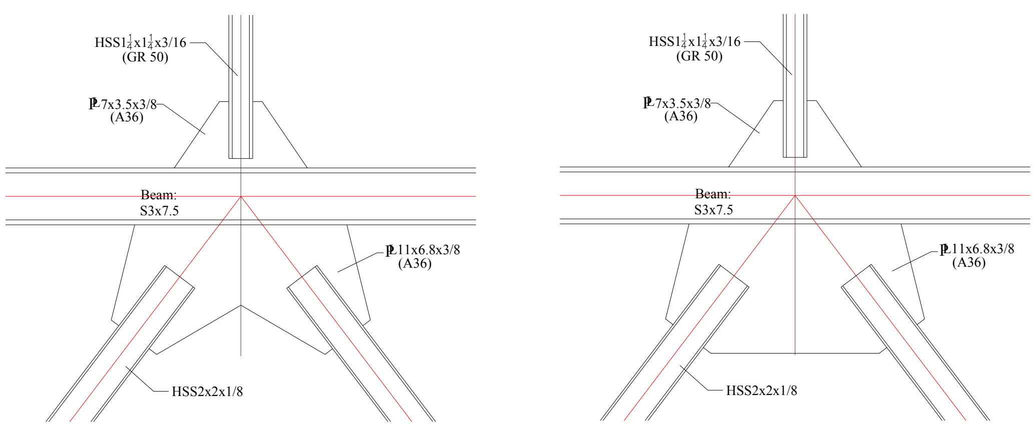

(a) (b)

Figure 4–7: Detail of beam to brace gusset plate. Designed (a), Constructed (b).

4.5.2 Instrumentation

The quantities that needed to be measured were:

- Axial force in the braces.
- Axial force in beams and columns.
- Moments in braces.
- Moments in beam and columns.
- Axial force in “zipper columns”.

Strain gauges were provided in form of half bridges (moments) and full bridges (axial) to read strains (which are directly related to forces through a stress-strain curve) at particular points along the members. In braces, axial force measurements were located far from the buckling point (midheight of the element), at approximately ¼ of its length in all three stories. Meanwhile, in plane moments were measured only in the first floor in 4 locations near the ends of the elements. In columns, only in plane moments were measured. The strain gauges were located 4” away from the beam to column connections. In “zipper columns”, axial strains were recorded at midheight of the element. In beams, axial forces were measured at quarter length and in plane moments were measured near the ends but at least 3” away from beam to column and beam to brace connections.

In addition to strain gauges, accelerometers were attached to each level of the structure to record lateral accelerations and were also attached to the extremes of the plates to record out of plane accelerations or possible torsion. Potentiometers were located at each level to record possible differences in lateral movement between the “zipper frame” and the “gravity frames”. String potentiometers were placed along each brace and each “zipper column” to record the axial displacements. They were also placed along the first floor beam to record its midpoint axial and vertical displacement. Finally, they were attached to each floor to measure the total displacements with respect to a reference frame.

Finally, the Krypton tracking system was also used during the test. The system consists of a camera capable of detecting and recording the spatial coordinate of a point in the structure. The points are defined by LEDs and the coordinate system can be defined anywhere in the range of view of the camera. For this test, the first story braces were instrumented with 7 LEDs each.

A complete list of instruments and drawings can be found in APPENDIX E.

4.5.3 Test Protocol

The chosen ground motion was LA22yy from the SAC set of scaled records for the L.A. area for the 2% probability of exceedance in 50 years (Somerville et al. 1997). This record corresponds to 1.15 times the Kobe earthquake. The peak ground acceleration (PGA) of the original Kobe ground motion is 0.8g and the PGA of LA22yy ground motion is 0.92g.

LA22yy was scaled in time according to Table 4–4 reducing its duration to approximate 12 seconds. The amplitude of the motion should be doubled to 1.84g however, the total weight of the model (51 kips) is very close to the maximum weight limit, therefore the maximum acceleration the shake table can reproduce is around 1.1g. It is not possible to perform a test with the 100% amplitude of the scaled LA22yy ground motion.

Since the real capacity of the frame before testing is not well known (only numerical analyses on an ideal 2D "zipper frame" model were performed before testing); it was decided to perform several tests amplifying the amplitude of the motion each time: incremental dynamic testing (IDT).

The sequence in Test #1 was: 0.138g, 0.276g, 0.414g, 0.552g. 0.736g and 0.920g (equivalent to the 7.5%, 15%, 22.5%, 30%, 40% and 50% of the PGA of the scaled LA22yy ground motion).

For identification purposes, the individual tests are named after the "% PGA" of the original LA22yy record. Thus for Test #1, the sequence was: "15% LA22yy", "30% LA22yy", "45% LA22yy", "60% LA22yy", "80% LA22yy" and "100% LA22yy" .

4.5.4 Test results

4.5.4.1 Test observations and data processing

During the "15% LA22yy" and the "30% LA22yy", the system remained elastic, as expected.

In the "45% LA22yy", the west brace in the 1st floor buckled elastically, while the east brace remained elastic. The buckled brace pulled the 1st floor beam down. As a consequence, both braces showed permanent compression strains, being those of the buckled brace greater than those of the elastic one. Braces in the 2nd floor remained elastic. No measurement of importance was registered in the "zipper column". The vertical potentiometer was not sensitive enough to record the beam displacement.

During the “60% LA22yy”, both braces in the first floor buckled and yielded, remaining with an important permanent deformation in tension. Even though the vertical string potentiometer was not sensitive enough to record the beam movement with accuracy, its sign showed that the bottom part of the gusset plate moved upwards, therefore, the bottom flange of the beam also moved upwards, coinciding with the fact that both braces were in tension at the end of the test. The “zipper column”, again did not record any axial strains of the magnitude of the calculated unbalanced vertical force from the braces, however it sign showed that it is in tension. Therefore, the top flange of the beam must have gone down. The only possible explanation for the beam movement is a rotation.

During the same test, the second floor east brace buckled inelastically, remaining with some compressive deformation. The time at which the braces on the east side at the first and second floor level buckled, was exactly the same. Therefore, the second floor brace did not require the addition of a big unbalanced axial force to buckle.

The second story “zipper column” showed to be engaged but the magnitude of the forces was very small.

The columns of the first floor both at the base and top showed signs of yielding.

During the “80% LA22yy” and “100% LA22yy” strain gauges at first story level either exceeded their maximum range or peeled off. At “80% LA22yy” the first story west brace was severely damaged and reached its axial compression capacity. During the same test, the east brace still showed buckling behavior. Both braces remained permanently in tension. Accordingly, the vertical string potentiometer showed that the bottom flange of the beam moved upwards. This again proves the importance of the rotation of the beam in the global behavior of the braces. The “zipper column” reached its largest force during this test, due to the fact that the west brace had already reached its minimum capacity, however the measured magnitude was again very small compared to the expected value.

The second story braces also buckled, remaining both in compression at the end of the motion. The beam at the second floor was considerably larger than the beam at the first floor and can resist the imposed torsion without substantial rotation. For the braces to remain in compression, the beam must have moved downwards. This is the expected behavior of the beam. Only at “100% LA22yy” the buckling in the second story braces was large enough to activate the third story “zipper column”. However, even in this case, the readings from strain measurements are very small, indicating that very small forces were present in the member.

4.5.4.2 Issues identified in test #1

The calibration of the full bridge strain gauges was found to have an error during testing. The calibration was 2.0 times larger than intended; reaching saturation (10 Volts max.) at 2500 μstrains when the expected value was 5000 μstrains. This is why, at the “80% LA22yy” level test, the readings from the gauges “saturated” at 2500 μstrains. Thus valuable data from the behavior of the braces was not properly recorded. This error was corrected in subsequent tests.

The data recorded with the “Krypton”coordinate tracking system presented problems. This was the first time that this instrument was used in the laboratory. The readings from the first 4 LEDs, numbers 1 to 4 on the west brace were correct, but all others were just a copy of the data for LED #4. This was due to a saturation of series scanned LEDs. This error was corrected in subsequent tests.

Moreover, the buckling of the braces occurred out of plane, thus the braces were subjected to a much larger out of plane moment (which was not recorded) than in plane moment. Although, the braces are designed such that the axial forces do not produce moments at the connections, in practice, a real hinge cannot be achieved. Thus, there are always moments at the ends of the braces and, depending on the gusset plate flexibility, these moments are transmitted to the beam. Since the braces buckle out of plane, the beam is subjected to torsion.

Preliminary numerical analysis and the design of the frame itself were done in two dimensions. Although the final design of the gusset plates considered the fact that the braces were going to buckle out of plane and provided enough room for the development of plastic hinges, the beam was not designed to carry any torsion because the connections were assumed “pinned”. The test setup did not use any lateral restraint and as a consequence, during the “80% LA22yy” test, the beam was subjected to torsion, yielded in shear and remained twisted when the test finished. The lateral displacements of the beam’ flanges were not recorded, since the beam was not instrumented to record such motion; however its rotation was evident from simple visual inspection.

The rotations of the beam had a major influence on the behavior of the “zipper column”. The gusset plate connecting these two elements is very rigid, thus it followed the rotation of the beam like a rigid body. As a consequence, the “zipper column” was also bent out of plane but did not elongate sufficiently to transfer axial loading to the upper braces.

4.5.5 Lessons and recommendations from test #1

Test #1 presented numerous problems with the strain gauges. The advantage of working with full or half Wheatstone bridges instead of individual gauges (quarter bridges) is the reduction in the number of channels and the simplification of the numerical analysis. However, with a full or half bridge is possible to record only one type of information: axial strains, in plane moments or out of plane moments. If individual gauges are used as independent channels, then all the above information can be obtained for the same section through data processing. With a consistent numbering of the channels it is easy to build a function that can do the calculations automatically. Therefore, for Test #2 it was decided to use single gauges instead of half or full bridges.

The insufficient redundancy of instrumentation was also a problem in Test #1. This is evident in the case of the “zipper columns”. It was not possible to conclude unequivocally from this test, that the “zipper columns” worked properly because there was not a second set of gauges along the member to measure axial strains. Therefore, for Test #2, two sets of gauges were used to record strains at the “zipper columns”.

The instrumentation did not include any shear measurement in beams to detect torsion or shear, therefore in Test #2, shear rosettes were placed along the beam.

It was found that the string potentiometers were not sufficiently sensitive to the small axial displacements of the braces. It was decided to replace them by high sensitivity rigid Temposonics^{TM} transducers .

Since the objective of the general work is to have comparable data to experimental results done at the other NEES Equipment Sites, it was decided to brace the beam against torsion in Test #2.

4.6 Test #2

4.6.1 Description of frame details in Test #2

As indicated in the previous section, following the results of Test #1, it was decided to restrain the beam against lateral movement at its midpoint (Figure 4–8). The bracing system consisted of a wide steel angle bolted to the mass simulating rigid plates of the "gravity frames". The angles hold a layer of Teflon™ which was in contact with the beam, if it moves. Teflon – steel has a very low friction coefficient (0.02 – 0.07) therefore, the Teflon surface does not interfere with the in plane movement of the frame.

The frame tested in Test #2 was built simultaneously with the frame tested in Test #1, thus it also has a full gusset at the beam to brace connection of the 1st floor (Figure 4–7, right).

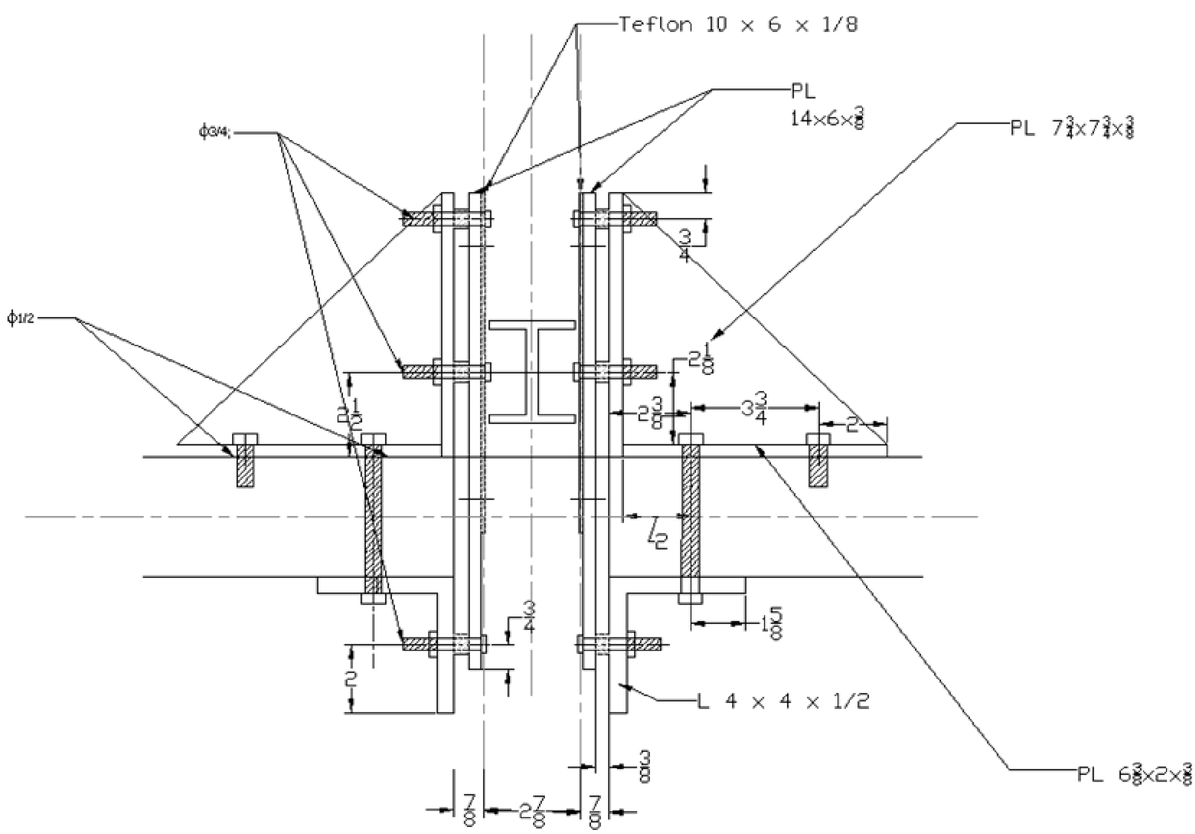

Figure 4–8: Restraint implemented in Test #2 for lateral movement.

4.6.2 Instrumentation

The quantities measured in this test were the same as in Test #1. After the instrumentation problems of Test #1, it was decided to connect every strain gauge as an individual channel (quarter bridge) and to perform the required processing after the test in order to obtain axial or moment strains.

The 1st floor braces had 4 sets of strain gauges along their length, while the braces of the 2nd floor had only 2 sets located near the ends. The 3rd floor braces had only 1 set of gauges and they were hooked into a full bridge because only the axial force was of interest in this floor.

Beams were instrumented with 4 sets of gauges located in the same places where the half bridges were in Test #1. At quarter points, strain rosettes were placed for shear measurements.

String potentiometers were used to record lateral movement and Temposonics^{TM} were used for recording the brace's axial displacements and 1st floor beam vertical movement

The Krypton camera was used again. The location of LEDs was the same as in Test #1. Two additional LEDs were place at the bottom gusset plates to detect out of plane motion.

Instrumentation in columns was not changed and accelerometers were used in the same way as in Test #1.

A complete list of instruments and its locations as well as drawings can be found in APPENDIX F.

4.6.3 Test protocol

As in Test #1, the ground motion for Test #2 was LA22yy. The sequence applied was: "30% LA22yy", "80% LA22yy", "100% LA22yy" and "120% LA22yy". The objective of this sequence was to minimize the effect of low cycle fatigue in the braces' performance.

4.6.4 Test results

4.6.4.1 Test observations and data processing

The first run scheduled for Test #2 was "30% LA22yy". During this run, the structure was expected to behave elastically. However, in a first attempt to perform "30% LA22yy", problems with the control of the shake table due to the weight of the specimen, created an input greater than the desirable, triggering buckling at the west brace. The east brace remained elastic. The loading was not large enough to create important permanent displacements in the brace but it did move the frame horizontally so that the east brace remained with some permanent tensile stress. In a second attempt, the frame performed elastically.

During the “80% LA22yy”, both braces in the first floor buckled and yielded. During this test, the Krypton camera worked very well and its readings show very clearly the buckling at the first story braces. As expected, the “zipper column” was engaged just after the braces buckled and it remained elastic during the entire ground motion. Readings from both sets of strain gauges were consistent and the calculated values of forces were in good agreement with what was expected. The vertical Temposonic^{TM} placed at the bottom of the 1st floor beam showed that the beam moved downwards, as expected. Braces in the second floor remained elastic. Readings from strain rosettes in the beam revealed that the beam was being subjected to some torsion, however its value was very small. When the beam moved out of plane, the sides of the flanges were in contact with the Teflon surface of the restraint, thus a large amount of the torsional moment was being transmitted to the bracing plates instead of to the beam itself.

During the “100% LA22yy”, the shake table exceeded its controllable rocking range, resulting in substantial base rotation. These additional vertical accelerations have to be considered in any numerical analysis that try to reproduce the results from this test. The 1st story braces showed a very small capacity in compression and extensive yielding while the 2nd story braces buckled. The 3rd floor “zipper column” was engaged when the 2nd floor braces buckled and remained with a permanent deformation in tension when the motion stopped. Consequently, the east brace of the 2nd floor remained in tension while the west brace of the 2nd floor remained in compression. However, the amount of permanent deformation in the 2nd floor was very small compared to 1st floor.

An additional test of amplitude “120% LA22yy” was performed because the frame was in good conditions after the “100% LA22yy”. During this test, the 1st story east brace ruptured in tension and the west brace had an important fracture (Figure 4–9). This test had to be stopped due to instability of the setup after the rupture of the brace.

After the “120% LA22yy”, the structure was inspected for signs of beam rotation and general frame displacements. It was found that the beam did rotate as shown in Figure 4–10. The 1st story brace to beam gusset plate also rotated (Figure 4–10 and Figure 4–11). The “zipper column” had some permanent deformation in the out of plane direction (Figure 4–12). The direction of the rotation was determined by the direction where the braces buckled. In the direction of excitation, there was no sign of permanent deformation in the first floor as shown in Figure 4–13.

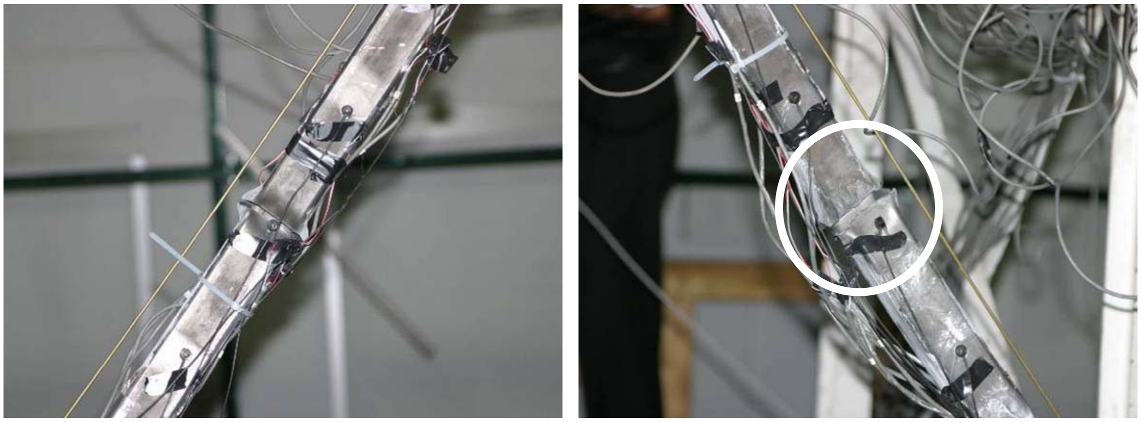

Figure 4–9: Damage in 1st floor braces after Test #2, "120% LA22yy". Local buckling and cracking in West brace (left) and fracture in East brace (right, see circle).

Figure 4–10: Picture of the rotation of the 1st floor beam after Test #2, "120% LA22yy".

Figure 4–11: Picture of the rotation of the 1st story brace to beam gusset plate after Test #2, "120% LA22yy".

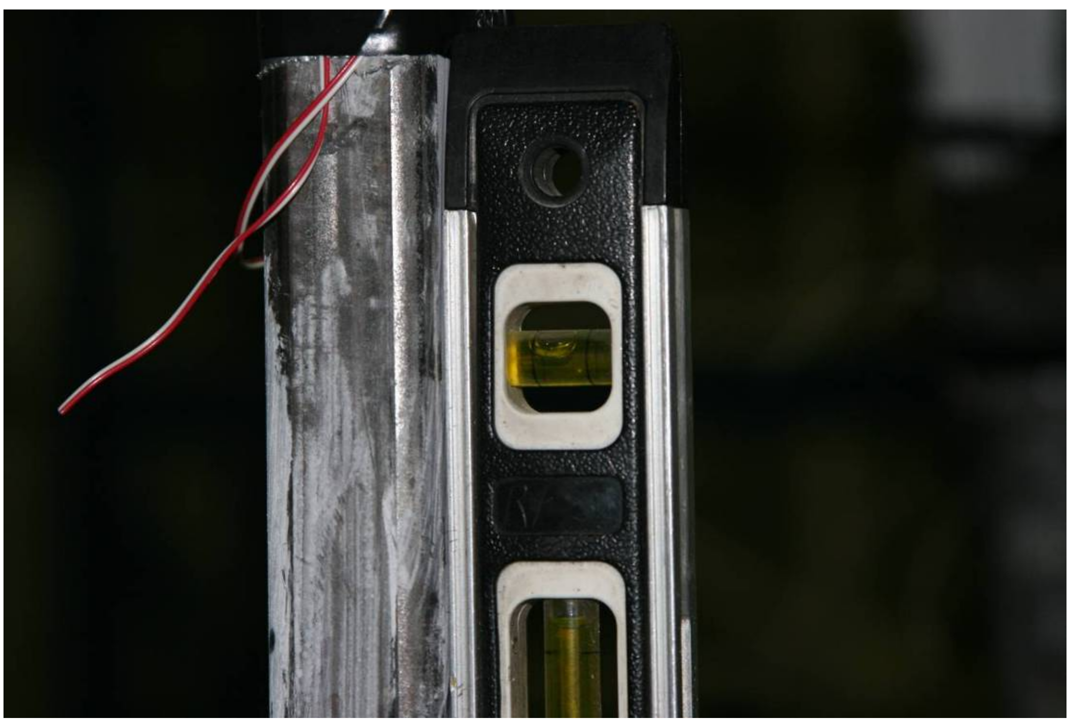

Figure 4–12: Picture of the out of plane bending in the 2nd story "zipper column" after Test #2, "120% LA22yy".

Figure 4–13: Picture of the 1st floor West column (left) and East column (right) after Test #2, "120% LA22yy".

4.6.4.2 Low cycle fatigue analysis of frame in test #2.

To assess the effects that the cumulative ground motions had on the failure of the braces, a low cycle fatigue analysis using the rainflow method (Matsuiski and Endo 1969) was performed. Assuming a linear distribution of strains along each brace, an interpolated value for the strains at the midpoint was obtained. Next, the history of strains for all ground motions of Test #2 were considered. Each history was re-arranged such that the cycles of similar amplitude were grouped together. The procedure (Nieslony 2003) obtains the average amplitude and number of times this cycle was repeated. Finally, a damage index for each test is calculated if the amplitude exceeds the yielding strain. The index is calculated with the formula developed by Boller et al. (Boller and Seeger 1987).

$$\frac{\Delta\varepsilon_p}{2} = 0.103 \cdot \left(2 \cdot N_f\right)^{-0.384} \tag{4.1}$$

where ε_p denotes plastic strains and N_f is the number of cycles to failure.

Because the tests were performed consecutively, the damage index is accumulated each time. The total number of inelastic cycles of each test was also added to find the total number of cycles needed for the brace to fail.

Results are shown in Table 4–6. At the end of "120% LA22yy", the cumulative damage index for the east brace is 0.9, very close to failure (failure = 1.0). These results are approximate since there is no certainty that the strains vary linearly in a segment where the section becomes plastic. However, from the analysis it can be concluded that it required only 7.5 cycles for the brace to fail.

Table 4–6: Low cycle fatigue analysis for Test #2.

Ground Motion	West brace			East brace		
	Number of damaging cycles	Cumulative number of damaging cycles.	Cumulative Damage Index	Number of damaging cycles	Cumulative number of damaging cycles.	Cumulative Damage Index
30%	0	0	0	0	0	0.0
80%	1	1	0.0002	1	1	0.0024
100%	2	3	0.1003	4	5	0.1068
120%	2	5	0.4805	2.5	7.5	0.9042

Lee and Goel (Lee and Goel 1987) developed a formula to calculate the theoretical fracture life Δ_f of a member. The meaning of Δ_f is not the number of cycles but is a parameter that depends on the strain history in a normalized hysteresis curve. This formula was developed for tubular braces under static cyclic loading. In a dynamic testing, however, the strain cycles are not necessarily completed which renders the calculation of this parameter very difficult.

Tang and Goel (Tang and Goel 1987) developed a formula to calculate the number of cycles to fracture given the properties of the section:

$$N_f = C_S \frac{\left(b/d\right)\left(KL/r\right)}{\left(\left(b-2t\right)/t\right)^2} = 116 \qquad (4.2)$$

This formula was also derived after static cyclic testing and it is well known that the data presented a large scatter. It can be observed that the total number of cycles predicted by this formula is much larger than the number of inelastic cycles the brace experienced.

4.6.5 Lessons and recommendations from test #2

The most important observation from Test #2 is the development of the expected "zipper mechanism" under dynamic loads. The frame behaved as expected: the restraint kept the beam straight and this fact made possible the engagement of the 2nd floor "zipper column" as early as in the first attempt of "30% LA22yy". The 3rd floor "zipper column" helped to resist the vertical unbalanced force coming from the first floor and was engaged (with a small amount of force) since "30% LA22yy". Therefore an important part of the vertical force is transmitted to the third floor braces. The beams at the 1st and 2nd level moved downwards when the braces at their respective levels buckle. And, although the 1st floor beam was rotated at the end of Test #2, it is possible that the rotations occurred only during the last sequence.

Test #2 proved that a correctly restrained beam ensures the development of the "zipper mechanism". However, Test #2 did not explain the results of Test #1. Therefore, another test was scheduled to repeat Test #1, providing a more complete instrumentation, as in Test #2.

4.7 Test #3

4.7.1 Description of frame details

The frame in Test #3 was built subsequently to the fabrication of the frames used in Test #1 and Test #2. Thus, special attention was paid to details. The 1st floor brace to beam gusset plate was constructed with the originally specified notch (see Figure 4–7, left).

No lateral restraint was provided during Test #3 to replicate Test #1.

4.7.2 Instrumentation

Test #3 used the same instrumentation distribution and names of channels as in Test #2. Only 2 more potentiometers were added to measure the beams' rotations.

4.7.3 Test portocol

As in Test #1 and Test #2, the ground motion for Test #3 was LA22yy. The sequence applied was: "30% LA22yy", "80% LA22yy", "100% LA22yy", "120% LA22yy", "140% LA22yy" and "160% LA22yy", as explained in section 4.5.3.

4.7.4 Test results

4.7.4.1 Test observations and data processing

During the "30% LA22yy", the frame remained elastic, as expected. During the "80% LA22yy", both braces of the first floor buckled. It was expected that the "zipper column"' measurements could be small as in Test #1. But, the readings from strain gauges showed that the "zipper column" was engaged and working properly. The Temposonic transducers measuring the vertical movement of the 1st floor beam showed that it moved downward, as expected. Forces transmitted to the 2nd floor level were not sufficiently large, so that the braces remained elastic. The third story "zipper column" was also engaged with some of the load which developed in the second story "zipper column".

Analysis of the beam rosettes and bimoment showed that the beam didn't experience a significant torsion.

During the "100% LA22yy", the braces of the 1st floor showed less compression capacity. Consequently, the forces in the "zipper column" were bigger and they triggered out of plane buckling in the 2nd floor. This was reflected in an increased amount of forces in the 3rd story "zipper column". The columns started to yield at the base. There was no sign of yielding in the beams. After the "100% LA22yy", the frame was inspected and it was found to be in very good conditions so the next level ground motion was conducted.

During the "120% LA22yy", the braces of the 1st floor have achieved their compression capacity. Braces at the 2nd floor buckled heavily. Important yielding at the base of the columns and at the beam to column joints was evident

During the "140% LA22yy", the braces showed a behavior very similar to the one exhibited at the "120% LA22yy". Due to the important yielding in tension of both braces, the out of plane displacements were reduced to zero for all the points along the brace. Thus the buckling load in this test was very similar to the one in the previous test. The "zipper mechanism" developed and yielding occurred at the base of the columns and at the beam to column connections. After the "140% LA22yy", the braces of the 1st floor looked damaged and with important permanent deformations, but not cracked. Therefore the next level amplitude was conducted.

During the "160% LA22yy", the west brace of the 1st floor broke in tension. This type of failure was the same as in Test #2. However, at this level, the 1st floor east brace was also severely damaged and the structure remained with an important permanent lateral deformation in the direction of the ground motion.

After "160% LA22yy", the frame was inspected for beam rotations and it was found that the beam did not rotate, although no torsional restraint was provided. The 1st floor brace to beam gusset plate was bent out of plane, however.

Figure 4–14: Picture of the frame's permanent deformation after Test #3, "160% LA22yy".

Figure 4–15: Picture of the beam's rotation (left) and the brace to beam gusset plate deformation (right) after Test #3, "160% LA22yy".

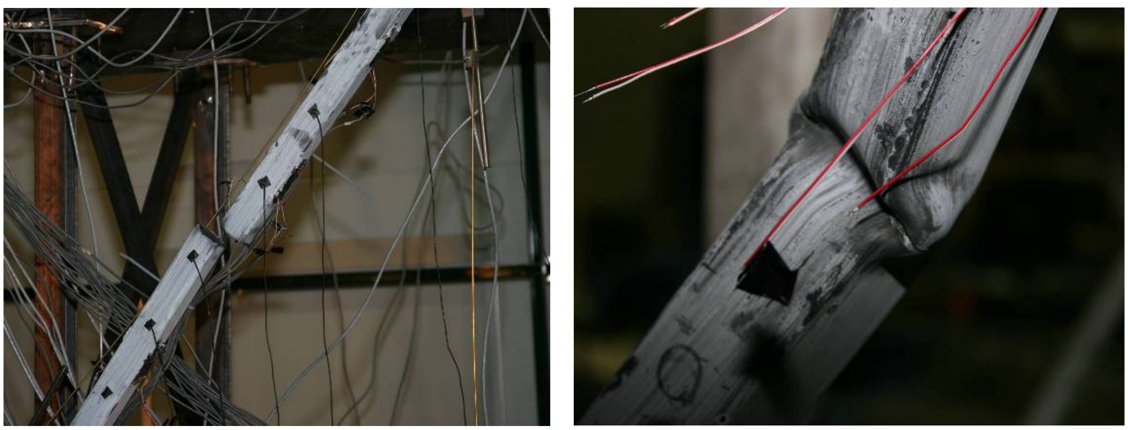

Figure 4–16: Picture of the West brace (left) and East brace (right) after Test #3, "160% LA22yy".

4.7.4.2 Low cycle fatigue analysis

The procedure described in section 2.6.4.2 was applied again to calculate the number of inelastic cycles the frame experienced until failure. In this case, the strain profile along the braces shows that the maximum strains are located around the position of the Set #3. Thus, the axial strains of Set #3 are used in the analysis. The results are shown in Table 4–7. The analysis indicates that the west brace fails at the "160% LA22yy" after 9 inelastic cycles, while the east brace doesn't fail and is subjected to 5.5 inelastic cycles. These results are in complete agreement with the Test observations.

Table 4–7: Low cycle fatigue analysis for Test #3.

Ground Motion	West brace			East brace		
	Number of damaging cycles	Cumulative number of damaging cycles.	Cumulative Damage Index	Number of damaging cycles	Cumulative number of damaging cycles.	Cumulative Damage Index
30%	0	0	0.0	0	0	0.0
80%	0	0	0.0	0.5	0.5	0.0
100%	1	1	0.003	0.5	1	0.005
120%	3	4	0.137	3	4	0.136
140%	4.5	8.5	0.496	1	5	0.615
160%	0.5	9	1.199	0.5	5.5	0.618

4.7.5 Remarks on test #3

The main objective of Test #3 was: to reproduce Test #1 with better instrumentation, to obtain measurements of the beam' rotations and to find the reason for the absence of the "zipper mechanism" without the lateral restraint of the beams. However, the frame during Test #3 behaved even better than in Test #2, resisting up to 160% PGA of LA22yy while developing the "zipper mechanism". The only difference between the frames in Test #1 and Test #3 was the *notch* in the 1st floor brace to beam gusset plate.

It should be noted that the notch reduces the out of plane stiffness of the gusset plate, allowing the plate to bend inelastically following the movement of the brace without transferring torsion to the beam. On the other hand, a stiff gusset plate behaves more like a rigid link, transmitting most of the out of plane moment as torsion to the beam without much inelastic deformation.

4.8 Remarks and conclusions from the experimental study

Three shake table tests were performed on the "zipper frames". The test setup for all tests was the same and the frames were built with the same dimensions and members. Thus, it was expected that the results from the different tests would be similar. However, a small detail in the 1st floor brace to beam gusset plate significantly changed the behavior of the system.

During Test #1 a stiff gusset plate was used with no lateral restraint on the beam. As a result, the beam rotated and yielded in torsion, the “zipper column” was bent out of plane and the “zipper mechanism” was compromised, although it is not possible to conclude that it did not develop entirely.

During Test #2, a stiff gusset plate and a lateral restraint for the beams were used. As a result the “zipper mechanism” developed and the frame behaved as expected until the “120% LA22yy” amplitude test when the east brace broke in tension.

During Test #3, a flexible gusset and no lateral restraint for the beams were used. As a result, the “zipper mechanism” also developed properly and the frame showed larger capacity than in Test #2. The west brace broke in tension at the “160% LA22yy” amplitude test after severe buckling in compression.

From the experimental study it can be concluded that:

4. The “zipper mechanism” can develop as expected if the system is built with adequate details.
5. The system is sensitive to the construction details which may render the system ineffective.
6. If the system is built with sufficient redundancy (such as lateral restraint) the “zipper mechanism” is ensured.
7. The flexibility of the gusset plates connecting braces and beams is an important factor in the development of the “zipper mechanism”.

It should be noted that the tests produced data on 3D buckling in dynamic conditions, as recorded by the coordinate tracking system, Krypton, which uses digital imagery technology.

Finally, all data from this experimental study is available in the NEES repository: https://central.nees.org/.

SECTION 5
ANALYTICAL EVALUATION OF THE PROPOSED FORMULATION

5.1 Introduction

The main objective of the following analysis is to verify that the new formulation is capable to analyze the structural models (such as the "zipper frame") and it is sufficiently sensitive to detect the influence of various parameters consistent with observations from experiments and from structural mechanics theory.

To test the performance of the element developed in Chapter 2, a model of the first story of the zipper frame is built and analyzed. While a full size model would be desirable, due to the high computational demands, a reduced size model was selected to explore the sensitivity of the modeling parameters. The objective of this model is to reproduce the 3D movement of the braces, like the one observed in the experimental work presented in Chapter 4.

The input motion is the 1st story lateral displacements obtained from string potentiometers at the beam level and from the beam axial deformations obtained from strain gauges readings.

The formulation is not capable of modeling a hinge because it cannot condense the rotational DOFs therefore, the connections are assumed fixed. The gusset plates are modeled with an element of equivalent section and material properties - a connection element. Because these properties are very difficult to determine, a bounding analysis is performed to assess the influence of each parameter in the global behavior of the braces. Then, the structure is analyzed with a combination of values for the parameters and the results are compared. In this Chapter, the results of the analysis of the model subjected to the input motion obtained from data of Test #2 are shown.

5.2 Analytical model

The analytical model consists of the 1st floor braces and 1st floor beam (Figure 5–1). The nodes are located at the same places were the sensors of the Krypton tracking system were placed during the experiment. This allows for a direct comparison of the analytical and experimental displacements. The only difference between the model and the experiment are the locations of nodes 2 and 8. In the model, they define the boundary between the gusset plate and the brace when the brace buckles out of plane. In the experiment node 2 is located in the middle of the gusset plate and node 8 is in the brace at the boundary with the gusset plate.

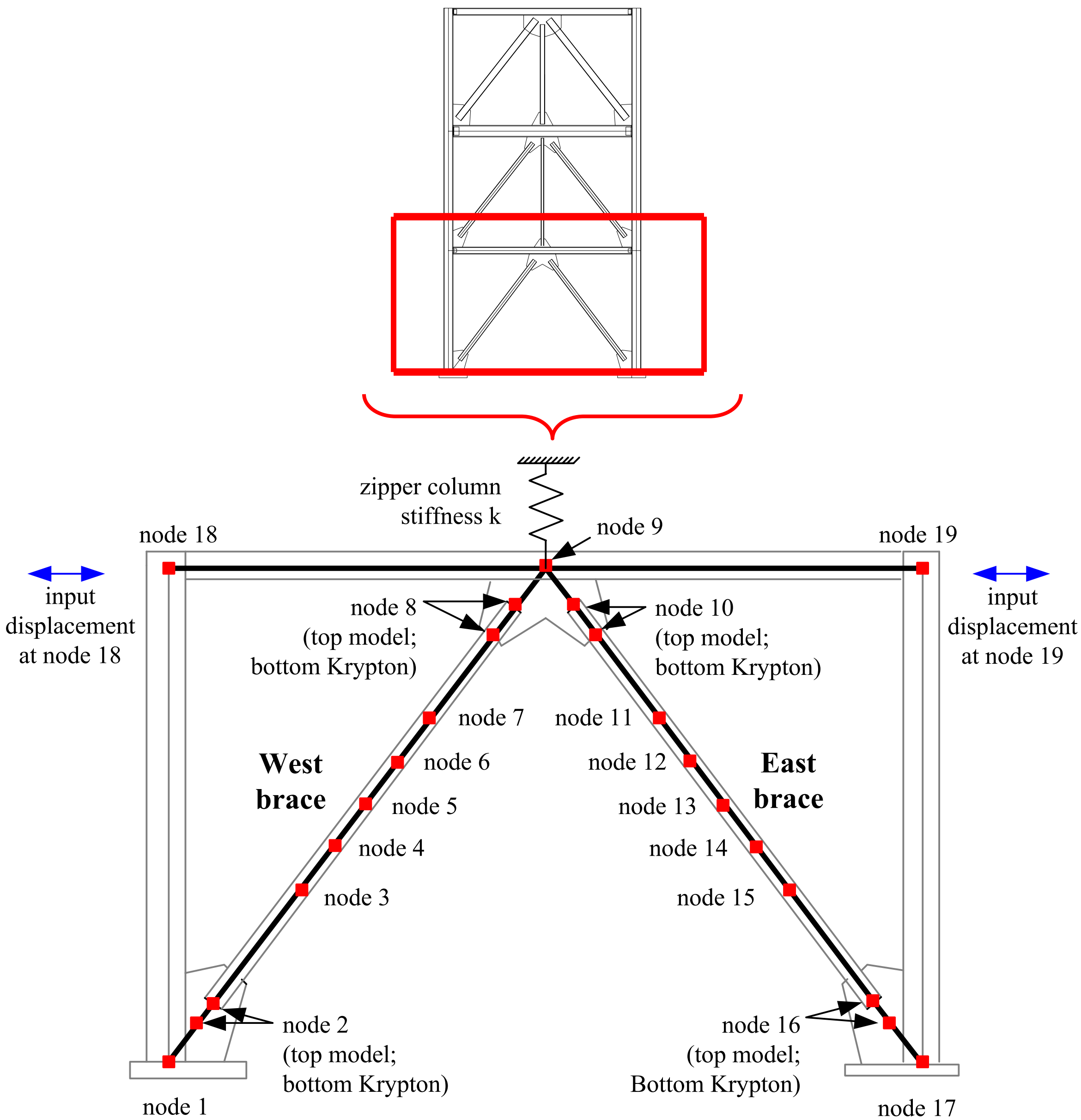

Figure 5–1: Schematic of model (black line) and node location (red dots).

Thus, there are 8 nodes and 8 elements per brace. The beam is described with 3 nodes and 2 elements. Ten integration points are used in each element. The material properties of the brace and beam were obtained through coupon testing and are detailed in Table **5–1**.

Table 5–1: Material properties per coupon testing.

	Brace	Beam
E (kip/in^2)	29000	29000
σ_y (kip/in^2)	60	50

The equivalent properties of the gusset plate are not known, therefore the same properties of the braces are initially assumed for the connection elements. This model, called "nominal", serves as a base for comparison in the bounding analysis.

The "zipper column" is modeled with an elastic spring. The assumption of elastic material is appropriate since the column did not yield during testing. The equivalent stiffness of this spring is not known since the column has a flexible boundary at the other end. The nominal axial stiffness of the column when connected rigidly is E A / L = 383 kip/in. However, the column is connected to flexible elements – the 2nd floor beam and braces. These elements are connected in series, thus the equivalent stiffness of the spring is smaller than the nominal stiffness of the "zipper column".

5.3 Analytical Results of test #2

The results of Test #2 are presented in Figure 5–2 to Figure 5–4. Although the displacements of all internal nodes can be compared, the boundary and the middle nodes are considered representative of the general behavior of the braces: the middle node allows for a comparison of the maximum in plane and out of plane displacements while the boundary nodes allow for a comparison of the gusset plates' behavior.

Vertical displacements are also important. From the experiment, it is clear that nodes below the buckling point have a positive permanent deformation (move upwards) and nodes above it have a negative permanent deformation (move downwards). In the west brace, node #5 goes upwards because the buckling point is not located exactly in the middle of the brace. In both braces, node #2 experiences the largest vertical vibration and it remains with no permanent deformation at the end of motion.

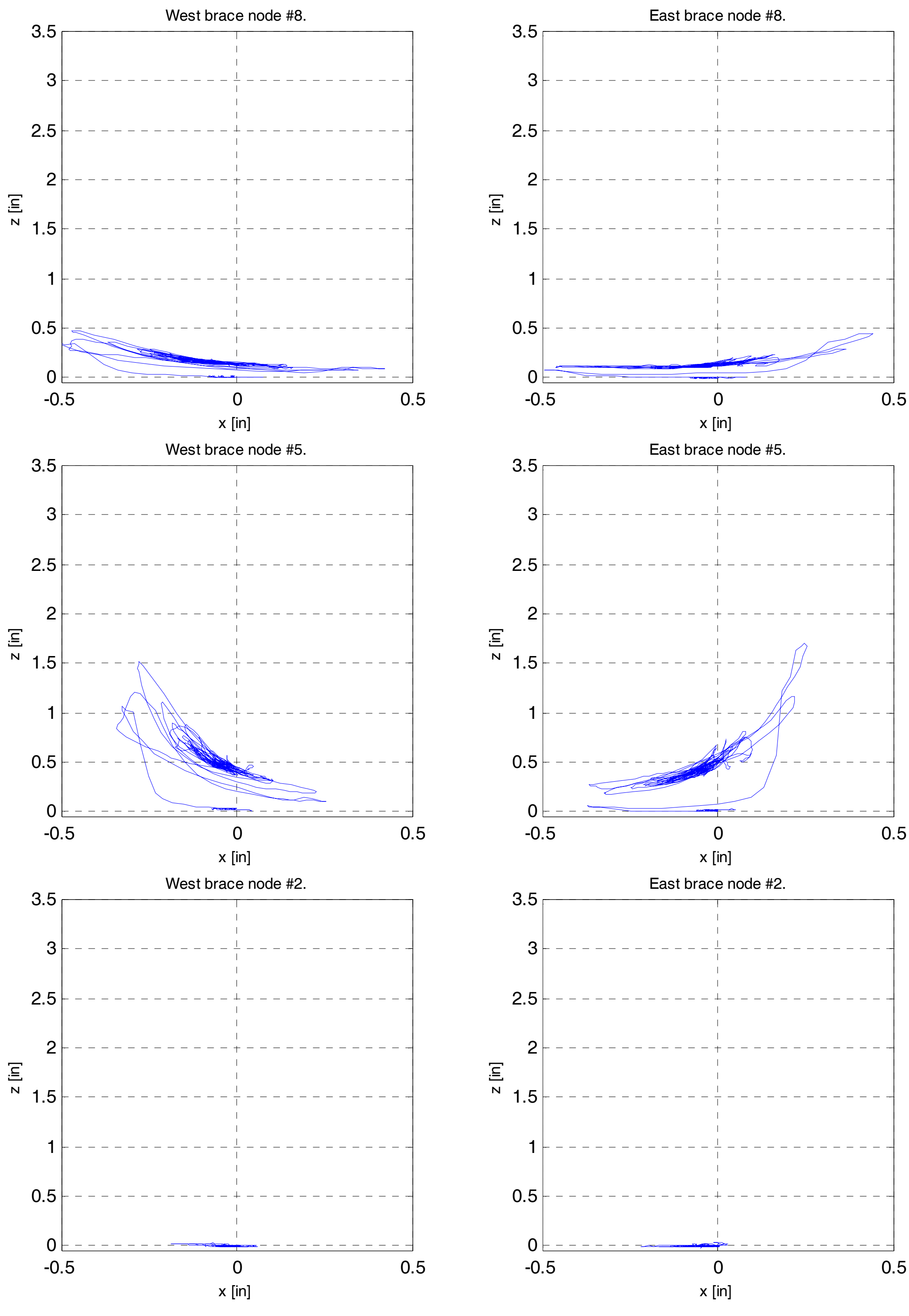

Figure 5–2: In plane (x) vs. out of plane (z) displacement at top (node 8), middle (node 5) and bottom (node 2) from Test #2 "80% LA22yy".

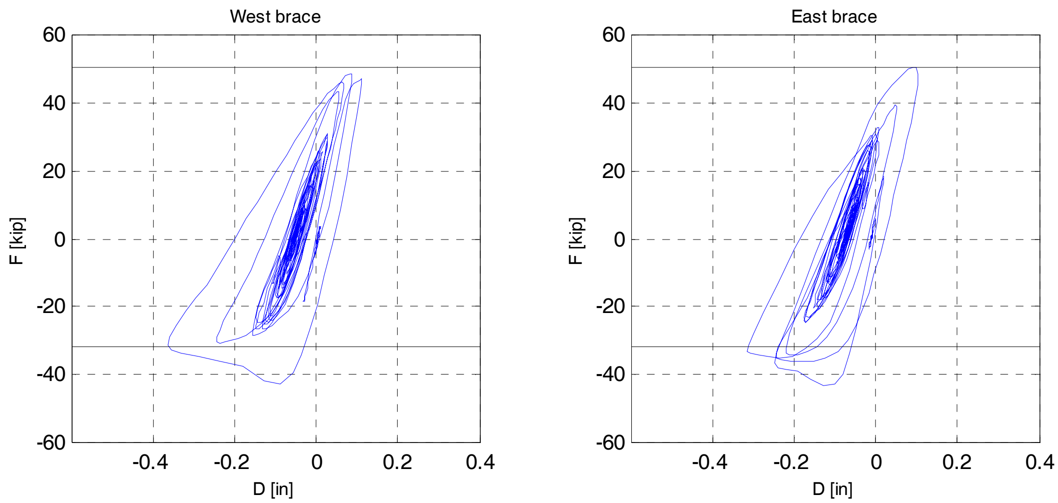

Figure 5–3: Hysteresis loops of west brace (left) and east brace (right) from Test #2, "80% LA22yy". Limits for actual yielding force P_y = 50.4 kip and Euler buckling force P_E = -31.77 kip included.

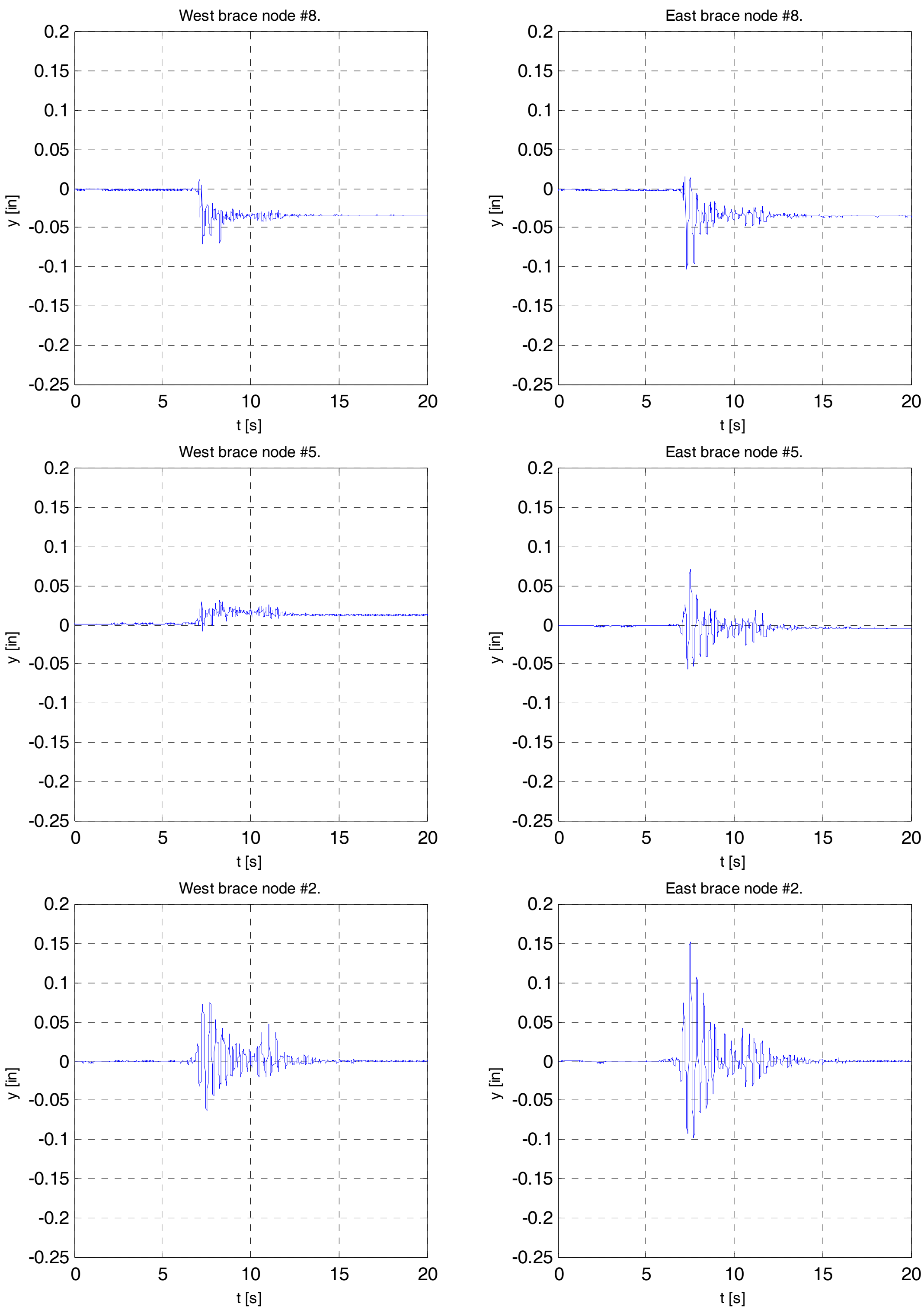

Figure 5–4: Vertical displacements of nodes 8 (top), 5 (middle) and 2 (bottom) for Test #2, “80% LA22yy”.

5.4 Bounding analysis

5.4.1 Connections: variation of the inertia of the connection elements

The inertia of the "nominal" model is assumed as the inertia of the brace's section: $I = 0.486\ in^4$. Two variations were analyzed: a flexible and a rigid connection element. The flexible connection has an assumed inertia ten times smaller than the nominal $I_{flexible} = I/10$, and the rigid connection has an assumed inertia ten times bigger than nominal $I_{rigid} = I\times 10$. The yield function used was HSS. When the inertia is 10 times smaller, the area of the section has to increase at least 10 times, otherwise the capacity of the section is very small compared to the brace and controls the behavior of the complete structure. It is expected that the end moments would be reduced when the gusset plates are more flexible and that the model would approach a hinged behavior. Accordingly, the calculated end moments in the flexible model are smaller than in the nominal model which in turn are slightly smaller than in the rigid model.

Figure 5–5 and Figure 5–6 show the in plane vs. out of plane displacements of node 2, 5 and 8 for west and east brace, respectively. When the connection is more flexible, the maximum out of plane displacements at all nodes increase significantly. Also, the curve becomes smoother and the residual out of plane displacement after buckling is considerably smaller, especially after the first cycle. The connection elements remain elastic, allowing the brace to recover all its out of plane deformation. As a consequence, the buckling loads of the first and second cycles are almost identical in the case of a flexible connection while they are clearly different when the gussets are rigid. This result is consistent with the theory: if the brace yields in tension such that it completely recovers its original out of plane imperfection, its buckling capacity remains unchanged.

From Figure 5–7 and Figure 5–8, it is observed that the value of the buckling load decreases when the connections are more flexible. This is consistent with the fact that stronger boundary conditions improve the capacity of a member to carry axial loads. The theoretical buckling load with hinge connections is 30 kip (see APPENDIX C) and the recorded experimental value is 42 kip, therefore, the gusset plates in the experimental model have some flexibility and do not behave like hinges.

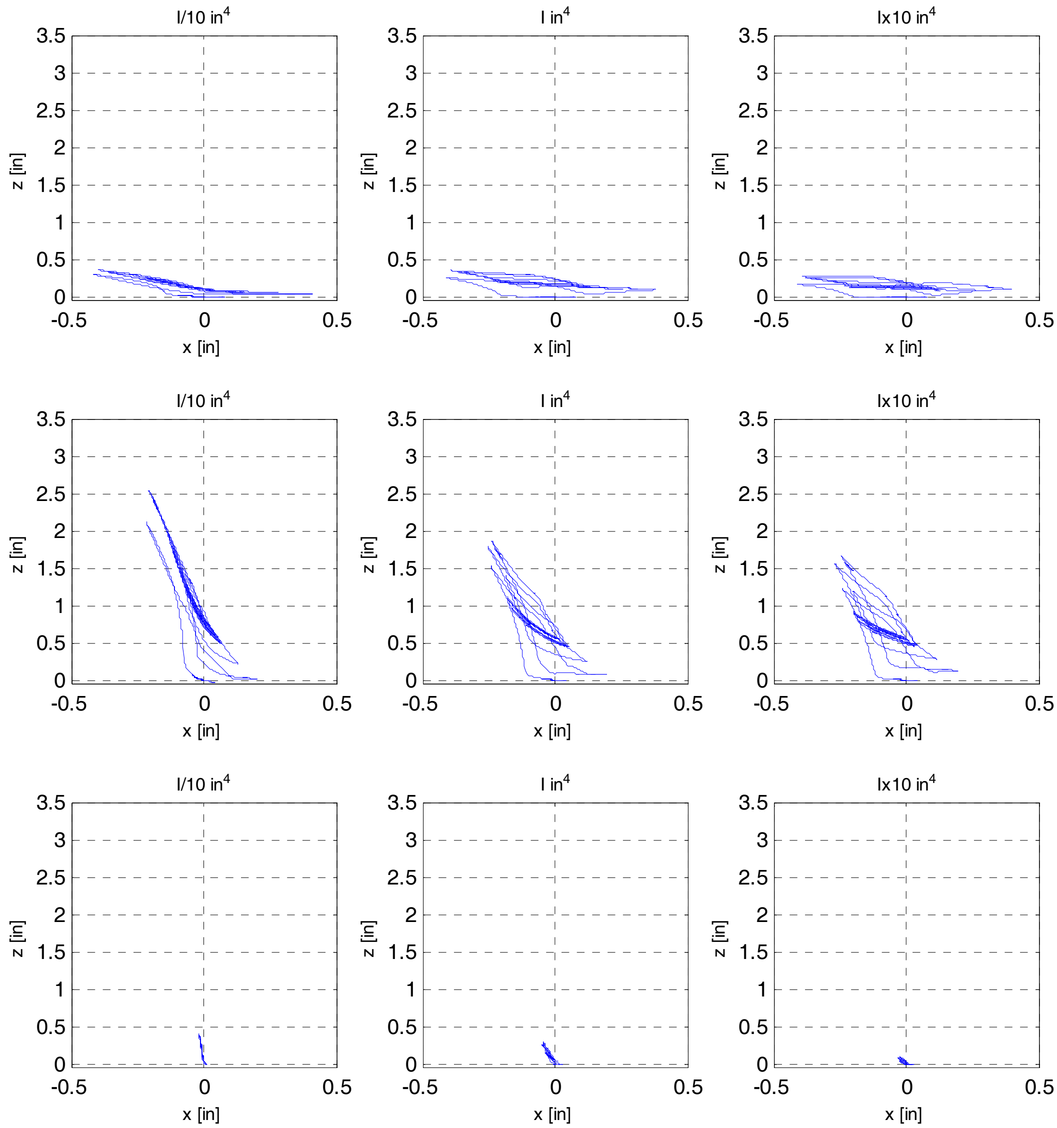

Figure 5–5: Comparison of the in plane (x) vs. out of plane (z) displacement at top (node 8), middle (node 5) and bottom (node 2) of the WEST brace. Flexible gusset plate (left), nominal (center), rigid gusset plate (right).

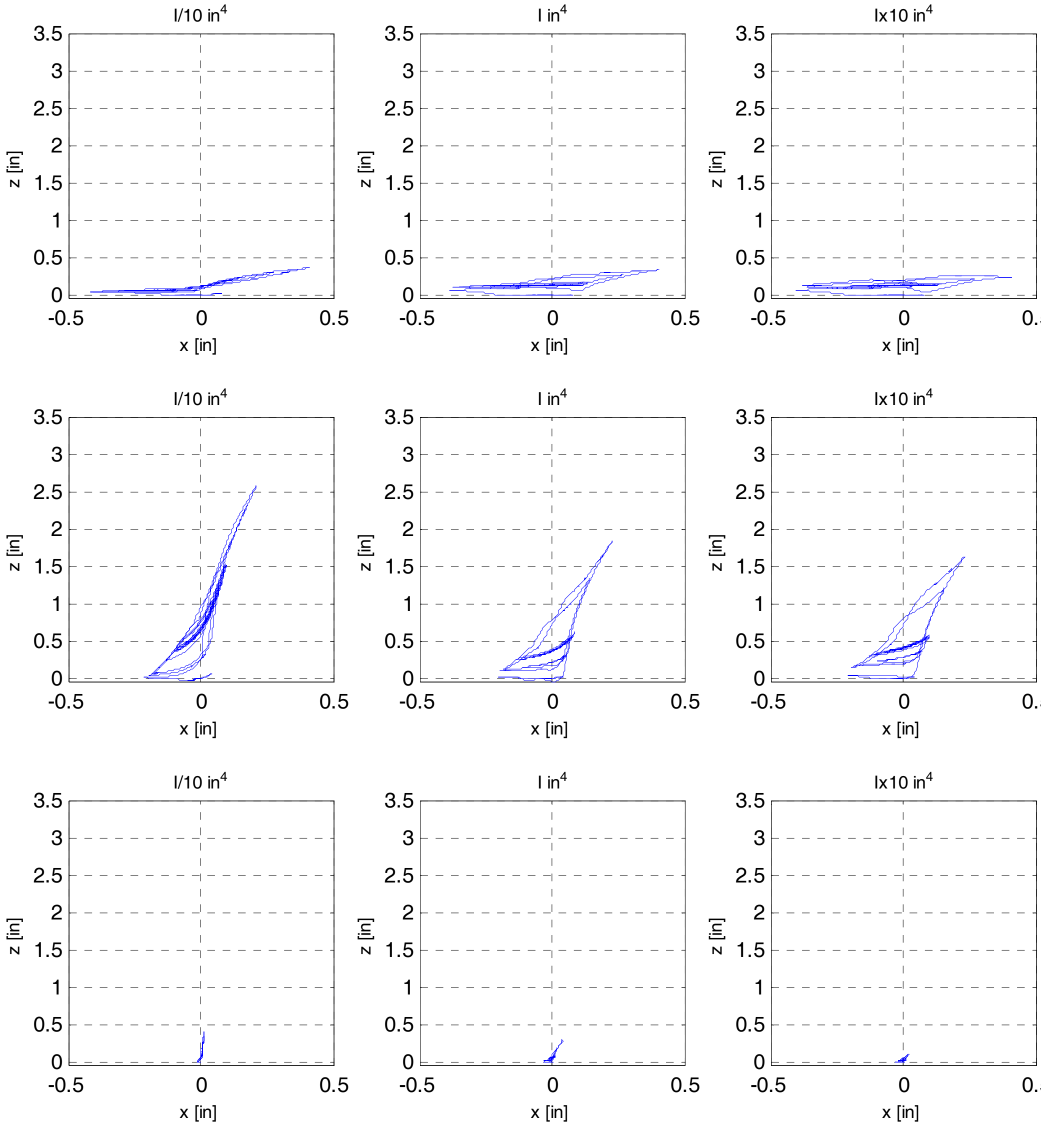

Figure 5–6: Comparison of the in plane (x) vs. out of plane (z) displacement at top (node 8), middle (node 5) and bottom (node 2) of the EAST brace. Flexible gusset plate (left), nominal (center), rigid gusset plate (right).

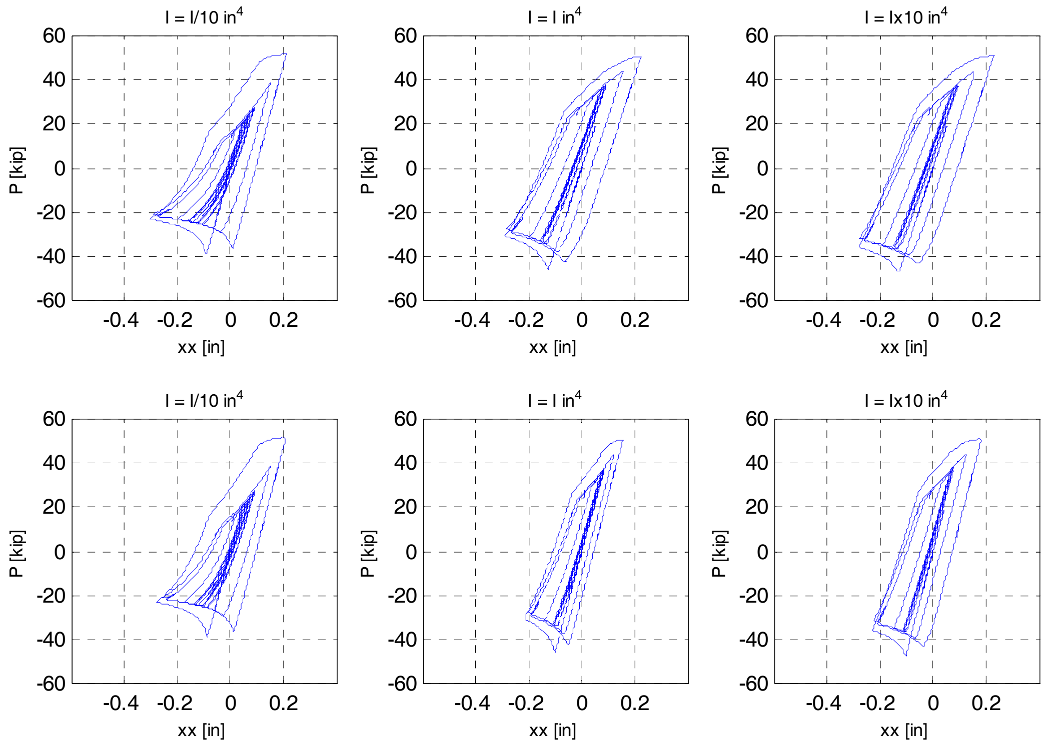

Figure 5–7: Comparison of the hysteresis loops of the WEST brace where the axial displacements considers the gusset plate (top) and does not consider the gusset plate (bottom) Flexible gusset plate (left), nominal value (center), rigid gusset plate (right)

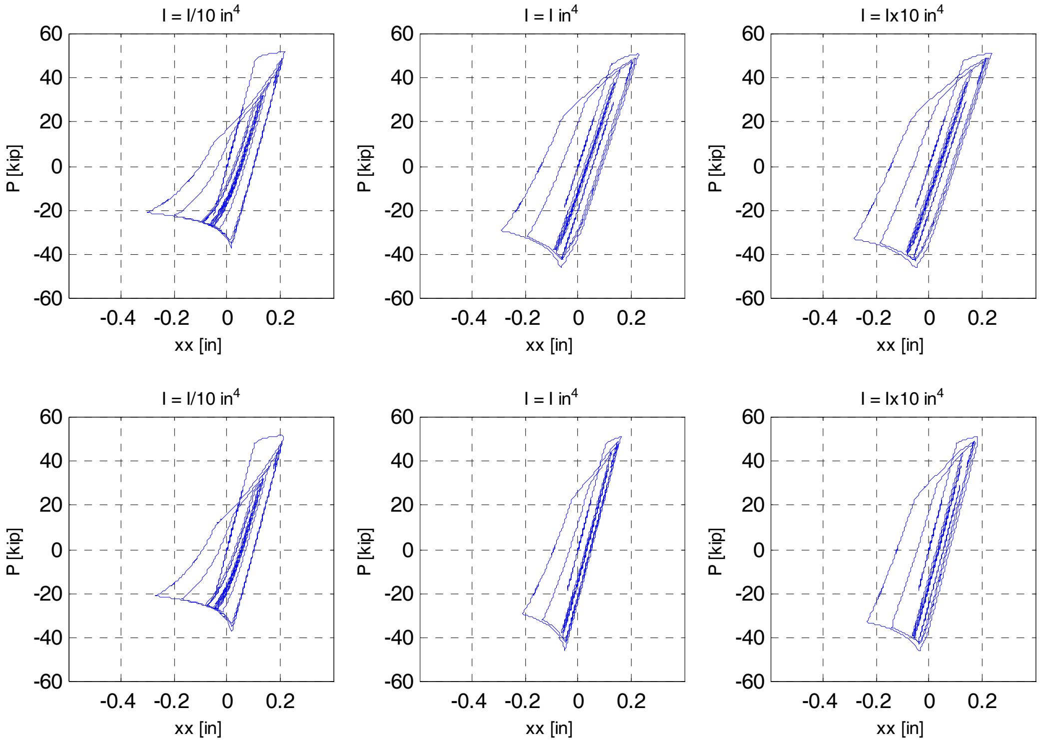

Figure 5–8: Comparison of the hysteresis loops of the EAST brace where the axial displacements considers the gusset plate (top) and does not consider the gusset plate (bottom). Flexible gusset plate (left), nominal value (center), rigid gusset plate (right).

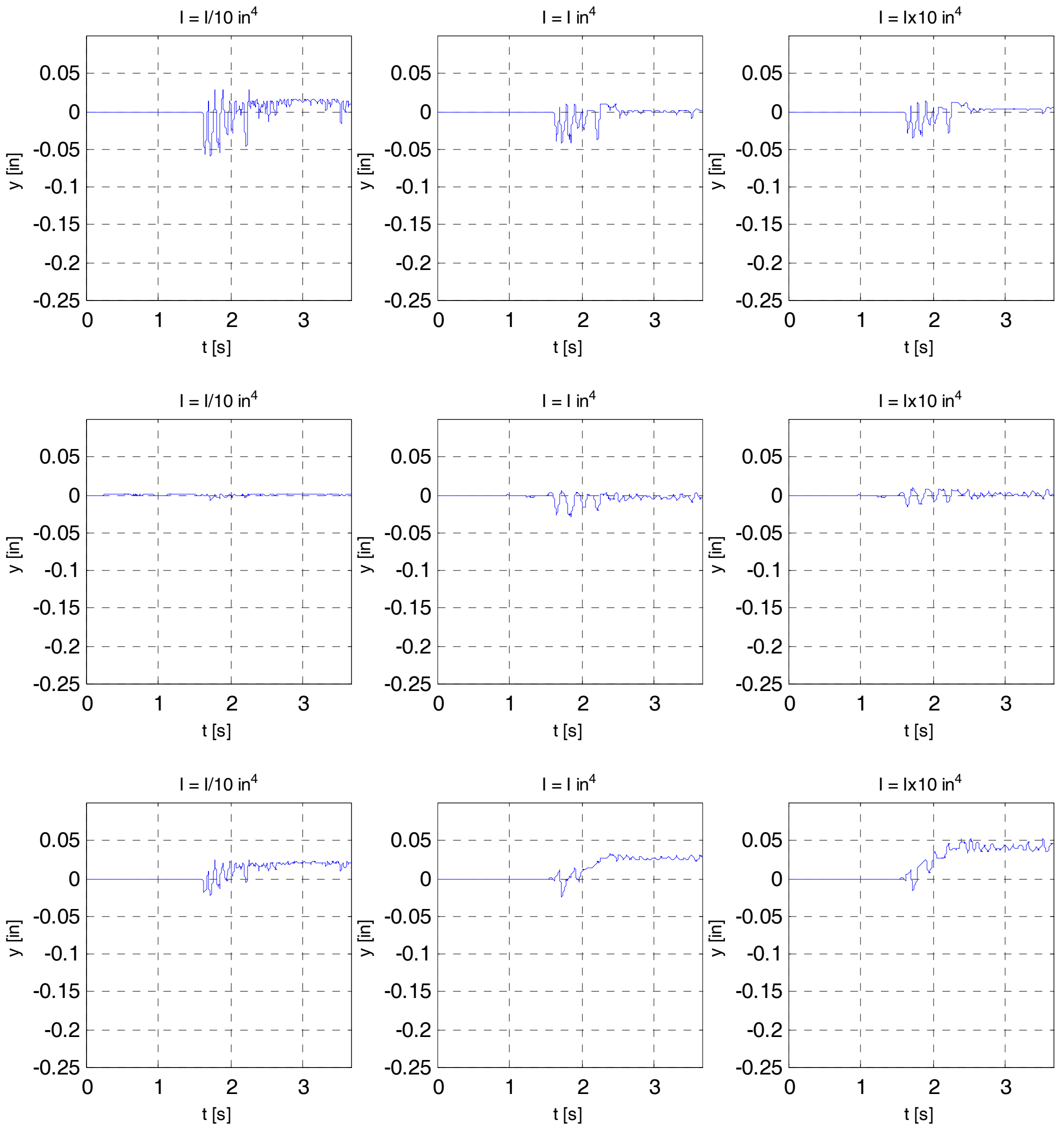

Figure 5–9: Comparison of the vertical displacements at the top (node 8), middle (node 5) and bottom (node 2) of the WEST brace. Flexible gusset plate (left), nominal value (center), rigid gusset plate (right)

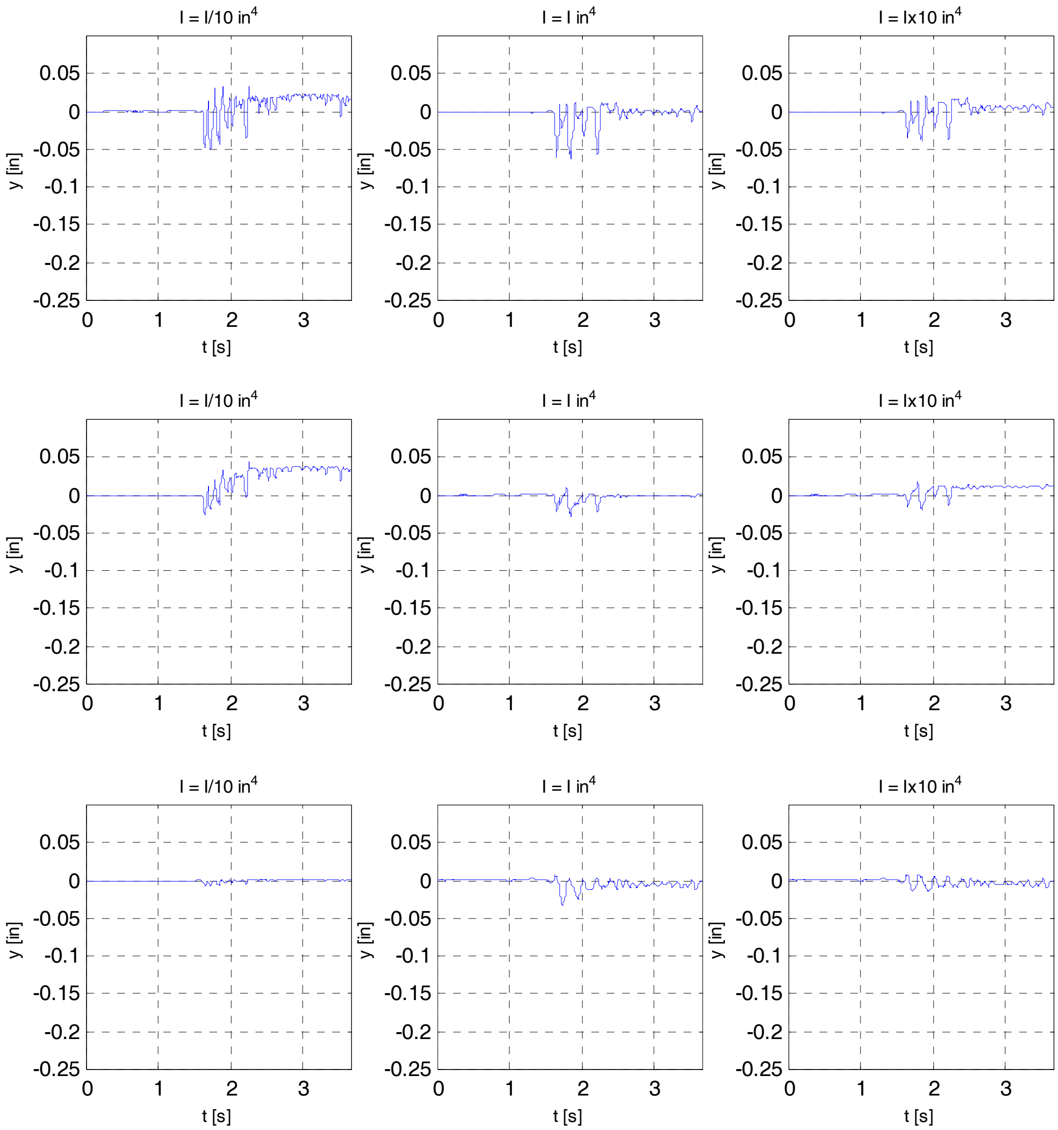

Figure 5–10: Comparison of the vertical displacements at the top (node 8), middle (node 5) and bottom (node 2) of the EAST brace. Flexible gusset plate (left), nominal value (center), rigid gusset plate (right)

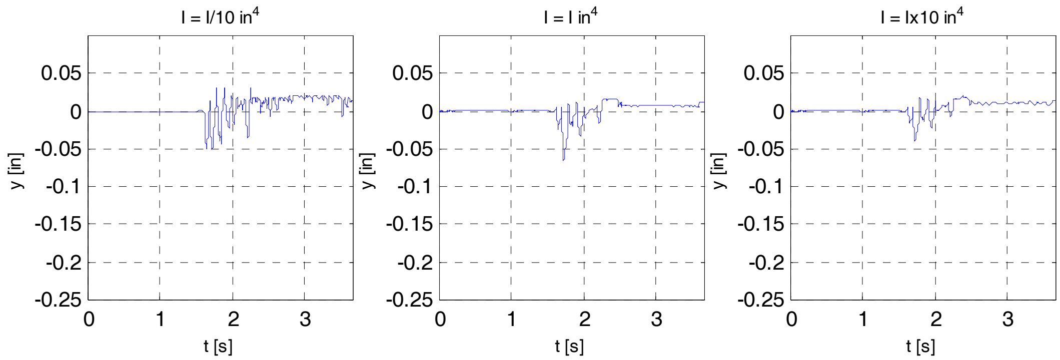

Figure 5–11: Comparison of the vertical displacements of the top node (9). Flexible gusset plate (left), nominal value (center), rigid gusset plate (right)

Comparing the top (brace + connection elements) with bottom (only brace) plots in Figure 5–7 and Figure 5–8, the influence of the flexibility of the gusset plate can be observed. The bottom plots are directly comparable to Figure 5–3, which represents the hysteretic loops of the braces during testing. In this case, the axial deformations are calculated using the Krypton system. It is apparent that when the gusset plates' deformation is considered, the total axial deformation increases. This effect is less important when the connection elements are flexible because they remain elastic. The same effect is observed when the brace is loaded in tension.

Figure 5–10 shows the vertical displacements of node 2, 5 and 8 for the west and east braces and Figure 5–11 shows the vertical displacement of node 9. The maximum values do not match the values of the test, however more importantly nodes 8 and 9 have positive residual displacements. Although the influence of the flexibility of the connection on the vertical displacements is not absolutely clear, the qualitative results match the ones obtained in the experiment.

5.4.2 Gusset plates: variation of the yield strength of the material

Figure 5–12 and Figure 5–13 show the displacements using the new analytical model when the yield strength of the gusset plates changes from 60 kip/in^2 to 36 kip/in^2 and 100 kip/in^2. When the yield strength is small, the braces do not buckle and the out of plane displacements are negligible. On the other hand, when the yield strength is very large, the connection elements remain elastic and the out of plane displacements are smaller than in the nominal case.

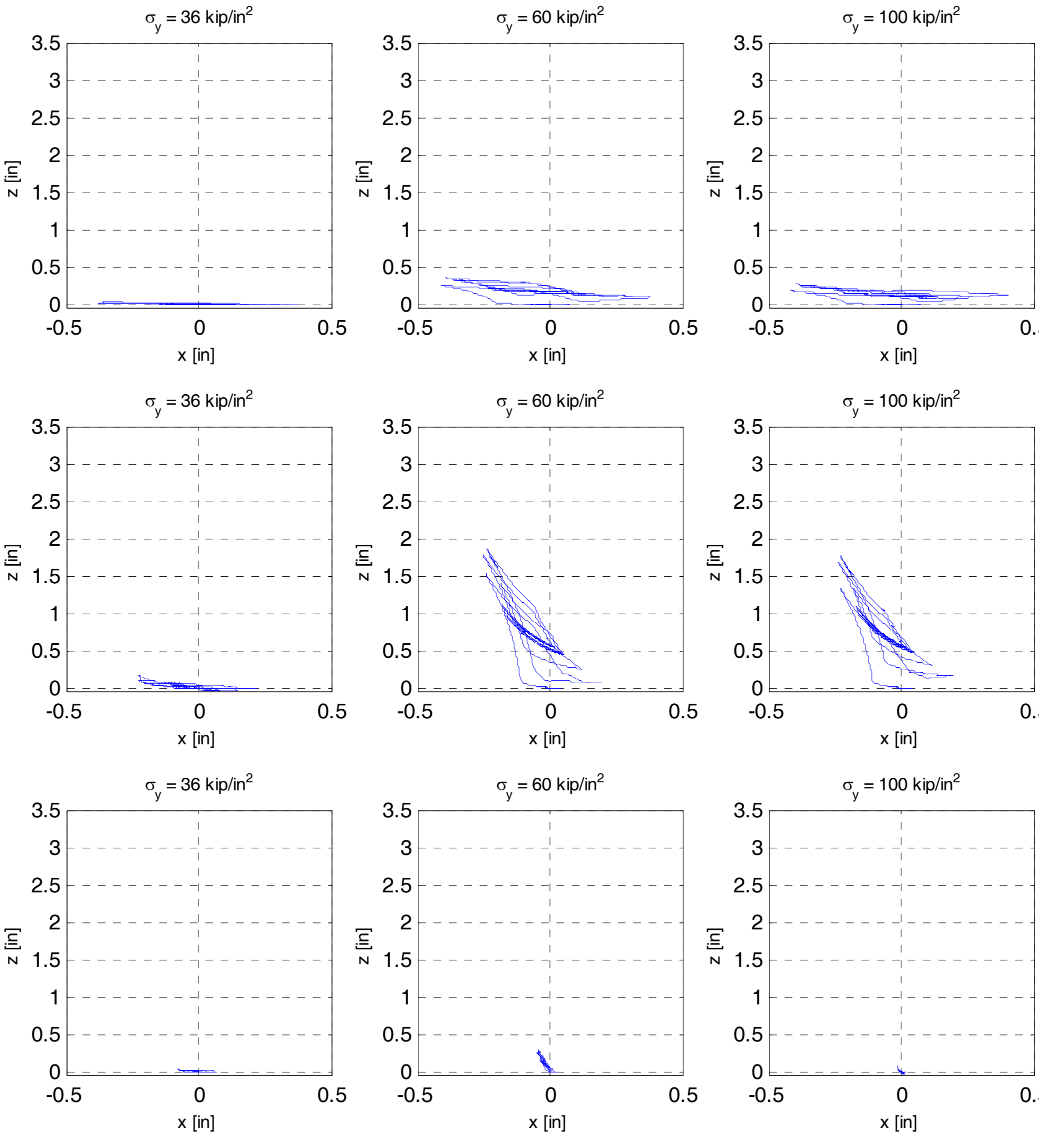

Figure 5–12: Comparison of the in plane (x) vs. out of plane (z) displacement at top (node 8), middle (node 5) and bottom (node 2) of the WEST brace. σ_ψ = 36 kip/in^2 (left), σ_ψ = 60 kip/in^2 (center), σ_ψ = 100 kip/in^2 (right).

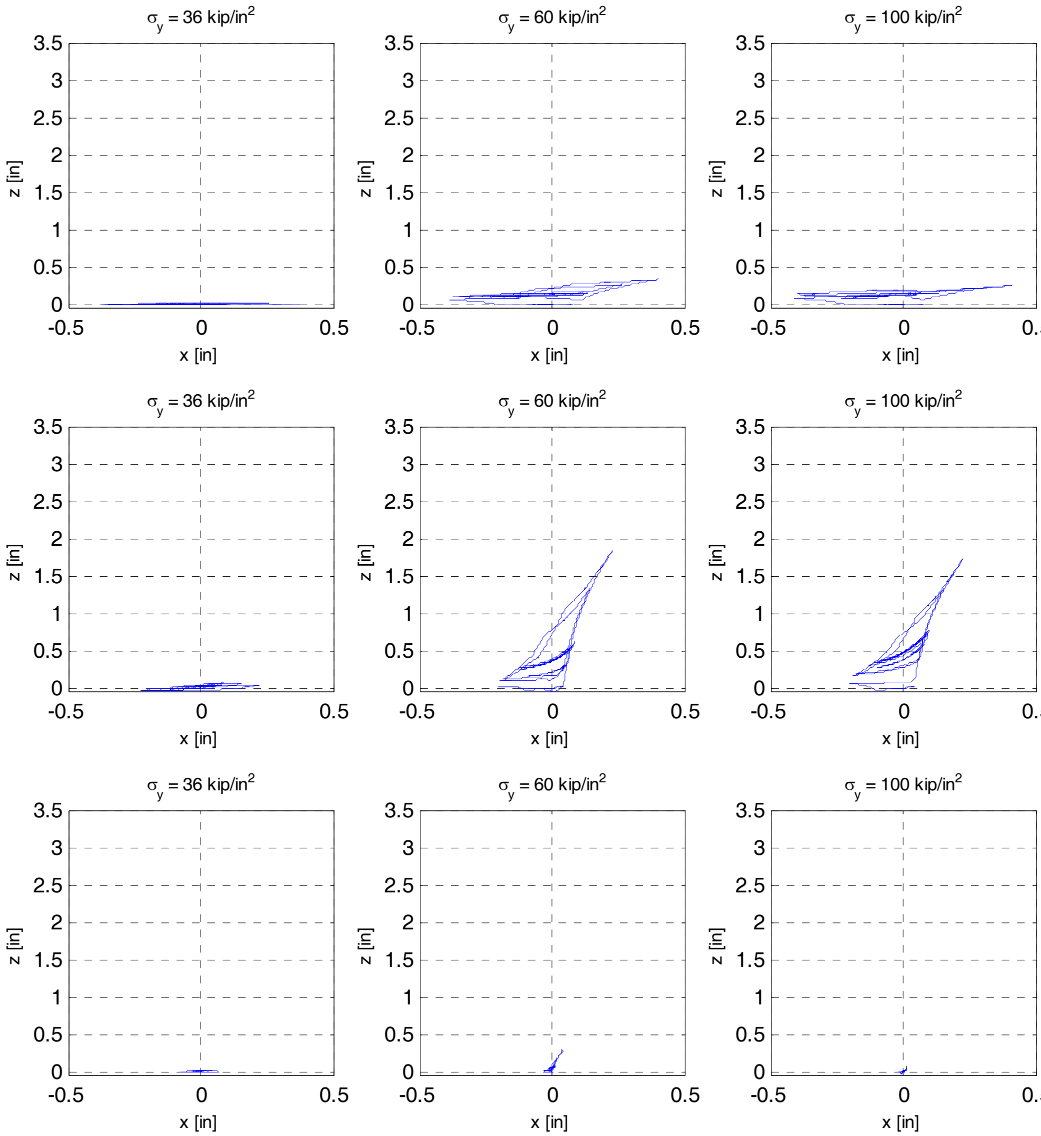

Figure 5–13: Comparison of the in plane (x) vs. out of plane (z) displacement at top (node 8), middle (node 5) and bottom (node 2) of the EAST brace. σ_ψ = 36 kip/in^2 (left), σ_ψ = 60 kip/in^2 (center), σ_ψ = 100 kip/in^2 (right).

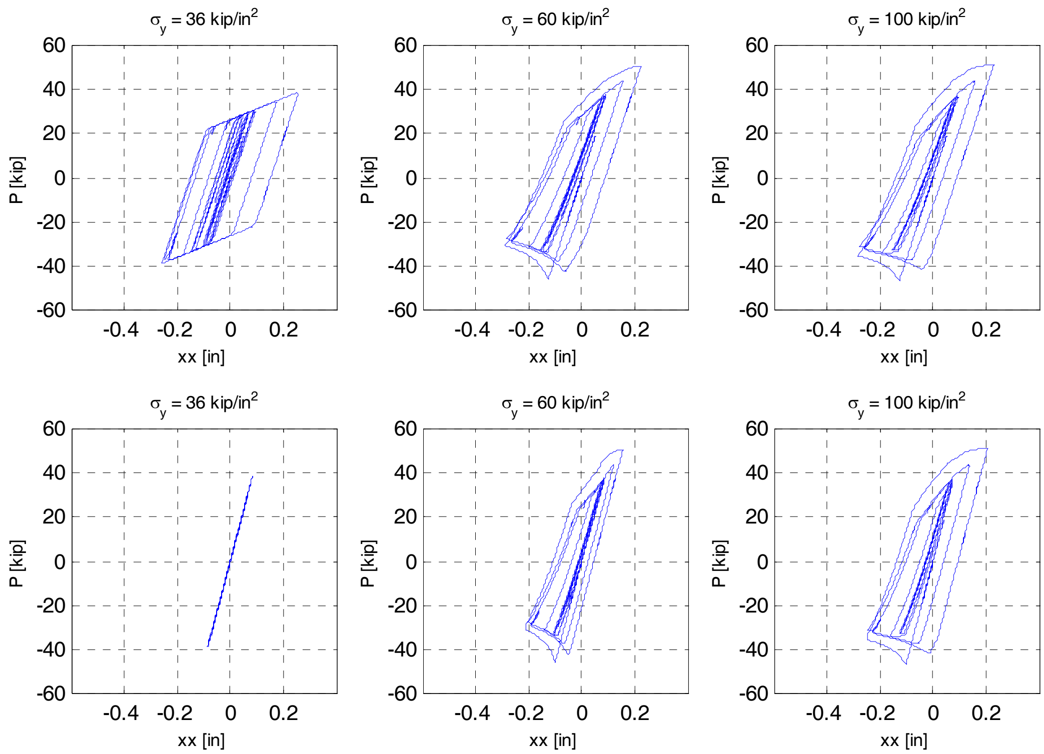

Figure 5–14: Comparison of the hysteresis loops of the WEST brace where the axial displacements considers the gusset plate (top) and does not consider the gusset plate (bottom).
σ_ψ = 36 kip/in^2 (left), σ_ψ = 60 kip/in^2 (center), σ_ψ = 100 kip/in^2 (right).

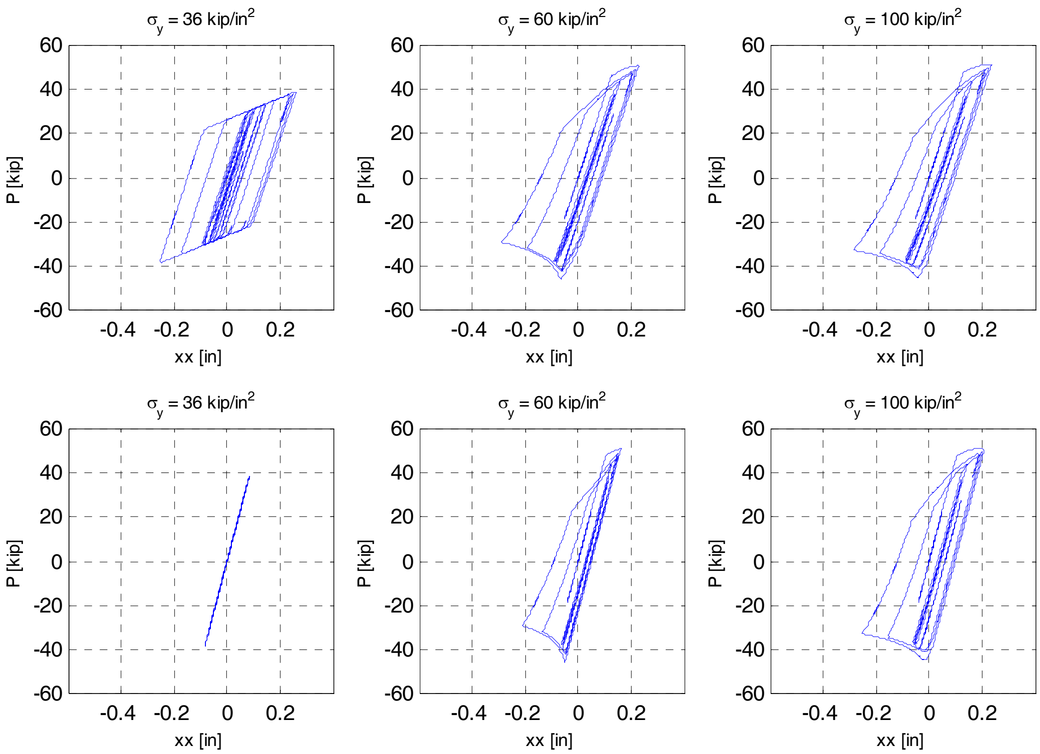

Figure 5–15: Comparison of the hysteresis loops of the EAST brace where the axial displacements considers the gusset plate (top) and does not consider the gusset plate (bottom).
σ_ψ = 36 kip/in^2 (left), σ_ψ = 60 kip/in^2 (center), σ_ψ = 100 kip/in^2 (right).

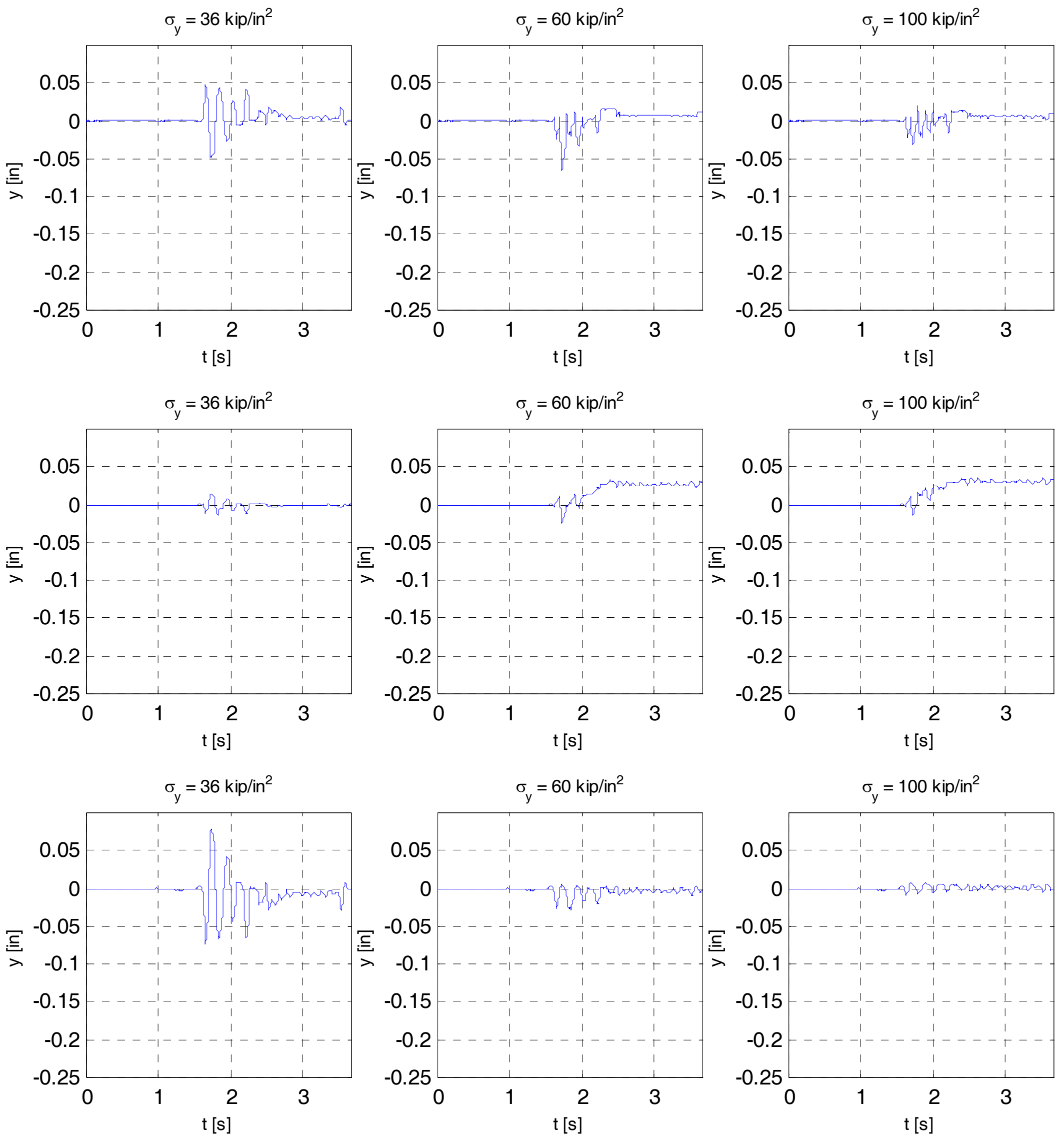

Figure 5–16: Comparison of the vertical displacements at the top (node 8), middle (node 5) and bottom (node 2) of the WEST brace. σ_ψ = 36 kip/in^2 (left), σ_ψ = 60 kip/in^2 (center), σ_ψ = 100 kip/in^2 (right).

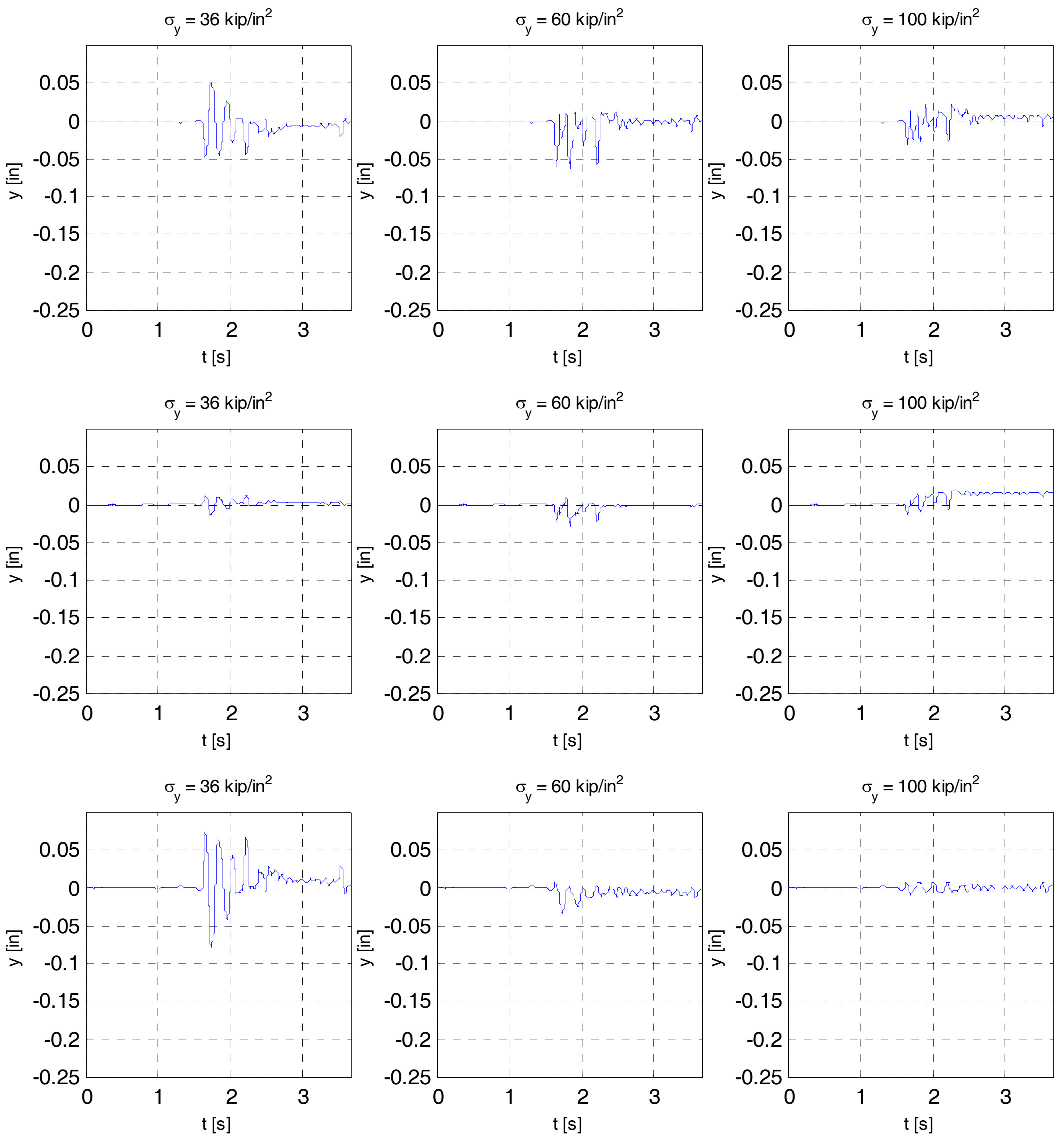

Figure 5–17: Comparison of the vertical displacements at the top (node 8), middle (node 5) and bottom (node 2) of the EAST brace. σ_ψ = 36 kip/in^2 (left), σ_ψ = 60 kip/in^2 (center), σ_ψ = 100 kip/in^2 (right).

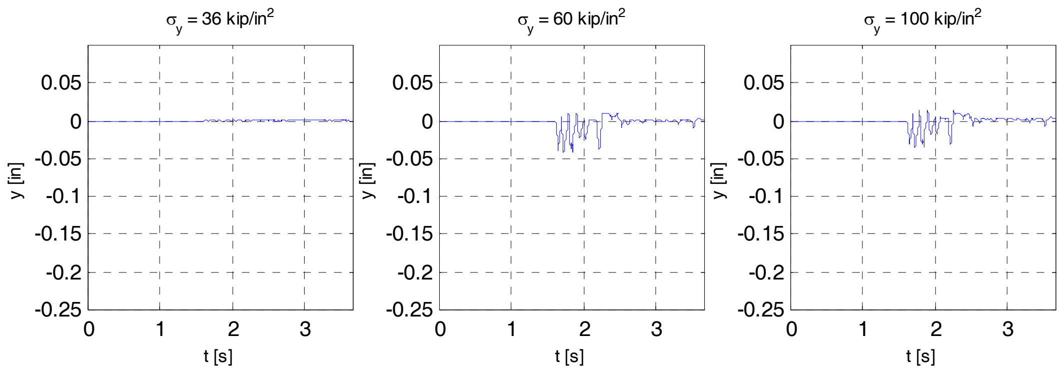

Figure 5–18: Comparison of the vertical displacements of the top node (9).
σ_ψ = 36 kip/in^2 (left), σ_ψ = 60 kip/in^2 (center), σ_ψ = 100 kip/in^2 (right).

Figure 5–14 and Figure 5–15 show the hysteretic curves of west and east braces, respectively. When the yield strength of the connection elements is small, they concentrate all the inelastic deformation while the braces remain elastic, which in turn explains why the brace does not buckle. The section properties are identical to those of the nominal model, however the lower yield strength limits the axial capacity of the braces, which develop a maximum compression force of only 38 kips, smaller than the nominal buckling load (46 kips).

When the yield strength is 100 kip/in^2, the brace concentrates all the inelastic deformation while the connections remain elastic. Thus, the hysteretic loops with and without the connection elements are identical.

Figure 5–16 and Figure 5–17 show the vertical displacements of nodes 2, 5 and 8 for different yield strengths. When a low yield strength is used in the analysis, nodes 2 and 8 (limits of the connection elements) have larger vertical vibrations and when the yield strength is very high, the vibrations are very small. Similar behavior can be observed in Figure 5–18.

In summary, the formulation is capable to predict the relationship between yield strength and plasticity distribution between different elements according to plasticity theories.

The yield strength of the gusset plates in the final model should be similar to the yield strength of the braces. A value between 50 kip/in^2 and 60 kip/in^2 is recommended for further analyses.

5.4.3 Connections: variation of the length of the element

In this case, variations of the properties of the gusset plates need also to be included otherwise the response of the structure is the same as in the nominal case. Only the case where the stiffness of the "zipper column" is nominal and the inertia of the connection elements is half of the nominal value is shown here, as an example. Three lengths are considered: the nominal length of 8 in; a smaller length of 4 in and a longer length of 12 in (See Figure 5–19). Results are presented in Figure 5–20 to Figure 5–26.

Since the inertia of the connection element is smaller than the one of the brace, a longer connection element adds flexibility to the complete system. Thus, it can be observed that the values for the maximum out of plane displacements are bigger, the buckling force is smaller and the permanent vertical displacements are larger.

The differences between the results with long and nominal connection elements are significant, however the results are very similar between the short and nominal length elements. Moreover, if a different inertia is assigned to the connection element, it is possible to obtain significantly different responses when different lengths are assumed. Thus, it is concluded that the inertia and the length of the element have a similar influence in the behavior of the system. Since the braces are more sensitive to the inertia, the element length is not considered further in this analysis.

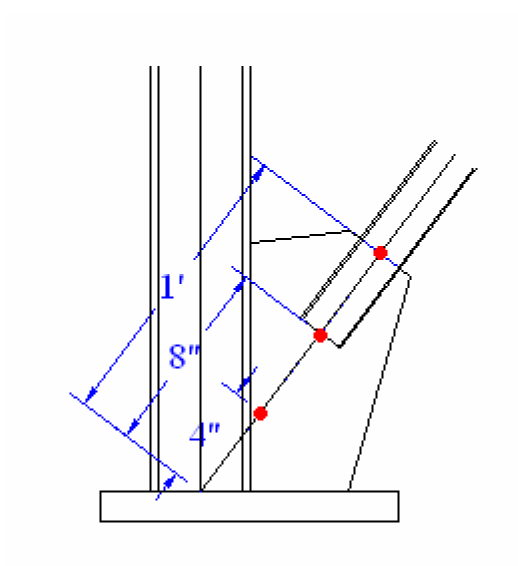

Figure 5–19: Sketch of gusset plate lengths.

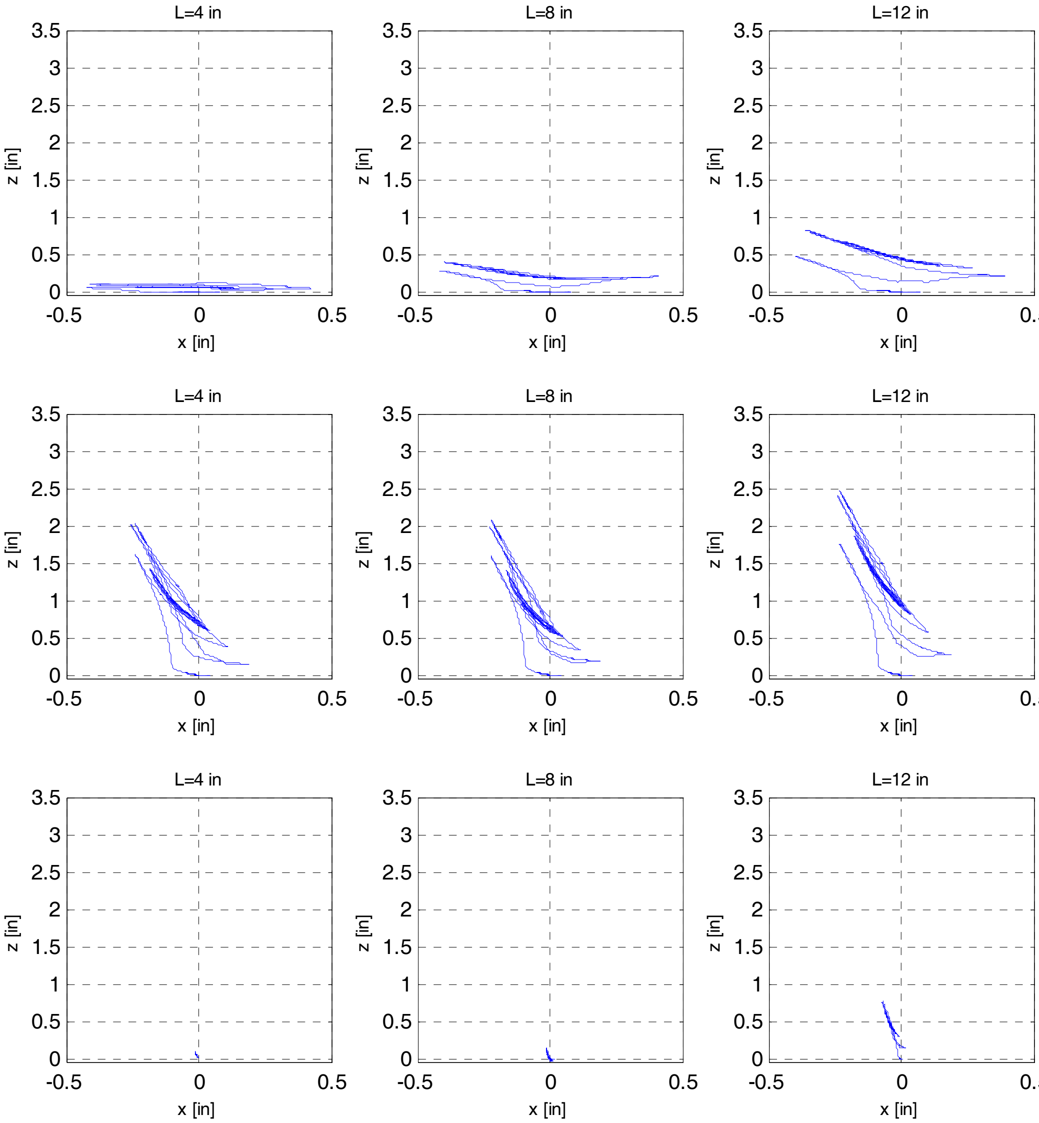

Figure 5–20: Comparison of the in plane (x) vs. out of plane (z) displacement at top (node 8), middle (node 5) and bottom (node 2) of the WEST brace.
Small connection element (left), nominal (center), Large connection element (right).

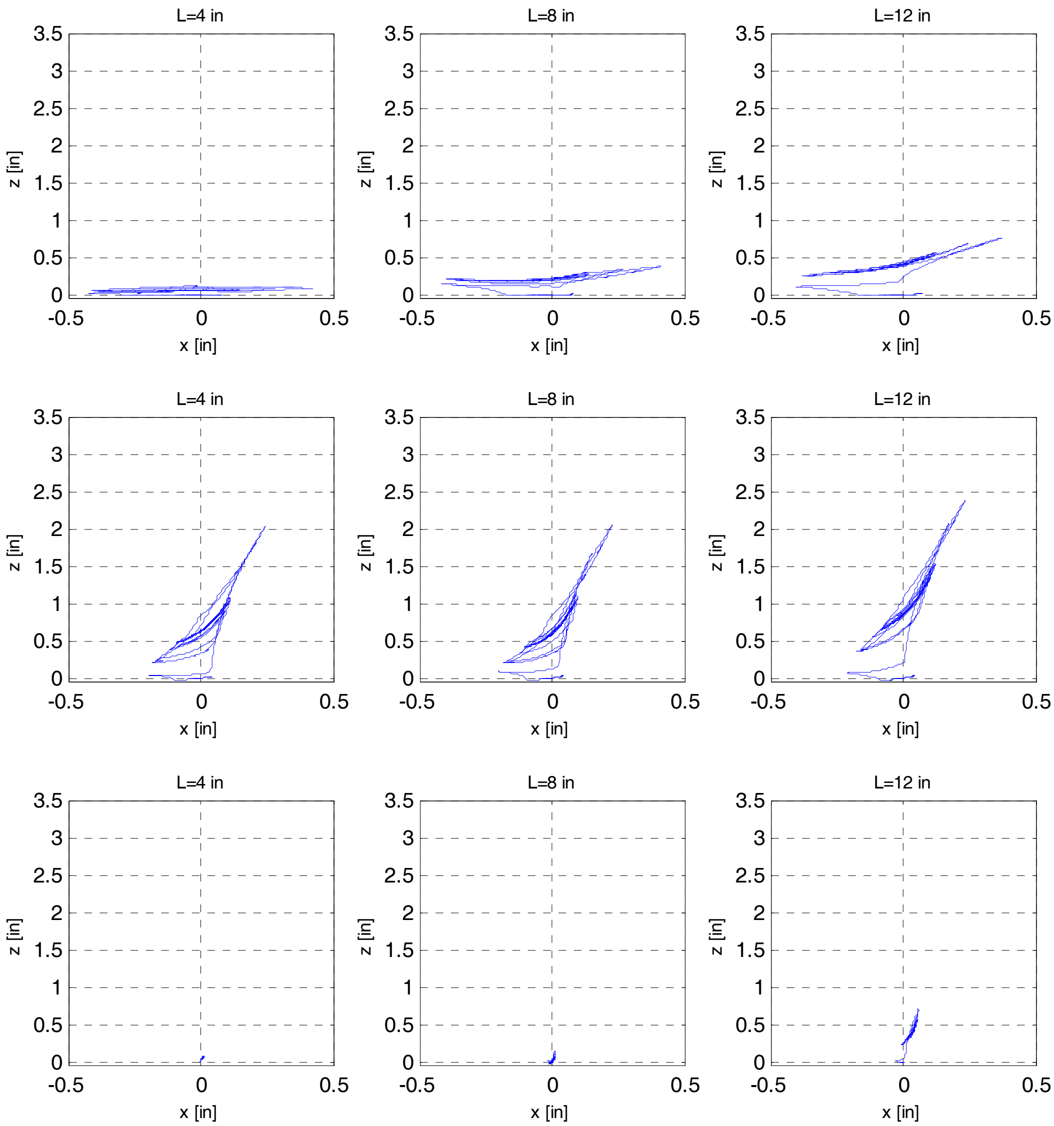

**Figure 5–21: Comparison of the in plane (x) vs. out of plane (z) displacement at top (node 8), middle (node 5) and bottom (node 2) of the EAST brace.
Small connection element (left), nominal (center), Large connection element (right).**

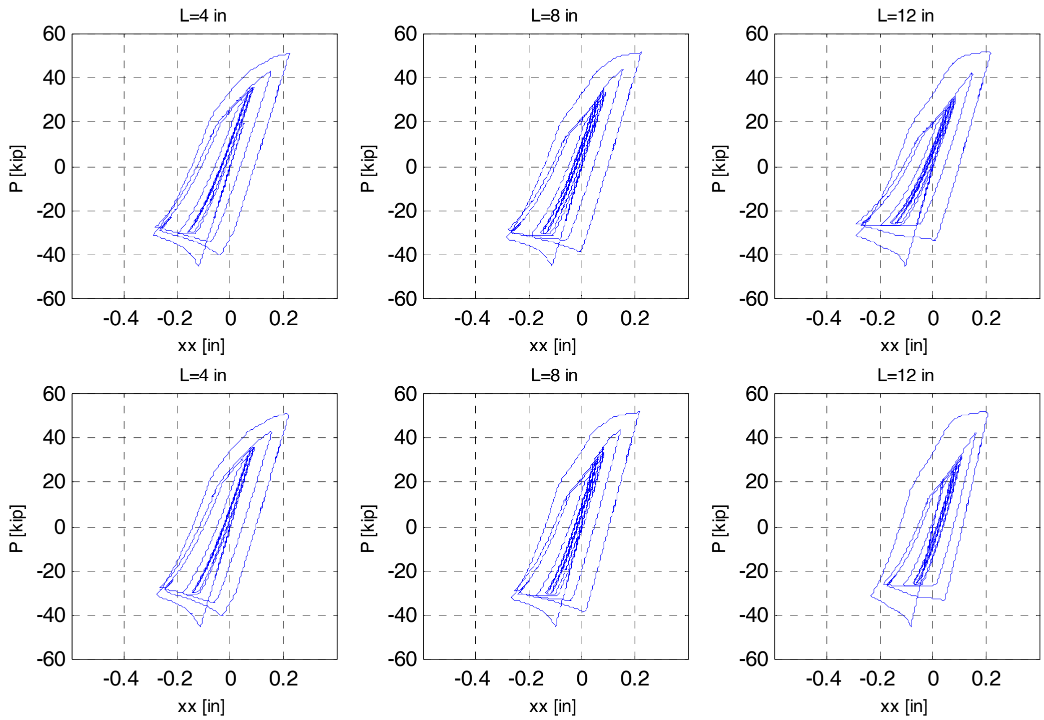

Figure 5–22: Comparison of the hysteresis loops of the WEST brace where the axial displacements considers the gusset plate (top) and does not consider the gusset plate (bottom). Small connection element (left), nominal (center), Large connection element (right).

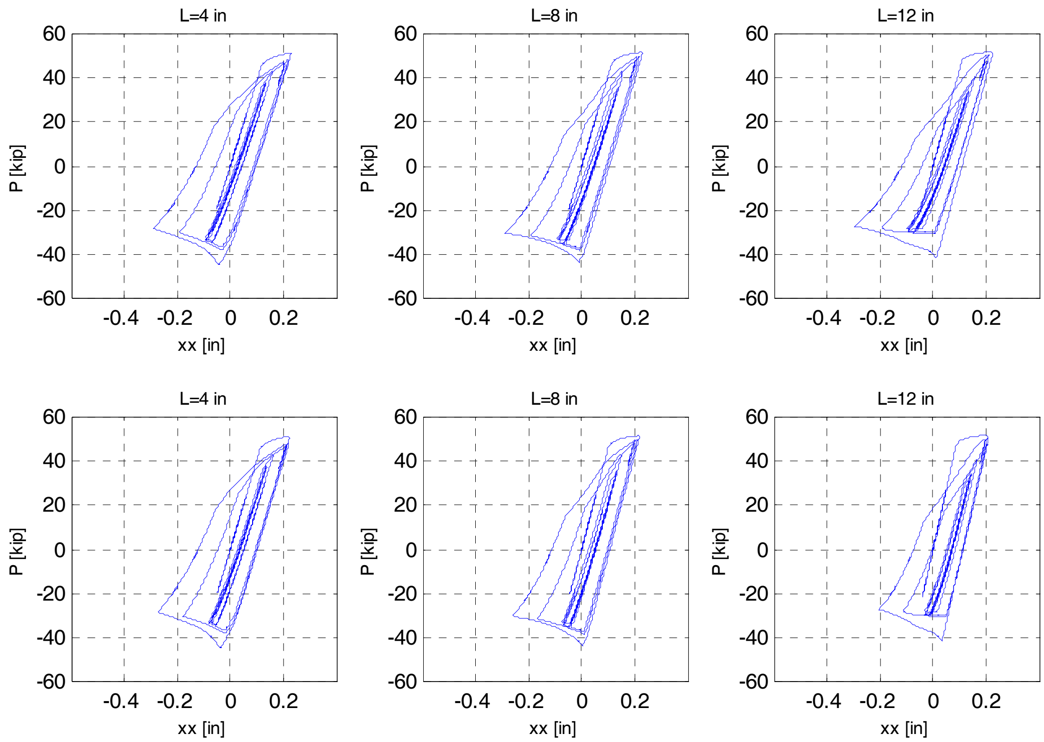

Figure 5–23: Comparison of the hysteresis loops of the EAST brace where the axial displacements considers the gusset plate (top) and does not consider the gusset plate (bottom). Small connection element (left), nominal (center), Large connection element (right).

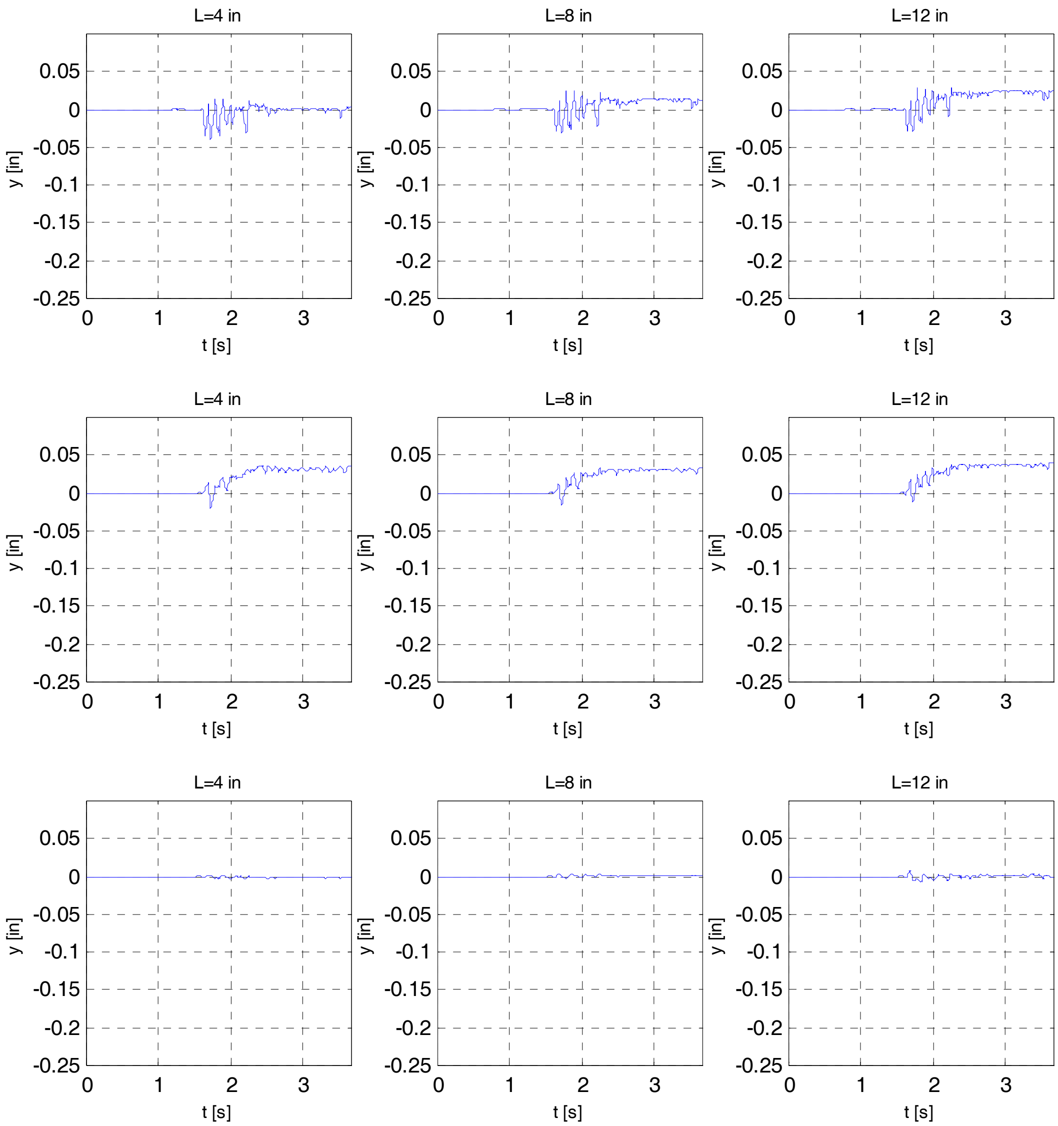

Figure 5–24: Comparison of the vertical displacements at the top (node 8), middle (node 5) and bottom (node 2) of the WEST brace. Small connection element (left), nominal (center), Large connection element (right).

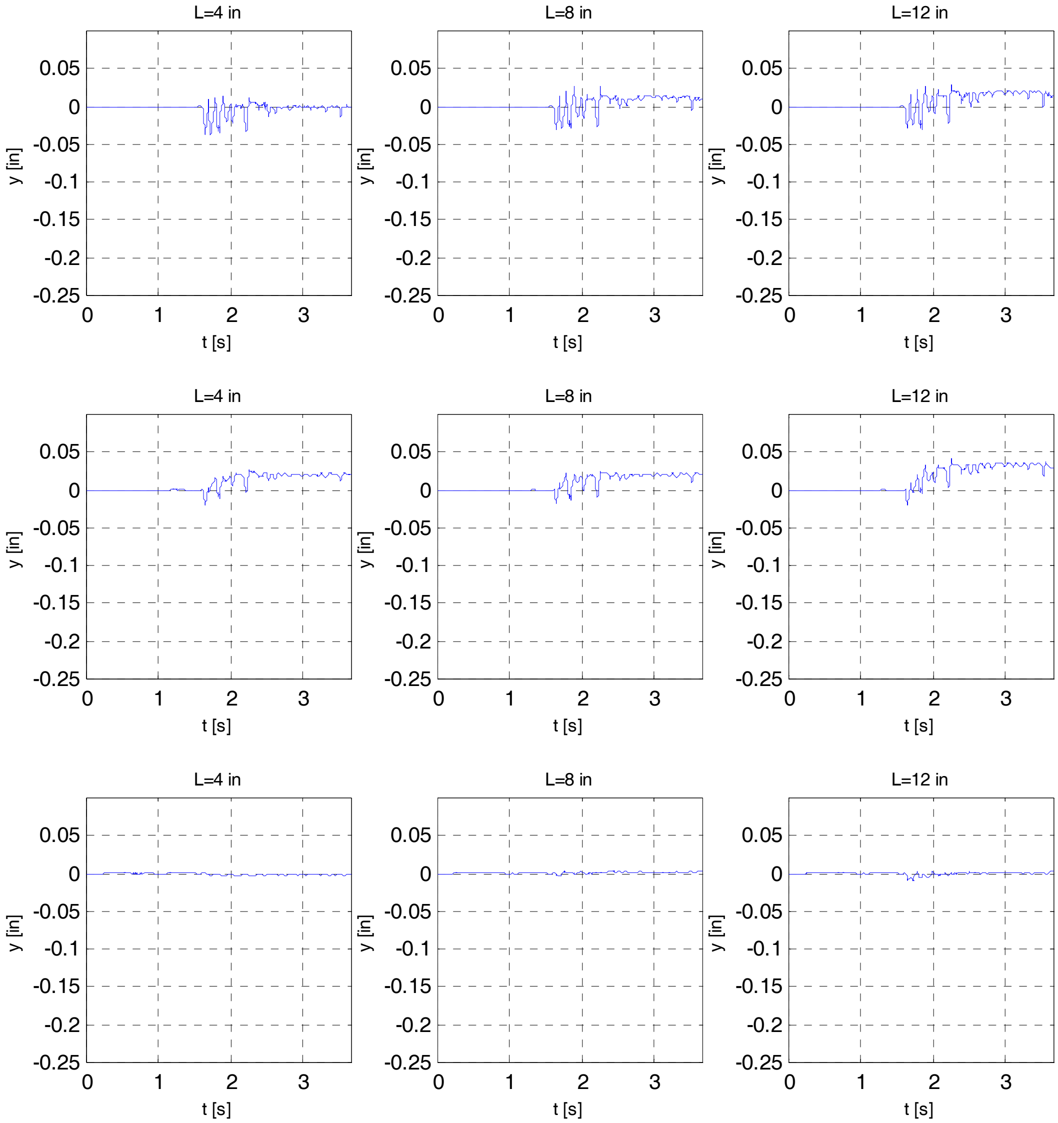

Figure 5–25: Comparison of the vertical displacements at the top (node 8), middle (node 5) and bottom (node 2) of the EAST brace. Small connection element (left), nominal (center), Large connection element (right).

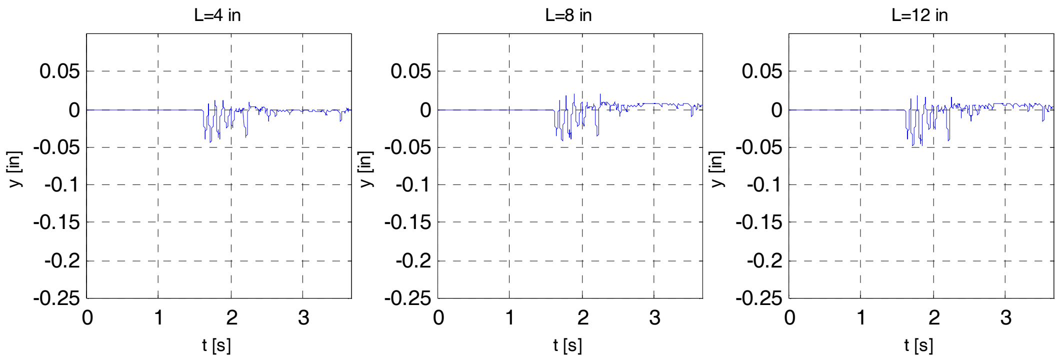

Figure 5–26: Comparison of the vertical displacements of the top node (9). Small connection element (left), nominal (center), Large connection element (right).

5.4.4 Zipper column: variation of the equivalent stiffness

The nominal value of the "zipper column's" stiffness is k=383 kip/in^2. This value was modified to evaluate the case of a very flexible column of stiffness equal to 10 kip/in^2 and the case of a very rigid column of stiffness equal to 1000 kip/in^2. The actual value of the zipper column's stiffness is expected to be smaller than the nominal value because it is connected to flexible elements. Results are presented in Figure 5–27 to Figure 5–33.

From Figure 5–27 and Figure 5–28 it is clear that the out of plane displacement increases 15% when the "zipper column" is very flexible. On the other hand, the results for a very stiff spring are not very different from the results with the nominal stiffness. A similar conclusion is obtained from to Figure 5–29 and Figure 5–30, where the hysteresis loops for k = 383 kip/in and k = 1000 kip/in are almost identical.

In the case of very flexible "zipper column", there is no yielding in tension in the connecting elements or in the braces. This is due to the fact that a flexible "zipper column" allows larger vertical displacements than a stiff "zipper column", for the same level of lateral force, as expected by structural mechanics. Therefore, the vertical movement increases the deformation in the brace under compression and decreases the deformation in the brace under tension. Thus, under compression force, the axial displacements are about 15% bigger than in the nominal case and the deformations of the connection elements are 33% of the total axial displacement. In the cases of a nominal, or rigid spring, the connections' deformations is 25% of the total value.

From Figure 5–31, Figure 5–32 and Figure 5–33 it can be concluded that the stiffness of the "zipper column" is the most important factor influencing the vertical displacements. For a flexible “zipper column”, all the nodes remain deformed with negative permanent displacements at the end of motion. For a rigid “zipper column”, only the nodes located at the middle of the brace remain deformed, with positive permanent displacements.

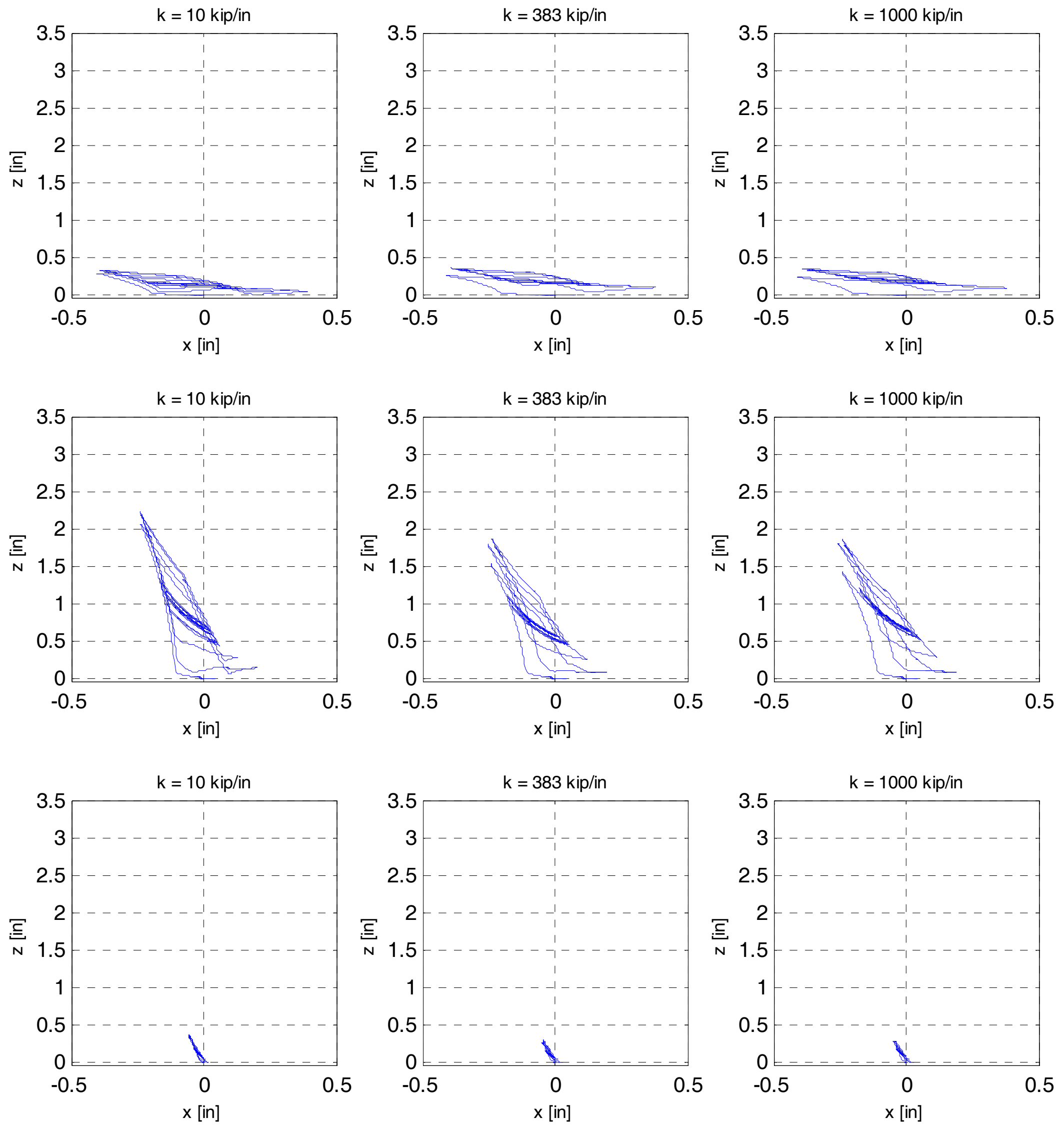

Figure 5–27: Comparison of the in plane (x) vs. out of plane (z) displacement at top (node 8), middle (node 5) and bottom (node 2) of the WEST brace.
Flexible spring (left), nominal (center), rigid spring (right).

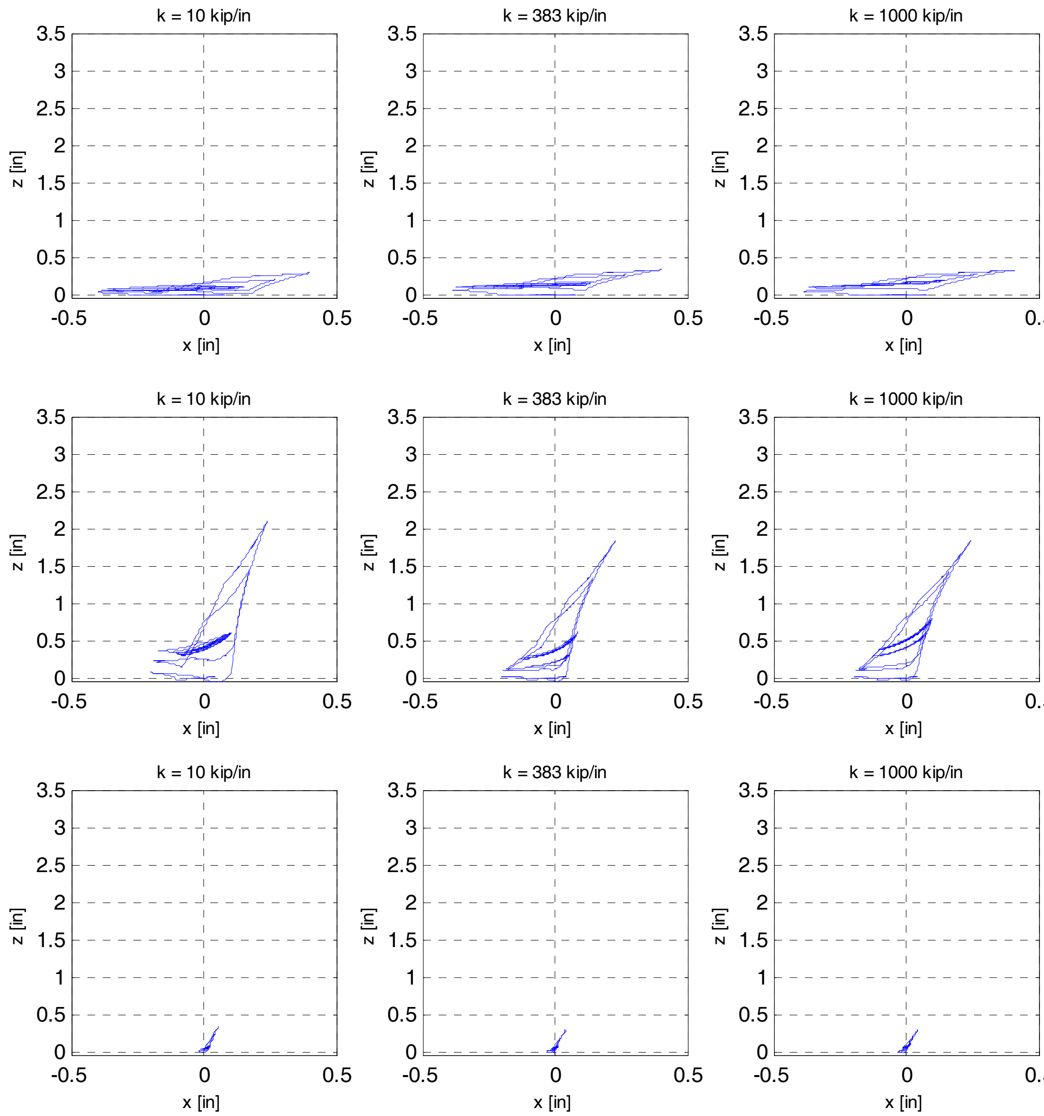

Figure 5–28: Comparison of the in plane (x) vs. out of plane (z) displacement at top (node 8), middle (node 5) and bottom (node 2) of the EAST brace.
Flexible spring (left), nominal (center), rigid spring (right).

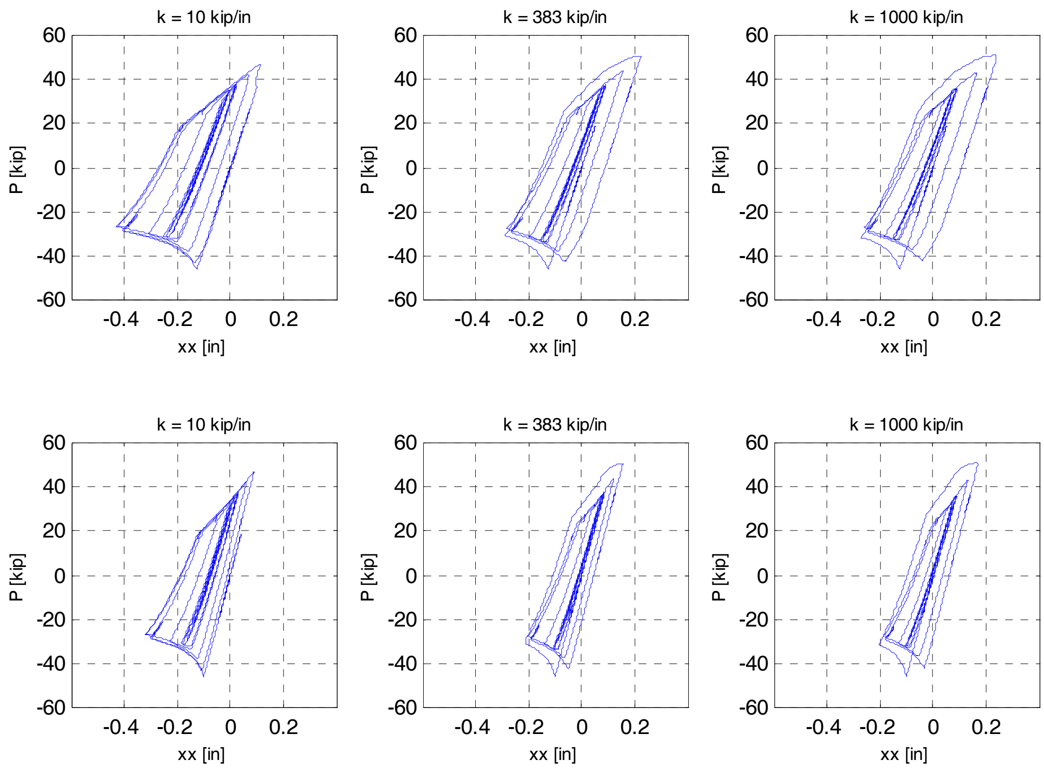

Figure 5–29: Comparison of the hysteresis loops of the WEST brace where the axial displacements considers the gusset plate (top) and does not consider the gusset plate (bottom). Flexible column (left), nominal stiffness (center), rigid column (right).

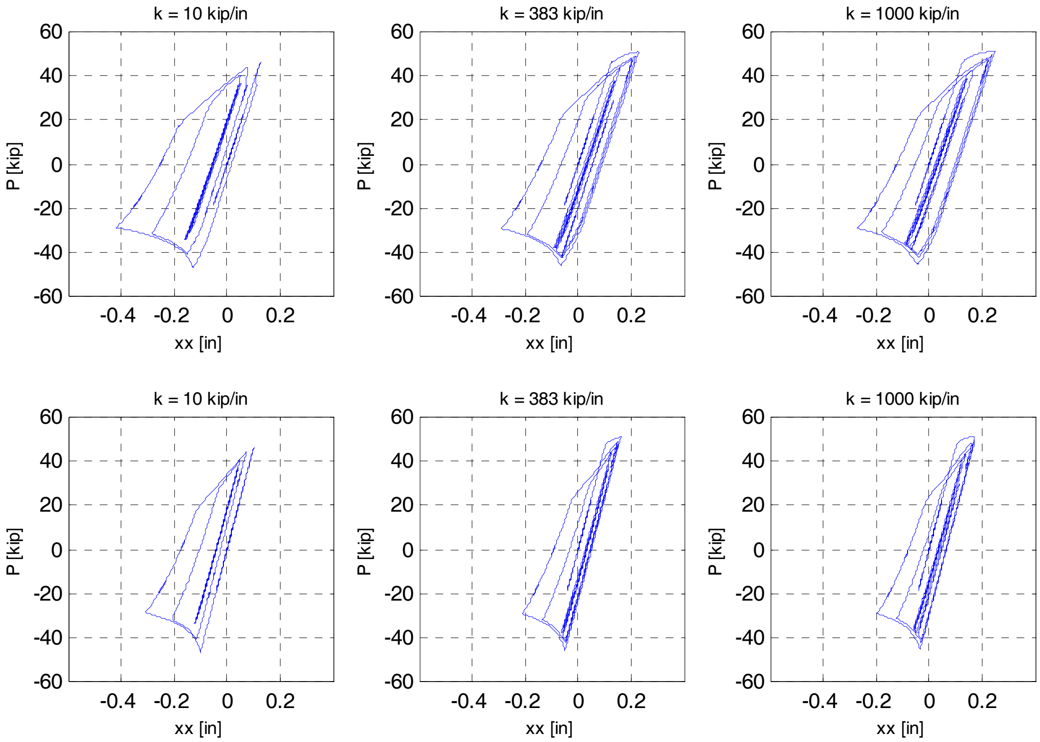

Figure 5–30: Comparison of the hysteresis loops of the EAST brace where the axial displacements considers the gusset plate (top) and does not consider the gusset plate (bottom). Flexible column (left), nominal stiffness (center), rigid column (right).

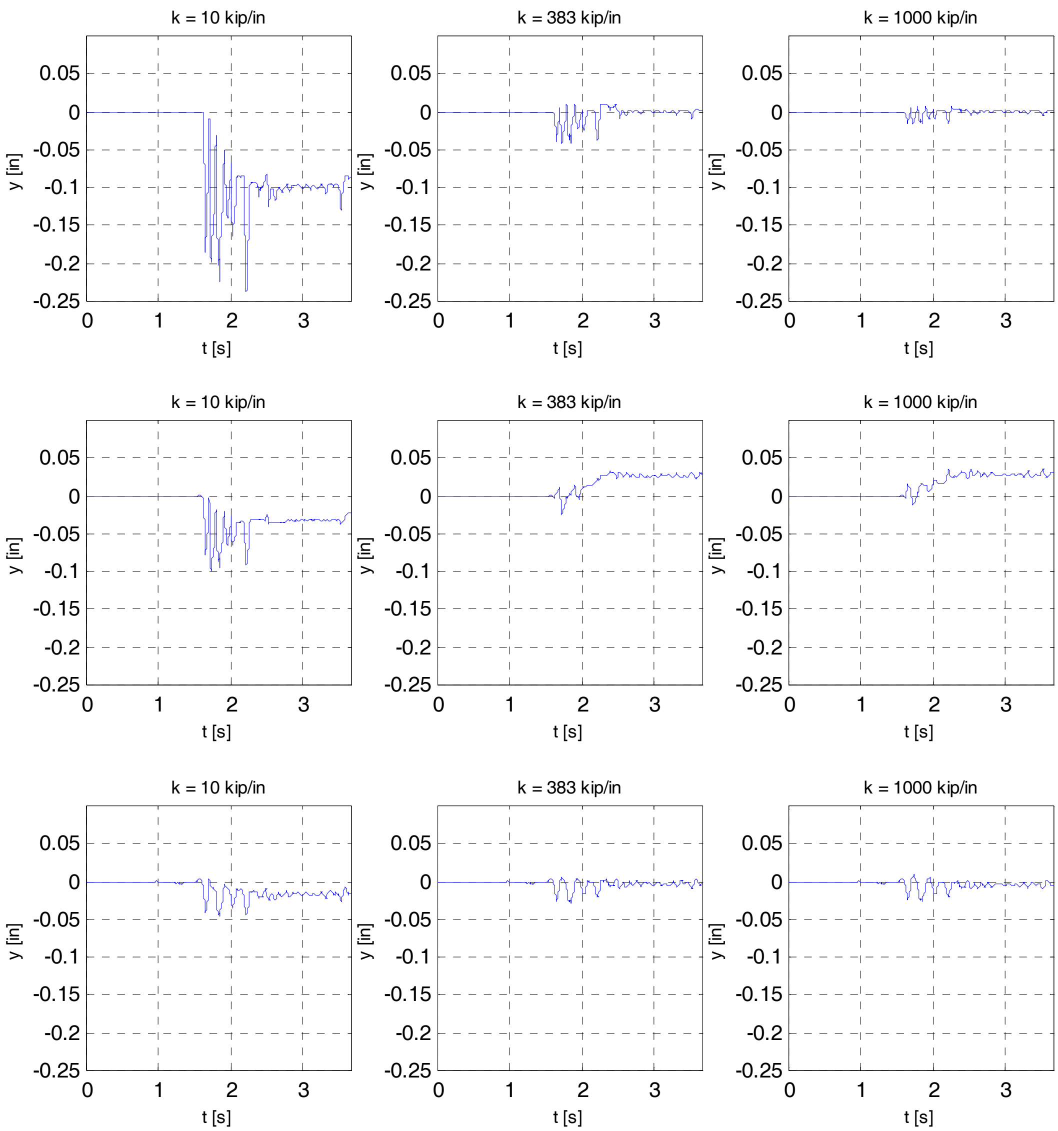

Figure 5–31: Comparison of the vertical displacements at the top (node 8), middle (node 5) and bottom (node 2) of the WEST brace Flexible column (left), nominal stiffness (center), rigid column (right).

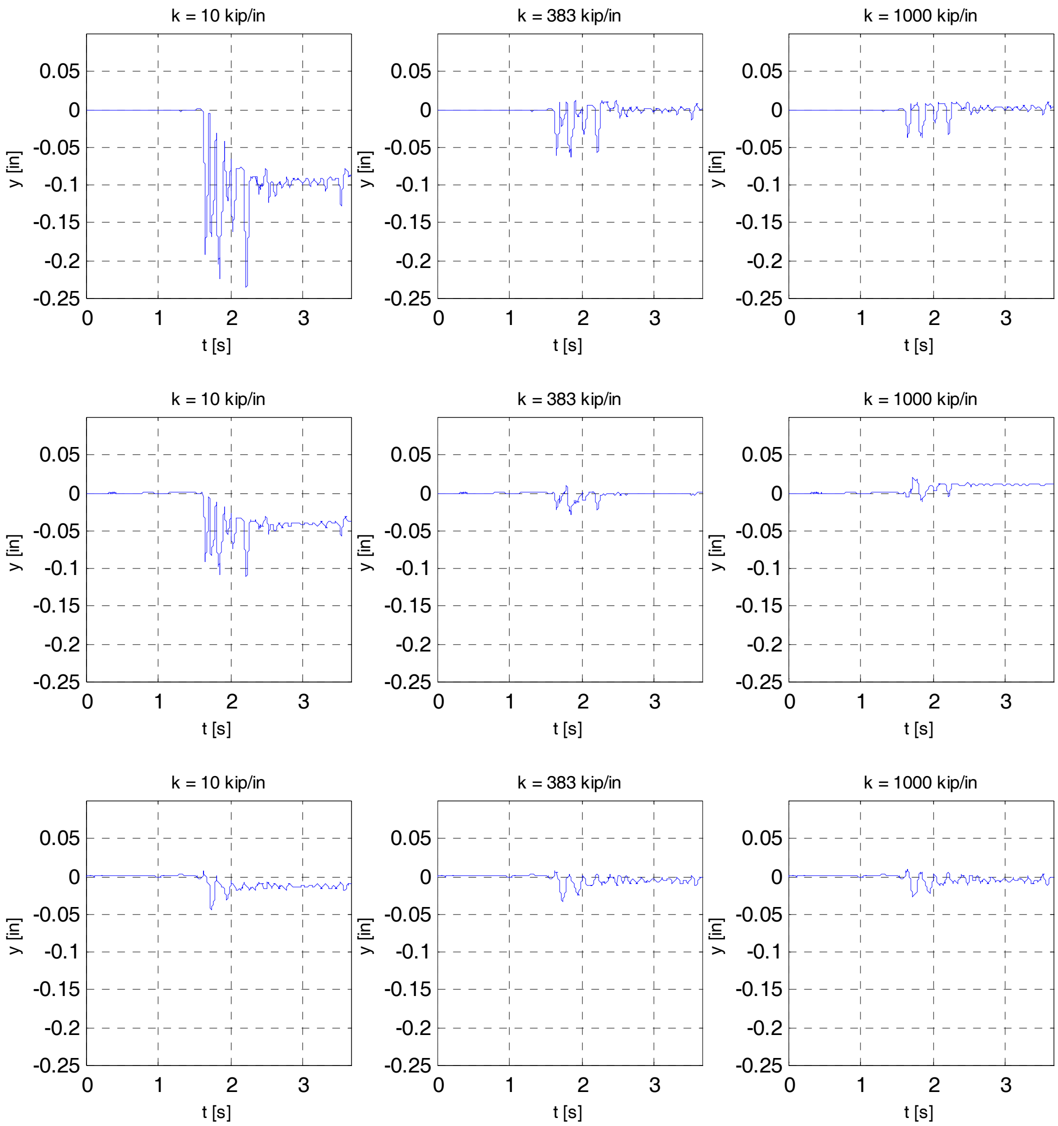

Figure 5–32: Comparison of the vertical displacements at the top (node 8), middle (node 5) and bottom (node 2) of the EAST brace Flexible column (left), nominal stiffness (center), rigid column (right).

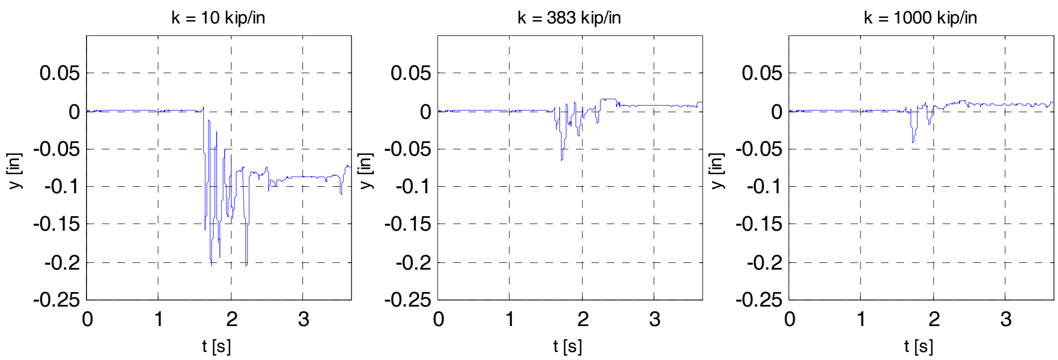

Figure 5–33: Comparison of the vertical displacements of the top node (9). Flexible column (left), nominal stiffness (center), rigid column (right).

5.4.5 Lateral restraint

Figure 5–34 and Figure 5–35 show the hysteretic curves of the braces (with and without connection elements) when an out of plane spring is added at node 9 and its stiffness is varied.

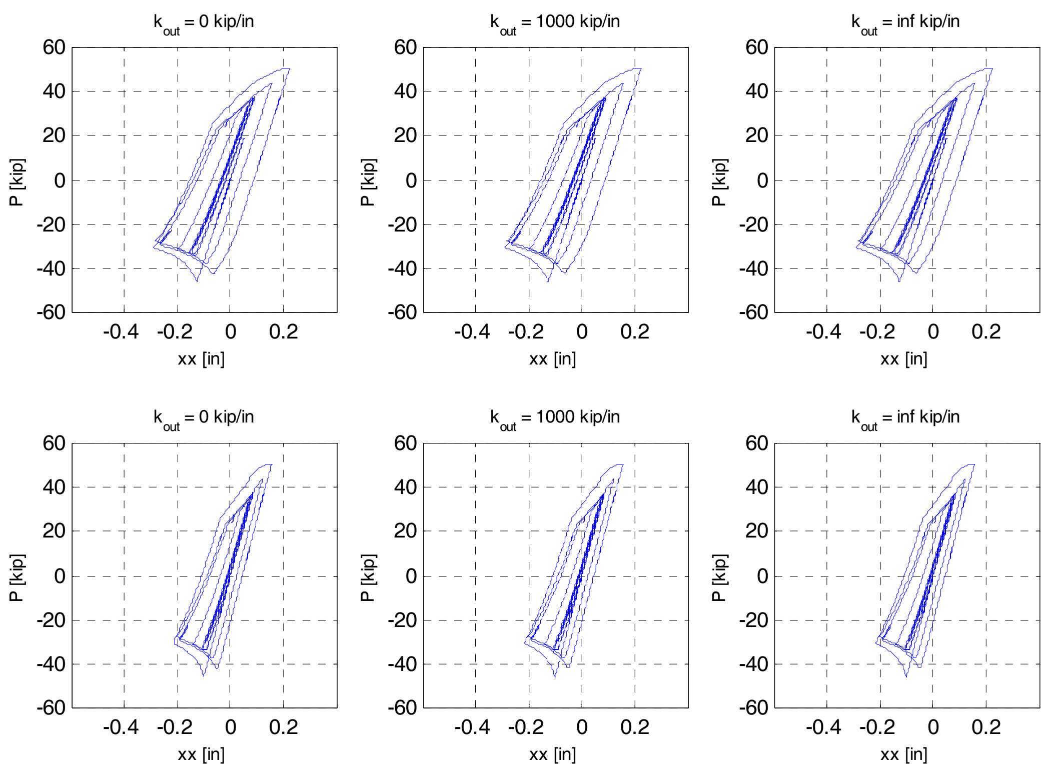

Figure 5–34: Comparison of the hysteresis loops of the EAST brace where the axial displacements considers the gusset plate (top) and does not consider the gusset plate (bottom). No out of plane restraint (left), rigid restraint (center), infinitely rigid restraint (right)

The spring' stiffness is set to 0 kip/in (no lateral restraint, nominal case), to 1000 kip/in and infinite stiffness (this is achieved by eliminating this DOF from the set of variables and setting its value to zero). It can be concluded that the presence of a lateral restraint in the analytical model has no influence in the behavior of the structure.

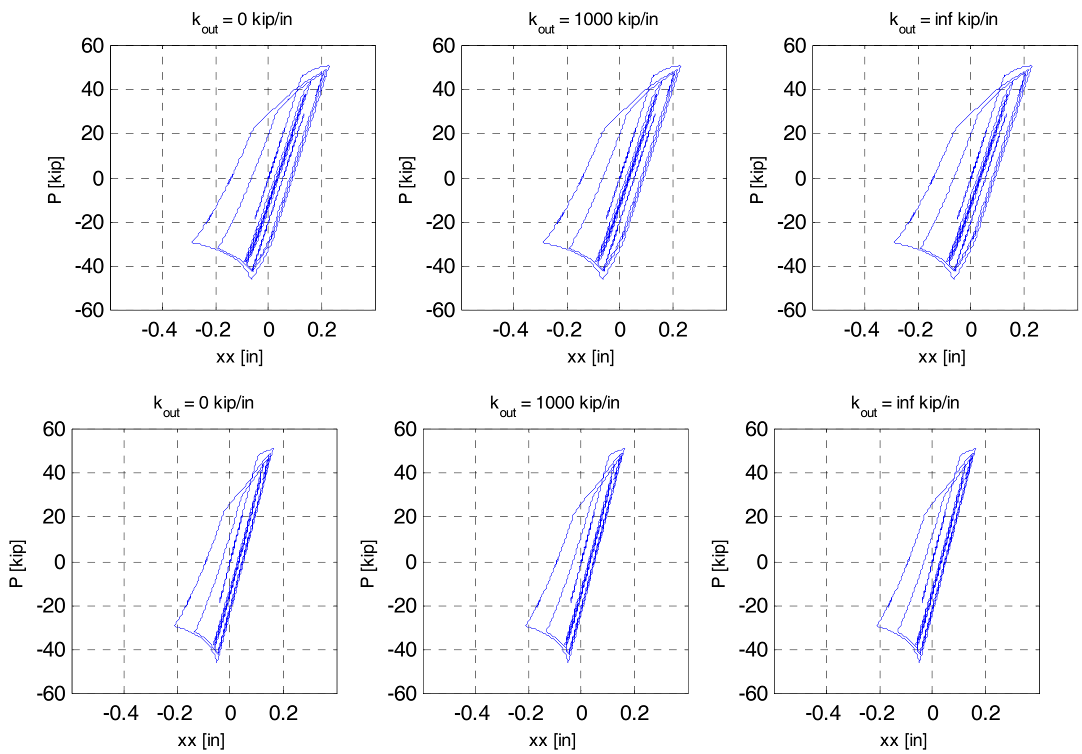

Figure 5–35: Comparison of the hysteresis loops of the WEST brace where the axial displacements considers the gusset plate (top) and does not consider the gusset plate (bottom). No out of plane restraint (left), rigid restraint (center), infinitely rigid restraint (right).

5.5 Comparison of analytical models with mixed parameters with test data for Test #2

From the shape of the in plane vs. the out of plane loop in Figure 5–2, it can be concluded that the braces are very flexible in the out of plane direction. However, their maximum displacement is only 1.64 in, a value that was achieved analytically only with a very stiff connection element. More importantly, the transition from the elastic to the buckling phases is slow and most of the deformation occurs in plane, while in the post buckling stage most of the deformation occurs out of plane. In all models discussed in the parametric study, the transition was fast and most of the in plane deformation occurred while the brace was buckling out of plane.

Several combinations of parameters were analyzed and the results are shown from Figure 5–36 to Figure 5–39. The experimental results are also shown for comparison purposes.

The properties of the connection elements are:

- Model 1: stiffness of "zipper column" 200 kip/in
  yield strength 60 kip/in^2
  out of plane inertia $I_{brace}/2$
- Model 2: stiffness of "zipper column" 200 kip/in
  yield strength 60 kip/in^2
  out of plane inertia $I_{brace}x2$
- Model 3: stiffness of "zipper column" 100 kip/in
  yield strength 60 kip/in^2
  out of plane inertia $I_{brace}x2$
- Model 4: stiffness of "zipper column" 100 kip/in
  yield strength 60 kip/in^2
  out of plane inertia I_{brace}
- Model 5: stiffness of "zipper column" 383 kip/in
  yield strength 60 kip/in^2
  out of plane inertia $I_{brace}/2$

Figure 5–36 and Figure 5–37 show the results for displacement loops of the west and east brace for the models detailed above. Comparing the results of Model 1 and Model 5, it can be concluded that when the connection elements are flexible, a variation in the "zipper column's" flexibility has an impact on the values of maximum displacements. However, when a very stiff connection element is used (model 2 and Model 3), a variation of the flexibility of the "zipper column" has no impact on the values of the maximum displacements and has a minimum influence in the shape of the curve. Therefore, the major parameter affecting the in plane and out of plane displacements of the braces is the stiffness of the connection elements.

Figure 5–38 and Figure 5–39 show the hysteretic loops of the west and east braces under the same combination of parameters. In this case, the stiffness of the spring is important because it controls the vertical displacements of the brace, thus it controls its total axial displacement. This is especially relevant when the brace is loaded in tension. When a soft spring is attached to the braces, the nodes move more freely in the vertical direction, thus for the brace under compression force the vertical displacements translate into more compression deformation. This brace will have larger buckling and permanent deformations. When the brace is under tension force, the vertical displacements also translate into compression deformation, thus reducing the amount of axial tension displacement. It is concluded that the models with a softer spring representing the “zipper column” approximate better the test results.

It appears also that a system with a soft spring dissipates less energy, but this conclusion must be wrong because the axial displacement is calculated as the length of the chord of the complete brace and does not account for permanent out of plane deformations.

Finally, a complete model of the “zipper frame” was not analyzed for the sensitivity study due to the high computational time required.

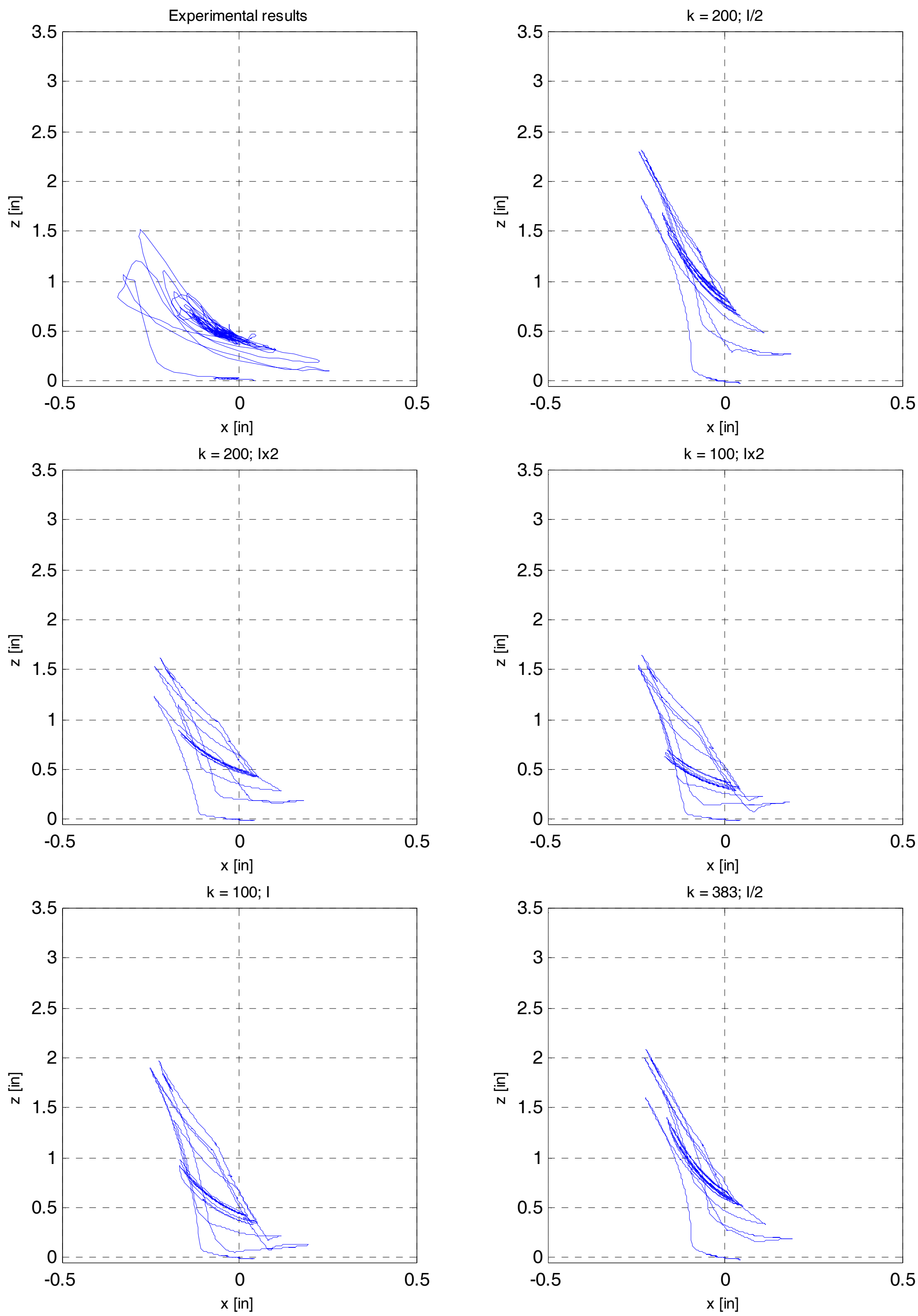

Figure 5–36: Comparison of in plane and out of plane displacement at the middle node (5) of WEST brace.

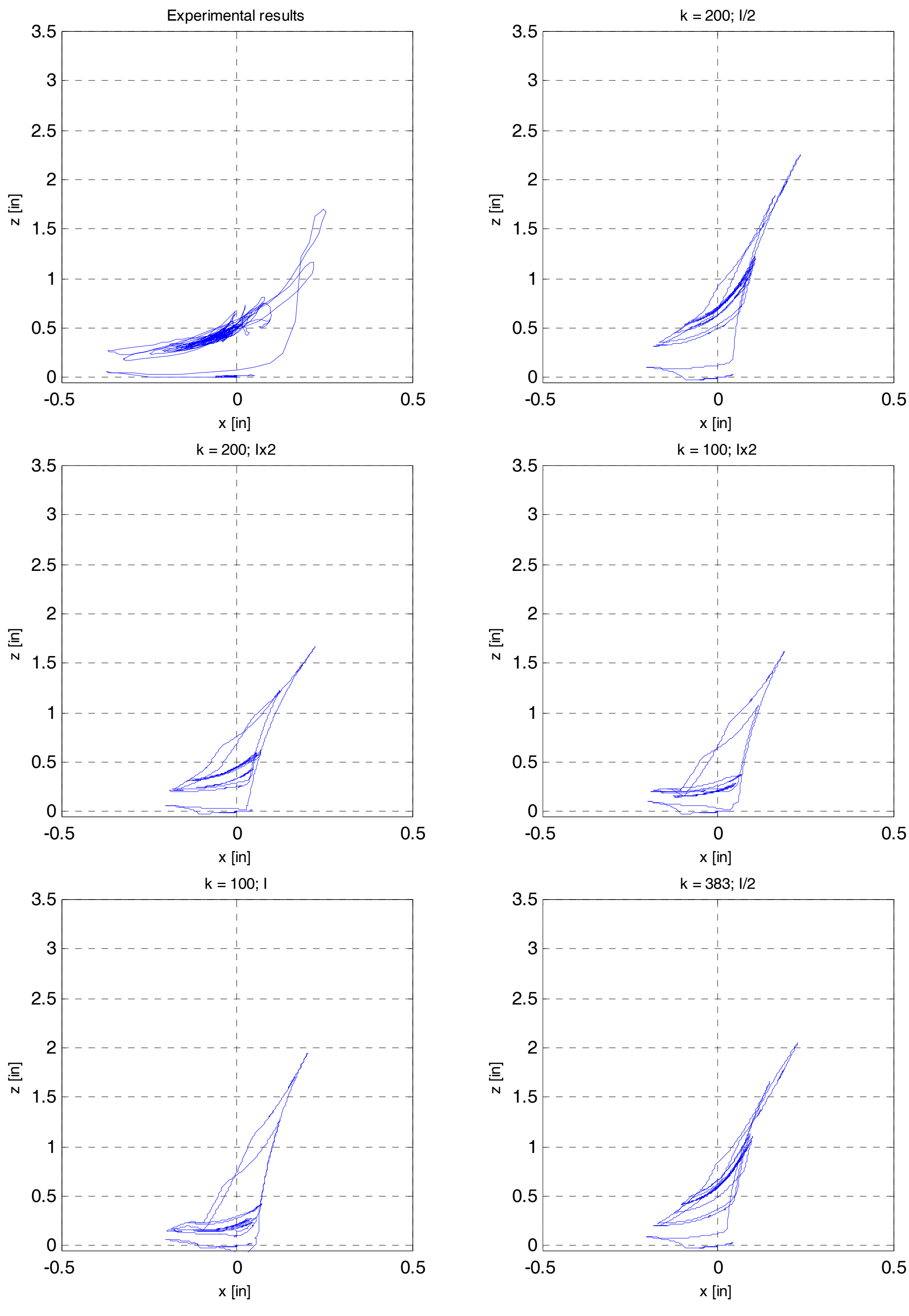

Figure 5–37: Comparison of in plane and out of plane at the middle node (5) of EAST brace.

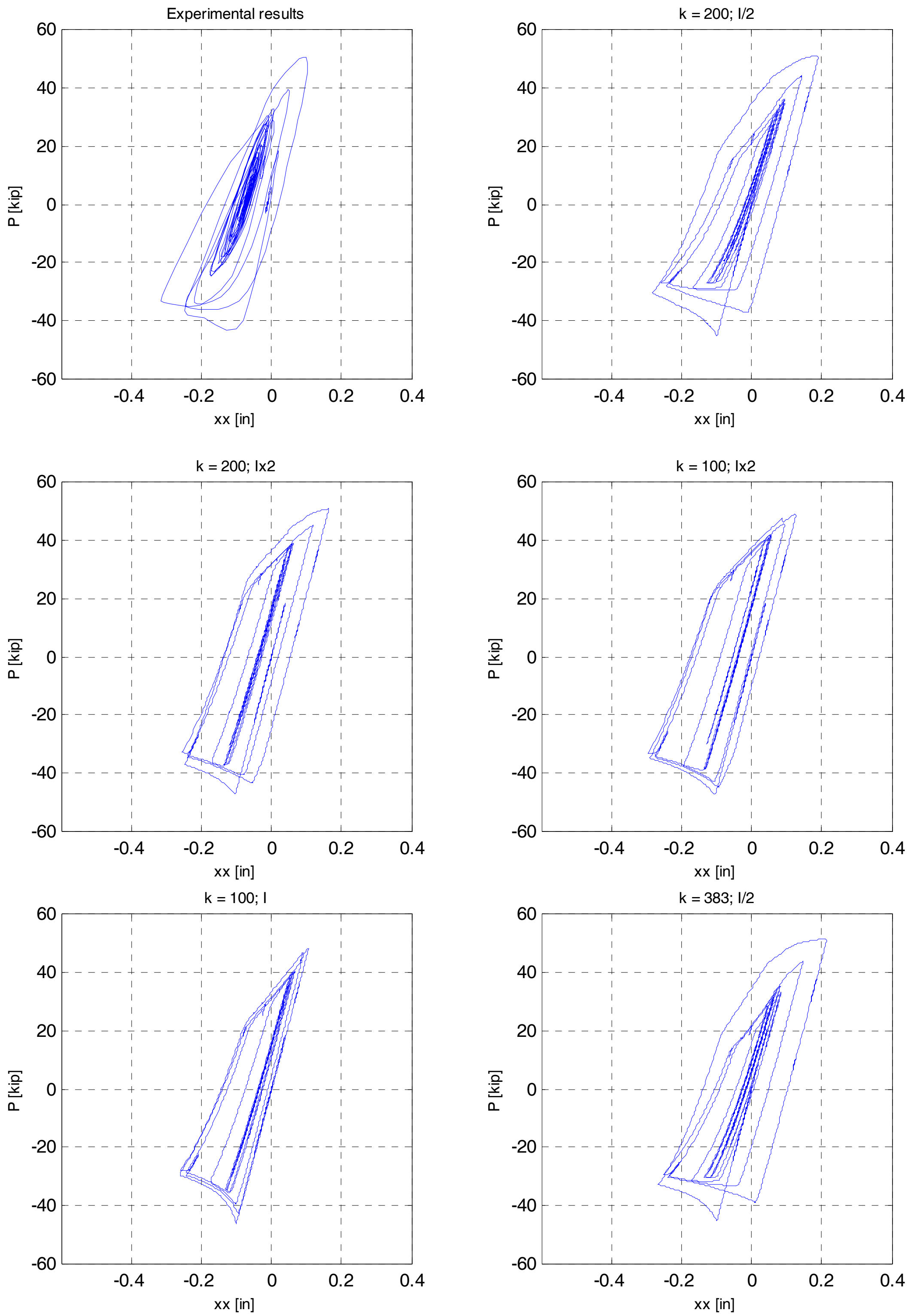

Figure 5–38: Comparison of hysteresis loops of WEST brace.

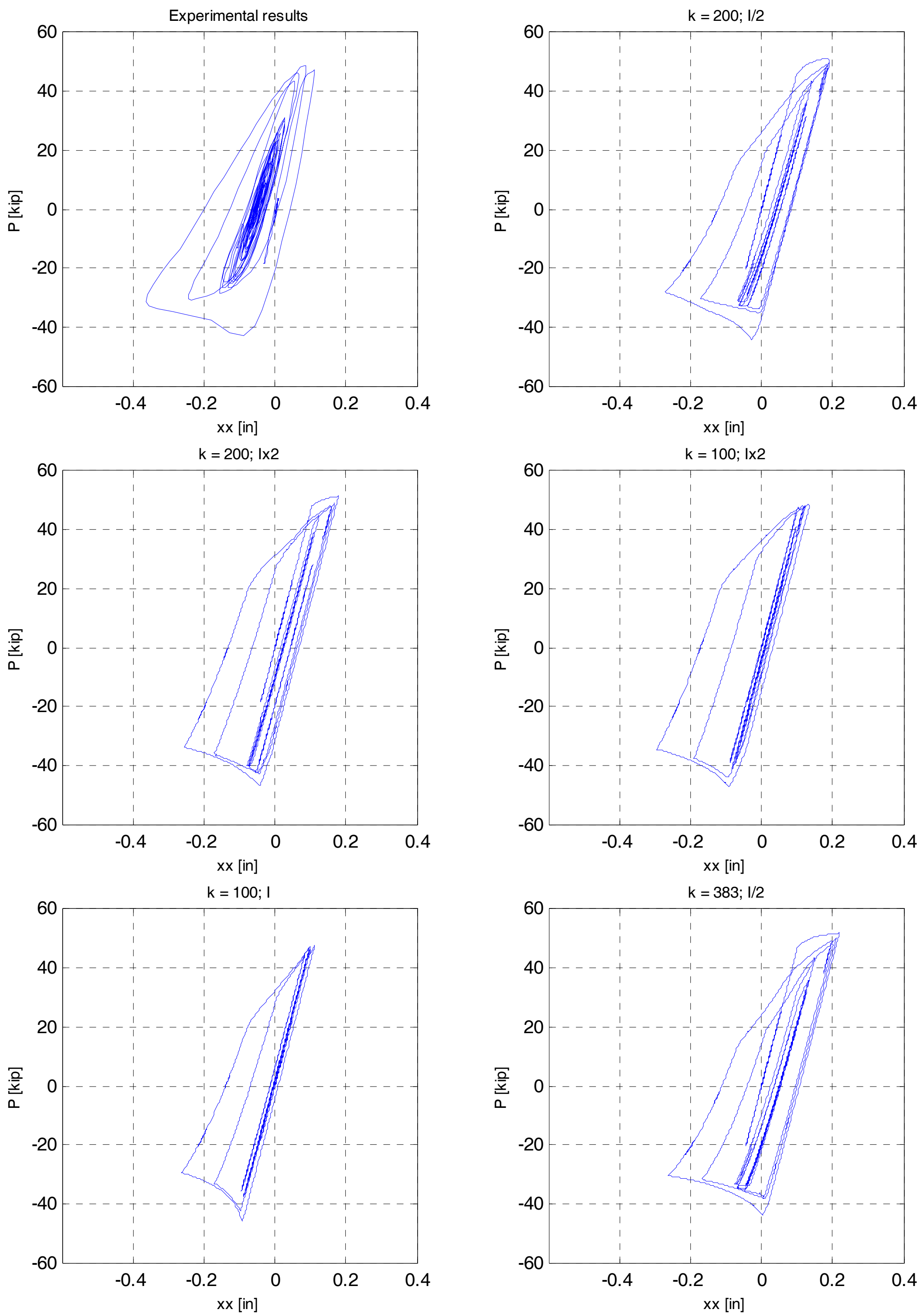

Figure 5–39: Comparison of hysteresis loops of EAST brace (right).

5.6 Conclusions

It can be concluded that the formulation developed in Chapter 2 reproduces all the important details that characterizes the inelastic buckling. The formulation is numerically stable and extremely sensitive to all modeling parameters. All the results obtained for each variation of each modeling parameter are consistent with structural mechanics theory.

Among the sources for discrepancies in the prediction are:

- Uncertain modeling parameters:
    - The gusset plates are modeled with connection elements of uncertain equivalent properties
    - The "zipper column" and the frame's upper stories are modeled with an elastic spring of uncertain equivalent stiffness.
- Uncertain yield functions: There are smooth continuous functions available in the literature that approximate the theoretical ultimate yield curves for typical sections. However, in the examples shown, a plate is being modeled with a conventional element and an appropriate equivalent yield function is not perfectly modeled. This is a key aspect in the solution of the system because the flexibility of the connection elements control the out of plane displacement of the braces and the relationship between the moment capacity of the connection and the moment capacity of the brace defines the shape of the hysteric loop.
- The implemented relationship between strains and forces (flexibility matrix) controls the relationship between the in plane and out of plane displacement. By allowing plastic deformations from the beginning of the ground motion, the brace moves in plane and out of plane simultaneously however, during the test, these displacements were almost independent. Figure 5–40 shows the in plane and out of plane displacements of the middle node of west and east braces when an elastic relationship between strains and forces is used in both braces and connection elements. The braces still buckle out of plane, although elastically. In that case, the shape of the displacement plots is very similar to the shapes in Figure 5–2 i.e. the braces develop most of their in plane displacement before buckling. The description of the material nonlinearity also controls the maximum and permanent lateral and vertical displacements and the distribution of the

section capacity between axial load and bending moments. Thus, a good yield function for both braces and connection elements is essential to obtain good predictions.

Despite all the uncertainties, the formulation predicts consistent responses when these parameters are varied to extreme values. The results of the study bound qualitatively the response observed during testing, although they do not match precisely. A more thorought parametric study is necessary to understand the exact sensitivity of the development of the "zipper mechanism" as identified in the experimental study.

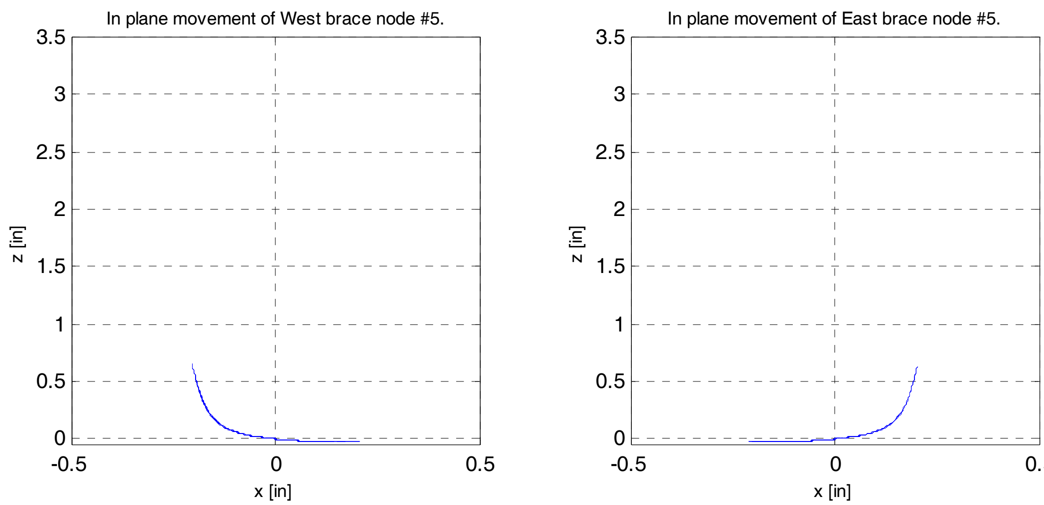

Figure 5–40: In plane (x) vs. out of plane (z) displacement at middle (node 5) of the West brace (left) and EAST brace (right).
Elastic material for all elements.

SECTION 6
REMARKS, CONCLUSIONS AND RECOMMENDATIONS

6.1 Summary

A new unified formulation capable of solving problems of large rotations and large deformations in inelastic frame structures was developed. An experimental study was carried out on a “zipper frame”. The frame was subjected to earthquake motion using the shake tables. Data from the inelastic behavior of the frame was collected for comparison with the analytical model predictions. Finally, an analytical model of the first story of the zipper frame was built and analyzed with the new formulation. A parametric study was performed and a few combinations of modeling parameters were selected to match the test results.

In order to incorporate large rotations and displacements, the formulation is based on the corotational method, where the rigid body motion and deformations are separated and analyzed independently by defining a local corotated coordinate system at the chord of the element in its deformed configuration. All the information needed to calculate the variations in strains and stresses is contained in the deformational part of the motion because a rigid body movement just changes the orientation of the strains. Usually deformations are assumed to be infinitesimal, however in the present formulation this hypothesis is relaxed and P-Δ effects are also accounted for at the chord level.

The proposed new formulation uses a flexibility based element and it is implemented in the state space. The main advantage of a flexibility based element is its exact interpolation of the forces along the length of the element while interpolating displacements using compatibility equations instead of approximated polynomials. In the state space, local and global variables and their evolution equations are defined. Global variables are total displacements and local variables are the elements' local forces and total strains at the Integration Points. The rates of all these variables are also variables of the system. The evolution equations for global variables are equilibrium equations and for local variables are plasticity equations. For a flexibility based element, the compatibility equations need to be considered explicitly because the internal forces are interpolated. In a stiffness based element, the compatibility is already accounted for when the strains (or displacement field) is approximated with interpolation functions. By solving all these equations simultaneously, convergence is achieved for all variables at the same time, thus eliminating the need for iterations between time steps.

The formulation derived therein combines the state space approach, the corotational method and a flexibility based element. Thus, after selecting the global and local variables, the equations of equilibrium compatibility and plasticity must be derived as rate equations, or algebraic equations. Equilibrium is readily obtained with the transformation of the element local forces. These equations are differential when mass is associated with a DOF and algebraic for all others DOFs. Incremental compatibility equations are based on a differential description of the deformed shape with respect to the chord. Both rotational and displacement deformations are considered to be finite. Plasticity equations are based on flow theory and are derived as rate equations linking force rates and strain rates. Therefore, the state space is an ideal framework to develop a unified formulation because it naturally integrates all the basics structural equations and ensures that convergence is achieved in all of them.

Finally, a comparison of the sensitivity of the analytical predictions from a model of the first story of a “zipper frame” with data from shaking table tests was performed. The primarily failure mode of the structure is inelastic buckling of its braces thus; this comparison is a good test of the capabilities of the developed formulation, which can handle problems of large rotations and inelastic material with great sensitivity.

6.2 Conclusions

From the comparison between analytical prediction and test results it can be concluded that:

- The formulation successfully solves problems of large rotations and displacements in three dimensions, like out of plane buckling of braces. A small imperfection of 1/500 of the length of the element is enough to trigger buckling.
- As a general conclusion, it can be said that the new formulation is sensitive to all parameters studied above and the variations of the response is always in agreement with structural principles.
- The formulation proved to be very sensitive to parameters that characterize the gusset plates (connection elements). The most sensitive parameters found are: the stiffness of

the vertical spring that models the influence of the zipper column and upper stories and the stiffness of the connection elements.

- It was found that the stiffness of the vertical spring controls the vertical displacement of the nodes, thus it controls the total axial deformation of the member and influences the shape of the hysteretic loop. Compared to a nominal stiffness calculated as (EA/L) with zipper column properties, the required stiffness of this element is much smaller. This result is in agreement with the fact that the nominal stiffness corresponds to an element that is rigidly supported at one end and that the actual zipper column is attached to flexible elements, thus the equivalent stiffness is smaller than the nominal.
- It was found that the stiffness of the connection elements controls the out of plane displacement of the nodes and thus controls the shape of the in plane vs. out of plane loop. The stiffness of these elements can be changed by changing the value of the equivalent inertia or by changing the length of the element. These possibilities were explored in the parametrical study performed. It was found that with flexible connection elements, the out of plane displacements are larger and the shapes of the loops are smoother. This behavior was the expected one. From the test results, the connection elements should be very flexible but the out of plane displacements are smaller than predicted.
- The variation in the response when the connection elements had different yield strengths was studied. It was found that if the connections' strength is very small compared to the braces, they yield first and do not allow the braces to develop all the axial force. Thus, by limiting the capacity of the connection elements, the overall capacity of the brace is also limited. In contrast, when their yield strength is much larger than the rest of the element, the connections remain elastic and the braces concentrate all plastic deformation.
- An important parameter not studied in this work is the yield function of the connection elements. The function used corresponds to a HSS section. Clearly, this is inadequate (because the gussets are plates not tubes) and a yield function that can replicate the plastic behavior of a plate is needed. During testing, the gusset plates yielded with a combination of axial force and bending moments, thus it is expected that a better description of the plate's plasticity will improve the overall response of the system.

- One of the most important differences between the predicted and recorded responses is the shape of the in plane/out of plane displacement. While the maximum in plane displacements are very similar, in the test during the pre-buckling phase most of the displacement occurs in the in plane direction and during the post-buckling phase the displacement is mostly in the out of plane direction. In the analytical response, however both displacements occur simultaneously. The explanation for this behavior lays in the adopted plasticity description. When the model is analyzed with an elastic material, a similar shape for in plane/out of plane loop is obtained although the maximum values are very different.
- In general, the new formulation and the experimental study indicate that the "zipper frame" is sensitive to the construction details which, if not properly considered, may render the system ineffective.
- The new formulation can identify the sensitive spots and can lead to better detail considerations and addition of redundancies.

In conclusion, the formulation can predict inelastic buckling and its accuracy depends on the knowledge of model details.

SECTION 7

REFERENCES.

AISC. (2003). *Manual of steel construction LRFD*, AISC, Chicago, IL.

AISC. (2005a). "Seismic provisions for structural steel buildings."

AISC. (2005b). "Specification for structural steel buildings."

Argyris, J. (1982). "An excursion into large rotations." *Computer Methods in Applied Mechanics and Engineering*, 32(1-3), 85-155.

Argyris, J. H., Balmer, H., Doltsinis, J. S., Dunne, P. C., Haase, M., Kleiber, M., Malejannakis, G. A., Mlejnek, H. P., Muller, M., and Scharpf, D. W. (1979). "Finite element method -- the natural approach." *Computer Methods in Applied Mechanics and Engineering*, 17-18(Part 1), 1-106.

ASCE. (2005). "Minimum design loads for buildings and other structures."

Bäcklund, J. (1976). "Large deflection analyis of elasto-plastic beams and frames." *International Journal of Mechanical Science*, 18, 269-277.

Battini, J.-M., and Pacoste, C. (2002a). "Co-rotational beam elements with warping effects in instability problems." *Computer Methods in Applied Mechanics and Engineering*, 191(17-18), 1755-1789.

Battini, J.-M., and Pacoste, C. (2002b). "Plastic instability of beam structures using co-rotational elements." *Computer Methods in Applied Mechanics and Engineering*, 191(51-52), 5811-5831.

Bazant, Z., and Cedolin, L. (1991). *Stability of structures.*, Oxford University Press., New York.

Behdinan, K., Stylianou, M. C., and Tabarrok, B. (1998). "Co-rotational dynamic analysis of flexible beams." *Computer Methods in Applied Mechanics and Engineering*, 154(3-4), 151-161.

Boller, C., and Seeger, T. (1987). *Material data for cyclic loading, part A: unalloyed steels*, Elsevier, Amsterdam.

Bouc, R. "Forced vibration of mechanical systems with hysteresis." *Proc., 4th Conference on Non-linear Oscillations*.

Brenan, K. E., Campbell, S. L., and Petzold, L. R. (1989). *Numerical solution of initial-value problems in differential-algebraic equations.*, SIAM, Philadelphia.

Cardona, A., and Geradin, M. (1988). "A beam finite element non-linear theory with finite rotations." *International Journal for Numerical Methods in Engineering*, 26(11), 2403-2438.

Chen, W. F. (2000). "Structural stability: from theory to practice." *Engineering Structures*, 22(2), 116-122.

Crisfield, M. A. (1990). "A consistent co-rotational formulation for non-linear, three-dimensional, beam-elements." *Computer Methods in Applied Mechanics and Engineering*, 81(2), 131-150.

Crisfield, M. A. (1991). *Non linear finite element analysis of solids and structures. v1: Essentials*, Wiley, Chichester.

Crisfield, M. A. (1997). *Non linear finite element analysis of solids and structures. v2: Advanced topics*, Wiley, Chichester.

Duan, L., and Chen, W.-F. (1990). "A yield surface equation for doubly symmetrical sections." *Engineering Structures*, 12(2), 114-119.

Felippa, C. A., and Haugen, B. (2005). "A unified formulation of small-strain corotational finite elements: I. Theory." *Computer Methods in Applied Mechanics and Engineering*, 194(21-24), 2285-2335.

FEMA. (2000). *355C: State of the art report on systems performance of steel moment frames subject to earthquake ground shaking*, Washington, DC, Prepared by the SAC joint venture for the Federal Emergency Management Agency.

Gruttmann, F., Sauer, R., and Wagner, W. (1998). "A geometrical nonlinear eccentric 3D-beam element with arbitrary cross-sections." *Computer Methods in Applied Mechanics and Engineering*, 160(3-4), 383-400.

Hall, J. F., and Challa, R. M. (1995). "Beam-Column Modeling." *Journal of Engineering Mechanics*, 121(2), 1284-1291.

Hindmarsh, A. C., and Serban, R. (2006). *User documentation for IDA v2.4.0*, LLNL.

Hsiao, K. M., Lin, J. Y., and Lin, W. Y. (1999). "A consistent co-rotational finite element formulation for geometrically nonlinear dynamic analysis of 3-D beams." *Computer Methods in Applied Mechanics and Engineering*, 169(1-2), 1-18.

Hsiao, K. M., and Lin, W. Y. (2000). "A co-rotational finite element formulation for buckling and postbuckling analyses of spatial beams." *Computer Methods in Applied Mechanics and Engineering*, 188(1-3), 567-594.

Huddleston, J. V. (1968). "Effect of axial strain on buckling and postbuckling behavior of elastic columns." Developments in theoretical and applied mechanics, Proceedings of the fourth southeastern conference on theoretical and applied mechanics, New Orleans, Louisiana, 263-273.

Ibrahimbegovic, A. (1995). "On finite element implementation of geometrically nonlinear Reissner's beam theory: three-dimensional curved beam elements." *Computer Methods in Applied Mechanics and Engineering*, 122(1-2), 11-26.

Ibrahimbegovic, A. (1997). "On the choice of finite rotation parameters." *Computer Methods in Applied Mechanics and Engineering*, 149(1-4), 49-71.

Izzuddin, B. A., and D.L.Smith. (1996). "Large-Displacement Analysis of Elastoplastic Thin-Walled Frames. I: Formulation and Implementation." *Journal of Structural Engineering*, 122(8), 905-914.

Jelenic, G., and Crisfield, M. A. (1999). "Geometrically exact 3D beam theory: implementation of a strain-invariant finite element for statics and dynamics." *Computer Methods in Applied Mechanics and Engineering*, 171(1-2), 141-171.

Jelenic, G., and Crisfield, M. A. (2001). "Dynamic analysis of 3D beams with joints in presence of large rotations." *Computer Methods in Applied Mechanics and Engineering*, 190(32-33), 4195-4230.

Jelenic, G., and Saje, M. (1995). "A kinematically exact space finite strain beam model - finite element formulation by generalized virtual work principle." *Computer Methods in Applied Mechanics and Engineering*, 120, 131-161.

Kanaan, A. E., and Powell, G. H. (1973). "DRAIN 2D - A general purpose computer program for dynamic analysis of inelastic plane structures." University of California, Berkeley.

Khatib, I. F., Mahin, S. A., and Pister, K. S. (1988). *Seismic Behavior of Concentrically Braced Steel Frames.*, Report No. UCB/EERC-88/01, Berkeley: Earthquake Engineering Research Center, University of California at Berkeley.

Kim, S.-E., and Lee, J. (2001). "Improved refined plastic-hinge analysis accounting for local buckling." *Engineering Structures*, 23(8), 1031-1042.

Kim, S.-E., and Lee, J. (2002). "Improved refined plastic-hinge analysis accounting for lateral torsional buckling." *Journal of Constructional Steel Research*, 58(11), 1431-1453.

Kim, S.-E., Lee, J., and Park, J.-S. (2003). "3-D second-order plastic-hinge analysis accounting for local buckling." *Engineering Structures*, 25(1), 81-90.

Kusumastuti, D. (2005). *A versatile experimentation model for study of structures near collapse*, PhD Dissertation, The State University of New York at Buffalo.

Lee, S., and Goel, S. C. (1987). "Seismic behavior of hollow and concrete filled square tubular bracing members." Ann Arbor, Michigan, The University of Michigan.

Leon, T. R., and Yang, C. S. (2003). "Special Inverted-V-braced Frames with Suspended Zipper Struts." International Workshop on Steel and Concrete Composite Construction, IWSCCC, National Center for Research on Earthquake, Taipei, Taiwan.

Lubliner, J. (1990). *Plasticity theory.*, Macmillan., New York.

Marsden, J. a. H., T. (1994). *Mathematical foundations of elasticity.*, Dover publications, Mineola.

Matsuiski, M., and Endo, T. (1969). *Fatigue of metals subjected to varying stress*, Japan Soc. Mech. Engrg.

Meek, J. L., and Xue, Q. (1998). "A study on the instability problem for 3D frames." *Computer Methods in Applied Mechanics and Engineering*, 158(3-4), 235-254.

Neuenhofer, A., and Filippou, F. C. (1997). "Evaluation of Nonlinear Frame Finite-Element Models." *Journal of Structural Engineering*, 123(7), 958-966.

Neuenhofer, A., and Filippou, F. C. (1998). "Geometrically Nonlinear Flexibility-Based Frame Finite Element." *Journal of Structural Engineering*, 124(6), 704-711.

Nieslony, A. (2003). "RainFlow Counting Method." Matlab Central.

Pacoste, C., and Eriksson, A. (1997). "Beam elements in instability problems." *Computer Methods in Applied Mechanics and Engineering*, 144(1-2), 163-197.

Park, Y., Reinhorn, A. M., and Kunnath, S. K. (1987). "IDARC: Inelastic damage analysis of reinforced concrete frame-shear wall structures." National Center for Earthquake Engineering Research, Buffalo, NY.

Pi, Y. L., and Bradford, M. A. (2001). "Effects of approximations in analyses of beams of open thin-walled cross-section - part I: Flexural-torsional stability." *International Journal for Numerical Methods in Engineering*, 51(7), 757-772.

Pi, Y. L., and Trahair, N. S. (1994). "Beam-Columns. I: Theory." *Journal of Structural Engineering*, 120(7), 2041-2061.

Pi, Y. L., Trahair, N. S., and Bradford, M. A. (2001a). "Effects of approximations in analyses of beams of open thin walled cross section-part I: Flexural-torsional stability." *International Journal for Numerical Methods in Engineering*, 51, 757-772.

Pi, Y. L., Trahair, N. S., and Bradford, M. A. (2001b). "Effects of approximations in analyses of beams of open thin walled cross section-part II: 3-D non-linear behaviour." *International Journal for Numerical Methods in Engineering*, 51, 773-790.

Prakash, V., Powell, G. H., and Campbell, S. D. (1994). "DRAIN-3DX: Base program description and user guide Version 1.10." Dept. of Civil Engineering, University of California, Berkeley.

Rankin, C. C., and Nour-Omid, B. (1988). "The use of projectors to improve finite element performance." *Computers & Structures*, 30(1-2), 257-267.

Schulz, M., and Filippou, F. C. (2001). "Non-linear spatial Timoshenko beam element with curvature interpolation." *International Journal for Numerical Methods in Engineering*, 50(4), 761-785.

Simeonov, V. (1999). *Three dimensional inelastic dynamic structural analysis of frame systems.*, PhD Dissertation, The State University of New York at Buffalo.

Simeonov, V., Sivaselvan, M. V., and Reinhorn, A. M. (2000). "Nonlinear analysis of structural frame systems by the state-space approach." *Computer-Aided Civil and Infrastructure Engineering*, 15(2), 76-89.

Simo, J. C., and Vu-Quoc, L. (1985). "A finite strain beam formulation. The three-dimensional dynamic problem. Part I." *Computer Methods in Applied Mechanics and Engineering*, 49(1), 55-70.

Simo, J. C., and Vu-Quoc, L. (1986). "A three-dimensional finite-strain rod model. part II: Computational aspects." *Computer Methods in Applied Mechanics and Engineering*, 58(1), 79-116.

Sivaselvan, M. V. (2003). *Nonlinear analysis towards collapse simulation – a dynamical systems approach.*, PhD dissertation., State University of New York at Buffalo.

Sivaselvan, M. V., and Reinhorn, A. M. (2001). "Hysteretic models for deteriorating inelastic structures." *Journal of Engineering Mechanics*, 126(6), 633-640.

Somerville, P. G., Smith, N., Punyamurthula, S., and Sun, J. (1997). "Development of ground motion time histories for phase 2 of the FEMA/SAC steel project."

Spacone, E., Ciampi, V., and Filippou, F. C. (1996). "Mixed formulation of nonlinear beam finite element." *Computers & Structures*, 58(1), 71-83.

Stavridis, A., and Shing, P. B. (2006). "Validation of a fast hybrid test system with substructure tests." 17th Analysis and computation specialty conference, St. Louis, Missouri.

Tang, X., and Goel, S. C. (1987). "Seismic analysis and design considerations of braced steel structures." Ann Arbor, Michigan, The University of Michigan.

Teh, L. H., and Clarke, M. J. (1997). "New Definition of Conservative Internal Moments in Space Frames." *Journal of Engineering Mechanics*, 123(2), 97-106.

Teh, L. H., and Clarke, M. J. (1998). "Co-rotational and Lagrangian formulations for elastic three-dimensional beam finite elements." *Journal of Constructional Steel Research*, 48(2-3), 123-144.

Trahair, N. S., and Chan, S. L. (2003). "Out of plane advanced analysis of steel structures." *Engineering Structures*, 25, 1627-1637.

Valles, R. E., Reinhorn, A. M., Kunnath, S. K., and Madan, A. (1996). "IDARC2D version 4.0: A computer program for the inelastic damage analysis of buildings." National Center for Earthquake Engineering Research, Buffalo, New York.

Wen, Y. K. (1976). "Method for random vibration of hysteretic systems." *Journal Engineering Mechanical Division, ASCE*, 102(2), 249-263.

Wongkaew, K., and Chen, W. F. (2002). "Consideration of out-of-plane buckling in advanced analysis for planar steel frame design." *Journal of Constructional Steel Research*, 58(5-8), 943-965.

Yang, C. S. (2006). *Analytical and experimental study of concentrically braced frames with zipper struts*, PhD Dissertation, Georgia Institute of Technology.

Yang, C. S., Leon, T. R., and DesRoches, R. (2006a). "Pushover test and analysis of a braced frame with zipper struts." *Journal of Structural Engineering*, in review.

Yang, C. S., Leon, T. R., and DesRoches, R. (2007a). "Cyclic behavior of zipper braced-frames." *Journal of Structural Engineering*, in review.

Yang, C. S., Leon, T. R., and DesRoches, R. (2007b). "Design and behavior of zipper braced frames." *Submitted for publication to Engineering Structures*.

Yang, T. Y., Stojadinovic, B., and Moehle, J. (2006b). "Hybrid simulation evaluation of innovative steel braced frame system." 8th NCEE, San Francisco, California.

Zienkiewicz, O. C., and Taylor, R. L. (2005). *The finite element method for solid and structural mechanics. 6th Edition.*, Elsevier, Boston.

APPENDIX A

DETAILS ON THE DEDUCTION OF COMPATIBILITY EQUATIONS

A.1 Deduction of equation 2.65

Equation (2.63) can be re-written to incorporate the results in Equation (2.64):

$$\frac{d\dot{\xi}}{dx} = \left(\mathbf{E}_1^t \cdot \mathbf{\Omega} \cdot \mathbf{t}_1\right)\left(1+\varepsilon\right) + \left(\mathbf{E}_1^t \cdot \mathbf{t}_1\right)\dot{\varepsilon} \tag{A.1}$$

Integrating from 0 to L:

$$\begin{aligned}
\int_0^L \frac{d\dot{\xi}}{dx}dx &= \int_0^L \left(\left(\mathbf{E}_1^t \cdot \mathbf{\Omega} \cdot \mathbf{t}_1\right)\left(1+\varepsilon\right) + \left(\mathbf{E}_1^t \cdot \mathbf{t}_1\right)\dot{\varepsilon}\right)dx \\
&= \int_0^L \left(\mathbf{E}_1^t \cdot \mathbf{\Omega} \cdot \mathbf{E}^t\right) \cdot \left(\mathbf{E} \cdot \mathbf{t}_1\left(1+\varepsilon\right)\right)dx + \int_0^L \mathbf{E}_1^t \cdot \mathbf{t}_1\dot{\varepsilon}dx \\
&= \int_0^L \left(\mathbf{E}_1^t \cdot \mathbf{\Omega} \cdot \mathbf{E}^t\right) \cdot \left(\begin{bmatrix} d\xi/dx \\ d\eta/dx \\ d\chi/dx \end{bmatrix}\right)dx + \int_0^L \mathbf{E}_1^t \cdot \mathbf{t}_1\dot{\varepsilon}dx
\end{aligned} \tag{A.2}$$

Integrating the first integral by parts:

$$\begin{aligned}
&u = \mathbf{E}_1^t \cdot \mathbf{\Omega} \cdot \mathbf{E}^t && du = \mathbf{E}_1^t \cdot \frac{d\mathbf{\Omega}}{dx} \cdot \mathbf{E}^t \\
&dv = \left(\begin{bmatrix} d\xi/dx \\ d\eta/dx \\ d\chi/dx \end{bmatrix}\right)dx && v = \begin{bmatrix} \xi \\ \eta \\ \chi \end{bmatrix}
\end{aligned} \tag{A.3}$$

$$
\begin{aligned}
\int_0^L \left(\mathbf{E}_1^t \cdot \boldsymbol{\Omega} \cdot \mathbf{E}^t\right) \cdot \left(\begin{bmatrix} d\xi/dx \\ d\eta/dx \\ d\chi/dx \end{bmatrix} \right) dx &= \left(\mathbf{E}_1^t \cdot \boldsymbol{\Omega} \cdot \mathbf{E}^t\right) \begin{bmatrix} \xi \\ \eta \\ \chi \end{bmatrix} \Bigg|_L^0 - \int_0^L \left(\mathbf{E}_1^t \cdot \frac{d\boldsymbol{\Omega}}{dx} \cdot \mathbf{E}^t \begin{bmatrix} \xi \\ \eta \\ \chi \end{bmatrix} \right) dx \\
&= \left(\mathbf{E}_1^t \cdot \boldsymbol{\Omega}(L) \cdot \mathbf{E}^t\right) \begin{bmatrix} \xi(L) \\ \eta(L) \\ \chi(L) \end{bmatrix} - \left(\mathbf{E}_1^t \cdot \boldsymbol{\Omega}(0) \cdot \mathbf{E}^t\right) \begin{bmatrix} \xi(0) \\ \eta(0) \\ \chi(0) \end{bmatrix} - \int_0^L \left(\mathbf{E}_1^t \cdot \frac{d\boldsymbol{\Omega}}{dx} \cdot \mathbf{E}^t \begin{bmatrix} \xi \\ \eta \\ \chi \end{bmatrix} \right) dx \\
&= \left(\mathbf{E}_1^t \cdot \boldsymbol{\Omega}(L) \cdot \mathbf{E}^t\right) \begin{bmatrix} \xi(L) \\ 0 \\ 0 \end{bmatrix} - \int_0^L \left(\mathbf{E}_1^t \cdot \frac{d\boldsymbol{\Omega}}{dx} \cdot \mathbf{E}^t \begin{bmatrix} \xi \\ \eta \\ \chi \end{bmatrix} \right) dx \\
&= \left(\mathbf{E}_1^t \cdot \boldsymbol{\Omega}(L) \cdot \mathbf{E}^t\right)_1 \xi(L) - \int_0^L \left(\mathbf{E}_1^t \cdot \frac{d\boldsymbol{\Omega}}{dx} \cdot \mathbf{E}^t \begin{bmatrix} \xi \\ \eta \\ \chi \end{bmatrix} \right) dx
\end{aligned} \tag{A.4}
$$

Since the origin of the **E** coordinate system is in node i, ξ(0)=η(0)=χ(0)=0, also by definition of the member's chord η(L)=χ(L)=0. Thus, Equation (A.2) becomes:

$$
\int_0^L \frac{d\dot{\xi}}{dx} dx = \left(\mathbf{E}_1^t \cdot \boldsymbol{\Omega} \cdot \mathbf{E}^t\right)_1 \xi_L - \int_0^L \left(\mathbf{E}_1^t \cdot \frac{d\boldsymbol{\Omega}}{dx} \cdot \mathbf{E}^t \begin{bmatrix} \xi \\ \eta \\ \chi \end{bmatrix} \right) dx + \int_0^L \mathbf{E}_1^t \cdot \mathbf{t}_1 \dot{\varepsilon} dx \tag{A.5}
$$

But since the skew-symmetric matrix is equivalent to a cross product, the first term is null.

$$
\int_0^L \frac{d\dot{\xi}}{dx} dx = -\int_0^L \left(\mathbf{E}_1^t \cdot \frac{d\boldsymbol{\Omega}}{dx} \cdot \mathbf{E}^t \begin{bmatrix} \xi \\ \eta \\ \chi \end{bmatrix} \right) dx + \int_0^L \mathbf{E}_1^t \cdot \mathbf{t}_1 \dot{\varepsilon} dx \tag{A.6}
$$

The equations for η and χ are found in a similar way. However, in those cases, the first terms in Equation (A.5) are:

$$
\begin{aligned}
C_2 &= \left(\mathbf{E}_2^t \cdot \boldsymbol{\Omega}(L) \cdot \mathbf{E}^t\right)_1 \xi(L) \\
C_3 &= \left(\mathbf{E}_3^t \cdot \boldsymbol{\Omega}(L) \cdot \mathbf{E}^t\right)_1 \xi(L)
\end{aligned} \tag{A.7}
$$

A.2 Derivation of Equation 2.68

Considering Equation (2.67) in spatial form:

$$\frac{d(\dot{\mathbf{R}})}{dx}=\frac{d}{dx}(\boldsymbol{\Omega}\cdot\mathbf{R})=\frac{d\boldsymbol{\Omega}}{dx}\cdot\mathbf{R}+\boldsymbol{\Omega}\cdot\frac{d\mathbf{R}}{dx}=\frac{d\boldsymbol{\Omega}}{dx}\cdot\mathbf{R}+\boldsymbol{\Omega}\cdot\boldsymbol{\Psi}\mathbf{R}(1+\varepsilon)$$

$$=\frac{d}{dt}\left(\boldsymbol{\Psi}\mathbf{R}(1+\varepsilon)\right)=\frac{d}{dt}(\boldsymbol{\Psi}\mathbf{R})(1+\varepsilon)+\boldsymbol{\Psi}\mathbf{R}\cdot\dot{\varepsilon}=\left(\dot{\boldsymbol{\Psi}}\mathbf{R}+\boldsymbol{\Psi}\dot{\mathbf{R}}\right)(1+\varepsilon)+\boldsymbol{\Psi}\mathbf{R}\cdot\dot{\varepsilon}$$

$$\frac{d\boldsymbol{\Omega}}{dx}\cdot\mathbf{R}=\dot{\boldsymbol{\Psi}}\mathbf{R}(1+\varepsilon)+\boldsymbol{\Psi}\mathbf{R}\cdot\dot{\varepsilon}+\boldsymbol{\Psi}\cdot\boldsymbol{\Omega}\cdot\mathbf{R}(1+\varepsilon)-\boldsymbol{\Omega}\cdot\boldsymbol{\Psi}\mathbf{R}(\mathbf{1}+\varepsilon) \tag{A.8}$$

$$\frac{d\boldsymbol{\Omega}}{dx}=\dot{\boldsymbol{\Psi}}(1+\varepsilon)+\boldsymbol{\Psi}\cdot\dot{\varepsilon}+(\boldsymbol{\Psi}\cdot\boldsymbol{\Omega}-\boldsymbol{\Omega}\cdot\boldsymbol{\Psi})(1+\varepsilon)$$

$$\frac{d\omega}{dx}=\left(\dot{\phi}-\omega\times\phi\right)(1+\varepsilon)+\phi\cdot\dot{\varepsilon}$$

$$=\widehat{\phi}(1+\varepsilon)+\phi\cdot\dot{\varepsilon}$$

The material representation:

$$\phi^{m}=\mathbf{R}^{t}\cdot\phi$$

$$\widehat{\phi}=\dot{\phi}-\omega\times\phi=\mathbf{R}\frac{d}{dt}\left(\mathbf{R}^{t}\cdot\phi\right)=\mathbf{R}\cdot\dot{\phi}^{m}$$

$$\frac{d\omega}{dx}=\mathbf{R}\cdot\dot{\phi}^{m}(1+\varepsilon)+\mathbf{R}\cdot\phi^{m}\dot{\varepsilon}=\mathbf{R}\cdot\left(\dot{\phi}^{m}(1+\varepsilon)+\phi^{m}\dot{\varepsilon}\right)$$

$$\mathbf{R}^{t}\frac{d\omega}{dx}=\left(\dot{\phi}^{m}(1+\varepsilon)+\phi^{m}\dot{\varepsilon}\right) \tag{A.9}$$

$$\frac{d\omega^{m}}{dx}=\frac{d\left(\mathbf{R}^{t}\omega\right)}{dx}=\frac{d\mathbf{R}^{t}}{dx}\omega+\mathbf{R}^{t}\frac{d\omega}{dx}=-\mathbf{R}^{t}\dot{\mathbf{R}}\mathbf{R}^{t}\omega+\mathbf{R}^{t}\frac{d\omega}{dx}=-\mathbf{R}^{t}\boldsymbol{\Omega}\mathbf{R}\mathbf{R}^{t}\omega+\mathbf{R}^{t}\frac{d\omega}{dx}=\mathbf{R}^{t}\frac{d\omega}{dx}$$

$$\frac{d\omega^{m}}{dx}=\left(\dot{\phi}^{m}(1+\varepsilon)+\phi^{m}\dot{\varepsilon}\right)$$

Where last expression is found by using the definition $\boldsymbol{\Omega}\omega=0$.

A.3 Compatibility equations in terms of material curvatures

Writing $d\boldsymbol{\Omega}/dx$ in material coordinates:

$$\frac{d\boldsymbol{\Omega}}{dx}=\frac{d}{dx}\left(\mathbf{R}\boldsymbol{\Omega}^{m}\mathbf{R}^{t}\right)=\frac{d\mathbf{R}}{dx}\boldsymbol{\Omega}^{m}\mathbf{R}^{t}+\mathbf{R}\frac{d\boldsymbol{\Omega}^{m}}{dx}\mathbf{R}^{t}+\mathbf{R}\boldsymbol{\Omega}^{m}\frac{d\mathbf{R}^{t}}{dx}$$

$$=\mathbf{R}\boldsymbol{\Omega}^{m}\boldsymbol{\Omega}^{m}\mathbf{R}^{t}+\mathbf{R}\frac{d\boldsymbol{\Omega}^{m}}{dx}\mathbf{R}^{t}-\mathbf{R}\boldsymbol{\Omega}^{m}\boldsymbol{\Omega}^{m}\mathbf{R}^{t} \tag{A.10}$$

$$=\mathbf{R}\frac{d\boldsymbol{\Omega}^{m}}{dx}\mathbf{R}^{t}$$

The compatibility equations become:

$$\int_0^L \frac{d\dot{\xi}}{dx}dx = -\int_0^L \left(\mathbf{E}_1^t \cdot \mathbf{R}\frac{d\mathbf{\Omega}^m}{dx}\mathbf{R}^t \cdot \mathbf{E}^t \begin{bmatrix} \xi \\ \eta \\ \chi \end{bmatrix} \right) dx + \int_0^L \mathbf{E}_1^t \cdot \mathbf{t}_1 \dot{\varepsilon} dx$$

$$\int_0^L \frac{d\dot{\eta}}{dx}dx = C_2 - \int_0^L \left(\mathbf{E}_2^t \cdot \mathbf{R}\frac{d\mathbf{\Omega}^m}{dx}\mathbf{R}^t \cdot \mathbf{E}^t \begin{bmatrix} \xi \\ \eta \\ \chi \end{bmatrix} \right) dx + \int_0^L \mathbf{E}_2^t \cdot \mathbf{t}_1 \dot{\varepsilon} dx \quad \text{(A.11)}$$

$$\int_0^L \frac{d\dot{\chi}}{dx}dx = C_3 - \int_0^L \left(\mathbf{E}_3^t \cdot \mathbf{R}\frac{d\mathbf{\Omega}^m}{dx}\mathbf{R}^t \cdot \mathbf{E}^t \begin{bmatrix} \xi \\ \eta \\ \chi \end{bmatrix} \right) dx + \int_0^L \mathbf{E}_3^t \cdot \mathbf{t}_1 \dot{\varepsilon} dx$$

And replacing the relationship between $d\mathbf{\Omega}^m/dx$ and ϕ^m:

$$\int_0^L \frac{d\dot{\xi}}{dx}dx = \int_0^L \left(\mathbf{-E}_1^t \cdot \mathbf{R}\left(\dot{\mathbf{\Psi}}^m (1+\varepsilon) + \mathbf{\Psi}^m \dot{\varepsilon} \right) \cdot \mathbf{R}^t \mathbf{E}^t \begin{bmatrix} \xi \\ \eta \\ \chi \end{bmatrix} + \mathbf{E}_1^t \cdot \mathbf{t}_1 \dot{\varepsilon} \right) dx$$

$$\dot{\xi}(L) - \dot{\xi}(0) = \dot{q}_1 = \int_0^L \begin{bmatrix} \mathbf{E}_1^t \cdot \mathbf{t}_1 - \mathbf{E}_1^t \mathbf{R}\mathbf{\Psi}^m \mathbf{R}^t \mathbf{E}^t \begin{bmatrix} \xi \\ \eta \\ \chi \end{bmatrix} & \mathbf{R}^t \mathbf{E}_1 \times \left(\begin{bmatrix} \xi & \eta & \chi \end{bmatrix} \mathbf{RE} \right)^t \end{bmatrix} \begin{bmatrix} \dot{\varepsilon} \\ \dot{\phi}^m \end{bmatrix} dx \quad \text{(A.12)}$$

$$\int_0^L \frac{d\dot{\eta}}{dx}dx = C_2 + \int_0^L \left(\mathbf{-E}_2^t \cdot \mathbf{R}\left(\dot{\mathbf{\Psi}}^m (1+\varepsilon) + \mathbf{\Psi}^m \dot{\varepsilon} \right) \cdot \mathbf{R}^t \mathbf{E}^t \begin{bmatrix} \xi \\ \eta \\ \chi \end{bmatrix} + \mathbf{E}_2^t \cdot \mathbf{t}_1 \dot{\varepsilon} \right) dx$$

$$\dot{\eta}\left(\tfrac{L}{2}\right) - \dot{\eta}\left(-\tfrac{L}{2}\right) = 0 = C_2 + \int_0^L \begin{bmatrix} \mathbf{E}_2^t \cdot \mathbf{t}_1 - \mathbf{E}_2^t \mathbf{R}\mathbf{\Psi}^m \mathbf{R}^t \mathbf{E}^t \begin{bmatrix} \xi \\ \eta \\ \chi \end{bmatrix} & \mathbf{R}^t \mathbf{E}_2 \times \left(\begin{bmatrix} \xi & \eta & \chi \end{bmatrix} \mathbf{RE} \right)^t \end{bmatrix} \begin{bmatrix} \dot{\varepsilon} \\ \dot{\phi}^m \end{bmatrix} dx \quad \text{(A.13)}$$

$$\int_0^L \frac{d\dot{\chi}}{dx}dx = C_3 + \int_0^L \left(\mathbf{-E}_3^t \cdot \mathbf{R}\left(\dot{\mathbf{\Psi}}^m (1+\varepsilon) + \mathbf{\Psi}^m \dot{\varepsilon} \right) \cdot \mathbf{R}^t \mathbf{E}^t \begin{bmatrix} \xi \\ \eta \\ \chi \end{bmatrix} + \mathbf{E}_3^t \cdot \mathbf{t}_1 \dot{\varepsilon} \right) dx$$

$$\dot{\chi}\left(\tfrac{L}{2}\right) - \dot{\chi}\left(-\tfrac{L}{2}\right) = 0 = C_3 + \int_0^L \begin{bmatrix} \mathbf{E}_3^t \cdot \mathbf{t}_1 - \mathbf{E}_3^t \mathbf{R}\mathbf{\Psi}^m \mathbf{R}^t \mathbf{E}^t \begin{bmatrix} \xi \\ \eta \\ \chi \end{bmatrix} & \mathbf{R}^t \mathbf{E}_3 \times \left(\begin{bmatrix} \xi & \eta & \chi \end{bmatrix} \mathbf{RE} \right)^t \end{bmatrix} \begin{bmatrix} \dot{\varepsilon} \\ \dot{\phi}^m \end{bmatrix} dx \quad \text{(A.14)}$$

A.4 Derivation of Matrix B

Replacing Equation (2.72) at the right hand side of Equation (2.71):

$$\begin{bmatrix} 1 & 0 & 0 & 0 & 0 & 0 \\ 0 & 0 & -\xi_L & 0 & 0 & 0 \\ 0 & 0 & 0 & 0 & \xi_L & 0 \\ 0 & 0 & 0 & 0 & 0 & 1 \\ 0 & 0 & 0 & -1 & 1 & 0 \\ 0 & -1 & 1 & 0 & 0 & 0 \end{bmatrix} \begin{bmatrix} \dot{q}_1 \\ \dot{q}_2 \\ \dot{q}_3 \\ \dot{q}_4 \\ \dot{q}_5 \\ \dot{q}_6 \end{bmatrix} =$$

$$= \int_0^L \begin{bmatrix} \mathbf{E}_1^t \cdot \mathbf{t}_1 - \mathbf{E}_1^t \mathbf{R} \mathbf{\Psi}^m \mathbf{R}^t \mathbf{E}^t \begin{bmatrix} \xi \\ \eta \\ \chi \end{bmatrix} & \left(\mathbf{R}^t \mathbf{E}_1 \times \left(\begin{bmatrix} \xi & \eta & \chi \end{bmatrix} \mathbf{E}^t \mathbf{R} \right)^t \right) (1+\varepsilon) \\ \mathbf{E}_2^t \cdot \mathbf{t}_1 - \mathbf{E}_2^t \mathbf{R} \mathbf{\Psi}^m \mathbf{R}^t \mathbf{E}^t \begin{bmatrix} \xi \\ \eta \\ \chi \end{bmatrix} & \left(\mathbf{R}^t \mathbf{E}_2 \times \left(\begin{bmatrix} \xi & \eta & \chi \end{bmatrix} \mathbf{E}^t \mathbf{R} \right)^t \right) (1+\varepsilon) \\ \mathbf{E}_3^t \cdot \mathbf{t}_1 - \mathbf{E}_3^t \mathbf{R} \mathbf{\Psi}^m \mathbf{R}^t \mathbf{E}^t \begin{bmatrix} \xi \\ \eta \\ \chi \end{bmatrix} & \left(\mathbf{R}^t \mathbf{E}_3 \times \left(\begin{bmatrix} \xi & \eta & \chi \end{bmatrix} \mathbf{E}^t \mathbf{R} \right)^t \right) (1+\varepsilon) \\ \mathbf{R}\boldsymbol{\phi} & \mathbf{R}(1+\varepsilon) \end{bmatrix} \begin{bmatrix} \dot{\varepsilon} \\ \dot{\phi}^m \end{bmatrix} dx \tag{A.15}$$

Defining:

$$\mathbf{D} = \begin{bmatrix} 1 & 0 & 0 & 0 & 0 & 0 \\ 0 & 0 & -\xi_L & 0 & 0 & 0 \\ 0 & 0 & 0 & 0 & \xi_L & 0 \\ 0 & 0 & 0 & 0 & 0 & 1 \\ 0 & 0 & 0 & -1 & 1 & 0 \\ 0 & -1 & 1 & 0 & 0 & 0 \end{bmatrix} \tag{A.16}$$

D is an invertible matrix and is invariable with respect to *x* (because it contains the boundary conditions), so it can be included under the integral:

$$\begin{bmatrix} \dot{q}_1 \\ \dot{q}_2 \\ \dot{q}_3 \\ \dot{q}_4 \\ \dot{q}_5 \end{bmatrix} = \int_0^L \mathbf{D}^{-1} \begin{bmatrix} \mathbf{E}_1^t \cdot \mathbf{t}_1 - \mathbf{E}_1^t \mathbf{R} \boldsymbol{\Psi}^m \mathbf{R}^t \mathbf{E}^t \begin{bmatrix} \xi \\ \eta \\ \chi \end{bmatrix} & \left(\mathbf{R}^t \mathbf{E}_1 \times \left(\begin{bmatrix} \xi & \eta & \chi \end{bmatrix} \mathbf{E}^t \mathbf{R} \right)^t \right)(1+\varepsilon) \\ \mathbf{E}_2^t \cdot \mathbf{t}_1 - \mathbf{E}_2^t \mathbf{R} \boldsymbol{\Psi}^m \mathbf{R}^t \mathbf{E}^t \begin{bmatrix} \xi \\ \eta \\ \chi \end{bmatrix} & \left(\mathbf{R}^t \mathbf{E}_2 \times \left(\begin{bmatrix} \xi & \eta & \chi \end{bmatrix} \mathbf{E}^t \mathbf{R} \right)^t \right)(1+\varepsilon) \\ \mathbf{E}_3^t \cdot \mathbf{t}_1 - \mathbf{E}_3^t \mathbf{R} \boldsymbol{\Psi}^m \mathbf{R}^t \mathbf{E}^t \begin{bmatrix} \xi \\ \eta \\ \chi \end{bmatrix} & \left(\mathbf{R}^t \mathbf{E}_3 \times \left(\begin{bmatrix} \xi & \eta & \chi \end{bmatrix} \mathbf{E}^t \mathbf{R} \right)^t \right)(1+\varepsilon) \\ \mathbf{R}\boldsymbol{\phi} & \mathbf{R}(1+\varepsilon) \end{bmatrix} \begin{bmatrix} \dot{\varepsilon} \\ \dot{\boldsymbol{\phi}}^m \end{bmatrix} dx \tag{A.17}$$

The inverse of matrix **D** is:

$$\mathbf{D}^{-1} = \begin{bmatrix} 1 & 0 & 0 & 0 & 0 & 0 \\ 0 & \frac{-1}{\xi_L} & 0 & 0 & -1 & 0 \\ 0 & \frac{-1}{\xi_L} & 0 & 0 & 0 & 0 \\ 0 & 0 & \frac{1}{\xi_L} & -1 & 0 & 0 \\ 0 & 0 & \frac{1}{\xi_L} & 0 & 0 & 0 \\ 0 & 0 & 0 & 0 & 0 & 1 \end{bmatrix} \tag{A.18}$$

Defining **B**:

$$\mathbf{B} = \mathbf{D}^{-1} \cdot \begin{bmatrix} \mathbf{E}_1^t \cdot \mathbf{t}_1 - \mathbf{E}_1^t \mathbf{R} \boldsymbol{\Psi}^m \mathbf{R}^t \mathbf{E}^t \begin{bmatrix} \xi \\ \eta \\ \chi \end{bmatrix} & \left(\mathbf{R}^t \mathbf{E}_1 \times \left(\begin{bmatrix} \xi & \eta & \chi \end{bmatrix} \mathbf{E}^t \mathbf{R} \right)^t \right)(1+\varepsilon) \\ \mathbf{E}_2^t \cdot \mathbf{t}_1 - \mathbf{E}_2^t \mathbf{R} \boldsymbol{\Psi}^m \mathbf{R}^t \mathbf{E}^t \begin{bmatrix} \xi \\ \eta \\ \chi \end{bmatrix} & \left(\mathbf{R}^t \mathbf{E}_2 \times \left(\begin{bmatrix} \xi & \eta & \chi \end{bmatrix} \mathbf{E}^t \mathbf{R} \right)^t \right)(1+\varepsilon) \\ \mathbf{E}_3^t \cdot \mathbf{t}_1 - \mathbf{E}_3^t \mathbf{R} \boldsymbol{\Psi}^m \mathbf{R}^t \mathbf{E}^t \begin{bmatrix} \xi \\ \eta \\ \chi \end{bmatrix} & \left(\mathbf{R}^t \mathbf{E}_3 \times \left(\begin{bmatrix} \xi & \eta & \chi \end{bmatrix} \mathbf{E}^t \mathbf{R} \right)^t \right)(1+\varepsilon) \\ \mathbf{R}\boldsymbol{\phi} & \mathbf{R}(1+\varepsilon) \end{bmatrix} \tag{A.19}$$

$$\mathbf{B}=\begin{bmatrix}1&0&0&0&0&0\\0&\frac{-1}{\xi_L}&0&0&-1&0\\0&\frac{-1}{\xi_L}&0&0&0&0\\0&0&\frac{1}{\xi_L}&-1&0&0\\0&0&\frac{1}{\xi_L}&0&0&0\\0&0&0&0&0&1\end{bmatrix}\cdot\begin{bmatrix}\mathbf{E}_1^t\cdot\mathbf{t}_1-\mathbf{E}_1^t\mathbf{R}\boldsymbol{\Psi}^m\mathbf{R}^t\mathbf{E}^t\begin{bmatrix}\xi\\\eta\\\chi\end{bmatrix} & \left(\mathbf{R}^t\mathbf{E}_1\times\left(\begin{bmatrix}\xi&\eta&\chi\end{bmatrix}\mathbf{RE}\right)^t\right)(1+\varepsilon)\\\mathbf{E}_2^t\cdot\mathbf{t}_1-\mathbf{E}_2^t\mathbf{R}\boldsymbol{\Psi}^m\mathbf{R}^t\mathbf{E}^t\begin{bmatrix}\xi\\\eta\\\chi\end{bmatrix} & \left(\mathbf{R}^t\mathbf{E}_2\times\left(\begin{bmatrix}\xi&\eta&\chi\end{bmatrix}\mathbf{RE}\right)^t\right)(1+\varepsilon)\\\mathbf{E}_3^t\cdot\mathbf{t}_1-\mathbf{E}_3^t\mathbf{R}\boldsymbol{\Psi}^m\mathbf{R}^t\mathbf{E}^t\begin{bmatrix}\xi\\\eta\\\chi\end{bmatrix} & \left(\mathbf{R}^t\mathbf{E}_3\times\left(\begin{bmatrix}\xi&\eta&\chi\end{bmatrix}\mathbf{RE}\right)^t\right)(1+\varepsilon)\\\mathbf{R}\boldsymbol{\phi} & \mathbf{R}(1+\varepsilon)\end{bmatrix} \tag{A.20}$$

A.5 Force transformation from corotated to deformed coordinates

The transformation to deformed coordinates $\mathbf{t}$ is done through $\mathbf{R}^t$, i.e. the elements in $\mathbf{E}$ coordinate system have to be written in terms of the $\mathbf{t}$ coordinate system.

$$\begin{aligned}M_x(x)&=M_x^E(x)\left(E_1^tt_1\right)+M_y^E(x)\left(E_1^tt_2\right)+M_z^E(x)\left(E_1^tt_3\right)\\&=\left(Q_6-V_y\chi-V_z\eta\right)R_{11}+\left(\left(Q_4+Q_5\right)\frac{\xi}{\xi_L}-Q_4-\chi Q_1\right)R_{21}+\left(\left(Q_2+Q_3\right)\frac{\xi}{\xi_L}-Q_2+\eta Q_1\right)R_{31}\\&=\left(Q_6-\frac{Q_2+Q_3}{\xi_L}\chi-\frac{Q_4+Q_5}{\xi_L}\eta\right)R_{11}+\left(\left(Q_4+Q_5\right)\frac{\xi}{\xi_L}-Q_4-\chi Q_1\right)R_{21}+\left(\left(Q_2+Q_3\right)\frac{\xi}{\xi_L}-Q_2+\eta Q_1\right)R_{31}\\&=Q_1R_{11}+\frac{Q_2+Q_3}{\xi_L}R_{21}-\frac{Q_4+Q_5}{\xi_L}R_{31}=Q_1R_{11}-\frac{Q_2+Q_3}{\xi_L}R_{12}+\frac{Q_4+Q_5}{\xi_L}R_{13}\end{aligned} \tag{A.21}$$

$$\begin{aligned}M_y(x)&=M_x^E(x)\left(E_2^tt_1\right)+M_y^E(x)\left(E_2^tt_2\right)+M_z^E(x)\left(E_2^tt_3\right)\\&=\left(Q_6-V_y\chi-V_z\eta\right)R_{12}+\left(\left(Q_4+Q_5\right)\frac{\xi}{\xi_L}-Q_4-\chi Q_1\right)R_{22}+\left(\left(Q_2+Q_3\right)\frac{\xi}{\xi_L}-Q_2+\eta Q_1\right)R_{32}\\&=\left(Q_6-\frac{Q_2+Q_3}{\xi_L}\chi-\frac{Q_4+Q_5}{\xi_L}\eta\right)R_{12}+\left(\left(Q_4+Q_5\right)\frac{\xi}{\xi_L}-Q_4-\chi Q_1\right)R_{22}+\left(\left(Q_2+Q_3\right)\frac{\xi}{\xi_L}-Q_2+\eta Q_1\right)R_{32}\end{aligned} \tag{A.22}$$

$$\begin{aligned}M_z(x)&=M_x^E(x)\left(E_3^tt_1\right)+M_y^E(x)\left(E_3^tt_2\right)+M_z^E(x)\left(E_3^tt_3\right)\\&=\left(Q_6-V_y\chi-V_z\eta\right)R_{13}+\left(\left(Q_4+Q_5\right)\frac{\xi}{\xi_L}-Q_4-\chi Q_1\right)R_{23}+\left(\left(Q_2+Q_3\right)\frac{\xi}{\xi_L}-Q_2+\eta Q_1\right)R_{33}\\&=\left(Q_6-\frac{Q_2+Q_3}{\xi_L}\chi-\frac{Q_4+Q_5}{\xi_L}\eta\right)R_{13}+\left(\left(Q_4+Q_5\right)\frac{\xi}{\xi_L}-Q_4-\chi Q_1\right)R_{23}+\left(\left(Q_2+Q_3\right)\frac{\xi}{\xi_L}-Q_2+\eta Q_1\right)R_{33}\end{aligned} \tag{A.23}$$

$$\begin{aligned}P(x)&=Q_1\left(E_1^tt_1\right)+V_y\left(E_2^tt_1\right)-V_z\left(E_3^tt_1\right)\\&=Q_1R_{11}+\frac{Q_2+Q_3}{\xi_L}R_{21}-\frac{Q_4+Q_5}{\xi_L}R_{31}=Q_1R_{11}-\frac{Q_2+Q_3}{\xi_L}R_{12}+\frac{Q_4+Q_5}{\xi_L}R_{13}\end{aligned} \tag{A.24}$$

Thus, one can write the above equations in matrix form:

$$
\mathbf{B}^{*t} = \begin{bmatrix} R_{11} & \dfrac{-R_{12}}{\xi_L} & \dfrac{-R_{12}}{\xi_L} & \dfrac{R_{13}}{\xi_L} & \dfrac{R_{13}}{\xi_L} & 0 \\ R_{31}\eta - R_{21}\chi & \left(\dfrac{\xi}{\xi_L} - 1\right) R_{31} - R_{11}\dfrac{\chi}{\xi_L} & \dfrac{\xi R_{31} - R_{11}\chi}{\xi_L} & \left(\dfrac{\xi}{\xi_L} - 1\right) R_{21} - R_{11}\dfrac{\eta}{\xi_L} & \dfrac{\xi R_{21} - R_{11}\eta}{\xi_L} & R_{11} \\ R_{32}\eta - R_{22}\chi & \left(\dfrac{\xi}{\xi_L} - 1\right) R_{32} - R_{12}\dfrac{\chi}{\xi_L} & \dfrac{\xi R_{32} - R_{12}\chi}{\xi_L} & \left(\dfrac{\xi}{\xi_L} - 1\right) R_{22} - R_{12}\dfrac{\eta}{\xi_L} & \dfrac{\xi R_{22} - R_{12}\eta}{\xi_L} & R_{12} \\ R_{33}\eta - R_{23}\chi & \left(\dfrac{\xi}{\xi_L} - 1\right) R_{33} - R_{13}\dfrac{\chi}{\xi_L} & \dfrac{\xi R_{33} - R_{13}\chi}{\xi_L} & \left(\dfrac{\xi}{\xi_L} - 1\right) R_{23} - R_{13}\dfrac{\eta}{\xi_L} & \dfrac{\xi R_{23} - R_{13}\eta}{\xi_L} & R_{13} \end{bmatrix} \tag{A.25}
$$

$$
\begin{bmatrix} P \\ M_x \\ M_y \\ M_z \end{bmatrix} (x) = \mathbf{B}^{*t} \begin{bmatrix} Q_1 \\ Q_2 \\ Q_3 \\ Q_4 \\ Q_5 \\ Q_6 \end{bmatrix}
$$

APPENDIX B

This appendix contains the description of the input file to Element.exe and an example.

B.1 Input file user's manual

B.1.1 Introduction

Element.exe is a program capable of solving 3-dimensional structures with large displacements and large rotations. The nodes' initial position, the elements' connectivity, materials' definition, initial conditions, restraints, loads and output information are contained in an "input file", which has a strict format. The objective of this format is to guide the program through the different options and ensure the proper interpretation of the data. The user's manual is a description of the input file format.

B.1.2 General considerations

- The input file has to be named "InputFile.dat".
- Input file, load files and executable file must be in the same folder to run properly. Output files are also written in the same folder, therefore if more than 1 output file is to be written, they have to have different names or the information will be written in a single file. If the file already exists, it will not be overwritten, it will be appended.
- Each line is preceded by a few words (written in bold letters below) that tells the program what part of the input file is reading. These words are essential to the correct interpretation of the input file.
- The input file is case sensitive.
- The loading can be static or dynamic. For static analysis, a history of displacements or forces can be prescribed at any node and in any direction. When a static analysis is being performed, the time step is still needed and can be set to a very large quantity (100). This ensures that the rates of the variables remain constant after the initial velocity required to get to the initial conditions is reached. For dynamic analysis, the frequency of the

recorded motion can be used as time step. Sometimes, if the structure is highly nonlinear, a very small time step will prompt the solver into numerical errors and it will fail.

- Initial conditions: the program is set such that the user needs only to input the initial conditions for the variables, not for its rates. Even in the case of dynamic analysis, where the velocities are part of the variable vector, its initial conditions are not needed. In general, the set of initial conditions must be a good approximation of the actual deformations, forces and strains under the specified loads. If the solver fails in the initial conditions calculation is because there is an error in the user's input. The loads for initial conditions must also be provided so that equilibrium can be satisfied. The loads can be prescribed displacements or forces, not accelerations and must be defined separately from the analysis loads. It is a good idea to use gravity loads for initial conditions purposes because the structure is easy to solve for them. Also, the loads can be carried as constant loads through the analysis. The user can always skip the verification of the initial conditions but must provide the complete set for both the variables and its rates. It is recommended to let the solver compute these values. If an initial condition of no loading (a vector of zero valued variables) is used, the program will not converge.
- Damping: damping in this program is considered to be only mass proportional. Because the program lacks the procedure to calculate the frequencies of the structure, the first frequency must be input by the user along with the damping ratio associated to that frequency. Since this program is based on a formulation in the state space, no mass, stiffness or damping matrices are created. The damping is considered in every equilibrium equation that has mass, the damping coefficient "c" is then calculated as the mass factor $a_0 = 2\zeta\omega$ times the mass at that dof: $c = a_0\ m$.

B.1.3 Input file format

title: 1 line with no more than 128 characters

Example: *Program description*
The actual word "title" is not needed but the program expects the first sentence to be an explanatory note.

total time Total number of points in the input load file

Example: *total time 745*

time step Frequency of the input motion.

Example: *time step 10*

node node # <SPACE> coordinate x <SPACE> coordinate y <SPACE> coordinate z

Example: *node 1 10 10 0*
node #1 has coordinates x=10, y=10 and z=0
all coordinates must be specified even if they are zero

element element # <SPACE> node i <SPACE> node j <SPACE> material # <SPACE> number of integration points

Example: *element 1 2 6 1 10*
element 1 goes from node 2 to node 6, has material properties #1 and 10 integration points.
The number of integration points has to be between 3 and 10 (including these numbers)

spring spring # <SPACE> node number <SPACE> stiffness x <SPACE> stiffness y <SPACE> stiffness z <SPACE> rotational stiffness x <SPACE> rotational stiffness y <SPACE> rotational stiffness z

Example: *spring 1 2 10 3 400 0.05 30 11*
Spring #1 is attached to node #2 and has the following stiffnesses: $K_x = 10$; $K_y = 3$; $K_z = 400$; $K_{\theta x} = 0.05$; $K_{\theta y} = 30$ *and* $K_{\theta z} = 11$

material material # <SPACE> section type <SPACE> E <SPACE> A <SPACE> G <SPACE> J <SPACE> Iy <SPACE> Iz <SPACE> Zy <SPACE> Zz <SPACE> σ_y <SPACE> a

Example: *material 1 HSS 29000 0.84 11600 0.796 0.486 0.486 0.584 0.584 60 0.03*
Section type can be 'HSS', 'W' or 'ELASTIC'
E: modulus of elasticity
A: area of the section
G: Shear modulus
J: torsional stiffness
I_y, I_z: *inertia in the weak and strong axis*

Z_y, Z_z: plastic modulus in the weak and strong axis
σ_y: yield strength
a: post yield stiffness, ratio of the elastic stiffness

restraint node number <SPACE> direction x <SPACE> direction y <SPACE> direction z <SPACE> rotation x <SPACE> rotation y <SPACE> rotation z

Example: *restraint 5 1 1 1 0 0 0*
Node 5 is restraint against displacement but not against rotation
restraint = 0: not restrained
restraint = 1: restrained

damping damping ratio <SPACE> frequency

Example: *damping 0.06 26.7*
In this case, the modal damping ratio is 6% and the frequency of the structure is ω =26.7 rad/s.

load analysis force node number <SPACE> direction <SPACE> file name

Example: *load analysis force 2 1 load.dat*
The load contained in file 'load.dat' is applied at node#2 in the direction 1.
direction = 1: global x translation
direction = 2: global y translation
direction = 3: global z translation
direction = 4: global x rotation
direction = 5: global y rotation
direction = 6: global z rotation

load analysis disp node number <SPACE> direction <SPACE> file name

Same as load force.

load analysis accel 0 <SPACE> direction <SPACE> gravity <SPACE> file name

Example: *load analysis accel 0 1 386.4 accel.dat*
In this case, the node number 0 is not considered by the program, so any number can be input.
directions are the same as in "load analysis force"
gravity is the constant by which the file "accel.dat" must be amplified to obtain proper acceleration units

analysis IC consistent <SPACE> permanent

Example: *analysis IC 0 0*
consistent IC: 0=no; 1=yes
permanent IC: 0=no; 1=yes

load IC force node number <SPACE> direction <SPACE> file name

Same as "load analysis force"

load IC disp node number <SPACE> direction <SPACE> file name

Same as "load analysis disp"

analysis type

Example: *analysis static*
Available types: static; dynamic

Numbering type

Example: *Numbering RCM*
Available types: PLAIN; RCM

IC node node # <SPACE> displ x <SPACE> displ y <SPACE> displ z <SPACE> rotation x <SPACE> rotation y <SPACE> rotation z

Example: *IC node 1 0.01 0.01 0 0 0 0.00004*
The initial displacement of node 1 is:
displacement x = 0.01
displacement y = 0.01
displacement z = 0
rotation x = 0
rotation y = 0
rotation z = 0.00004

IC element element # <SPACE> axial force <SPACE> moment z node i <SPACE> moment z node j <SPACE> moment y node i <SPACE> moment y node j <SPACE> torsion

Example: *IC element 5 10.8 -2.3 3.5 4.8 6.6 0.1*
Element 5 in CR coordinates is in equilibrium with the following forces:
Axial force = 10.8
Moment z (strong) node i = -2.3

Moment z (strong) node j = 3.5
Moment y (weak) node i = 4.8
Moment y (weak) node j = 6.6
Torsion = 0.1

IC ip element number <SPACE> integration point # <SPACE> axial deformation ε <SPACE> curvature x <SPACE> curvature y <SPACE> curvature z

Example: *IC ip 1 3 0.0002 0.00004 0.000005 0.000003*
Integration point # 3 on element #1 has the following strains:
Axial strain e = 0.0002
Curvature in x (axial)direction = 0.00004
Curvature in y (weak) direction = 0.000005
Curvature in z (strong) direction = 0.000003

outputfiles number of files <SPACE> number of points in each file

Example: *outputfiles 3 120 380 245*
There will be 3 output files, the first one will have 120 points, the second one will have 380 points and the third one will have 245 points. The total number of points (120+380+245) = 745 cannot exceed the **total time** *specified in line 2.*

output node node # <SPACE> directions

Example: *output node 1 1 1 1 0 0 0*
Print output = 1 do not print output = 0
In the example, only displacements will be printed for node 1.

file file name for output node above

Example: *file node1_1.out*
file node 1_2.out
file node1_3.out
Since 3 files were specified in the line **outputfiles**, *3 lines of input with names for the different files are expected by the program.*

output element element # <SPACE> type <SPACE> forces

Example: *output element 5 global 1 1 1 1 1 0*

All forces except torsion will be written to files for element #5.
Available types: global; local

file file name for output element above

Same as for output node.

output ip ip # <SPACE> strains

Example: *output ip 260 1 0 0 0*
Only axial strains will be written to file for IP #260.

file file name for output ip above

Same as in output node.

B.2 Example of input file

This input file corresponds to the 1st story zipper frame model analyzed in Chapter 5.

ZipperHinged

total time 15000

time step 10

node 1 0 0 0

node 2 4.8337693005949358 6.3745332651595712 0.037058924051024691

node 3 14.010378207193135 18.476186260735943 0.089137627700906039

node 4 17.409122246673949 22.958279962801267 0.097936784822100817

node 5 20.807866286154763 27.440373664866591 0.099798774491541772

node 6 24.206610325635577 31.922467366931915 0.094591706182561006

node 7 27.6053543651163911 36.404561068997239 0.082684412758701434

node 8 3.67819632717145881 4.8506214064573612 0.025006173300166315

node 9 40 52.75 0

node 10 43.218036728285412 48.506214064573612 0.025006173300166315

node 11 52.394645634883609 36.404561068997239 0.082684412758701434

node 12 55.793389674364420 31.922467366931915 0.094591706182561006

node 13 59.192133713845237 27.440373664866591 0.099798774491541772

node 14 62.590877753326055 22.958279962801267 0.097936784822100817 node 15 65.989621792806872 18.476186260735943 0.089137627700906039

node 16 75.166230699405062 6.3745332651595712 0.037058924051024691

node 17 80 0 0

node 18 0 52.75 0

node 19 80 52.75 0

mass 18 0.022 0 0 0 0 0

mass 19 0.022 0 0 0 0 0

element 1 1 2 2 10

element 2 2 3 1 10

element 3 3 4 1 10

element 4 4 5 1 10

element 5 5 6 1 10

element 6 6 7 1 10

element 7 7 8 1 10

element 8 8 9 2 10

element 9 10 9 2 10

element 10 11 10 1 10

element 11 12 11 1 10

element 12 13 12 1 10

element 13 14 13 1 10

element 14 15 14 1 10

element 15 16 15 1 10

element 16 17 16 2 10

element 17 18 9 3 10

element 18 9 19 3 10

spring 1 9 0 383 0 0 0 0

material 1 HSS 29000 0.84 11600 0.796 0.486 0.486 0.584 0.584 60 0.03

material 2 HSS 29000 4.2 11600 0.796 0.0972 0.0486 0.292 0.292 60 0.03

material 3 W 29000 2.2 11600 0.07 0.461 1.94 0.821 2.35 50 0.03

restraint 1 1 1 1 1 1 1

restraint 17 1 1 1 1 1 1

```
restraint 18 0 1 1 1 1 1
restraint 19 0 1 1 1 1 1
Numbering RCM
analysis dynamic
damping 0.06 26.7
load analysis accel 0 1 386.4 Test2_accel.dat
analysis IC 0 0
load IC disp 18 1 ICbeamW_floor1.dat
load IC disp 19 1 ICbeamE_floor1.dat

IC node 1       0 0 0 0 0 0
IC node 2       -4.8922121782979389e-5 8.1590734168912604e-11 0 0 0 0
IC node 3       -1.4179771235589556e-4 2.3648638602935534e-10 0 0 0 0
IC node 4       -1.7619607923435865e-4 2.9385560651462583e-10 0 0 0 0
IC node 5       -2.1059444611637446e-4 3.5121772157253872e-10 0 0 0 0
IC node 6       -2.4499281299128484e-4 4.0859049477148801e-10 0 0 0 0
IC node 7       -2.7939117987330064e-4 4.6595260982940090e-10 0 0 0 0
IC node 8       -3.7226677044088774e-4 6.2085803165246034e-10 0 0 0 0
IC node 9       -4.0483621572496540e-4 6.7517461471324837e-10 0 0 0 0
IC node 10      -3.7226677044088774e-4 6.2085092622510274e-10 0 0 0 0
IC node 11      -2.7939117987330064e-4 4.659597152567585e-10 0  0 0 0
IC node 12      -2.44992812994837550e-4 4.0860115291252441e-10 0 0 0 0
IC node 13      -2.10594446116374460e-4 3.5122837971357512e-10 0 0 0 0
IC node 14      -1.76196079237911360e-4 2.9385560651462583e-10 0 0 0 0
IC node 15      -1.41797712359448270e-4 2.3648638602935534e-10 0 0 0 0
IC node 16      -4.89221217776503180e-5 8.1590734168912604e-11 0  0 0 0
IC node 17      0 0 0 0 0 0
IC node 18      -4.38933638844259E-04 0 0 0 0 0
IC node 19      -4.38933638844259E-04 0 0 0 0 0
IC element 1    -9.00E-02 0 7.67E-06 0 3.34E-03      0
IC element 2    -9.00E-02  -5.68E-06  1.37E-05  -3.34E-03  8.02E-03  0
```

IC element 3 -9.00E-02 -6.23E-06 6.85E-06 -8.02E-03 8.82E-03 0

IC element 4 -9.00E-02 -1.45E-06 1.48E-06 -8.82E-03 8.98E-03 0

IC element 5 -9.00E-02 4.13E-06 -3.91E-06 -8.98E-03 8.51E-03 0

IC element 6 -9.00E-02 8.95E-06 -7.83E-06 -8.51E-03 7.44E-03 0

IC element 7 -9.00E-02 1.40E-05 -4.25E-06 -7.44E-03 2.25E-03 0

IC element 8 -9.00E-02 5.25E-06 4.97E-17 -2.25E-03 -3.04E-18 0

IC element 9 9.00E-02 -2.13E-05 -1.12E-15 2.25E-03 -1.30E-18 0

IC element 10 9.00E-02 -5.69E-05 1.72E-05 7.44E-03 -2.25E-03 0

IC element 11 9.00E-02 -3.63E-05 3.17E-05 8.51E-03 -7.44E-03 0

IC element 12 9.00E-02 -1.67E-05 1.59E-05 8.98E-03 -8.51E-03 0

IC element 13 9.00E-02 5.87E-06 -5.99E-06 8.82E-03 -8.98E-03 0

IC element 14 9.00E-02 2.53E-05 -2.78E-05 8.02E-03 -8.82E-03 0

IC element 15 9.00E-02 2.30E-05 -5.54E-05 3.34E-03 -8.02E-03 0

IC element 16 9.00E-02 0 -3.11E-05 0 -3.34E-03 0

IC element 17 5.44E-02 0 0 0 0 0

IC element 18 -5.44E-02 0 0 0 0 0

IC ip 1 1	-3.69E-06	0.00E+00	0.00E+00	0.00E+00
IC ip 1 2	-3.69E-06	0.00E+00	1.39E-08	3.09E-11
IC ip 1 3	-3.69E-06	0.00E+00	4.50E-08	1.00E-10
IC ip 1 4	-3.69E-06	0.00E+00	8.99E-08	2.01E-10
IC ip 1 5	-3.69E-06	0.00E+00	1.44E-07	3.21E-10
IC ip 1 6	-3.69E-06	0.00E+00	2.01E-07	4.48E-10
IC ip 1 7	-3.69E-06	0.00E+00	2.54E-07	5.68E-10
IC ip 1 8	-3.69E-06	0.00E+00	2.99E-07	6.68E-10
IC ip 1 9	-3.69E-06	0.00E+00	3.30E-07	7.38E-10
IC ip 1 10	-3.69E-06	0.00E+00	3.44E-07	7.68E-10
IC ip 2 1	-3.69E-06	1.27E-23	3.44E-07	5.38E-10
IC ip 2 2	-3.69E-06	1.27E-23	3.53E-07	5.53E-10
IC ip 2 3	-3.69E-06	1.27E-23	3.74E-07	5.84E-10
IC ip 2 4	-3.69E-06	1.27E-23	4.03E-07	6.30E-10
IC ip 2 5	-3.69E-06	1.27E-23	4.38E-07	6.85E-10

IC ip 2 6	-3.69E-06	1.27E-23	4.75E-07	7.43E-10
IC ip 2 7	-3.69E-06	1.27E-23	5.11E-07	7.98E-10
IC ip 2 8	-3.69E-06	1.27E-23	5.40E-07	8.44E-10
IC ip 2 9	-3.69E-06	1.27E-23	5.60E-07	8.76E-10
IC ip 2 10	-3.69E-06	1.27E-23	5.69E-07	8.90E-10
IC ip 3 1	-3.69E-06	3.23E-23	5.69E-07	4.42E-10
IC ip 3 2	-3.69E-06	3.23E-23	5.72E-07	4.44E-10
IC ip 3 3	-3.69E-06	3.23E-23	5.77E-07	4.48E-10
IC ip 3 4	-3.69E-06	3.23E-23	5.84E-07	4.54E-10
IC ip 3 5	-3.69E-06	3.23E-23	5.93E-07	4.61E-10
IC ip 3 6	-3.69E-06	3.23E-23	6.02E-07	4.68E-10
IC ip 3 7	-3.69E-06	3.23E-23	6.11E-07	4.75E-10
IC ip 3 8	-3.69E-06	3.23E-23	6.18E-07	4.80E-10
IC ip 3 9	-3.69E-06	3.23E-23	6.23E-07	4.84E-10
IC ip 3 10	-3.69E-06	3.23E-23	6.25E-07	4.86E-10
IC ip 4 1	-3.69E-06	-8.86E-23	6.25E-07	1.03E-10
IC ip 4 2	-3.69E-06	-8.86E-23	6.26E-07	1.03E-10
IC ip 4 3	-3.69E-06	-8.86E-23	6.27E-07	1.03E-10
IC ip 4 4	-3.69E-06	-8.86E-23	6.29E-07	1.03E-10
IC ip 4 5	-3.69E-06	-8.86E-23	6.30E-07	1.04E-10
IC ip 4 6	-3.69E-06	-8.86E-23	6.32E-07	1.04E-10
IC ip 4 7	-3.69E-06	-8.86E-23	6.34E-07	1.04E-10
IC ip 4 8	-3.69E-06	-8.86E-23	6.36E-07	1.05E-10
IC ip 4 9	-3.69E-06	-8.86E-23	6.37E-07	1.05E-10
IC ip 4 10	-3.69E-06	-8.86E-23	6.37E-07	1.05E-10
IC ip 5 1	-3.69E-06	-1.59E-23	6.37E-07	-2.93E-10
IC ip 5 2	-3.69E-06	-1.59E-23	6.36E-07	-2.92E-10
IC ip 5 3	-3.69E-06	-1.59E-23	6.33E-07	-2.91E-10
IC ip 5 4	-3.69E-06	-1.59E-23	6.29E-07	-2.89E-10
IC ip 5 5	-3.69E-06	-1.59E-23	6.23E-07	-2.87E-10
IC ip 5 6	-3.69E-06	-1.59E-23	6.18E-07	-2.84E-10

IC ip 5 7	-3.69E-06	-1.59E-23	6.13E-07	-2.82E-10
IC ip 5 8	-3.69E-06	-1.59E-23	6.08E-07	-2.80E-10
IC ip 5 9	-3.69E-06	-1.59E-23	6.05E-07	-2.78E-10
IC ip 5 10	-3.69E-06	-1.59E-23	6.04E-07	-2.78E-10
IC ip 6 1	-3.69E-06	-1.19E-22	6.04E-07	-6.35E-10
IC ip 6 2	-3.69E-06	-1.19E-22	6.01E-07	-6.32E-10
IC ip 6 3	-3.69E-06	-1.19E-22	5.94E-07	-6.25E-10
IC ip 6 4	-3.69E-06	-1.19E-22	5.84E-07	-6.14E-10
IC ip 6 5	-3.69E-06	-1.19E-22	5.72E-07	-6.02E-10
IC ip 6 6	-3.69E-06	-1.19E-22	5.60E-07	-5.89E-10
IC ip 6 7	-3.69E-06	-1.19E-22	5.48E-07	-5.76E-10
IC ip 6 8	-3.69E-06	-1.19E-22	5.38E-07	-5.66E-10
IC ip 6 9	-3.69E-06	-1.19E-22	5.31E-07	-5.58E-10
IC ip 6 10	-3.69E-06	-1.19E-22	5.28E-07	-5.55E-10
IC ip 7 1	-3.69E-06	-1.81E-22	5.28E-07	-9.34E-10
IC ip 7 2	-3.69E-06	-1.81E-22	5.18E-07	-9.16E-10
IC ip 7 3	-3.69E-06	-1.81E-22	4.95E-07	-8.76E-10
IC ip 7 4	-3.69E-06	-1.81E-22	4.62E-07	-8.17E-10
IC ip 7 5	-3.69E-06	-1.81E-22	4.22E-07	-7.46E-10
IC ip 7 6	-3.69E-06	-1.81E-22	3.80E-07	-6.72E-10
IC ip 7 7	-3.69E-06	-1.81E-22	3.40E-07	-6.02E-10
IC ip 7 8	-3.69E-06	-1.81E-22	3.07E-07	-5.43E-10
IC ip 7 9	-3.69E-06	-1.81E-22	2.84E-07	-5.02E-10
IC ip 7 10	-3.69E-06	-1.81E-22	2.74E-07	-4.84E-10
IC ip 8 1	-3.69E-06	-2.65E-22	2.74E-07	-6.24E-10
IC ip 8 2	-3.69E-06	-2.65E-22	2.62E-07	-5.99E-10
IC ip 8 3	-3.69E-06	-2.65E-22	2.38E-07	-5.42E-10
IC ip 8 4	-3.69E-06	-2.65E-22	2.02E-07	-4.61E-10
IC ip 8 5	-3.69E-06	-2.65E-22	1.59E-07	-3.63E-10
IC ip 8 6	-3.69E-06	-2.65E-22	1.14E-07	-2.60E-10
IC ip 8 7	-3.69E-06	-2.65E-22	7.14E-08	-1.63E-10

IC ip 8 8	-3.69E-06	-2.65E-22	3.57E-08	-8.15E-11
IC ip 8 9	-3.69E-06	-2.65E-22	1.10E-08	-2.51E-11
IC ip 8 10	-3.69E-06	-2.65E-22	-1.85E-22	1.47E-20
IC ip 9 1	3.69E-06	2.22E-22	-2.73E-07	2.53E-09
IC ip 9 2	3.69E-06	2.22E-22	-2.62E-07	2.43E-09
IC ip 9 3	3.69E-06	2.22E-22	-2.38E-07	2.20E-09
IC ip 9 4	3.69E-06	2.22E-22	-2.02E-07	1.87E-09
IC ip 9 5	3.69E-06	2.22E-22	-1.59E-07	1.47E-09
IC ip 9 6	3.69E-06	2.22E-22	-1.14E-07	1.06E-09
IC ip 9 7	3.69E-06	2.22E-22	-7.14E-08	6.60E-10
IC ip 9 8	3.69E-06	2.22E-22	-3.57E-08	3.30E-10
IC ip 9 9	3.69E-06	2.22E-22	-1.10E-08	1.02E-10
IC ip 9 10	3.69E-06	2.22E-22	-1.85E-22	-3.69E-20
IC ip 10 1	3.69E-06	2.68E-22	-5.28E-07	3.79E-09
IC ip 10 2	3.69E-06	2.68E-22	-5.18E-07	3.71E-09
IC ip 10 3	3.69E-06	2.68E-22	-4.95E-07	3.55E-09
IC ip 10 4	3.69E-06	2.68E-22	-4.62E-07	3.31E-09
IC ip 10 5	3.69E-06	2.68E-22	-4.22E-07	3.03E-09
IC ip 10 6	3.69E-06	2.68E-22	-3.80E-07	2.72E-09
IC ip 10 7	3.69E-06	2.68E-22	-3.40E-07	2.44E-09
IC ip 10 8	3.69E-06	2.68E-22	-3.07E-07	2.20E-09
IC ip 10 9	3.69E-06	2.68E-22	-2.84E-07	2.04E-09
IC ip 10 10	3.69E-06	2.68E-22	-2.73E-07	1.96E-09
IC ip 11 1	3.69E-06	5.42E-22	-6.04E-07	2.57E-09
IC ip 11 2	3.69E-06	5.42E-22	-6.01E-07	2.56E-09
IC ip 11 3	3.69E-06	5.42E-22	-5.94E-07	2.53E-09
IC ip 11 4	3.69E-06	5.42E-22	-5.84E-07	2.49E-09
IC ip 11 5	3.69E-06	5.42E-22	-5.72E-07	2.44E-09
IC ip 11 6	3.69E-06	5.42E-22	-5.60E-07	2.39E-09
IC ip 11 7	3.69E-06	5.42E-22	-5.48E-07	2.34E-09
IC ip 11 8	3.69E-06	5.42E-22	-5.38E-07	2.29E-09

IC ip 11 9	3.69E-06	5.42E-22	-5.31E-07	2.26E-09
IC ip 11 10	3.69E-06	5.42E-22	-5.28E-07	2.25E-09
IC ip 12 1	3.69E-06	-3.71E-22	-6.37E-07	1.19E-09
IC ip 12 2	3.69E-06	-3.71E-22	-6.36E-07	1.19E-09
IC ip 12 3	3.69E-06	-3.71E-22	-6.33E-07	1.18E-09
IC ip 12 4	3.69E-06	-3.71E-22	-6.29E-07	1.17E-09
IC ip 12 5	3.69E-06	-3.71E-22	-6.23E-07	1.16E-09
IC ip 12 6	3.69E-06	-3.71E-22	-6.18E-07	1.15E-09
IC ip 12 7	3.69E-06	-3.71E-22	-6.13E-07	1.14E-09
IC ip 12 8	3.69E-06	-3.71E-22	-6.08E-07	1.13E-09
IC ip 12 9	3.69E-06	-3.71E-22	-6.05E-07	1.13E-09
IC ip 12 10	3.69E-06	-3.71E-22	-6.04E-07	1.13E-09
IC ip 13 1	3.69E-06	-1.93E-22	-6.25E-07	-4.17E-10
IC ip 13 2	3.69E-06	-1.93E-22	-6.26E-07	-4.17E-10
IC ip 13 3	3.69E-06	-1.93E-22	-6.27E-07	-4.18E-10
IC ip 13 4	3.69E-06	-1.93E-22	-6.29E-07	-4.19E-10
IC ip 13 5	3.69E-06	-1.93E-22	-6.30E-07	-4.20E-10
IC ip 13 6	3.69E-06	-1.93E-22	-6.32E-07	-4.21E-10
IC ip 13 7	3.69E-06	-1.93E-22	-6.34E-07	-4.23E-10
IC ip 13 8	3.69E-06	-1.93E-22	-6.36E-07	-4.24E-10
IC ip 13 9	3.69E-06	-1.93E-22	-6.37E-07	-4.24E-10
IC ip 13 10	3.69E-06	-1.93E-22	-6.37E-07	-4.25E-10
IC ip 14 1	3.69E-06	-5.45E-22	-5.69E-07	-1.79E-09
IC ip 14 2	3.69E-06	-5.45E-22	-5.72E-07	-1.80E-09
IC ip 14 3	3.69E-06	-5.45E-22	-5.77E-07	-1.82E-09
IC ip 14 4	3.69E-06	-5.45E-22	-5.84E-07	-1.84E-09
IC ip 14 5	3.69E-06	-5.45E-22	-5.93E-07	-1.87E-09
IC ip 14 6	3.69E-06	-5.45E-22	-6.02E-07	-1.90E-09
IC ip 14 7	3.69E-06	-5.45E-22	-6.11E-07	-1.92E-09
IC ip 14 8	3.69E-06	-5.45E-22	-6.18E-07	-1.95E-09
IC ip 14 9	3.69E-06	-5.45E-22	-6.23E-07	-1.96E-09

IC ip 14 10	3.69E-06	-5.45E-22	-6.25E-07	-1.97E-09
IC ip 15 1	3.69E-06	-2.75E-22	-3.44E-07	-2.18E-09
IC ip 15 2	3.69E-06	-2.75E-22	-3.53E-07	-2.24E-09
IC ip 15 3	3.69E-06	-2.75E-22	-3.74E-07	-2.37E-09
IC ip 15 4	3.69E-06	-2.75E-22	-4.03E-07	-2.55E-09
IC ip 15 5	3.69E-06	-2.75E-22	-4.38E-07	-2.78E-09
IC ip 15 6	3.69E-06	-2.75E-22	-4.75E-07	-3.01E-09
IC ip 15 7	3.69E-06	-2.75E-22	-5.11E-07	-3.24E-09
IC ip 15 8	3.69E-06	-2.75E-22	-5.40E-07	-3.42E-09
IC ip 15 9	3.69E-06	-2.75E-22	-5.60E-07	-3.55E-09
IC ip 15 10	3.69E-06	-2.75E-22	-5.69E-07	-3.61E-09
IC ip 16 1	3.69E-06	0.00E+00	0.00E+00	0.00E+00
IC ip 16 2	3.69E-06	0.00E+00	-1.39E-08	-1.25E-10
IC ip 16 3	3.69E-06	0.00E+00	-4.50E-08	-4.07E-10
IC ip 16 4	3.69E-06	0.00E+00	-8.99E-08	-8.13E-10
IC ip 16 5	3.69E-06	0.00E+00	-1.44E-07	-1.30E-09
IC ip 16 6	3.69E-06	0.00E+00	-2.01E-07	-1.81E-09
IC ip 16 7	3.69E-06	0.00E+00	-2.54E-07	-2.30E-09
IC ip 16 8	3.69E-06	0.00E+00	-2.99E-07	-2.71E-09
IC ip 16 9	3.69E-06	0.00E+00	-3.30E-07	-2.99E-09
IC ip 16 10	3.69E-06	0.00E+00	-3.44E-07	-3.11E-09

IC ip 17 1	8.52E-07	0	0	0
IC ip 17 2	8.52E-07	0	0	0
IC ip 17 3	8.52E-07	0	0	0
IC ip 17 4	8.52E-07	0	0	0
IC ip 17 5	8.52E-07	0	0	0
IC ip 17 6	8.52E-07	0	0	0
IC ip 17 7	8.52E-07	0	0	0
IC ip 17 8	8.52E-07	0	0	0
IC ip 17 9	8.52E-07	0	0	0
IC ip 17 10	8.52E-07	0	0	0

```
IC ip 18 1    -8.52E-07   0   0   0
IC ip 18 2    -8.52E-07   0   0   0
IC ip 18 3    -8.52E-07   0   0   0
IC ip 18 4    -8.52E-07   0   0   0
IC ip 18 5    -8.52E-07   0   0   0
IC ip 18 6    -8.52E-07   0   0   0
IC ip 18 7    -8.52E-07   0   0   0
IC ip 18 8    -8.52E-07   0   0   0
IC ip 18 9    -8.52E-07   0   0   0
IC ip 18 10   -8.52E-07   0   0   0
outputfiles 1 15000
output node disp 2 1 1 1 0 0 0
file node2_80.out
output node disp 3 1 1 1 0 0 0
file node3_80.out
output node disp 4 1 1 1 0 0 0
file node4_80.out
output node disp 5 1 1 1 0 0 0
file node5_80.out
output node disp 6 1 1 1 0 0 0
file node6_80.out
output node disp 7 1 1 1 0 0 0
file node7_80.out
output node disp 8 1 1 1 0 0 0
file node8_80.out
output node disp 9 1 1 1 1 1 1
file node9_80.out
output node disp 10 1 1 1 0 0 0
file node10_80.out
output node disp 11 1 1 1 0 0 0
file node11_80.out
```

```
output node disp 12 1 1 1 0 0 0
file node12_80.out
output node disp 13 1 1 1 0 0 0
file node13_80.out
output node disp 14 1 1 1 0 0 0
file node14_80.out
output node disp 15 1 1 1 0 0 0
file node15_80.out
output node disp 16 1 1 1 0 0 0
file node16_80.out
output node accel 18 1
file aacelnode18_80.out
output node accel 19 1
file aacelnode19_80.out
output element 1 global 1 1 1 1 1 1
file element1_80.out
output element 2 local 1 1 1 1 1 1
file element2_80.out
output element 3 local 1 1 1 1 1 1
file element3_80.out
output element 4 local 1 1 1 1 1 1
file element4_80.out
output element 5 local 1 1 1 1 1 1
file element5_80.out
output element 6 local 1 1 1 1 1 1
file element6_80.out
output element 7 local 1 1 1 1 1 1
file element7_80.out
output element 8 global 1 1 1 1 1 1
file element8_80.out
output element 9 global 1 1 1 1 1 1
```

file element9_80.out
output element 10 local 1 1 1 1 1 1
file element10_80.out
output element 11 local 1 1 1 1 1 1
file element11_80.out
output element 12 local 1 1 1 1 1 1
file element12_80.out
output element 13 local 1 1 1 1 1 1
file element13_80.out
output element 14 local 1 1 1 1 1 1
file element14_80.out
output element 15 local 1 1 1 1 1 1
file element15_80.out
output element 16 global 1 1 1 1 1 1
file element16_80.out
output element 17 local 1 1 1 1 1 1
file element17_80.out
output element 18 local 1 1 1 1 1 1
file element18_80.out

APPENDIX C
DESIGN OF THE "ZIPPER FRAME"

This Appendix contains information about the general design procedure of a full scale "zipper frame" prototype as developed by Yang (Yang 2006) (all the information presented here has been kindly provided by Walter Yang). In addition, seismic requirements on compactness, slenderness and bracing length for the 1/3 scaled "zipper frame" model are also presented.

C.1 Suspended "zipper frame" design methodology

The methodology proposed by Yang (Yang 2006) is a two step design procedure. Step I is a design by strength where the frame is analyzed without considering the contribution from the "zipper columns" i.e. like a conventional chevron braced frame. All the frame members, except for the top story braces, are designed to resist the actions from combined gravity and lateral loads.

Step II is a design by capacity where the frame is analyzed considering the "zipper columns". The introduction of these new elements will change the design of all the other structural members except for the braces below the top story.

The "zipper column" is designed to resist the vertical unbalanced forces generated by the braces below the floor under consideration, assuming P_y (not R_y P_y) for the braces in tension and 0.3 times ϕ_c P_n for the braces in compression. The use of a tension brace force of P_y in the capacity calculation prevents excessive deformations in the tension brace and forces the "zipper column" to yield soon after the brace under tension force yields, preventing drift concentration in a single floor. The value used for the compression capacity is in accordance with current codes, and reflects the capacity of a moderately slender brace after buckling. The shear capacity of the beams is ignored.

The top-story braces need to resist both the vertical unbalanced forces and the top-floor level equivalent lateral earthquake force. A factor of 1.7 times the top-floor level equivalent earthquake force is used because the top-story braces need to be elastic throughout the load history. As mentioned by Yang (Yang 2006), this value needs further research.

A flow chart of the design procedure is found in Figure C–1.

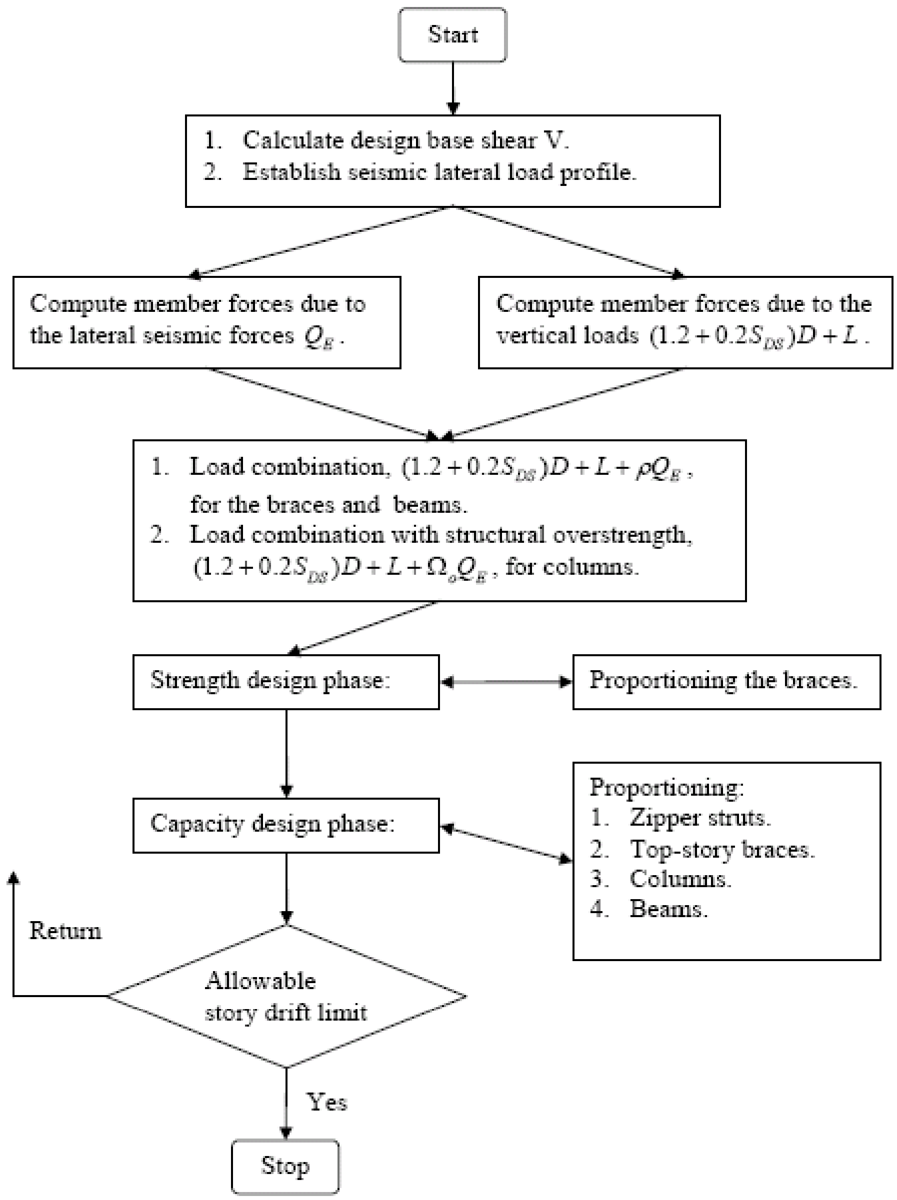

Figure C–1: Flow chart of the design procedure of a "zipper" braced frame. (From Yang, 2006 Figure 6.3)

C.2 Design of the 3 story prototype

A detailed calculation of the member sizes for the three stories prototype can be found in (Yang 2006). For completeness, the most important features of the procedure are repeated here.

The chosen prototype is the 3 story SAC moment resisting frame (FEMA 2000) designed for downtown Los Angeles. For the 2 % probability of exceedance in 50 years, the mapped spectral accelerations for the short and 1 sec period are 2.16g and 0.72g, respectively, with a PGA of 0.90 g.

The design code is the 2005 ASCE-7 (ASCE 2005) for loads and the 2005 AISC LRFD, Seismic Provisions and Specifications for members and frame design (AISC 2003; AISC 2005a; AISC 2005b). The building is designed as if located on stiff soil (site class D as per ASCE 7-05 definitions). An importance factor of 1.5 is assigned to the building in accordance of Occupancy Category IV. The response modification coefficient, R is 6, consistent with other ductile braced systems (special steel concentrically braced frames).

The lateral load design was controlled by the seismic load provisions from Chapter 12 of ASCE 7-05. For design, the beam-to-column connections as well as brace-to-beam and "zipper column"-to-beam intersections are assumed to be pinned.

The calculated seismic base shear was 390 kips per braced bay, with the floor loads being 203 kips, 125 kips, and 62 kips from the roof to second floor levels, respectively.

The seismic load combination 5 (ASCE 7-05, Section 12.4.2.3, Equation 4.1) is adopted as the critical basic load combination for strength design and the system overstrength factor for concentrically braced frames is 2. A summary of demands of the members in the strength design phase is shown in Table C–1. In this phase only the 1st and 2nd story braces are designed because they provide most of the lateral resistance of the entire frame. The section HSS 8x8x1/2 is selected for the first story braces. This section also meets the requirements for slenderness ratio and compactness stipulated in Section 13.2 and Table I-8-1 of the Seismic Provisions (AISC 2005a).

Table C–1: Demands on the structural members in the strength design phase. (From Yang, 2006 Table 6.5)

Story	Braces		Columns		Left beams		Right beams	
	Left (kip)	Right (kip)	Left (kip)	Right (kip)	Axial Force (kip)	Bending Moment (kip ft)	Axial Force (kip)	Bending Moment (kip ft)
3	144	-205	-12	-12	-264	61	0	61
2	247	-317	130	-222	-271	69	155	69
1	301	-371	377	-542	-268	69	239	69

After the sizes of the braces are determined, the design of "zipper columns" and redesign of other structural members is performed using the brace's capacities. The sequence coincides with the load path of the forces in the desired "zipper mechanism": "zipper columns", top-story braces, columns, and beams.

The required strength for the second-story "zipper columns" is the combination of the unbalanced vertical force and the reaction at midspan of the second-floor beam induced by unfactored vertical loads. The selected section are W 12x45 for the second and W 12x96 for the third story. These sections meet the seismic requirements.

The top-story braces are designed at this stage because they have to remain elastic when the structure develops its ultimate strength. Accordingly, the required strength for the third-story braces should consider both the required forces in the third story "zipper column" and the forces induced by the horizontal seismic loads including structural overstrength. The section W 14x132 is selected.

For the first-story column, the required force is calculated by superimposing the force from the third-story brace, the minimum postbuckling strength from the second-story brace, and the axial member force induced by the unfactored vertical loads. The selected section is W 12x96.

Both the top-story braces are subjected compression, leading to tension in the third-floor beam. The section selected for this component is W 10x88.

A summary of all the members is found in Table C–2.

Table C–2: Summary of the member sizes for the three stories "zipper" braced frame. (From Yang, 2006 Table 6.6)

Story	Braces	Columns	Beams	"Zipper columns"
3	W14x332	W12x96	W8x58	W12x96
2	HSS8x8x1/2	W12x96	W10x88	W12x45
1	HSS8x8x5/8	W12x96	W10x88	

C.3 Design check of the 1/3 scaled "zipper frame" model

The braces as well as the "zipper columns" in the "zipper"-braced frame model were cold-formed welded and seamless hollow square section (HSS) made of ASTM A500 Grade B steel (nominal F_y =46 ksi and F_u = 58 ksi). The section HSS2x2x1/8 was used in the first and second-story braces while an HSS3x3x3/16 was used in the third floor braces.: The rest of the members (beam and columns) were designed using A572 Grade 50 (nominal F_y = 50 ksi and F_u = 65 ksi). The chosen sections were: S4x9.5 for all columns, S3x7.5 for the beam at 1st story, S5x10 at the beam of the 2nd story and S3x5.7 at the beam of the third story. The column base and gusset plates were made of ASTM A36 steel (nominal F_y =36 ksi and F_u = 58ksi).

Table C–3 provides the main characteristics of the sections obtained from AISC manual (AISC 2003), Table C–4 provides a check for compactness and Table C–5 provides the check for brace slenderness.

Section 13.4a of the Seismic provisions specifies the maximum unbraced length for beams in special concentrically braced frames which cannot exceed the value given by Equation 1-1-7 of the Specifications (AISC 2005a): $L_{pd} = (0.12+0.076\ M_1/M_2)\ (E/F_y)\ r_y$. The evaluation of this equation for $M_1/M_2 = 0$ (the beams are designed as pinned connections) results in 35.7 in, which exceeds the unbraced length of the beam = 80 in. The beam should have been braced laterally.

Table C–3: Properties of the selected sections of the 1/3 scale model. (From AISC 2005).

Section	Location	Area (in^2)	Inertia (in^3)	Radius of Gyration (in)
HSS 2x2x1/8	Braces 1st and 2nd floors	0.84	0.486	0.761
HSS 3x3x3/16	Braces 3rd floor	1.89	2.46	1.14
S4x9.5	Columns	2.79	6.76	1.56
S3x7.5	Beam 1st floor	2.2	2.91	1.15
S5x10	Beam 2nd floor	2.93	12.3	2.05
S3x5.7	Beam 3rd floor	1.66	2.5	1.23
HSS1.25x1.25xx3/16	“Zipper column” 2nd floor	0.671	0.122	0.426
HSS2x2x3/16	“Zipper column” 3rd floor	1.19	0.641	0.733

Table C–4: Verification of section compactness of the 1/3 scale model (From AISC Seismic Provisions Table I-8-1).

Section	b/t	h/t_w	Seismic compact limits λ_{ps}
HSS 2x2x1/8	14.2	14.2	$0.64\sqrt{(E/F_y)} = 16.1$
HSS 3x3x3/16	14.2	14.2	$0.64\sqrt{(E/F_y)} = 16.1$
S4x9.5	4.78	12.27	Flanges: $0.3\sqrt{(E/F_y)} = 7.22$ Webs: $1.12\sqrt{(E/F_y)}\,(2.23-0.144) = 56.27$
S3x7.5	4.83	8.60	Flanges: $0.3\sqrt{(E/F_y)} = 7.22$ Webs: $1.12\sqrt{(E/F_y)}\,(2.23-0.144) = 56.27$
S5x10	4.60	23.36	Flanges: $0.3\sqrt{(E/F_y)} = 7.22$ Webs: $1.12\sqrt{(E/F_y)}\,(2.23-0.144) = 56.27$
S3x5.7	4.48	17.65	Flanges: $0.3\sqrt{(E/F_y)} = 7.22$ Webs: $1.12\sqrt{(E/F_y)}\,(2.23-0.144) = 56.27$
HSS1.25x1.25xx3/16	4.18	4.18	$0.64\sqrt{(E/F_y)} = 16.1$
HSS2x2x3/16	8.49	8.49	$0.64\sqrt{(E/F_y)} = 16.1$

Table C–5: Verification of slenderness for brace members of the 1/3 scale model (From AISC Seismic Provisions section 13.4a).

Member	L (in)	K L / r	Limit	P_y (kip)	P_E (kip)
Brace 1st and 2nd floor	66.2	87.00	$4\sqrt{(E/F_y)} = 100.43$	38.64	31.77
Brace 3rd floor	53.5	46.92	100.43	86.94	245.62

APPENDIX D

In this appendix, all drawings and specifications for the zipper frame model tested at the University at Buffalo are presented.

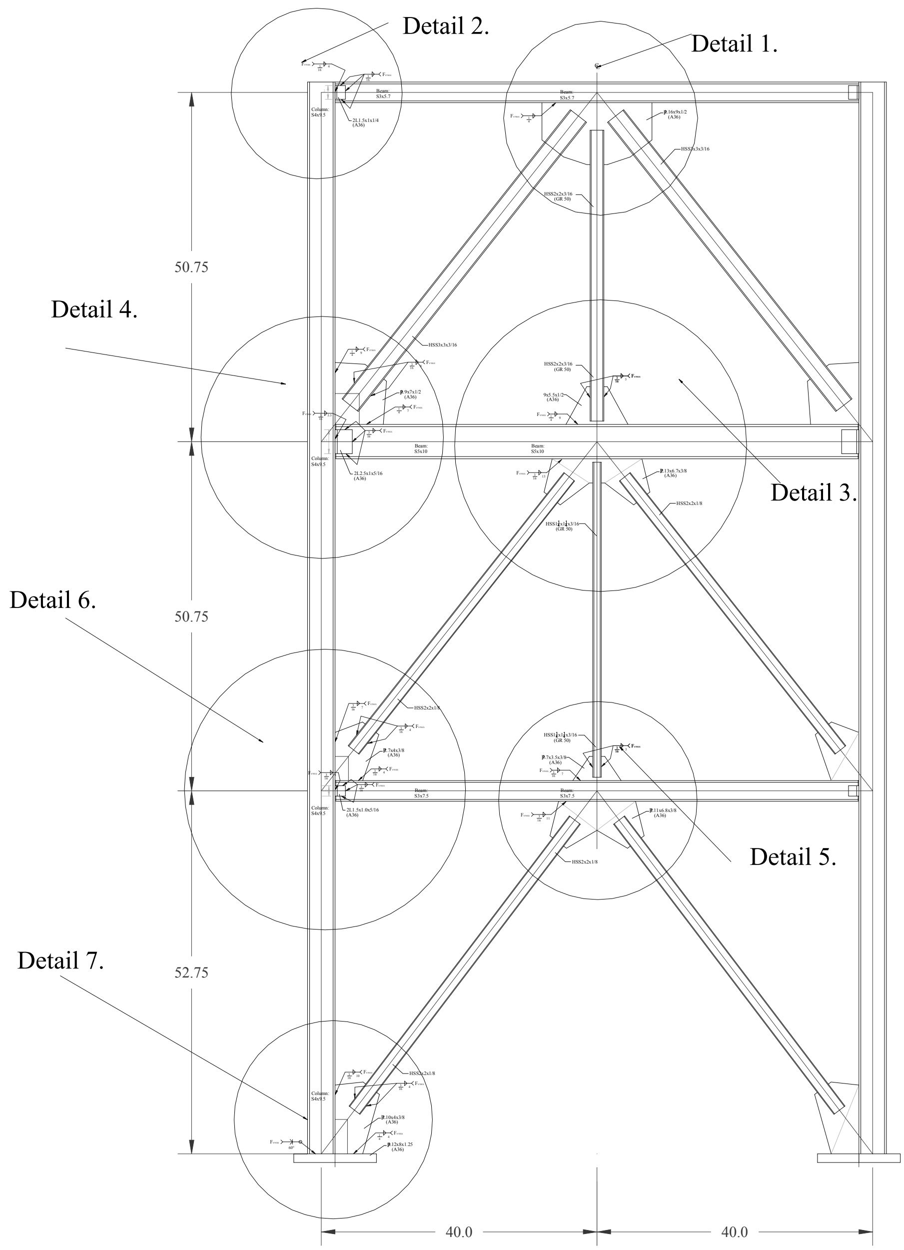

Figure D–1: General view of the model and connection details.

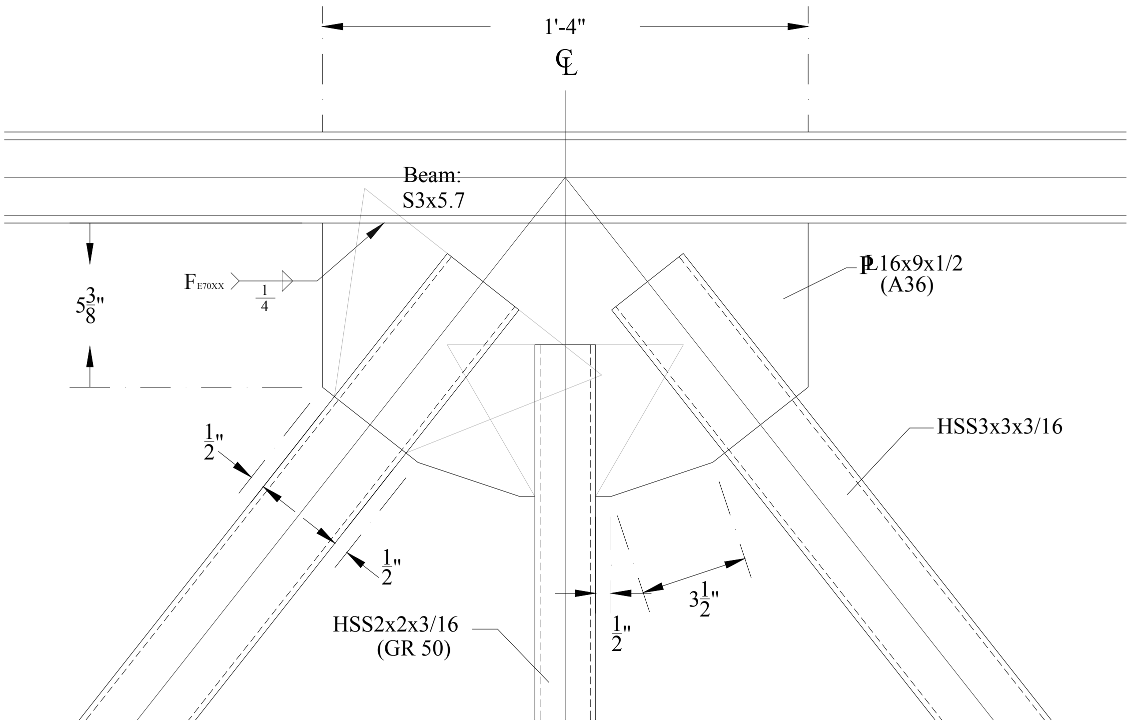

Figure D–2: Detail 1.

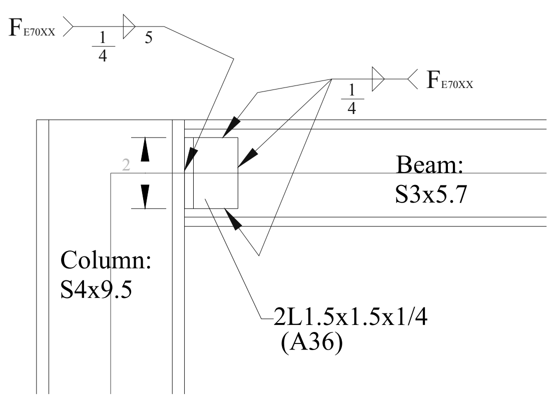

Figure D–3: Detail 2.

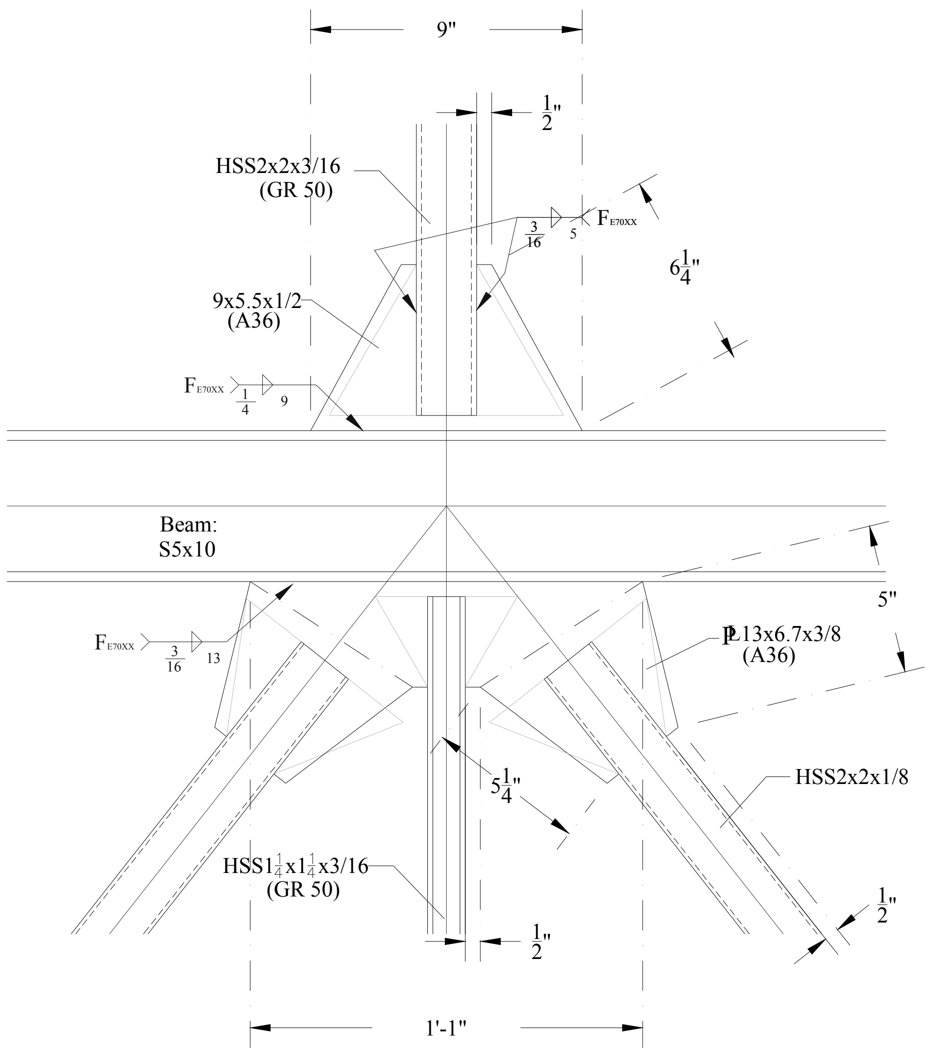

Figure D–4: Detail 3.

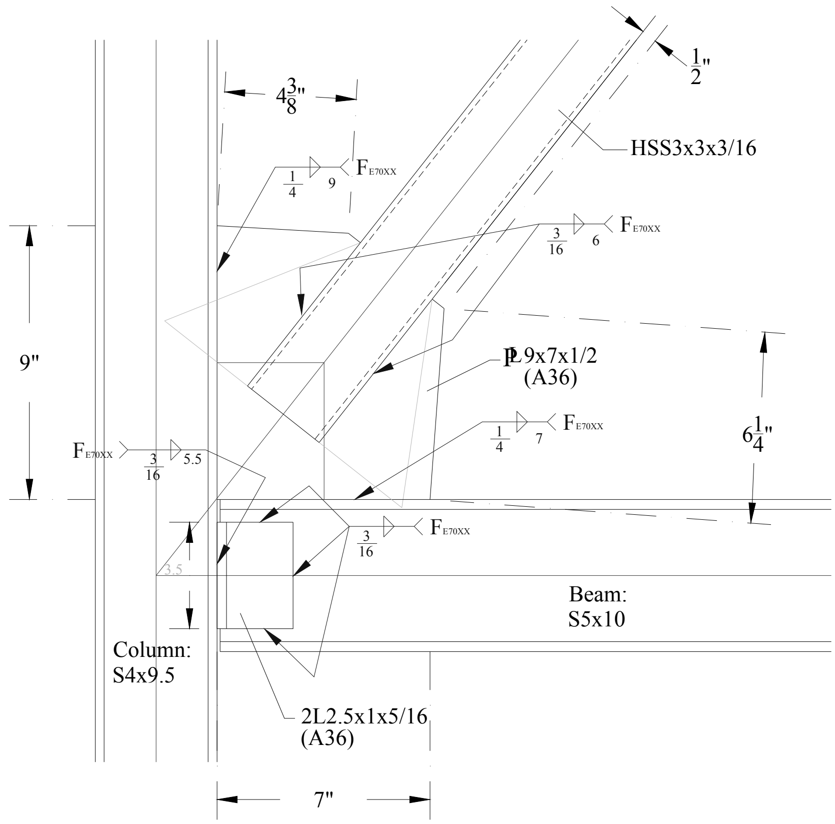

Figure D–5: Detail 4.

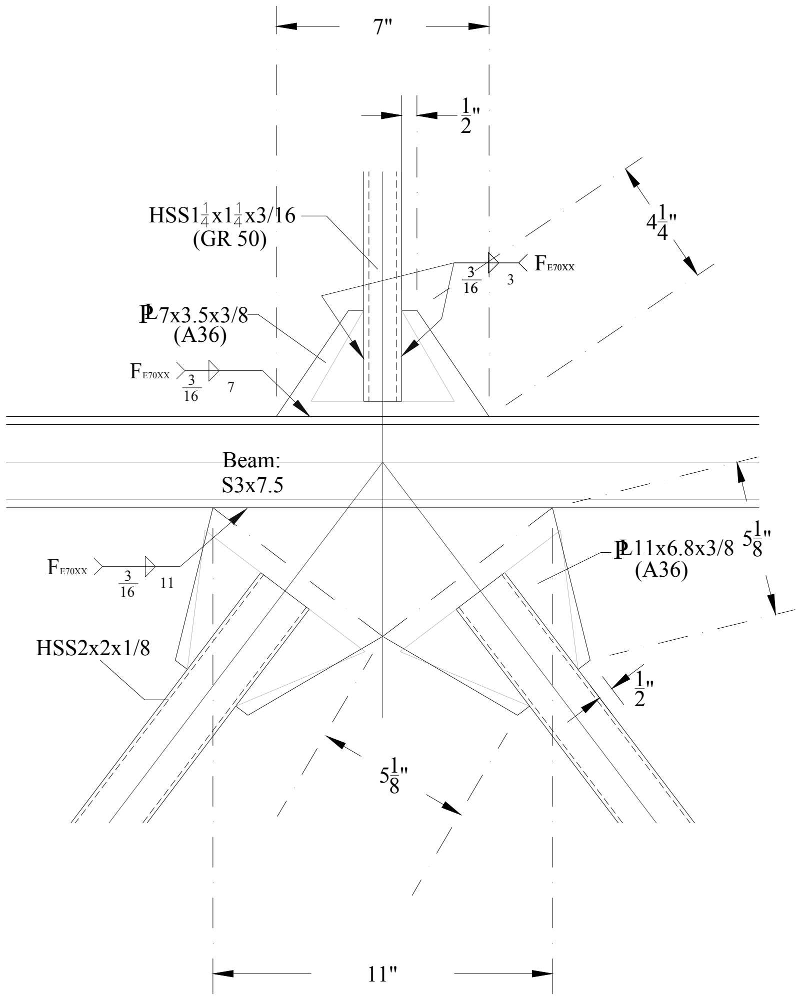

Figure D–6: Detail 5.

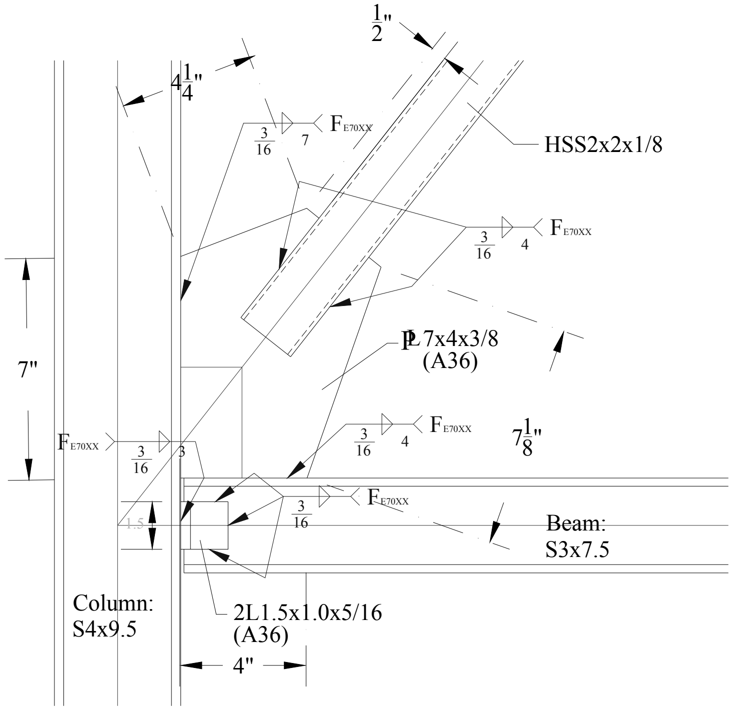

Figure D–7: Detail 6.

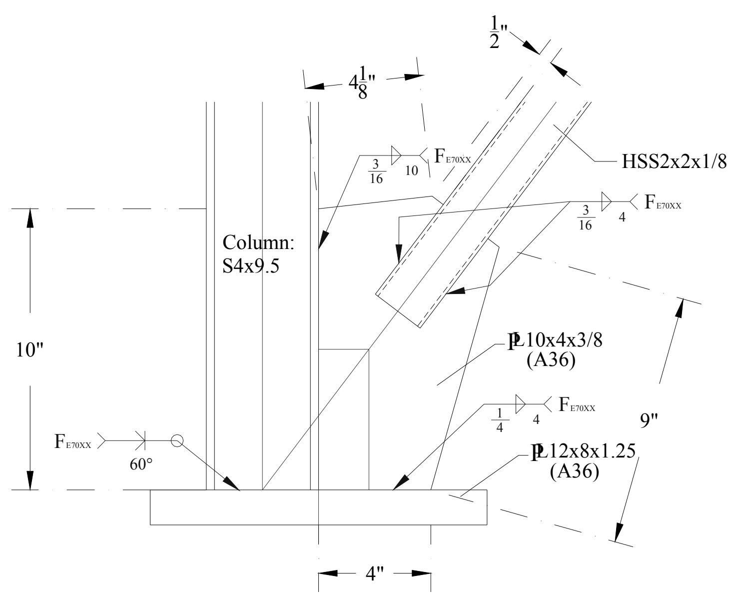

Figure D–8: Detail 7.

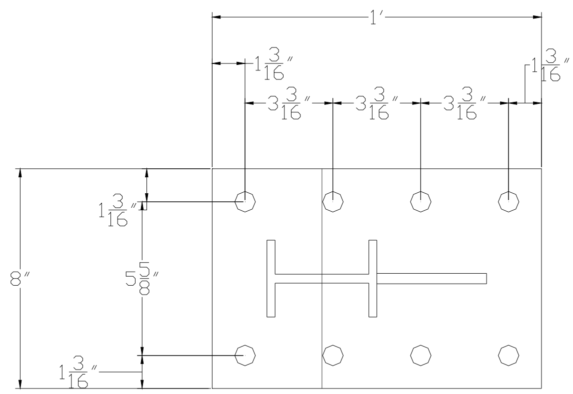

Figure D–9: Detail connection to base plate.

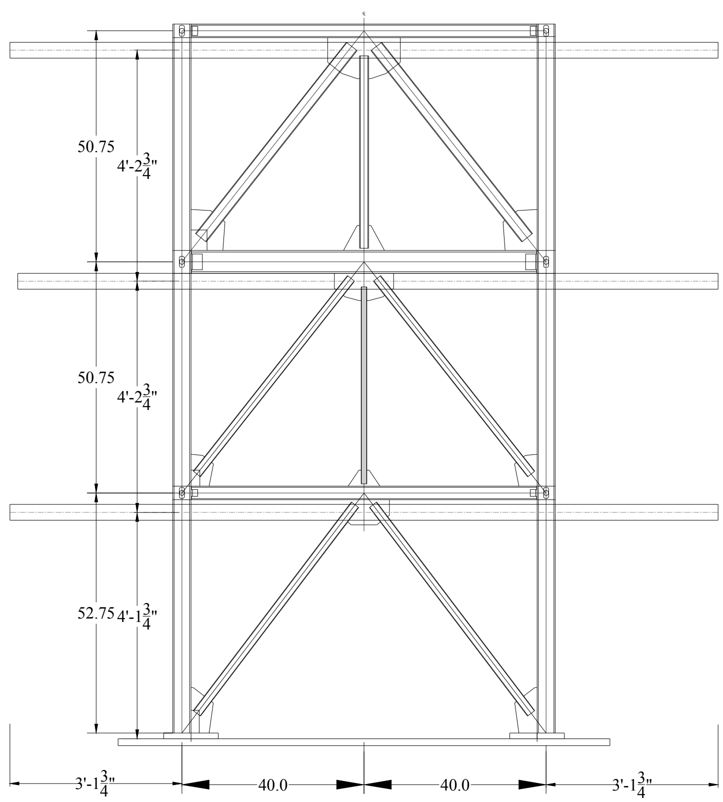

Figure D–10: Front view setup.

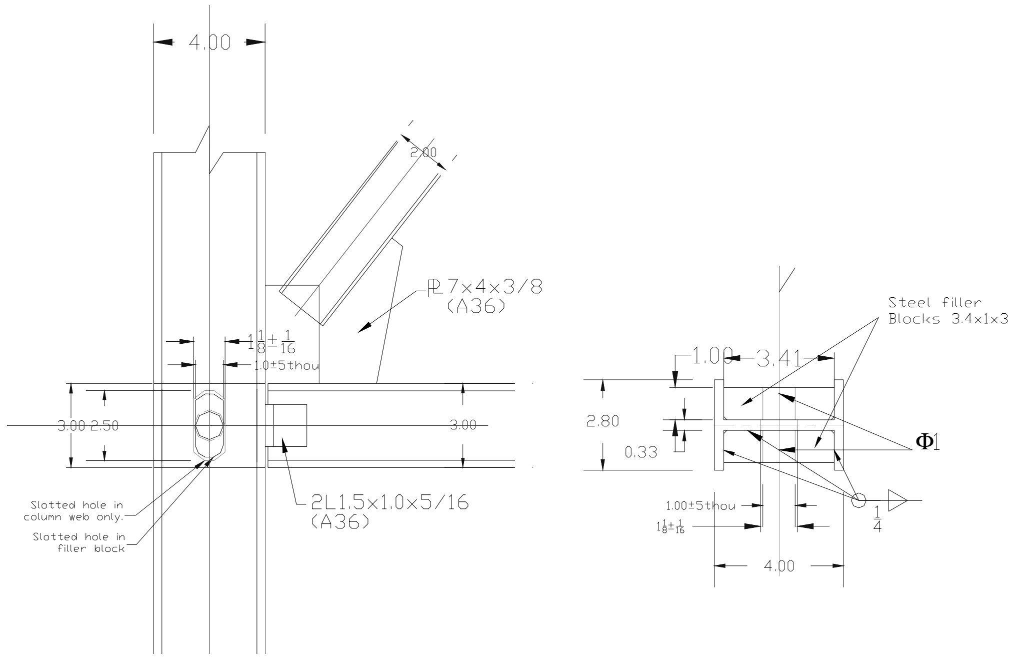

Figure D–11: Detail of beam to column and gravity frame to zipper frame connection.

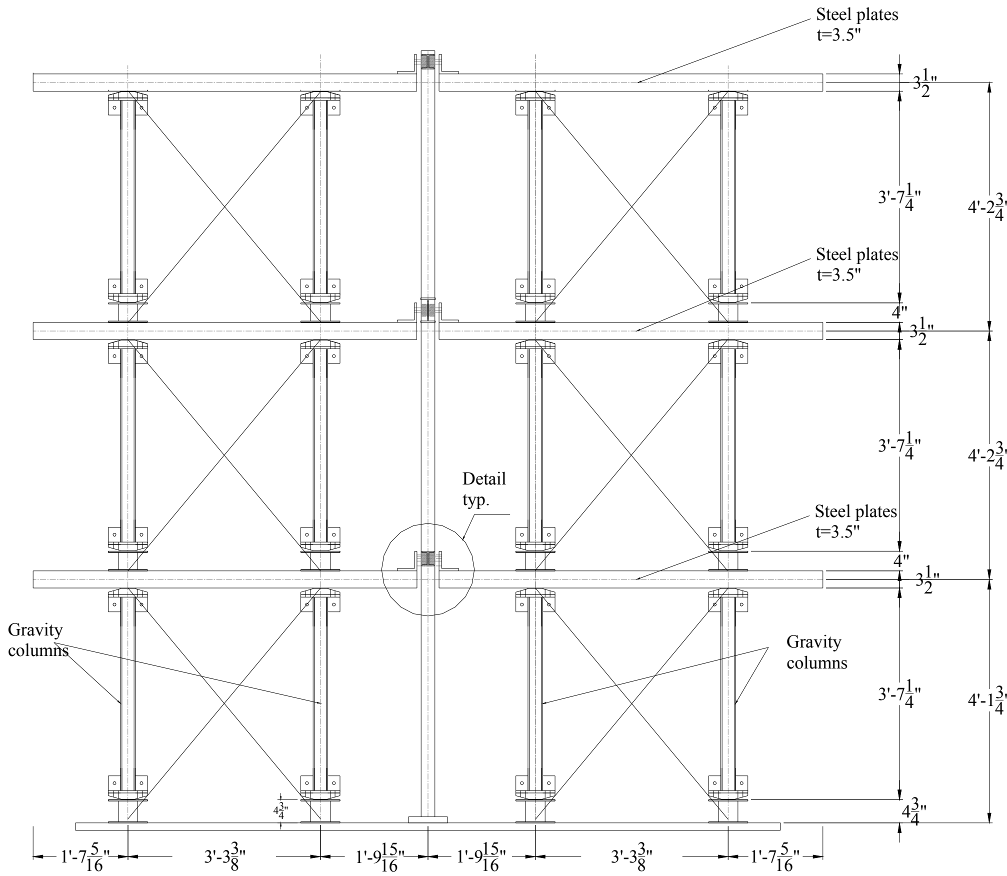

Figure D–12: Lateral view setup.

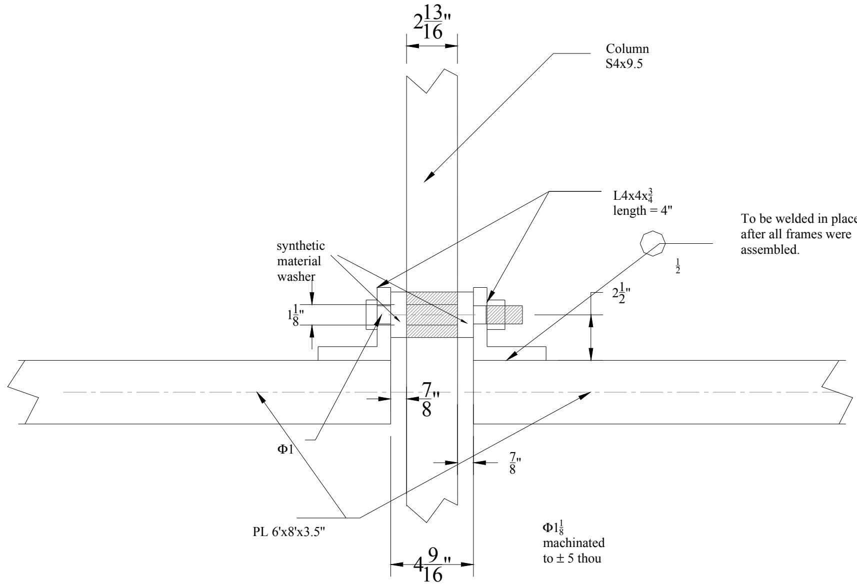

Figure D–13: Detail typ. From lateral view of test setup.

APPENDIX E.

This appendix contains a list of instrumentation and drawings with locations of the instruments for Test #1.

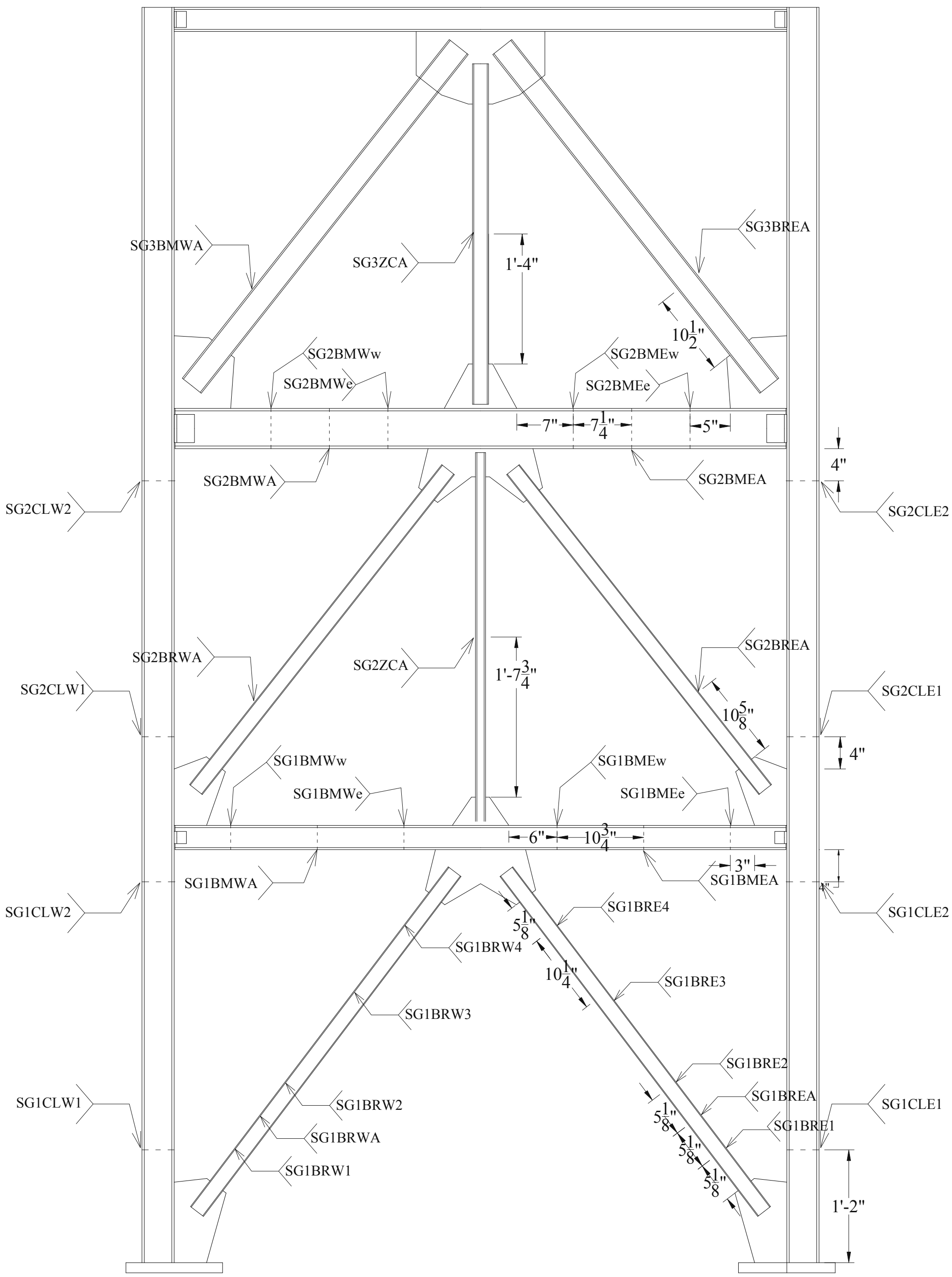

Figure E–1: Location of strain gauges.

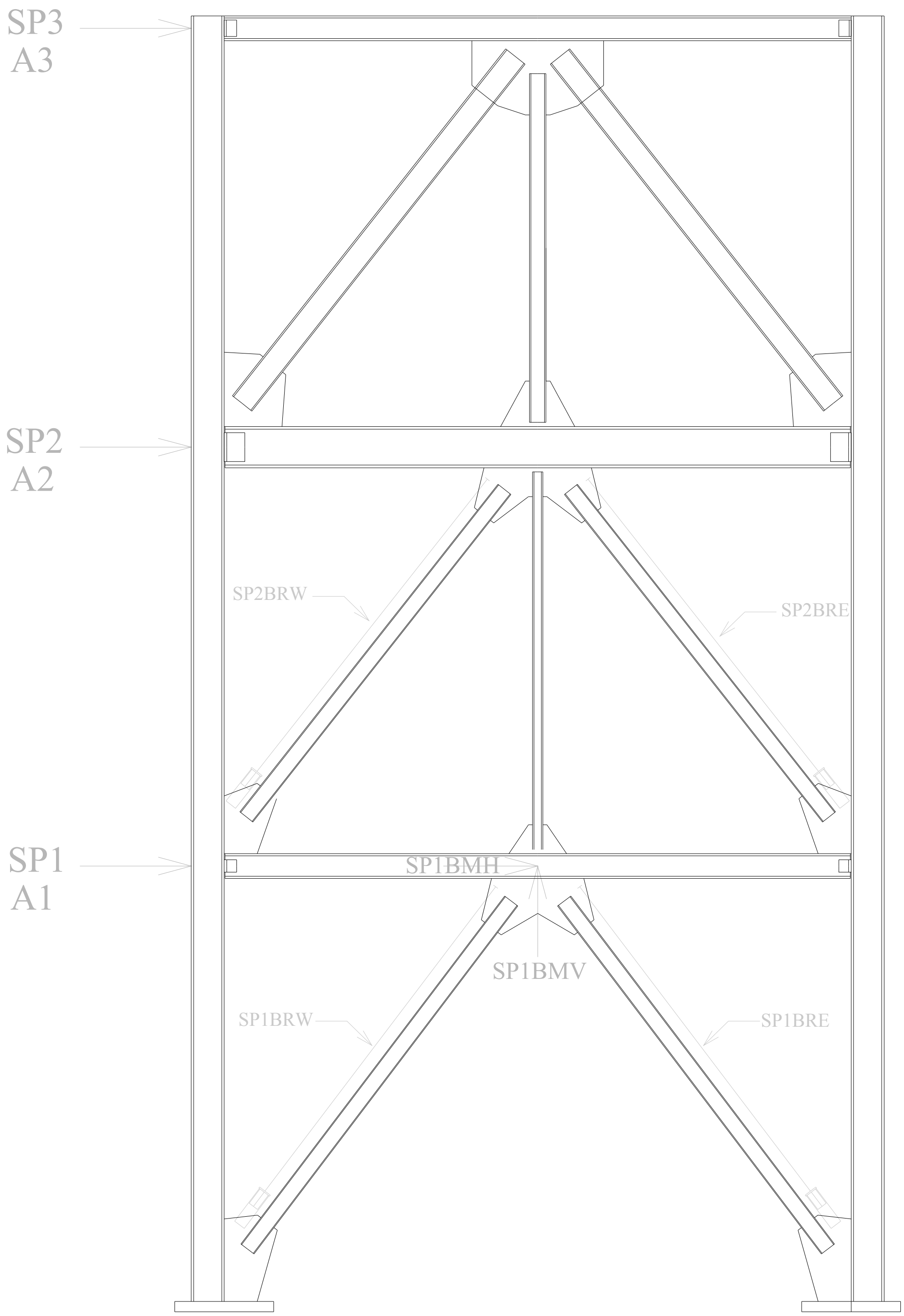

Figure E–2: Location f accelerometers and string potentiometers.

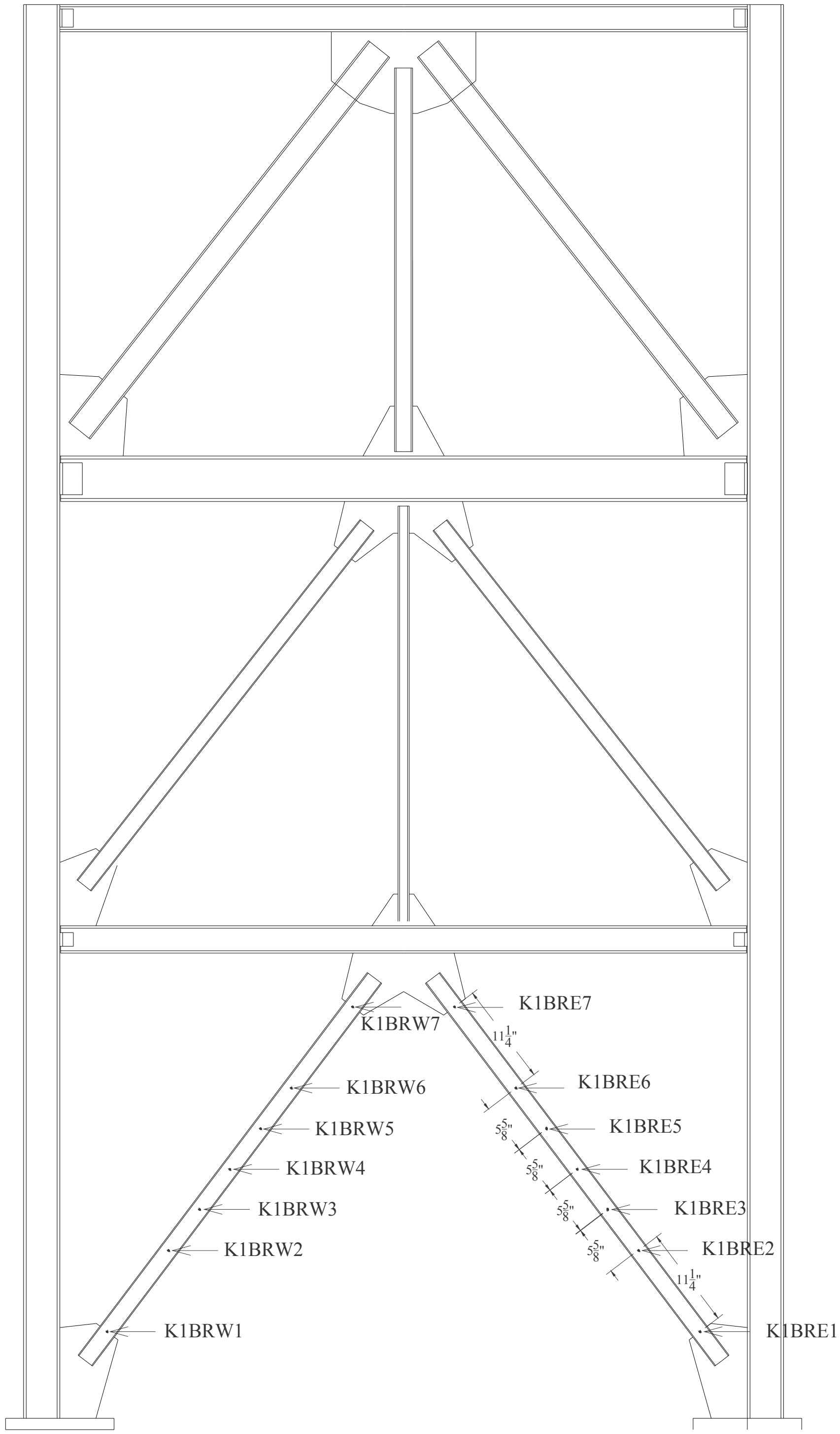

Figure E–3: Location of LED sensors for Krypton camera.

Table E–1: List of all instruments, their location and calibration.

NUMBER	NAME	TYPE OF SENSOR	Location	Calibration
1	A1	accelerometer	1st floor, east-west acceleration	+ facing West
2	A2	accelerometer	2nd floor, east-west acceleration	+ facing West
3	A3	accelerometer	3rd floor, east-west acceleration	+ facing West
4	AGnd	accelerometer	Base plate, east-west acceleration	+ facing West
4	AT1	accelerometer	1st floor plate , north-south acceleration	+ facing North
5	AT2	accelerometer	2nd floor plate , north-south acceleration	+ facing North
6	AT3	accelerometer	3rd floor plate , north-south acceleration	+ facing North
7	AP1N	accelerometer	1st floor plate , east-west acceleration	+ facing West
8	AP1S	accelerometer	1st floor plate , east-west acceleration	+ facing West
9	AP2N	accelerometer	2nd floor plate , east-west acceleration	+ facing West
10	AP2S	accelerometer	2nd floor plate , east-west acceleration	+ facing West
11	AP3N	accelerometer	3rd floor plate , east-west acceleration	+ facing West
12	AP3S	accelerometer	3rd floor plate , east-west acceleration	+ facing West
13	SP1BRW	string pot	1st floor brace, west side	+ compression
14	SP1BRE	string pot	1st floor brace, east side	+ compression
15	SP1BMH	string pot	center of 1st floor beam, horizontal	+ compression from zipper column to column.

NUMBER	NAME	TYPE OF SENSOR	Location	Calibration
16	SP1BMV	string pot	center of 1st floor beam, vertical	+ if beam goes down
17	SP1	string pot	1st floor, lateral displ.	+ goes West
18	SP2BRW	string pot	2nd floor brace, west side	+ compression
19	SP2BRE	string pot	2nd floor brace, east side	+ compression
20	SP2	string pot	2nd floor, lateral displ.	+ goes West
21	SP3	string pot	3rd floor, lateral displ.	+ goes West
22	SPGnd	string pot	Base plate, lateral displ.	+ goes West
23	P1NW	string pot	1st floor, north plate, towards west.	+ goes west, i.e. plate moves east
24	P1SW	string pot	1st floor, south plate, towards west.	+ goes west, i.e. plate moves east
25	P2NW	string pot	2nd floor, north plate, towards west.	+ goes west, i.e. plate moves east
26	P2SW	string pot	2nd floor, south plate, towards west.	+ goes west, i.e. plate moves east
27	P3NW	string pot	3rd floor, north plate, towards west.	+ goes west, i.e. plate moves east
28	P3SW	string pot	3rd floor, south plate, towards west.	+ goes west, i.e. plate moves east
29	SG1BRW1	Strain Gauge	1st floor, north plate, towards west.	+ tension
30	SG1BRWA	Strain Gauge	Brace West 1^{st} floor	+ tension
31	SG1BRW2	Strain Gauge	Brace West 1^{st} floor	+ tension
32	SG1BRW3	Strain Gauge	Brace West 1^{st} floor	+ tension
33	SG1BRW4	Strain Gauge	Brace West 1^{st} floor	+ tension
34	SG1BRE1	Strain Gauge	Brace East 1^{st} floor	+ tension
35	SG1BREA	Strain Gauge	Brace East 1^{st} floor	+ tension
36	SG1BRE2	Strain Gauge	Brace East 1^{st} floor	+ tension
37	SG1BRE3	Strain Gauge	Brace East 1^{st} floor	+ tension
38	SG1BRE4	Strain Gauge	Brace East 1^{st} floor	+ tension

NUMBER	NAME	TYPE OF SENSOR	Location	Calibration
39	SG1BMWw	Strain Gauge	West beam, 1st floor	+ tension
40	SG1BMWA	Strain Gauge	West beam, 1st floor	+ tension
41	SG1BMWe	Strain Gauge	West beam, 1st floor	+ tension
42	SG1BMEw	Strain Gauge	East beam, 1st floor	+ tension
43	SG1BMEA	Strain Gauge	East beam, 1st floor	+ tension
44	SG1BMEe	Strain Gauge	East beam, 1st floor	+ tension
45	SG1CLW1	Strain Gauge	West column, 1st floor	+ tension
46	SG1CLW2	Strain Gauge	West column, 1st floor	+ tension
47	SG1CLE1	Strain Gauge	East column, 1st floor	+ tension
48	SG1CLE2	Strain Gauge	East column, 1st floor	+ tension
49	SG2ZCA	Strain Gauge	Zipper column, 2nd floor	+ tension
50	SG2BRWA	Strain Gauge	Brace west, 2nd floor	+ tension
51	SG2BREA	Strain Gauge	Brace east, 2nd floor	+ tension
52	SG2BMWw	Strain Gauge	West beam, 2nd floor	+ tension
53	SG2BMWA	Strain Gauge	West beam, 2nd floor	+ tension
54	SG2BMWe	Strain Gauge	West beam, 2nd floor	+ tension
55	SG2BMEw	Strain Gauge	East beam, 2nd floor	+ tension
56	SG2BMEA	Strain Gauge	East beam, 2nd floor	+ tension
57	SG2BMEe	Strain Gauge	East beam, 2nd floor	+ tension
58	SG2CLW1	Strain Gauge	West column, 2nd floor	+ tension
59	SG2CLW2	Strain Gauge	West column, 2nd floor	+ tension
60	SG2CLE1	Strain Gauge	East column, 2nd floor	+ tension
61	SG2CLE2	Strain Gauge	East column, 2nd floor	+ tension
62	SG3ZCA	Strain Gauge	Zipper column, 3rd floor	+ tension
63	SG3BRWA	Strain Gauge	Brace W 3rd floor	+ tension
64	SG3BREA	Strain Gauge	Brace east 3rd floor	+ tension
65	K1BRW1	krypton	1st floor brace, west side	+ towards east (X), north(Y), up(Z)
66	K1BRW2	krypton	1st floor brace, west side	Same as above

NUMBER	NAME	TYPE OF SENSOR	Location	Calibration
67	K1BRW3	krypton	1st floor brace, west side	Same as above
68	K1BRW4	krypton	1st floor brace, west side	Same as above
69	K1BRW5	krypton	1st floor brace, west side	Same as above
70	K1BRW6	krypton	1st floor brace, west side	Same as above
71	K1BRW7	krypton	1st floor brace, west side	Same as above
72	K1BRE1	krypton	1st floor brace, east side	Same as above
73	K1BRE2	krypton	1st floor brace, east side	Same as above
74	K1BRE3	krypton	1st floor brace, east side	Same as above
75	K1BRE4	krypton	1st floor brace, east side	Same as above
76	K1BRE5	krypton	1st floor brace, east side	Same as above
77	K1BRE6	krypton	1st floor brace, east side	Same as above
78	K1BRE7	krypton	1st floor brace, east side	Same as above

APPENDIX F.

This appendix contains a list of instrumentation and drawings with locations of the instruments for Test #2.

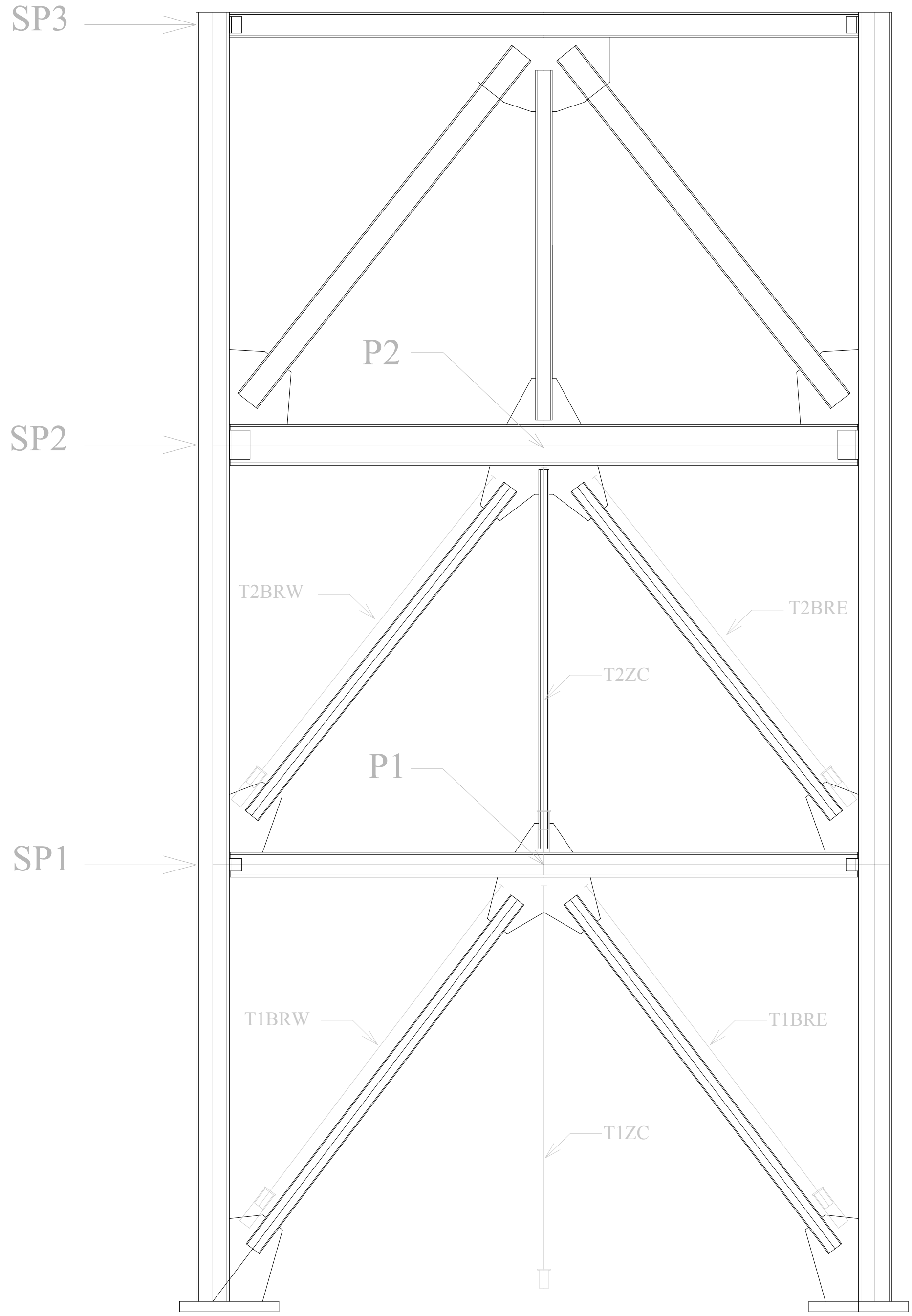

Figure F–1: Location of Temposonics and String potentiometers.

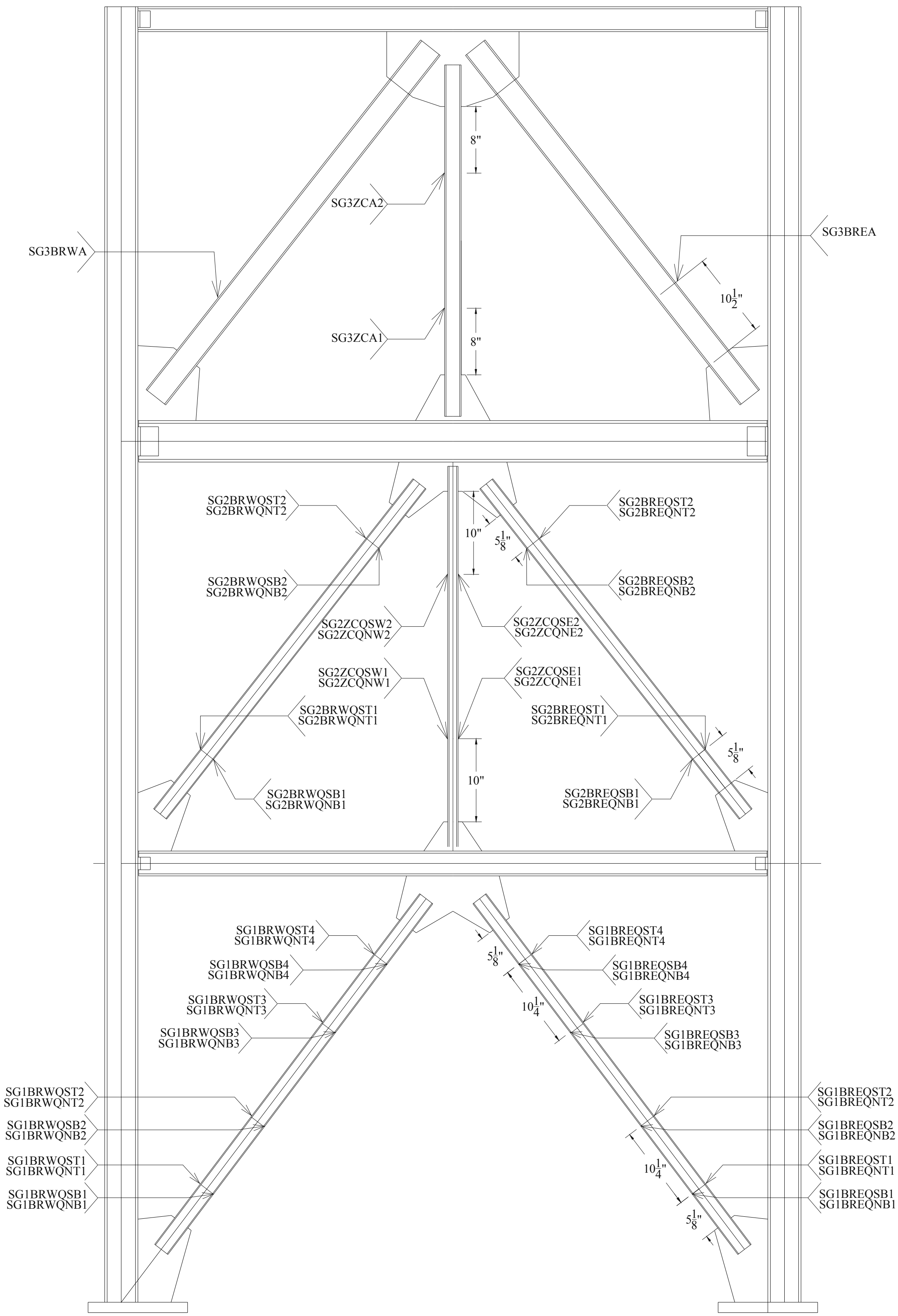

Figure F–2: Location of strain gauges in braces and zipper columns.

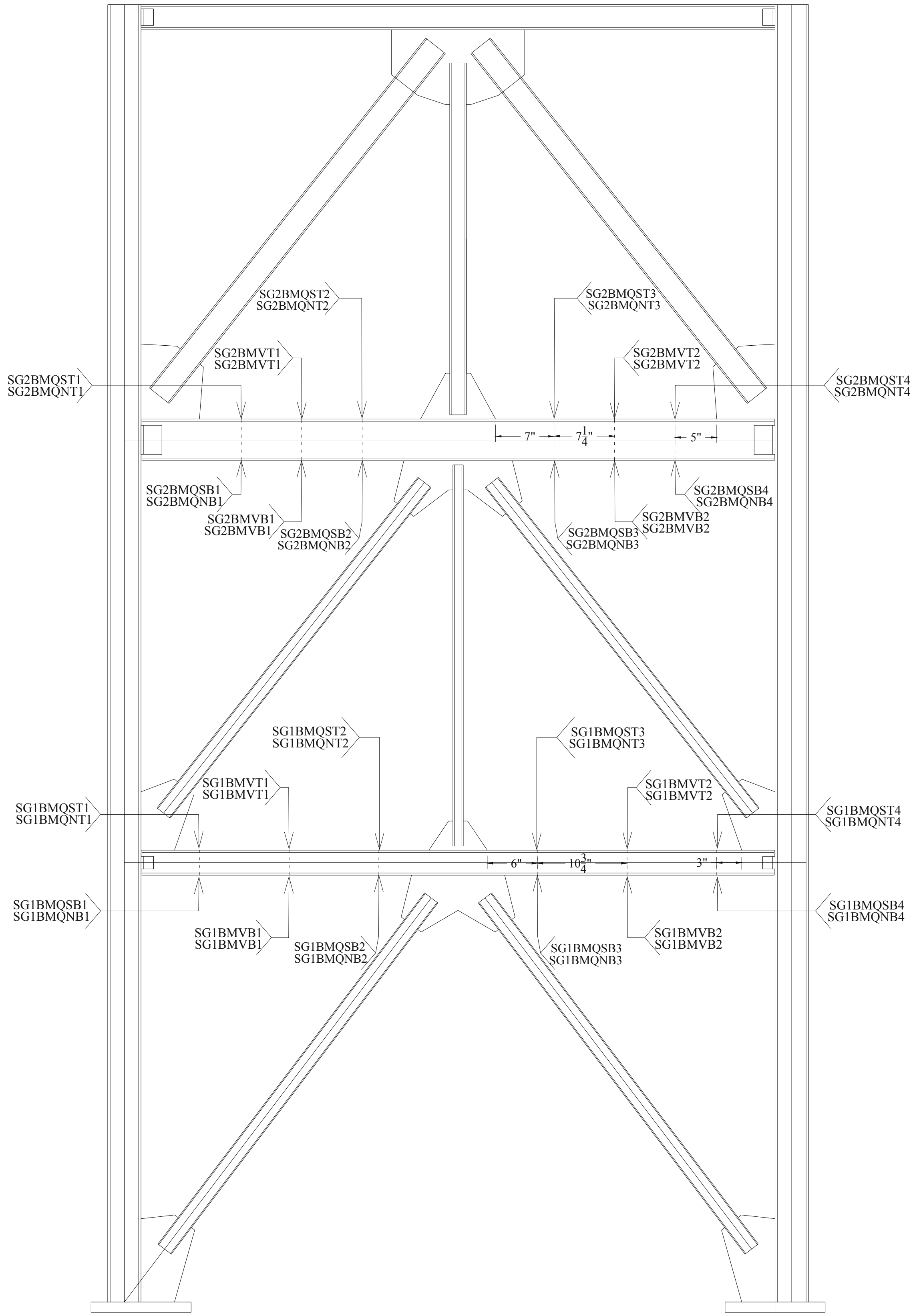

Figure F–3: Location of strain gauges in beams.

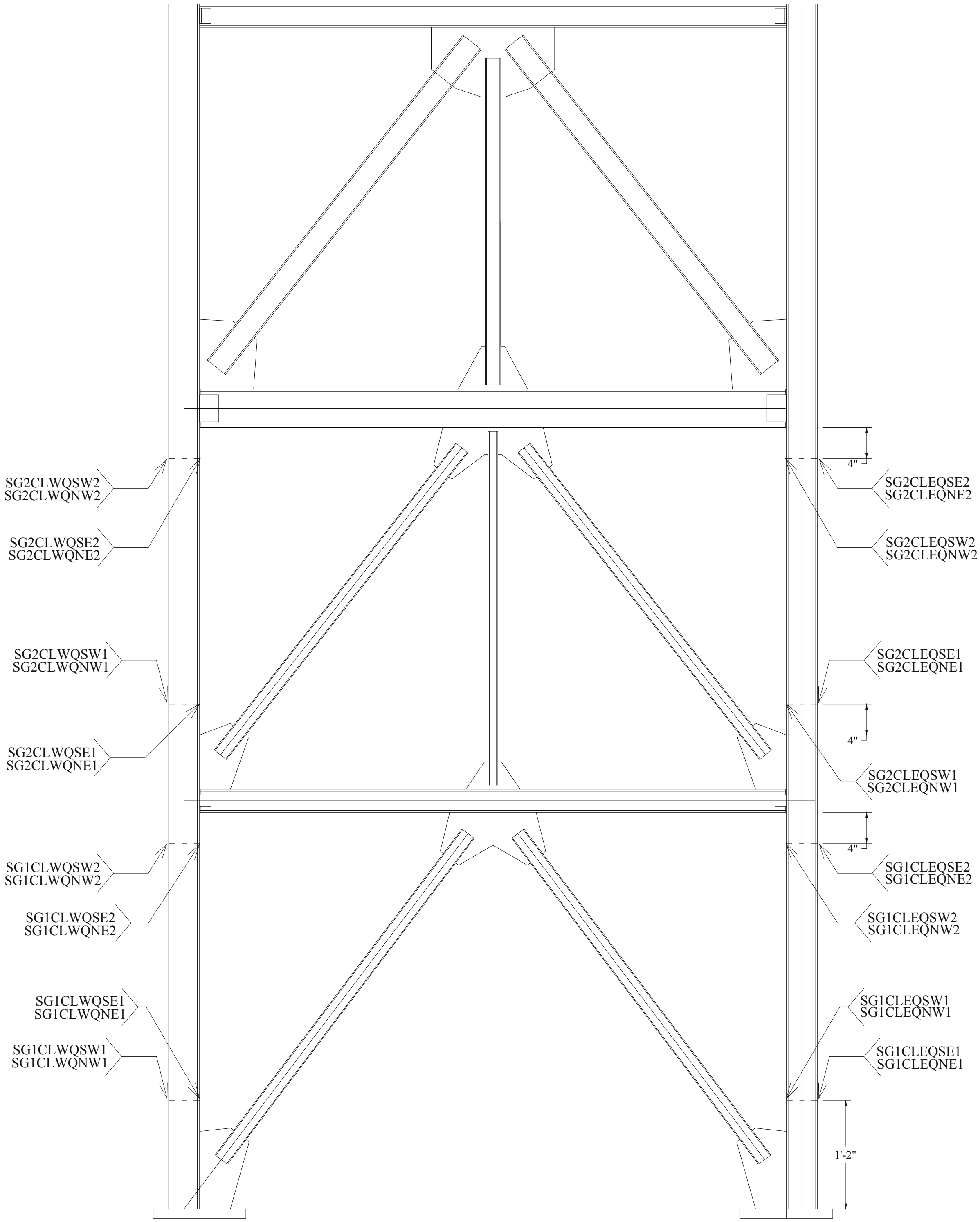

Figure F–4: Location of strain gauges in columns.

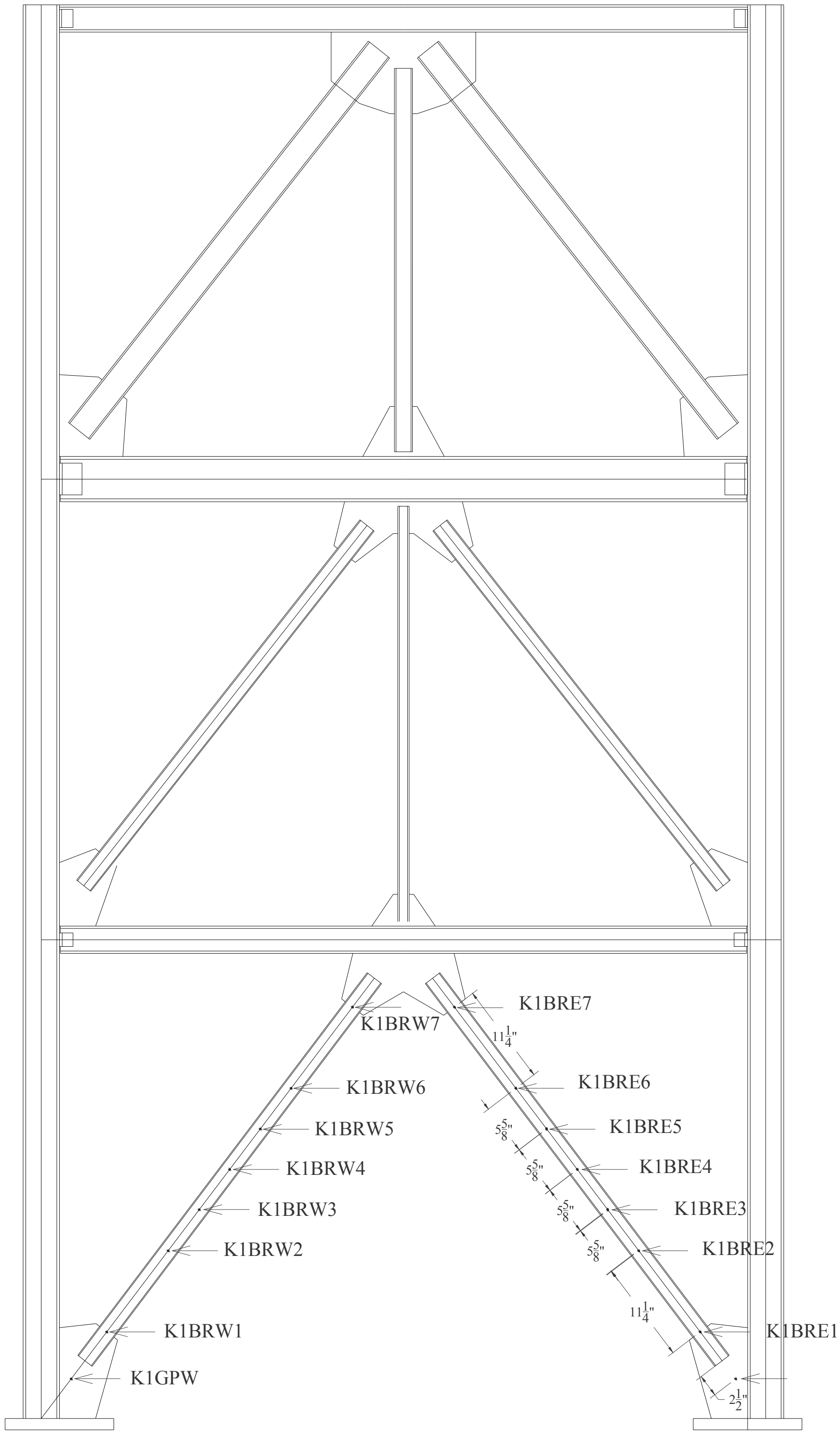

Figure F–5: Location of LED sensors for Krypton camera.

Table F–1: List of all instruments, their location and calibration.

NUMBER	NAME	TYPE OF SENSOR	Location	Calibration
1	A1	accelerometer	1st floor, east-west acceleration	+ facing West
2	A2	accelerometer	2nd floor, east-west acceleration	+ facing West
3	A3	accelerometer	3rd floor, east-west acceleration	+ facing West
4	AGnd	accelerometer	Base plate, east-west acceleration	+ facing West
4	AT1	accelerometer	1st floor plate , north-south acceleration	+ facing North
5	AT2	accelerometer	2nd floor plate , north-south acceleration	+ facing North
6	AT3	accelerometer	3rd floor plate , north-south acceleration	+ facing North
7	AP1N	accelerometer	1st floor plate , east-west acceleration	+ facing West
8	AP1S	accelerometer	1st floor plate , east-west acceleration	+ facing West
9	AP2N	accelerometer	2nd floor plate , east-west acceleration	+ facing West
10	AP2S	accelerometer	2nd floor plate , east-west acceleration	+ facing West
11	AP3N	accelerometer	3rd floor plate , east-west acceleration	+ facing West
12	AP3S	accelerometer	3rd floor plate , east-west acceleration	+ facing West
13	SP1	string pot	1st floor, lateral displ.	+ goes East
14	SP2	string pot	2nd floor, lateral displ.	+ goes East
15	SP3	string pot	3rd floor, lateral displ.	+ goes East
16	SPGnd	string pot	Base plate, lateral displ.	+ goes East
17	P1	Potentiometer	1st floor beam to brace	+ goes north

			connection	
NUMBER	**NAME**	**TYPE OF SENSOR**	**Location**	**Calibration**
18	P2	Potentiometer	2nd floor beam to brace connection	+ goes north
19	T1BRE	Temposonic	1^{st} floor brace E	+ compression
20	T1BRW	Temposonic	1^{st} floor brace W	+ compression
21	T2BRE	Temposonic	2^{nd} floor brace E	+ compression
22	T2BRW	Temposonic	2^{nd} floor brace W	+ compression
23	T1ZC	Temposonic	1^{st} floor gusset plate vertical movement	+ goes down
24	T2ZC	Temposonic	2^{nd} floor ZC vertical movement	+ compression
25	SG1BMQNB1	Strain Gauge	Beam 1^{st} floor north bottom, location 1.	+ compression
26	SG1BMQNB2	Strain Gauge	Beam 1^{st} floor north bottom, location 2.	+ compression
27	SG1BMQNB3	Strain Gauge	Beam 1^{st} floor north bottom, location 3.	+ compression
28	SG1BMQNB4	Strain Gauge	Beam 1^{st} floor north bottom, location 4.	+ compression
29	SG1BMQNT1	Strain Gauge	Beam 1^{st} floor north top, location 1.	+ compression
30	SG1BMQNT2	Strain Gauge	Beam 1^{st} floor north top, location 2.	+ compression
31	SG1BMQNT3	Strain Gauge	Beam 1^{st} floor north top, location 3.	+ compression
32	SG1BMQNT4	Strain Gauge	Beam 1^{st} floor north top, location 4.	+ compression
33	SG1BMQSB1	Strain Gauge	Beam 1^{st} floor south bottom, location 1.	+ compression
34	SG1BMQSB2	Strain Gauge	Beam 1^{st} floor south bottom, location 2.	+ compression
35	SG1BMQSB3	Strain Gauge	Beam 1^{st} floor south bottom,	+ compression

			location 3.	
NUMBER	**NAME**	**TYPE OF SENSOR**	**Location**	**Calibration**
36	SG1BMQSB4	Strain Gauge	Beam 1st floor south bottom, location 4.	+ compression
37	SG1BMQST1	Strain Gauge	Beam 1st floor south top, location 1.	+ compression
38	SG1BMQST2	Strain Gauge	Beam 1st floor south top, location 2.	+ compression
39	SG1BMQST3	Strain Gauge	Beam 1st floor south top, location 3.	+ compression
40	SG1BMQST4	Strain Gauge	Beam 1st floor south top, location 4.	+ compression
41	SG1BMVB1	Strain Gauge	Beam 1st floor, shear rosette, bottom location1.	+ compression
42	SG1BMVB2	Strain Gauge	Beam 1st floor, shear rosette, bottom location2.	+ compression
43	SG1BMVT1	Strain Gauge	Beam 1st floor, shear rosette, top location1.	+ compression
44	SG1BMVT2	Strain Gauge	Beam 1st floor, shear rosette, top location2.	+ compression
45	SG2BMQNB1	Strain Gauge	Beam 2nd floor north bottom, location 1.	+ compression
46	SG2BMQNB2	Strain Gauge	Beam 2nd floor north bottom, location 2.	+ compression
47	SG2BMQNB3	Strain Gauge	Beam 2nd floor north bottom, location 3.	+ compression
48	SG2BMQNB4	Strain Gauge	Beam 2nd floor north bottom, location 4.	+ compression
49	SG2BMQNT1	Strain Gauge	Beam 2nd floor north top, location 1.	+ compression

50	SG2BMQNT2	Strain Gauge	Beam 2nd floor north top, location 2.	+ compression
NUMBER	**NAME**	**TYPE OF SENSOR**	**Location**	**Calibration**
51	SG2BMQNT3	Strain Gauge	Beam 2nd floor north top, location 3.	+ compression
52	SG2BMQNT4	Strain Gauge	Beam 2nd floor north top, location 4.	+ compression
53	SG2BMQSB1	Strain Gauge	Beam 2nd floor south bottom, location 1.	+ compression
54	SG2BMQSB2	Strain Gauge	Beam 2nd floor south bottom, location 2.	+ compression
55	SG2BMQSB3	Strain Gauge	Beam 2nd floor south bottom, location 3.	+ compression
56	SG2BMQSB4	Strain Gauge	Beam 2nd floor south bottom, location 4.	+ compression
57	SG2BMQST1	Strain Gauge	Beam 2nd floor south top, location 1.	+ compression
58	SG2BMQST2	Strain Gauge	Beam 2nd floor south top, location 2.	+ compression
59	SG2BMQST3	Strain Gauge	Beam 2nd floor south top, location 3.	+ compression
60	SG2BMQST4	Strain Gauge	Beam 2nd floor south top, location 4.	+ compression
61	SG2BMVB1	Strain Gauge	Beam 2nd floor, shear rosette, bottom location1.	+ compression
62	SG2BMVB2	Strain Gauge	Beam 2nd floor, shear rosette, bottom location2.	+ compression
63	SG2BMVT1	Strain Gauge	Beam 2nd floor, shear rosette, top location1.	+ compression
64	SG2BMVT2	Strain Gauge	Beam 2nd floor, shear rosette, top location2.	+ compression

65	SG1BREQNB1	Strain Gauge	Brace 1st floor east, north bottom location 1.	+ compression
NUMBER	**NAME**	**TYPE OF SENSOR**	**Location**	**Calibration**
66	SG1BREQNB2	Strain Gauge	Brace 1st floor east, north bottom location 2.	+ compression
67	SG1BREQNB3	Strain Gauge	Brace 1st floor east, north bottom location 3.	+ compression
68	SG1BREQNB4	Strain Gauge	Brace 1st floor east, north bottom location 4.	+ compression
69	SG1BREQNT1	Strain Gauge	Brace 1st floor east, north top location 1.	+ compression
70	SG1BREQNT2	Strain Gauge	Brace 1st floor east, north top location 2.	+ compression
71	SG1BREQNT3	Strain Gauge	Brace 1st floor east, north top location 3.	+ compression
72	SG1BREQNT4	Strain Gauge	Brace 1st floor east, north top location 4.	+ compression
73	SG1BREQSB1	Strain Gauge	Brace 1st floor east, south bottom location 1.	+ compression
74	SG1BREQSB2	Strain Gauge	Brace 1st floor east, south bottom location 2.	+ compression
75	SG1BREQSB3	Strain Gauge	Brace 1st floor east, south bottom location 3.	+ compression
76	SG1BREQSB4	Strain Gauge	Brace 1st floor east, south bottom location 4.	+ compression
77	SG1BREQST1	Strain Gauge	Brace 1st floor east, south top location 1.	+ compression
78	SG1BREQST2	Strain Gauge	Brace 1st floor east, south top location 2.	+ compression
79	SG1BREQST3	Strain Gauge	Brace 1st floor east, south top location 3.	+ compression

80	SG1BREQST4	Strain Gauge	Brace 1st floor east, south top location 4.	+ compression
NUMBER	**NAME**	**TYPE OF SENSOR**	**Location**	**Calibration**
81	SG1BRWQNB1	Strain Gauge	Brace 1st floor west, north bottom location 1.	+ compression
82	SG1BRWQNB2	Strain Gauge	Brace 1st floor west, north bottom location 2.	+ compression
83	SG1BRWQNB3	Strain Gauge	Brace 1st floor west, north bottom location 3.	+ compression
84	SG1BRWQNB4	Strain Gauge	Brace 1st floor west, north bottom location 4.	+ compression
85	SG1BRWQNT1	Strain Gauge	Brace 1st floor west, north top location 1.	+ compression
86	SG1BRWQNT2	Strain Gauge	Brace 1st floor west, north top location 2.	+ compression
87	SG1BRWQNT3	Strain Gauge	Brace 1st floor west, north top location 3.	+ compression
88	SG1BRWQNT4	Strain Gauge	Brace 1st floor west, north top location 4.	+ compression
89	SG1BRWQSB1	Strain Gauge	Brace 1st floor west, south bottom location 1.	+ compression
90	SG1BRWQSB2	Strain Gauge	Brace 1st floor west, south bottom location 2.	+ compression
91	SG1BRWQSB3	Strain Gauge	Brace 1st floor west, south bottom location 3.	+ compression
92	SG1BRWQSB4	Strain Gauge	Brace 1st floor west, south bottom location 4.	+ compression
93	SG1BRWQST1	Strain Gauge	Brace 1st floor west, south top location 1.	+ compression
94	SG1BRWQST2	Strain Gauge	Brace 1st floor west, south top location 2.	+ compression

95	SG1BRWQST3	Strain Gauge	Brace 1st floor west, south top location 3.	+ compression
NUMBER	**NAME**	**TYPE OF SENSOR**	**Location**	**Calibration**
96	SG1BRWQST4	Strain Gauge	Brace 1st floor west, south top location 4.	+ compression
97	SG2BREQNB1	Strain Gauge	Brace 2nd floor east, north bottom location 1.	+ compression
98	SG2BREQNB2	Strain Gauge	Brace 2nd floor east, north bottom location 2.	+ compression
99	SG2BREQNT1	Strain Gauge	Brace 2nd floor east, north top location 1.	+ compression
100	SG2BREQNT2	Strain Gauge	Brace 2nd floor east, north top location 2.	+ compression
101	SG2BREQSB1	Strain Gauge	Brace 2nd floor east, south bottom location 1.	+ compression
102	SG2BREQSB2	Strain Gauge	Brace 2nd floor east, south bottom location 2.	+ compression
103	SG2BREQST1	Strain Gauge	Brace 2nd floor east, south top location 1.	+ compression
104	SG2BREQST2	Strain Gauge	Brace 2nd floor east, south top location 2.	+ compression
105	SG2BRWQNB1	Strain Gauge	Brace 2nd floor west, north bottom location 1.	+ compression
106	SG2BRWQNB2	Strain Gauge	Brace 2nd floor west, north bottom location 2.	+ compression
107	SG2BRWQNT1	Strain Gauge	Brace 2nd floor west, north top location 1.	+ compression
108	SG2BRWQNT2	Strain Gauge	Brace 2nd floor west, north top location 2.	+ compression
109	SG2BRWQSB1	Strain Gauge	Brace 2nd floor west, south bottom location 1.	+ compression

110	SG2BRWQSB2	Strain Gauge	Brace 2^{nd} floor west, south bottom location 2.	+ compression
NUMBER	**NAME**	**TYPE OF SENSOR**	**Location**	**Calibration**
111	SG2BRWQST1	Strain Gauge	Brace 2^{nd} floor west, south top location 1.	+ compression
112	SG2BRWQST2	Strain Gauge	Brace 2^{nd} floor west, south top location 2.	+ compression
113	SG3BREA	Strain Gauge	Full bridge for axial force, brace east 3^{rd} floor.	+ compression
114	SG3BRWA	Strain Gauge	Full bridge for axial force, brace west 3^{rd} floor.	+ compression
115	SG1CLEQNE1	Strain Gauge	Column, 1^{st} floor east, north east location1.	+ compression
116	SG1CLEQNE2	Strain Gauge	Column, 1^{st} floor east, north east location2.	+ compression
117	SG1CLEQNW1	Strain Gauge	Column, 1^{st} floor east, north west location1.	+ compression
118	SG1CLEQNW2	Strain Gauge	Column, 1^{st} floor east, north west location2.	+ compression
119	SG1CLEQSE1	Strain Gauge	Column, 1^{st} floor east, south east location1.	+ compression
120	SG1CLEQSE2	Strain Gauge	Column, 1^{st} floor east, south east location2.	+ compression
121	SG1CLEQSW1	Strain Gauge	Column, 1^{st} floor east, south west location1.	+ compression
122	SG1CLEQSW2	Strain Gauge	Column, 1^{st} floor east, south west location2.	+ compression
123	SG1CLWQNE1	Strain Gauge	Column, 1^{st} floor west, north east location1.	+ compression
124	SG1CLWQNE2	Strain Gauge	Column, 1^{st} floor west, north east location2.	+ compression

125	SG1CLWQNW1	Strain Gauge	Column, 1st floor west, north west location1.	+ compression
NUMBER	**NAME**	**TYPE OF SENSOR**	**Location**	**Calibration**
126	SG1CLWQNW2	Strain Gauge	Column, 1st floor west, north west location2.	+ compression
127	SG1CLWQSE1	Strain Gauge	Column, 1st floor west, south east location1.	+ compression
128	SG1CLWQSE2	Strain Gauge	Column, 1st floor west, south east location2.	+ compression
129	SG1CLWQSW1	Strain Gauge	Column, 1st floor west, south west location1.	+ compression
130	SG1CLWQSW2	Strain Gauge	Column, 1st floor west, south west location2.	+ compression
131	SG2CLEQNE1	Strain Gauge	Column, 2nd floor east, north east location1.	+ compression
132	SG2CLEQNE2	Strain Gauge	Column, 2nd floor east, north east location2.	+ compression
133	SG2CLEQNW1	Strain Gauge	Column, 2nd floor east, north west location1.	+ compression
134	SG2CLEQNW2	Strain Gauge	Column, 2nd floor east, north west location2.	+ compression
135	SG2CLEQSE1	Strain Gauge	Column, 2nd floor east, south east location1.	+ compression
136	SG2CLEQSE2	Strain Gauge	Column, 2nd floor east, south east location2.	+ compression
137	SG2CLEQSW1	Strain Gauge	Column, 2nd floor east, south west location1.	+ compression
138	SG2CLEQSW2	Strain Gauge	Column, 2nd floor east, south west location2.	+ compression
139	SG2CLWQNE1	Strain Gauge	Column, 2nd floor west, north east location1.	+ compression

140	SG2CLWQNE2	Strain Gauge	Column, 2^{nd} floor west, north east location2.	+ compression
NUMBER	**NAME**	**TYPE OF SENSOR**	**Location**	**Calibration**
141	SG2CLWQNW1	Strain Gauge	Column, 2^{nd} floor west, north west location1.	+ compression
142	SG2CLWQNW2	Strain Gauge	Column, 2^{nd} floor west, north west location2.	+ compression
143	SG2CLWQSE1	Strain Gauge	Column, 2^{nd} floor west, south east location1.	+ compression
144	SG2CLWQSE2	Strain Gauge	Column, 2^{nd} floor west, south east location2.	+ compression
145	SG2CLWQSW1	Strain Gauge	Column, 2^{nd} floor west, south west location1.	+ compression
146	SG2CLWQSW2	Strain Gauge	Column, 2^{nd} floor west, south west location2.	+ compression
147	SG2ZCQNE1	Strain Gauge	Zipper column 2^{nd} floor, north east location 1.	+ compression
148	SG2ZCQNE2	Strain Gauge	Zipper column 2^{nd} floor, north east location 2.	+ compression
149	SG2ZCQNW1	Strain Gauge	Zipper column 2^{nd} floor, north west location 1.	+ compression
150	SG2ZCQNW2	Strain Gauge	Zipper column 2^{nd} floor, north west location 2.	+ compression
151	SG2ZCQSE1	Strain Gauge	Zipper column 2^{nd} floor, south east location 1.	+ compression
152	SG2ZCQSE1	Strain Gauge	Zipper column 2^{nd} floor, south east location 2.	+ compression
153	SG2ZCQSW1	Strain Gauge	Zipper column 2^{nd} floor, south west location 1.	+ compression
154	SG2ZCQSW2	Strain Gauge	Zipper column 2^{nd} floor, south west location 1.	+ compression

155	SG3ZCA1	Strain Gauge	Full bridge for axial force, zipper column east 3rd floor.	+ compression
NUMBER	**NAME**	**TYPE OF SENSOR**	**Location**	**Calibration**
156	SG3ZCA2	Strain Gauge	Full bridge for axial force, zipper column west 3rd floor.	+ compression
158	K1BRW1	krypton	1st floor brace, west side	+ east (X), north(Y), up(Z)
159	K1BRW2	krypton	1st floor brace, west side	Same as above
160	K1BRW3	krypton	1st floor brace, west side	Same as above
161	K1BRW4	krypton	1st floor brace, west side	Same as above
162	K1BRW5	krypton	1st floor brace, west side	Same as above
163	K1BRW6	krypton	1st floor brace, west side	Same as above
164	K1BRW7	krypton	1st floor brace, west side	Same as above
165	K1BRE1	krypton	1st floor brace, east side	Same as above
166	K1BRE2	krypton	1st floor brace, east side	Same as above
167	K1BRE3	krypton	1st floor brace, east side	Same as above
168	K1BRE4	krypton	1st floor brace, east side	Same as above
169	K1BRE5	krypton	1st floor brace, east side	Same as above
170	K1BRE6	krypton	1st floor brace, east side	Same as above
171	K1BRE7	krypton	1st floor brace, east side	Same as above
172	K1GPE	krypton	1st floor gusset plate brace to column connection, east side	Same as above
173	K1GPW	krypton	1st floor gusset plate brace to column connection, west side	Same as above

APPENDIX G

VERIFICATION OF THE FORMULATION WITH STANDARIZED CASE STUDY: LATERAL BUCKLING OF A CANTILIVER RIGHT ANGLE FRAME UNDER END LOAD

The formulation resented in Chapter 2 was initially verified with a standardized structure that has three dimensional buckling effects and that has been studied by numerous authors (Argyris et al. 1979; Simo and Vu-Quoc 1986). The results of the verification are shown below.

The problem (see Figure G–1) consists of a right angle frame, clamped in one of its ends and free in the other end. The frame is subjected to a lateral in plane load P and buckles out of plane. This problem was solved numerically by Argyris (Argyris et al. 1979), Simo and Vu-Quoc (Simo and Vu-Quoc 1986) and other authors.

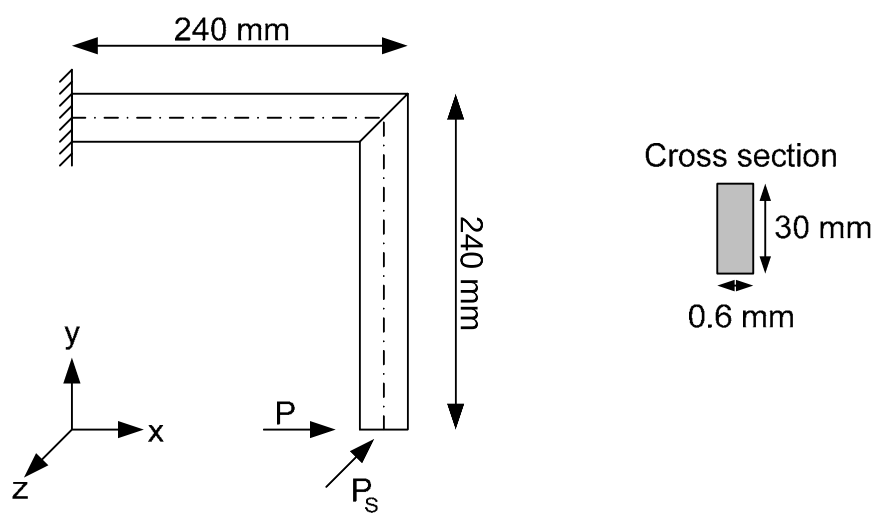

Figure G–1: Data of the problem.

The dimensions of the frame are 240 mm x 240 mm. The cross section is rectangular of dimensions 30 mm x 0.6 mm. The value for the modulus of elasticity is 71240 N/mm and the Poisson's ratio is 0.31. Only one element with 10 integration points was used for each member.

The buckling mode is achieved using a perturbation load, P_S, applied at the free end of the frame in the out of plane (z) direction. Its value varies with time and its equal to 1/1000 times the value of the lateral load P. The results, applied lateral load vs. out of plane tip displacement, are presented in Figure G–2. The critical load was found to be 1.04 N while Argyris (Argyris et al.

1979) provided the value 1.09 N (Figure G–3, a) and Simo (Simo and Vu-Quoc 1986) the value 1.088 N (Figure G–3, b). It has to be noted that Argyris used 10 elements per member.

In general, the performance of the formulation is very satisfactory.

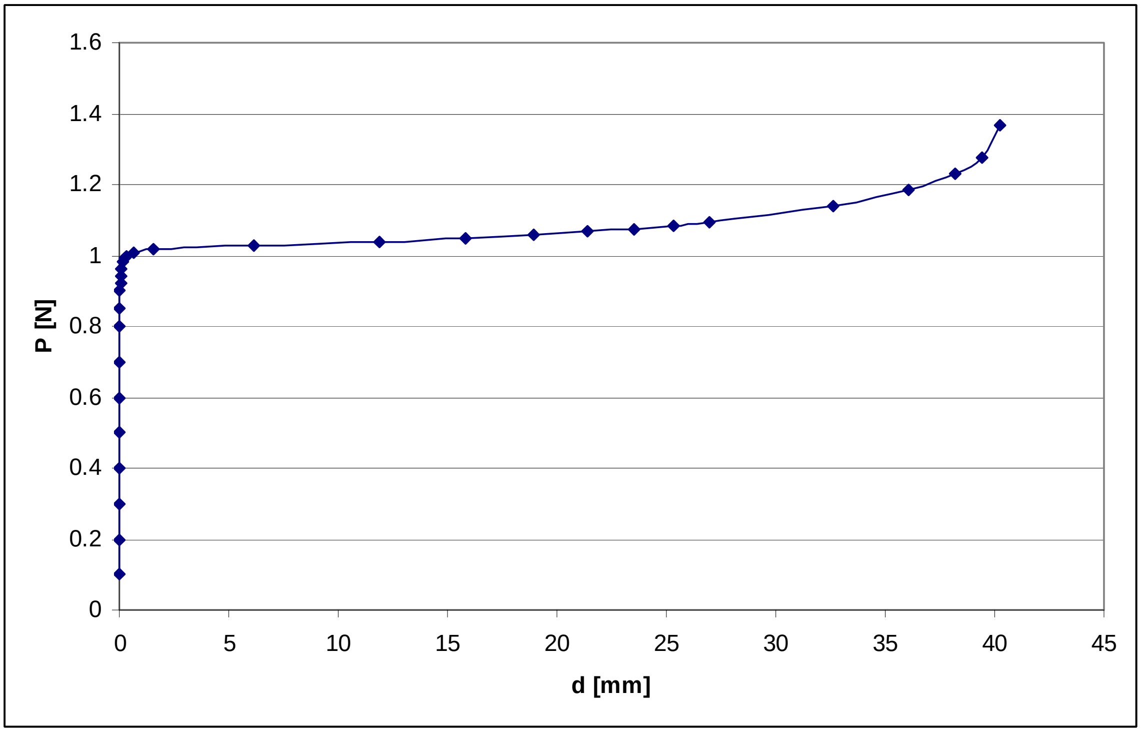

Figure G–2: Load displacement diagram.

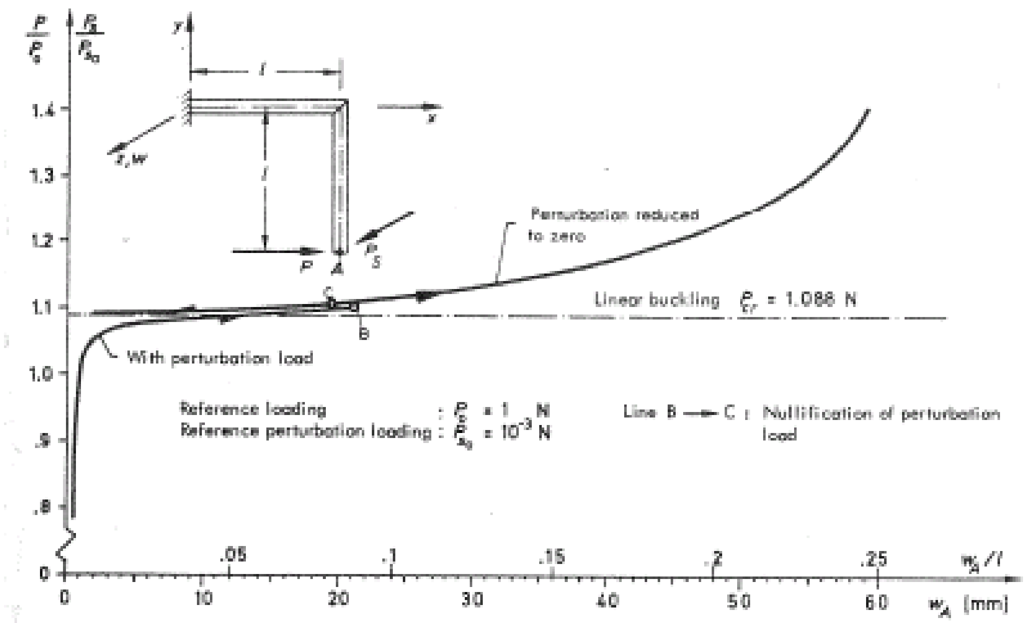

(a)

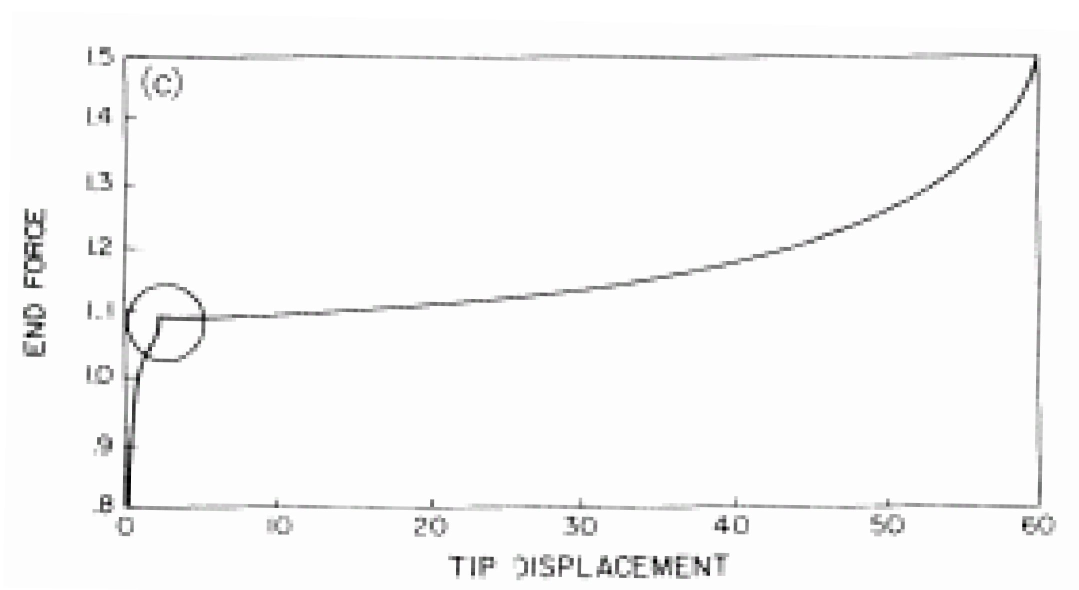

(b)

Figure G–3: Solutions to the problem by (a) Argyris (1979) and Simo et al. (1986).

MCEER Technical Reports

MCEER publishes technical reports on a variety of subjects written by authors funded through MCEER. These reports are available from both MCEER Publications and the National Technical Information Service (NTIS). Requests for reports should be directed to MCEER Publications, MCEER, University at Buffalo, State University of New York, Red Jacket Quadrangle, Buffalo, New York 14261. Reports can also be requested through NTIS, 5285 Port Royal Road, Springfield, Virginia 22161. NTIS accession numbers are shown in parenthesis, if available.

NCEER-87-0001 "First-Year Program in Research, Education and Technology Transfer," 3/5/87, (PB88-134275, A04, MF-A01).

NCEER-87-0002 "Experimental Evaluation of Instantaneous Optimal Algorithms for Structural Control," by R.C. Lin, T.T. Soong and A.M. Reinhorn, 4/20/87, (PB88-134341, A04, MF-A01).

NCEER-87-0003 "Experimentation Using the Earthquake Simulation Facilities at University at Buffalo," by A.M. Reinhorn and R.L. Ketter, to be published.

NCEER-87-0004 "The System Characteristics and Performance of a Shaking Table," by J.S. Hwang, K.C. Chang and G.C. Lee, 6/1/87, (PB88-134259, A03, MF-A01). This report is available only through NTIS (see address given above).

NCEER-87-0005 "A Finite Element Formulation for Nonlinear Viscoplastic Material Using a Q Model," by O. Gyebi and G. Dasgupta, 11/2/87, (PB88-213764, A08, MF-A01).

NCEER-87-0006 "Symbolic Manipulation Program (SMP) - Algebraic Codes for Two and Three Dimensional Finite Element Formulations," by X. Lee and G. Dasgupta, 11/9/87, (PB88-218522, A05, MF-A01).

NCEER-87-0007 "Instantaneous Optimal Control Laws for Tall Buildings Under Seismic Excitations," by J.N. Yang, A. Akbarpour and P. Ghaemmaghami, 6/10/87, (PB88-134333, A06, MF-A01). This report is only available through NTIS (see address given above).

NCEER-87-0008 "IDARC: Inelastic Damage Analysis of Reinforced Concrete Frame - Shear-Wall Structures," by Y.J. Park, A.M. Reinhorn and S.K. Kunnath, 7/20/87, (PB88-134325, A09, MF-A01). This report is only available through NTIS (see address given above).

NCEER-87-0009 "Liquefaction Potential for New York State: A Preliminary Report on Sites in Manhattan and Buffalo," by M. Budhu, V. Vijayakumar, R.F. Giese and L. Baumgras, 8/31/87, (PB88-163704, A03, MF-A01). This report is available only through NTIS (see address given above).

NCEER-87-0010 "Vertical and Torsional Vibration of Foundations in Inhomogeneous Media," by A.S. Veletsos and K.W. Dotson, 6/1/87, (PB88-134291, A03, MF-A01). This report is only available through NTIS (see address given above).

NCEER-87-0011 "Seismic Probabilistic Risk Assessment and Seismic Margins Studies for Nuclear Power Plants," by Howard H.M. Hwang, 6/15/87, (PB88-134267, A03, MF-A01). This report is only available through NTIS (see address given above).

NCEER-87-0012 "Parametric Studies of Frequency Response of Secondary Systems Under Ground-Acceleration Excitations," by Y. Yong and Y.K. Lin, 6/10/87, (PB88-134309, A03, MF-A01). This report is only available through NTIS (see address given above).

NCEER-87-0013 "Frequency Response of Secondary Systems Under Seismic Excitation," by J.A. HoLung, J. Cai and Y.K. Lin, 7/31/87, (PB88-134317, A05, MF-A01). This report is only available through NTIS (see address given above).

NCEER-87-0014 "Modelling Earthquake Ground Motions in Seismically Active Regions Using Parametric Time Series Methods," by G.W. Ellis and A.S. Cakmak, 8/25/87, (PB88-134283, A08, MF-A01). This report is only available through NTIS (see address given above).

NCEER-87-0015 "Detection and Assessment of Seismic Structural Damage," by E. DiPasquale and A.S. Cakmak, 8/25/87, (PB88-163712, A05, MF-A01). This report is only available through NTIS (see address given above).

NCEER-87-0016 "Pipeline Experiment at Parkfield, California," by J. Isenberg and E. Richardson, 9/15/87, (PB88-163720, A03, MF-A01). This report is available only through NTIS (see address given above).

NCEER-87-0017 "Digital Simulation of Seismic Ground Motion," by M. Shinozuka, G. Deodatis and T. Harada, 8/31/87, (PB88-155197, A04, MF-A01). This report is available only through NTIS (see address given above).

NCEER-87-0018 "Practical Considerations for Structural Control: System Uncertainty, System Time Delay and Truncation of Small Control Forces," J.N. Yang and A. Akbarpour, 8/10/87, (PB88-163738, A08, MF-A01). This report is only available through NTIS (see address given above).

NCEER-87-0019 "Modal Analysis of Nonclassically Damped Structural Systems Using Canonical Transformation," by J.N. Yang, S. Sarkani and F.X. Long, 9/27/87, (PB88-187851, A04, MF-A01).

NCEER-87-0020 "A Nonstationary Solution in Random Vibration Theory," by J.R. Red-Horse and P.D. Spanos, 11/3/87, (PB88-163746, A03, MF-A01).

NCEER-87-0021 "Horizontal Impedances for Radially Inhomogeneous Viscoelastic Soil Layers," by A.S. Veletsos and K.W. Dotson, 10/15/87, (PB88-150859, A04, MF-A01).

NCEER-87-0022 "Seismic Damage Assessment of Reinforced Concrete Members," by Y.S. Chung, C. Meyer and M. Shinozuka, 10/9/87, (PB88-150867, A05, MF-A01). This report is available only through NTIS (see address given above).

NCEER-87-0023 "Active Structural Control in Civil Engineering," by T.T. Soong, 11/11/87, (PB88-187778, A03, MF-A01).

NCEER-87-0024 "Vertical and Torsional Impedances for Radially Inhomogeneous Viscoelastic Soil Layers," by K.W. Dotson and A.S. Veletsos, 12/87, (PB88-187786, A03, MF-A01).

NCEER-87-0025 "Proceedings from the Symposium on Seismic Hazards, Ground Motions, Soil-Liquefaction and Engineering Practice in Eastern North America," October 20-22, 1987, edited by K.H. Jacob, 12/87, (PB88-188115, A23, MF-A01). This report is available only through NTIS (see address given above).

NCEER-87-0026 "Report on the Whittier-Narrows, California, Earthquake of October 1, 1987," by J. Pantelic and A. Reinhorn, 11/87, (PB88-187752, A03, MF-A01). This report is available only through NTIS (see address given above).

NCEER-87-0027 "Design of a Modular Program for Transient Nonlinear Analysis of Large 3-D Building Structures," by S. Srivastav and J.F. Abel, 12/30/87, (PB88-187950, A05, MF-A01). This report is only available through NTIS (see address given above).

NCEER-87-0028 "Second-Year Program in Research, Education and Technology Transfer," 3/8/88, (PB88-219480, A04, MF-A01).

NCEER-88-0001 "Workshop on Seismic Computer Analysis and Design of Buildings With Interactive Graphics," by W. McGuire, J.F. Abel and C.H. Conley, 1/18/88, (PB88-187760, A03, MF-A01). This report is only available through NTIS (see address given above).

NCEER-88-0002 "Optimal Control of Nonlinear Flexible Structures," by J.N. Yang, F.X. Long and D. Wong, 1/22/88, (PB88-213772, A06, MF-A01).

NCEER-88-0003 "Substructuring Techniques in the Time Domain for Primary-Secondary Structural Systems," by G.D. Manolis and G. Juhn, 2/10/88, (PB88-213780, A04, MF-A01).

NCEER-88-0004 "Iterative Seismic Analysis of Primary-Secondary Systems," by A. Singhal, L.D. Lutes and P.D. Spanos, 2/23/88, (PB88-213798, A04, MF-A01).

NCEER-88-0005 "Stochastic Finite Element Expansion for Random Media," by P.D. Spanos and R. Ghanem, 3/14/88, (PB88-213806, A03, MF-A01).

NCEER-88-0006 "Combining Structural Optimization and Structural Control," by F.Y. Cheng and C.P. Pantelides, 1/10/88, (PB88-213814, A05, MF-A01).

NCEER-88-0007 "Seismic Performance Assessment of Code-Designed Structures," by H.H-M. Hwang, J-W. Jaw and H-J. Shau, 3/20/88, (PB88-219423, A04, MF-A01). This report is only available through NTIS (see address given above).

NCEER-88-0008 "Reliability Analysis of Code-Designed Structures Under Natural Hazards," by H.H-M. Hwang, H. Ushiba and M. Shinozuka, 2/29/88, (PB88-229471, A07, MF-A01). This report is only available through NTIS (see address given above).

NCEER-88-0009 "Seismic Fragility Analysis of Shear Wall Structures," by J-W Jaw and H.H-M. Hwang, 4/30/88, (PB89-102867, A04, MF-A01).

NCEER-88-0010 "Base Isolation of a Multi-Story Building Under a Harmonic Ground Motion - A Comparison of Performances of Various Systems," by F-G Fan, G. Ahmadi and I.G. Tadjbakhsh, 5/18/88, (PB89-122238, A06, MF-A01). This report is only available through NTIS (see address given above).

NCEER-88-0011 "Seismic Floor Response Spectra for a Combined System by Green's Functions," by F.M. Lavelle, L.A. Bergman and P.D. Spanos, 5/1/88, (PB89-102875, A03, MF-A01).

NCEER-88-0012 "A New Solution Technique for Randomly Excited Hysteretic Structures," by G.Q. Cai and Y.K. Lin, 5/16/88, (PB89-102883, A03, MF-A01).

NCEER-88-0013 "A Study of Radiation Damping and Soil-Structure Interaction Effects in the Centrifuge," by K. Weissman, supervised by J.H. Prevost, 5/24/88, (PB89-144703, A06, MF-A01).

NCEER-88-0014 "Parameter Identification and Implementation of a Kinematic Plasticity Model for Frictional Soils," by J.H. Prevost and D.V. Griffiths, to be published.

NCEER-88-0015 "Two- and Three- Dimensional Dynamic Finite Element Analyses of the Long Valley Dam," by D.V. Griffiths and J.H. Prevost, 6/17/88, (PB89-144711, A04, MF-A01).

NCEER-88-0016 "Damage Assessment of Reinforced Concrete Structures in Eastern United States," by A.M. Reinhorn, M.J. Seidel, S.K. Kunnath and Y.J. Park, 6/15/88, (PB89-122220, A04, MF-A01). This report is only available through NTIS (see address given above).

NCEER-88-0017 "Dynamic Compliance of Vertically Loaded Strip Foundations in Multilayered Viscoelastic Soils," by S. Ahmad and A.S.M. Israil, 6/17/88, (PB89-102891, A04, MF-A01).

NCEER-88-0018 "An Experimental Study of Seismic Structural Response With Added Viscoelastic Dampers," by R.C. Lin, Z. Liang, T.T. Soong and R.H. Zhang, 6/30/88, (PB89-122212, A05, MF-A01). This report is available only through NTIS (see address given above).

NCEER-88-0019 "Experimental Investigation of Primary - Secondary System Interaction," by G.D. Manolis, G. Juhn and A.M. Reinhorn, 5/27/88, (PB89-122204, A04, MF-A01).

NCEER-88-0020 "A Response Spectrum Approach For Analysis of Nonclassically Damped Structures," by J.N. Yang, S. Sarkani and F.X. Long, 4/22/88, (PB89-102909, A04, MF-A01).

NCEER-88-0021 "Seismic Interaction of Structures and Soils: Stochastic Approach," by A.S. Veletsos and A.M. Prasad, 7/21/88, (PB89-122196, A04, MF-A01). This report is only available through NTIS (see address given above).

NCEER-88-0022 "Identification of the Serviceability Limit State and Detection of Seismic Structural Damage," by E. DiPasquale and A.S. Cakmak, 6/15/88, (PB89-122188, A05, MF-A01). This report is available only through NTIS (see address given above).

NCEER-88-0023 "Multi-Hazard Risk Analysis: Case of a Simple Offshore Structure," by B.K. Bhartia and E.H. Vanmarcke, 7/21/88, (PB89-145213, A05, MF-A01).

NCEER-88-0024 "Automated Seismic Design of Reinforced Concrete Buildings," by Y.S. Chung, C. Meyer and M. Shinozuka, 7/5/88, (PB89-122170, A06, MF-A01). This report is available only through NTIS (see address given above).

NCEER-88-0025 "Experimental Study of Active Control of MDOF Structures Under Seismic Excitations," by L.L. Chung, R.C. Lin, T.T. Soong and A.M. Reinhorn, 7/10/88, (PB89-122600, A04, MF-A01).

NCEER-88-0026 "Earthquake Simulation Tests of a Low-Rise Metal Structure," by J.S. Hwang, K.C. Chang, G.C. Lee and R.L. Ketter, 8/1/88, (PB89-102917, A04, MF-A01).

NCEER-88-0027 "Systems Study of Urban Response and Reconstruction Due to Catastrophic Earthquakes," by F. Kozin and H.K. Zhou, 9/22/88, (PB90-162348, A04, MF-A01).

NCEER-88-0028 "Seismic Fragility Analysis of Plane Frame Structures," by H.H-M. Hwang and Y.K. Low, 7/31/88, (PB89-131445, A06, MF-A01).

NCEER-88-0029 "Response Analysis of Stochastic Structures," by A. Kardara, C. Bucher and M. Shinozuka, 9/22/88, (PB89-174429, A04, MF-A01).

NCEER-88-0030 "Nonnormal Accelerations Due to Yielding in a Primary Structure," by D.C.K. Chen and L.D. Lutes, 9/19/88, (PB89-131437, A04, MF-A01).

NCEER-88-0031 "Design Approaches for Soil-Structure Interaction," by A.S. Veletsos, A.M. Prasad and Y. Tang, 12/30/88, (PB89-174437, A03, MF-A01). This report is available only through NTIS (see address given above).

NCEER-88-0032 "A Re-evaluation of Design Spectra for Seismic Damage Control," by C.J. Turkstra and A.G. Tallin, 11/7/88, (PB89-145221, A05, MF-A01).

NCEER-88-0033 "The Behavior and Design of Noncontact Lap Splices Subjected to Repeated Inelastic Tensile Loading," by V.E. Sagan, P. Gergely and R.N. White, 12/8/88, (PB89-163737, A08, MF-A01).

NCEER-88-0034 "Seismic Response of Pile Foundations," by S.M. Mamoon, P.K. Banerjee and S. Ahmad, 11/1/88, (PB89-145239, A04, MF-A01).

NCEER-88-0035 "Modeling of R/C Building Structures With Flexible Floor Diaphragms (IDARC2)," by A.M. Reinhorn, S.K. Kunnath and N. Panahshahi, 9/7/88, (PB89-207153, A07, MF-A01).

NCEER-88-0036 "Solution of the Dam-Reservoir Interaction Problem Using a Combination of FEM, BEM with Particular Integrals, Modal Analysis, and Substructuring," by C-S. Tsai, G.C. Lee and R.L. Ketter, 12/31/88, (PB89-207146, A04, MF-A01).

NCEER-88-0037 "Optimal Placement of Actuators for Structural Control," by F.Y. Cheng and C.P. Pantelides, 8/15/88, (PB89-162846, A05, MF-A01).

NCEER-88-0038 "Teflon Bearings in Aseismic Base Isolation: Experimental Studies and Mathematical Modeling," by A. Mokha, M.C. Constantinou and A.M. Reinhorn, 12/5/88, (PB89-218457, A10, MF-A01). This report is available only through NTIS (see address given above).

NCEER-88-0039 "Seismic Behavior of Flat Slab High-Rise Buildings in the New York City Area," by P. Weidlinger and M. Ettouney, 10/15/88, (PB90-145681, A04, MF-A01).

NCEER-88-0040 "Evaluation of the Earthquake Resistance of Existing Buildings in New York City," by P. Weidlinger and M. Ettouney, 10/15/88, to be published.

NCEER-88-0041 "Small-Scale Modeling Techniques for Reinforced Concrete Structures Subjected to Seismic Loads," by W. Kim, A. El-Attar and R.N. White, 11/22/88, (PB89-189625, A05, MF-A01).

NCEER-88-0042 "Modeling Strong Ground Motion from Multiple Event Earthquakes," by G.W. Ellis and A.S. Cakmak, 10/15/88, (PB89-174445, A03, MF-A01).

NCEER-88-0043 "Nonstationary Models of Seismic Ground Acceleration," by M. Grigoriu, S.E. Ruiz and E. Rosenblueth, 7/15/88, (PB89-189617, A04, MF-A01).

NCEER-88-0044 "SARCF User's Guide: Seismic Analysis of Reinforced Concrete Frames," by Y.S. Chung, C. Meyer and M. Shinozuka, 11/9/88, (PB89-174452, A08, MF-A01).

NCEER-88-0045 "First Expert Panel Meeting on Disaster Research and Planning," edited by J. Pantelic and J. Stoyle, 9/15/88, (PB89-174460, A05, MF-A01).

NCEER-88-0046 "Preliminary Studies of the Effect of Degrading Infill Walls on the Nonlinear Seismic Response of Steel Frames," by C.Z. Chrysostomou, P. Gergely and J.F. Abel, 12/19/88, (PB89-208383, A05, MF-A01).

NCEER-88-0047 "Reinforced Concrete Frame Component Testing Facility - Design, Construction, Instrumentation and Operation," by S.P. Pessiki, C. Conley, T. Bond, P. Gergely and R.N. White, 12/16/88, (PB89-174478, A04, MF-A01).

NCEER-89-0001 "Effects of Protective Cushion and Soil Compliancy on the Response of Equipment Within a Seismically Excited Building," by J.A. HoLung, 2/16/89, (PB89-207179, A04, MF-A01).

NCEER-89-0002 "Statistical Evaluation of Response Modification Factors for Reinforced Concrete Structures," by H.H-M. Hwang and J-W. Jaw, 2/17/89, (PB89-207187, A05, MF-A01).

NCEER-89-0003 "Hysteretic Columns Under Random Excitation," by G-Q. Cai and Y.K. Lin, 1/9/89, (PB89-196513, A03, MF-A01).

NCEER-89-0004 "Experimental Study of `Elephant Foot Bulge' Instability of Thin-Walled Metal Tanks," by Z-H. Jia and R.L. Ketter, 2/22/89, (PB89-207195, A03, MF-A01).

NCEER-89-0005 "Experiment on Performance of Buried Pipelines Across San Andreas Fault," by J. Isenberg, E. Richardson and T.D. O'Rourke, 3/10/89, (PB89-218440, A04, MF-A01). This report is available only through NTIS (see address given above).

NCEER-89-0006 "A Knowledge-Based Approach to Structural Design of Earthquake-Resistant Buildings," by M. Subramani, P. Gergely, C.H. Conley, J.F. Abel and A.H. Zaghw, 1/15/89, (PB89-218465, A06, MF-A01).

NCEER-89-0007 "Liquefaction Hazards and Their Effects on Buried Pipelines," by T.D. O'Rourke and P.A. Lane, 2/1/89, (PB89-218481, A09, MF-A01).

NCEER-89-0008 "Fundamentals of System Identification in Structural Dynamics," by H. Imai, C-B. Yun, O. Maruyama and M. Shinozuka, 1/26/89, (PB89-207211, A04, MF-A01).

NCEER-89-0009 "Effects of the 1985 Michoacan Earthquake on Water Systems and Other Buried Lifelines in Mexico," by A.G. Ayala and M.J. O'Rourke, 3/8/89, (PB89-207229, A06, MF-A01).

NCEER-89-R010 "NCEER Bibliography of Earthquake Education Materials," by K.E.K. Ross, Second Revision, 9/1/89, (PB90-125352, A05, MF-A01). This report is replaced by NCEER-92-0018.

NCEER-89-0011 "Inelastic Three-Dimensional Response Analysis of Reinforced Concrete Building Structures (IDARC-3D), Part I - Modeling," by S.K. Kunnath and A.M. Reinhorn, 4/17/89, (PB90-114612, A07, MF-A01). This report is available only through NTIS (see address given above).

NCEER-89-0012 "Recommended Modifications to ATC-14," by C.D. Poland and J.O. Malley, 4/12/89, (PB90-108648, A15, MF-A01).

NCEER-89-0013 "Repair and Strengthening of Beam-to-Column Connections Subjected to Earthquake Loading," by M. Corazao and A.J. Durrani, 2/28/89, (PB90-109885, A06, MF-A01).

NCEER-89-0014 "Program EXKAL2 for Identification of Structural Dynamic Systems," by O. Maruyama, C-B. Yun, M. Hoshiya and M. Shinozuka, 5/19/89, (PB90-109877, A09, MF-A01).

NCEER-89-0015 "Response of Frames With Bolted Semi-Rigid Connections, Part I - Experimental Study and Analytical Predictions," by P.J. DiCorso, A.M. Reinhorn, J.R. Dickerson, J.B. Radziminski and W.L. Harper, 6/1/89, to be published.

NCEER-89-0016 "ARMA Monte Carlo Simulation in Probabilistic Structural Analysis," by P.D. Spanos and M.P. Mignolet, 7/10/89, (PB90-109893, A03, MF-A01).

NCEER-89-P017 "Preliminary Proceedings from the Conference on Disaster Preparedness - The Place of Earthquake Education in Our Schools," Edited by K.E.K. Ross, 6/23/89, (PB90-108606, A03, MF-A01).

NCEER-89-0017 "Proceedings from the Conference on Disaster Preparedness - The Place of Earthquake Education in Our Schools," Edited by K.E.K. Ross, 12/31/89, (PB90-207895, A012, MF-A02). This report is available only through NTIS (see address given above).

NCEER-89-0018 "Multidimensional Models of Hysteretic Material Behavior for Vibration Analysis of Shape Memory Energy Absorbing Devices, by E.J. Graesser and F.A. Cozzarelli, 6/7/89, (PB90-164146, A04, MF-A01).

NCEER-89-0019 "Nonlinear Dynamic Analysis of Three-Dimensional Base Isolated Structures (3D-BASIS)," by S. Nagarajaiah, A.M. Reinhorn and M.C. Constantinou, 8/3/89, (PB90-161936, A06, MF-A01). This report has been replaced by NCEER-93-0011.

NCEER-89-0020 "Structural Control Considering Time-Rate of Control Forces and Control Rate Constraints," by F.Y. Cheng and C.P. Pantelides, 8/3/89, (PB90-120445, A04, MF-A01).

NCEER-89-0021 "Subsurface Conditions of Memphis and Shelby County," by K.W. Ng, T-S. Chang and H-H.M. Hwang, 7/26/89, (PB90-120437, A03, MF-A01).

NCEER-89-0022 "Seismic Wave Propagation Effects on Straight Jointed Buried Pipelines," by K. Elhmadi and M.J. O'Rourke, 8/24/89, (PB90-162322, A10, MF-A02).

NCEER-89-0023 "Workshop on Serviceability Analysis of Water Delivery Systems," edited by M. Grigoriu, 3/6/89, (PB90-127424, A03, MF-A01).

NCEER-89-0024 "Shaking Table Study of a 1/5 Scale Steel Frame Composed of Tapered Members," by K.C. Chang, J.S. Hwang and G.C. Lee, 9/18/89, (PB90-160169, A04, MF-A01).

NCEER-89-0025 "DYNA1D: A Computer Program for Nonlinear Seismic Site Response Analysis - Technical Documentation," by Jean H. Prevost, 9/14/89, (PB90-161944, A07, MF-A01). This report is available only through NTIS (see address given above).

NCEER-89-0026 "1:4 Scale Model Studies of Active Tendon Systems and Active Mass Dampers for Aseismic Protection," by A.M. Reinhorn, T.T. Soong, R.C. Lin, Y.P. Yang, Y. Fukao, H. Abe and M. Nakai, 9/15/89, (PB90-173246, A10, MF-A02). This report is available only through NTIS (see address given above).

NCEER-89-0027 "Scattering of Waves by Inclusions in a Nonhomogeneous Elastic Half Space Solved by Boundary Element Methods," by P.K. Hadley, A. Askar and A.S. Cakmak, 6/15/89, (PB90-145699, A07, MF-A01).

NCEER-89-0028 "Statistical Evaluation of Deflection Amplification Factors for Reinforced Concrete Structures," by H.H.M. Hwang, J-W. Jaw and A.L. Ch'ng, 8/31/89, (PB90-164633, A05, MF-A01).

NCEER-89-0029 "Bedrock Accelerations in Memphis Area Due to Large New Madrid Earthquakes," by H.H.M. Hwang, C.H.S. Chen and G. Yu, 11/7/89, (PB90-162330, A04, MF-A01).

NCEER-89-0030 "Seismic Behavior and Response Sensitivity of Secondary Structural Systems," by Y.Q. Chen and T.T. Soong, 10/23/89, (PB90-164658, A08, MF-A01).

NCEER-89-0031 "Random Vibration and Reliability Analysis of Primary-Secondary Structural Systems," by Y. Ibrahim, M. Grigoriu and T.T. Soong, 11/10/89, (PB90-161951, A04, MF-A01).

NCEER-89-0032 "Proceedings from the Second U.S. - Japan Workshop on Liquefaction, Large Ground Deformation and Their Effects on Lifelines, September 26-29, 1989," Edited by T.D. O'Rourke and M. Hamada, 12/1/89, (PB90-209388, A22, MF-A03).

NCEER-89-0033 "Deterministic Model for Seismic Damage Evaluation of Reinforced Concrete Structures," by J.M. Bracci, A.M. Reinhorn, J.B. Mander and S.K. Kunnath, 9/27/89, (PB91-108803, A06, MF-A01).

NCEER-89-0034 "On the Relation Between Local and Global Damage Indices," by E. DiPasquale and A.S. Cakmak, 8/15/89, (PB90-173865, A05, MF-A01).

NCEER-89-0035 "Cyclic Undrained Behavior of Nonplastic and Low Plasticity Silts," by A.J. Walker and H.E. Stewart, 7/26/89, (PB90-183518, A10, MF-A01).

NCEER-89-0036 "Liquefaction Potential of Surficial Deposits in the City of Buffalo, New York," by M. Budhu, R. Giese and L. Baumgrass, 1/17/89, (PB90-208455, A04, MF-A01).

NCEER-89-0037 "A Deterministic Assessment of Effects of Ground Motion Incoherence," by A.S. Veletsos and Y. Tang, 7/15/89, (PB90-164294, A03, MF-A01).

NCEER-89-0038 "Workshop on Ground Motion Parameters for Seismic Hazard Mapping," July 17-18, 1989, edited by R.V. Whitman, 12/1/89, (PB90-173923, A04, MF-A01).

NCEER-89-0039 "Seismic Effects on Elevated Transit Lines of the New York City Transit Authority," by C.J. Costantino, C.A. Miller and E. Heymsfield, 12/26/89, (PB90-207887, A06, MF-A01).

NCEER-89-0040 "Centrifugal Modeling of Dynamic Soil-Structure Interaction," by K. Weissman, Supervised by J.H. Prevost, 5/10/89, (PB90-207879, A07, MF-A01).

NCEER-89-0041 "Linearized Identification of Buildings With Cores for Seismic Vulnerability Assessment," by I-K. Ho and A.E. Aktan, 11/1/89, (PB90-251943, A07, MF-A01).

NCEER-90-0001 "Geotechnical and Lifeline Aspects of the October 17, 1989 Loma Prieta Earthquake in San Francisco," by T.D. O'Rourke, H.E. Stewart, F.T. Blackburn and T.S. Dickerman, 1/90, (PB90-208596, A05, MF-A01).

NCEER-90-0002 "Nonnormal Secondary Response Due to Yielding in a Primary Structure," by D.C.K. Chen and L.D. Lutes, 2/28/90, (PB90-251976, A07, MF-A01).

NCEER-90-0003 "Earthquake Education Materials for Grades K-12," by K.E.K. Ross, 4/16/90, (PB91-251984, A05, MF-A05). This report has been replaced by NCEER-92-0018.

NCEER-90-0004 "Catalog of Strong Motion Stations in Eastern North America," by R.W. Busby, 4/3/90, (PB90-251984, A05, MF-A01).

NCEER-90-0005 "NCEER Strong-Motion Data Base: A User Manual for the GeoBase Release (Version 1.0 for the Sun3)," by P. Friberg and K. Jacob, 3/31/90 (PB90-258062, A04, MF-A01).

NCEER-90-0006 "Seismic Hazard Along a Crude Oil Pipeline in the Event of an 1811-1812 Type New Madrid Earthquake," by H.H.M. Hwang and C-H.S. Chen, 4/16/90, (PB90-258054, A04, MF-A01).

NCEER-90-0007 "Site-Specific Response Spectra for Memphis Sheahan Pumping Station," by H.H.M. Hwang and C.S. Lee, 5/15/90, (PB91-108811, A05, MF-A01).

NCEER-90-0008 "Pilot Study on Seismic Vulnerability of Crude Oil Transmission Systems," by T. Ariman, R. Dobry, M. Grigoriu, F. Kozin, M. O'Rourke, T. O'Rourke and M. Shinozuka, 5/25/90, (PB91-108837, A06, MF-A01).

NCEER-90-0009 "A Program to Generate Site Dependent Time Histories: EQGEN," by G.W. Ellis, M. Srinivasan and A.S. Cakmak, 1/30/90, (PB91-108829, A04, MF-A01).

NCEER-90-0010 "Active Isolation for Seismic Protection of Operating Rooms," by M.E. Talbott, Supervised by M. Shinozuka, 6/8/9, (PB91-110205, A05, MF-A01).

NCEER-90-0011 "Program LINEARID for Identification of Linear Structural Dynamic Systems," by C-B. Yun and M. Shinozuka, 6/25/90, (PB91-110312, A08, MF-A01).

NCEER-90-0012 "Two-Dimensional Two-Phase Elasto-Plastic Seismic Response of Earth Dams," by A.N. Yiagos, Supervised by J.H. Prevost, 6/20/90, (PB91-110197, A13, MF-A02).

NCEER-90-0013 "Secondary Systems in Base-Isolated Structures: Experimental Investigation, Stochastic Response and Stochastic Sensitivity," by G.D. Manolis, G. Juhn, M.C. Constantinou and A.M. Reinhorn, 7/1/90, (PB91-110320, A08, MF-A01).

NCEER-90-0014 "Seismic Behavior of Lightly-Reinforced Concrete Column and Beam-Column Joint Details," by S.P. Pessiki, C.H. Conley, P. Gergely and R.N. White, 8/22/90, (PB91-108795, A11, MF-A02).

NCEER-90-0015 "Two Hybrid Control Systems for Building Structures Under Strong Earthquakes," by J.N. Yang and A. Danielians, 6/29/90, (PB91-125393, A04, MF-A01).

NCEER-90-0016 "Instantaneous Optimal Control with Acceleration and Velocity Feedback," by J.N. Yang and Z. Li, 6/29/90, (PB91-125401, A03, MF-A01).

NCEER-90-0017 "Reconnaissance Report on the Northern Iran Earthquake of June 21, 1990," by M. Mehrain, 10/4/90, (PB91-125377, A03, MF-A01).

NCEER-90-0018 "Evaluation of Liquefaction Potential in Memphis and Shelby County," by T.S. Chang, P.S. Tang, C.S. Lee and H. Hwang, 8/10/90, (PB91-125427, A09, MF-A01).

NCEER-90-0019 "Experimental and Analytical Study of a Combined Sliding Disc Bearing and Helical Steel Spring Isolation System," by M.C. Constantinou, A.S. Mokha and A.M. Reinhorn, 10/4/90, (PB91-125385, A06, MF-A01). This report is available only through NTIS (see address given above).

NCEER-90-0020 "Experimental Study and Analytical Prediction of Earthquake Response of a Sliding Isolation System with a Spherical Surface," by A.S. Mokha, M.C. Constantinou and A.M. Reinhorn, 10/11/90, (PB91-125419, A05, MF-A01).

NCEER-90-0021 "Dynamic Interaction Factors for Floating Pile Groups," by G. Gazetas, K. Fan, A. Kaynia and E. Kausel, 9/10/90, (PB91-170381, A05, MF-A01).

NCEER-90-0022 "Evaluation of Seismic Damage Indices for Reinforced Concrete Structures," by S. Rodriguez-Gomez and A.S. Cakmak, 9/30/90, PB91-171322, A06, MF-A01).

NCEER-90-0023 "Study of Site Response at a Selected Memphis Site," by H. Desai, S. Ahmad, E.S. Gazetas and M.R. Oh, 10/11/90, (PB91-196857, A03, MF-A01).

NCEER-90-0024 "A User's Guide to Strongmo: Version 1.0 of NCEER's Strong-Motion Data Access Tool for PCs and Terminals," by P.A. Friberg and C.A.T. Susch, 11/15/90, (PB91-171272, A03, MF-A01).

NCEER-90-0025 "A Three-Dimensional Analytical Study of Spatial Variability of Seismic Ground Motions," by L-L. Hong and A.H.-S. Ang, 10/30/90, (PB91-170399, A09, MF-A01).

NCEER-90-0026 "MUMOID User's Guide - A Program for the Identification of Modal Parameters," by S. Rodriguez-Gomez and E. DiPasquale, 9/30/90, (PB91-171298, A04, MF-A01).

NCEER-90-0027 "SARCF-II User's Guide - Seismic Analysis of Reinforced Concrete Frames," by S. Rodriguez-Gomez, Y.S. Chung and C. Meyer, 9/30/90, (PB91-171280, A05, MF-A01).

NCEER-90-0028 "Viscous Dampers: Testing, Modeling and Application in Vibration and Seismic Isolation," by N. Makris and M.C. Constantinou, 12/20/90 (PB91-190561, A06, MF-A01).

NCEER-90-0029 "Soil Effects on Earthquake Ground Motions in the Memphis Area," by H. Hwang, C.S. Lee, K.W. Ng and T.S. Chang, 8/2/90, (PB91-190751, A05, MF-A01).

NCEER-91-0001 "Proceedings from the Third Japan-U.S. Workshop on Earthquake Resistant Design of Lifeline Facilities and Countermeasures for Soil Liquefaction, December 17-19, 1990," edited by T.D. O'Rourke and M. Hamada, 2/1/91, (PB91-179259, A99, MF-A04).

NCEER-91-0002 "Physical Space Solutions of Non-Proportionally Damped Systems," by M. Tong, Z. Liang and G.C. Lee, 1/15/91, (PB91-179242, A04, MF-A01).

NCEER-91-0003 "Seismic Response of Single Piles and Pile Groups," by K. Fan and G. Gazetas, 1/10/91, (PB92-174994, A04, MF-A01).

NCEER-91-0004 "Damping of Structures: Part 1 - Theory of Complex Damping," by Z. Liang and G. Lee, 10/10/91, (PB92-197235, A12, MF-A03).

NCEER-91-0005 "3D-BASIS - Nonlinear Dynamic Analysis of Three Dimensional Base Isolated Structures: Part II," by S. Nagarajaiah, A.M. Reinhorn and M.C. Constantinou, 2/28/91, (PB91-190553, A07, MF-A01). This report has been replaced by NCEER-93-0011.

NCEER-91-0006 "A Multidimensional Hysteretic Model for Plasticity Deforming Metals in Energy Absorbing Devices," by E.J. Graesser and F.A. Cozzarelli, 4/9/91, (PB92-108364, A04, MF-A01).

NCEER-91-0007 "A Framework for Customizable Knowledge-Based Expert Systems with an Application to a KBES for Evaluating the Seismic Resistance of Existing Buildings," by E.G. Ibarra-Anaya and S.J. Fenves, 4/9/91, (PB91-210930, A08, MF-A01).

NCEER-91-0008 "Nonlinear Analysis of Steel Frames with Semi-Rigid Connections Using the Capacity Spectrum Method," by G.G. Deierlein, S-H. Hsieh, Y-J. Shen and J.F. Abel, 7/2/91, (PB92-113828, A05, MF-A01).

NCEER-91-0009 "Earthquake Education Materials for Grades K-12," by K.E.K. Ross, 4/30/91, (PB91-212142, A06, MF-A01). This report has been replaced by NCEER-92-0018.

NCEER-91-0010 "Phase Wave Velocities and Displacement Phase Differences in a Harmonically Oscillating Pile," by N. Makris and G. Gazetas, 7/8/91, (PB92-108356, A04, MF-A01).

NCEER-91-0011 "Dynamic Characteristics of a Full-Size Five-Story Steel Structure and a 2/5 Scale Model," by K.C. Chang, G.C. Yao, G.C. Lee, D.S. Hao and Y.C. Yeh," 7/2/91, (PB93-116648, A06, MF-A02).

NCEER-91-0012 "Seismic Response of a 2/5 Scale Steel Structure with Added Viscoelastic Dampers," by K.C. Chang, T.T. Soong, S-T. Oh and M.L. Lai, 5/17/91, (PB92-110816, A05, MF-A01).

NCEER-91-0013 "Earthquake Response of Retaining Walls; Full-Scale Testing and Computational Modeling," by S. Alampalli and A-W.M. Elgamal, 6/20/91, to be published.

NCEER-91-0014 "3D-BASIS-M: Nonlinear Dynamic Analysis of Multiple Building Base Isolated Structures," by P.C. Tsopelas, S. Nagarajaiah, M.C. Constantinou and A.M. Reinhorn, 5/28/91, (PB92-113885, A09, MF-A02).

NCEER-91-0015 "Evaluation of SEAOC Design Requirements for Sliding Isolated Structures," by D. Theodossiou and M.C. Constantinou, 6/10/91, (PB92-114602, A11, MF-A03).

NCEER-91-0016 "Closed-Loop Modal Testing of a 27-Story Reinforced Concrete Flat Plate-Core Building," by H.R. Somaprasad, T. Toksoy, H. Yoshiyuki and A.E. Aktan, 7/15/91, (PB92-129980, A07, MF-A02).

NCEER-91-0017 "Shake Table Test of a 1/6 Scale Two-Story Lightly Reinforced Concrete Building," by A.G. El-Attar, R.N. White and P. Gergely, 2/28/91, (PB92-222447, A06, MF-A02).

NCEER-91-0018 "Shake Table Test of a 1/8 Scale Three-Story Lightly Reinforced Concrete Building," by A.G. El-Attar, R.N. White and P. Gergely, 2/28/91, (PB93-116630, A08, MF-A02).

NCEER-91-0019 "Transfer Functions for Rigid Rectangular Foundations," by A.S. Veletsos, A.M. Prasad and W.H. Wu, 7/31/91, to be published.

NCEER-91-0020 "Hybrid Control of Seismic-Excited Nonlinear and Inelastic Structural Systems," by J.N. Yang, Z. Li and A. Danielians, 8/1/91, (PB92-143171, A06, MF-A02).

NCEER-91-0021 "The NCEER-91 Earthquake Catalog: Improved Intensity-Based Magnitudes and Recurrence Relations for U.S. Earthquakes East of New Madrid," by L. Seeber and J.G. Armbruster, 8/28/91, (PB92-176742, A06, MF-A02).

NCEER-91-0022 "Proceedings from the Implementation of Earthquake Planning and Education in Schools: The Need for Change - The Roles of the Changemakers," by K.E.K. Ross and F. Winslow, 7/23/91, (PB92-129998, A12, MF-A03).

NCEER-91-0023 "A Study of Reliability-Based Criteria for Seismic Design of Reinforced Concrete Frame Buildings," by H.H.M. Hwang and H-M. Hsu, 8/10/91, (PB92-140235, A09, MF-A02).

NCEER-91-0024 "Experimental Verification of a Number of Structural System Identification Algorithms," by R.G. Ghanem, H. Gavin and M. Shinozuka, 9/18/91, (PB92-176577, A18, MF-A04).

NCEER-91-0025 "Probabilistic Evaluation of Liquefaction Potential," by H.H.M. Hwang and C.S. Lee," 11/25/91, (PB92-143429, A05, MF-A01).

NCEER-91-0026 "Instantaneous Optimal Control for Linear, Nonlinear and Hysteretic Structures - Stable Controllers," by J.N. Yang and Z. Li, 11/15/91, (PB92-163807, A04, MF-A01).

NCEER-91-0027 "Experimental and Theoretical Study of a Sliding Isolation System for Bridges," by M.C. Constantinou, A. Kartoum, A.M. Reinhorn and P. Bradford, 11/15/91, (PB92-176973, A10, MF-A03).

NCEER-92-0001 "Case Studies of Liquefaction and Lifeline Performance During Past Earthquakes, Volume 1: Japanese Case Studies," Edited by M. Hamada and T. O'Rourke, 2/17/92, (PB92-197243, A18, MF-A04).

NCEER-92-0002 "Case Studies of Liquefaction and Lifeline Performance During Past Earthquakes, Volume 2: United States Case Studies," Edited by T. O'Rourke and M. Hamada, 2/17/92, (PB92-197250, A20, MF-A04).

NCEER-92-0003 "Issues in Earthquake Education," Edited by K. Ross, 2/3/92, (PB92-222389, A07, MF-A02).

NCEER-92-0004 "Proceedings from the First U.S. - Japan Workshop on Earthquake Protective Systems for Bridges," Edited by I.G. Buckle, 2/4/92, (PB94-142239, A99, MF-A06).

NCEER-92-0005 "Seismic Ground Motion from a Haskell-Type Source in a Multiple-Layered Half-Space," A.P. Theoharis, G. Deodatis and M. Shinozuka, 1/2/92, to be published.

NCEER-92-0006 "Proceedings from the Site Effects Workshop," Edited by R. Whitman, 2/29/92, (PB92-197201, A04, MF-A01).

NCEER-92-0007 "Engineering Evaluation of Permanent Ground Deformations Due to Seismically-Induced Liquefaction," by M.H. Baziar, R. Dobry and A-W.M. Elgamal, 3/24/92, (PB92-222421, A13, MF-A03).

NCEER-92-0008 "A Procedure for the Seismic Evaluation of Buildings in the Central and Eastern United States," by C.D. Poland and J.O. Malley, 4/2/92, (PB92-222439, A20, MF-A04).

NCEER-92-0009 "Experimental and Analytical Study of a Hybrid Isolation System Using Friction Controllable Sliding Bearings," by M.Q. Feng, S. Fujii and M. Shinozuka, 5/15/92, (PB93-150282, A06, MF-A02).

NCEER-92-0010 "Seismic Resistance of Slab-Column Connections in Existing Non-Ductile Flat-Plate Buildings," by A.J. Durrani and Y. Du, 5/18/92, (PB93-116812, A06, MF-A02).

NCEER-92-0011 "The Hysteretic and Dynamic Behavior of Brick Masonry Walls Upgraded by Ferrocement Coatings Under Cyclic Loading and Strong Simulated Ground Motion," by H. Lee and S.P. Prawel, 5/11/92, to be published.

NCEER-92-0012 "Study of Wire Rope Systems for Seismic Protection of Equipment in Buildings," by G.F. Demetriades, M.C. Constantinou and A.M. Reinhorn, 5/20/92, (PB93-116655, A08, MF-A02).

NCEER-92-0013 "Shape Memory Structural Dampers: Material Properties, Design and Seismic Testing," by P.R. Witting and F.A. Cozzarelli, 5/26/92, (PB93-116663, A05, MF-A01).

NCEER-92-0014 "Longitudinal Permanent Ground Deformation Effects on Buried Continuous Pipelines," by M.J. O'Rourke, and C. Nordberg, 6/15/92, (PB93-116671, A08, MF-A02).

NCEER-92-0015 "A Simulation Method for Stationary Gaussian Random Functions Based on the Sampling Theorem," by M. Grigoriu and S. Balopoulou, 6/11/92, (PB93-127496, A05, MF-A01).

NCEER-92-0016 "Gravity-Load-Designed Reinforced Concrete Buildings: Seismic Evaluation of Existing Construction and Detailing Strategies for Improved Seismic Resistance," by G.W. Hoffmann, S.K. Kunnath, A.M. Reinhorn and J.B. Mander, 7/15/92, (PB94-142007, A08, MF-A02).

NCEER-92-0017 "Observations on Water System and Pipeline Performance in the Limón Area of Costa Rica Due to the April 22, 1991 Earthquake," by M. O'Rourke and D. Ballantyne, 6/30/92, (PB93-126811, A06, MF-A02).

NCEER-92-0018 "Fourth Edition of Earthquake Education Materials for Grades K-12," Edited by K.E.K. Ross, 8/10/92, (PB93-114023, A07, MF-A02).

NCEER-92-0019 "Proceedings from the Fourth Japan-U.S. Workshop on Earthquake Resistant Design of Lifeline Facilities and Countermeasures for Soil Liquefaction," Edited by M. Hamada and T.D. O'Rourke, 8/12/92, (PB93-163939, A99, MF-E11).

NCEER-92-0020 "Active Bracing System: A Full Scale Implementation of Active Control," by A.M. Reinhorn, T.T. Soong, R.C. Lin, M.A. Riley, Y.P. Wang, S. Aizawa and M. Higashino, 8/14/92, (PB93-127512, A06, MF-A02).

NCEER-92-0021 "Empirical Analysis of Horizontal Ground Displacement Generated by Liquefaction-Induced Lateral Spreads," by S.F. Bartlett and T.L. Youd, 8/17/92, (PB93-188241, A06, MF-A02).

NCEER-92-0022 "IDARC Version 3.0: Inelastic Damage Analysis of Reinforced Concrete Structures," by S.K. Kunnath, A.M. Reinhorn and R.F. Lobo, 8/31/92, (PB93-227502, A07, MF-A02).

NCEER-92-0023 "A Semi-Empirical Analysis of Strong-Motion Peaks in Terms of Seismic Source, Propagation Path and Local Site Conditions, by M. Kamiyama, M.J. O'Rourke and R. Flores-Berrones, 9/9/92, (PB93-150266, A08, MF-A02).

NCEER-92-0024 "Seismic Behavior of Reinforced Concrete Frame Structures with Nonductile Details, Part I: Summary of Experimental Findings of Full Scale Beam-Column Joint Tests," by A. Beres, R.N. White and P. Gergely, 9/30/92, (PB93-227783, A05, MF-A01).

NCEER-92-0025 "Experimental Results of Repaired and Retrofitted Beam-Column Joint Tests in Lightly Reinforced Concrete Frame Buildings," by A. Beres, S. El-Borgi, R.N. White and P. Gergely, 10/29/92, (PB93-227791, A05, MF-A01).

NCEER-92-0026 "A Generalization of Optimal Control Theory: Linear and Nonlinear Structures," by J.N. Yang, Z. Li and S. Vongchavalitkul, 11/2/92, (PB93-188621, A05, MF-A01).

NCEER-92-0027 "Seismic Resistance of Reinforced Concrete Frame Structures Designed Only for Gravity Loads: Part I - Design and Properties of a One-Third Scale Model Structure," by J.M. Bracci, A.M. Reinhorn and J.B. Mander, 12/1/92, (PB94-104502, A08, MF-A02).

NCEER-92-0028 "Seismic Resistance of Reinforced Concrete Frame Structures Designed Only for Gravity Loads: Part II - Experimental Performance of Subassemblages," by L.E. Aycardi, J.B. Mander and A.M. Reinhorn, 12/1/92, (PB94-104510, A08, MF-A02).

NCEER-92-0029 "Seismic Resistance of Reinforced Concrete Frame Structures Designed Only for Gravity Loads: Part III - Experimental Performance and Analytical Study of a Structural Model," by J.M. Bracci, A.M. Reinhorn and J.B. Mander, 12/1/92, (PB93-227528, A09, MF-A01).

NCEER-92-0030 "Evaluation of Seismic Retrofit of Reinforced Concrete Frame Structures: Part I - Experimental Performance of Retrofitted Subassemblages," by D. Choudhuri, J.B. Mander and A.M. Reinhorn, 12/8/92, (PB93-198307, A07, MF-A02).

NCEER-92-0031 "Evaluation of Seismic Retrofit of Reinforced Concrete Frame Structures: Part II - Experimental Performance and Analytical Study of a Retrofitted Structural Model," by J.M. Bracci, A.M. Reinhorn and J.B. Mander, 12/8/92, (PB93-198315, A09, MF-A03).

NCEER-92-0032 "Experimental and Analytical Investigation of Seismic Response of Structures with Supplemental Fluid Viscous Dampers," by M.C. Constantinou and M.D. Symans, 12/21/92, (PB93-191435, A10, MF-A03). This report is available only through NTIS (see address given above).

NCEER-92-0033 "Reconnaissance Report on the Cairo, Egypt Earthquake of October 12, 1992," by M. Khater, 12/23/92, (PB93-188621, A03, MF-A01).

NCEER-92-0034 "Low-Level Dynamic Characteristics of Four Tall Flat-Plate Buildings in New York City," by H. Gavin, S. Yuan, J. Grossman, E. Pekelis and K. Jacob, 12/28/92, (PB93-188217, A07, MF-A02).

NCEER-93-0001 "An Experimental Study on the Seismic Performance of Brick-Infilled Steel Frames With and Without Retrofit," by J.B. Mander, B. Nair, K. Wojtkowski and J. Ma, 1/29/93, (PB93-227510, A07, MF-A02).

NCEER-93-0002 "Social Accounting for Disaster Preparedness and Recovery Planning," by S. Cole, E. Pantoja and V. Razak, 2/22/93, (PB94-142114, A12, MF-A03).

NCEER-93-0003 "Assessment of 1991 NEHRP Provisions for Nonstructural Components and Recommended Revisions," by T.T. Soong, G. Chen, Z. Wu, R-H. Zhang and M. Grigoriu, 3/1/93, (PB93-188639, A06, MF-A02).

NCEER-93-0004 "Evaluation of Static and Response Spectrum Analysis Procedures of SEAOC/UBC for Seismic Isolated Structures," by C.W. Winters and M.C. Constantinou, 3/23/93, (PB93-198299, A10, MF-A03).

NCEER-93-0005 "Earthquakes in the Northeast - Are We Ignoring the Hazard? A Workshop on Earthquake Science and Safety for Educators," edited by K.E.K. Ross, 4/2/93, (PB94-103066, A09, MF-A02).

NCEER-93-0006 "Inelastic Response of Reinforced Concrete Structures with Viscoelastic Braces," by R.F. Lobo, J.M. Bracci, K.L. Shen, A.M. Reinhorn and T.T. Soong, 4/5/93, (PB93-227486, A05, MF-A02).

NCEER-93-0007 "Seismic Testing of Installation Methods for Computers and Data Processing Equipment," by K. Kosar, T.T. Soong, K.L. Shen, J.A. HoLung and Y.K. Lin, 4/12/93, (PB93-198299, A07, MF-A02).

NCEER-93-0008 "Retrofit of Reinforced Concrete Frames Using Added Dampers," by A. Reinhorn, M. Constantinou and C. Li, to be published.

NCEER-93-0009 "Seismic Behavior and Design Guidelines for Steel Frame Structures with Added Viscoelastic Dampers," by K.C. Chang, M.L. Lai, T.T. Soong, D.S. Hao and Y.C. Yeh, 5/1/93, (PB94-141959, A07, MF-A02).

NCEER-93-0010 "Seismic Performance of Shear-Critical Reinforced Concrete Bridge Piers," by J.B. Mander, S.M. Waheed, M.T.A. Chaudhary and S.S. Chen, 5/12/93, (PB93-227494, A08, MF-A02).

NCEER-93-0011 "3D-BASIS-TABS: Computer Program for Nonlinear Dynamic Analysis of Three Dimensional Base Isolated Structures," by S. Nagarajaiah, C. Li, A.M. Reinhorn and M.C. Constantinou, 8/2/93, (PB94-141819, A09, MF-A02).

NCEER-93-0012 "Effects of Hydrocarbon Spills from an Oil Pipeline Break on Ground Water," by O.J. Helweg and H.H.M. Hwang, 8/3/93, (PB94-141942, A06, MF-A02).

NCEER-93-0013 "Simplified Procedures for Seismic Design of Nonstructural Components and Assessment of Current Code Provisions," by M.P. Singh, L.E. Suarez, E.E. Matheu and G.O. Maldonado, 8/4/93, (PB94-141827, A09, MF-A02).

NCEER-93-0014 "An Energy Approach to Seismic Analysis and Design of Secondary Systems," by G. Chen and T.T. Soong, 8/6/93, (PB94-142767, A11, MF-A03).

NCEER-93-0015 "Proceedings from School Sites: Becoming Prepared for Earthquakes - Commemorating the Third Anniversary of the Loma Prieta Earthquake," Edited by F.E. Winslow and K.E.K. Ross, 8/16/93, (PB94-154275, A16, MF-A02).

NCEER-93-0016 "Reconnaissance Report of Damage to Historic Monuments in Cairo, Egypt Following the October 12, 1992 Dahshur Earthquake," by D. Sykora, D. Look, G. Croci, E. Karaesmen and E. Karaesmen, 8/19/93, (PB94-142221, A08, MF-A02).

NCEER-93-0017 "The Island of Guam Earthquake of August 8, 1993," by S.W. Swan and S.K. Harris, 9/30/93, (PB94-141843, A04, MF-A01).

NCEER-93-0018 "Engineering Aspects of the October 12, 1992 Egyptian Earthquake," by A.W. Elgamal, M. Amer, K. Adalier and A. Abul-Fadl, 10/7/93, (PB94-141983, A05, MF-A01).

NCEER-93-0019 "Development of an Earthquake Motion Simulator and its Application in Dynamic Centrifuge Testing," by I. Krstelj, Supervised by J.H. Prevost, 10/23/93, (PB94-181773, A-10, MF-A03).

NCEER-93-0020 "NCEER-Taisei Corporation Research Program on Sliding Seismic Isolation Systems for Bridges: Experimental and Analytical Study of a Friction Pendulum System (FPS)," by M.C. Constantinou, P. Tsopelas, Y-S. Kim and S. Okamoto, 11/1/93, (PB94-142775, A08, MF-A02).

NCEER-93-0021 "Finite Element Modeling of Elastomeric Seismic Isolation Bearings," by L.J. Billings, Supervised by R. Shepherd, 11/8/93, to be published.

NCEER-93-0022 "Seismic Vulnerability of Equipment in Critical Facilities: Life-Safety and Operational Consequences," by K. Porter, G.S. Johnson, M.M. Zadeh, C. Scawthorn and S. Eder, 11/24/93, (PB94-181765, A16, MF-A03).

NCEER-93-0023 "Hokkaido Nansei-oki, Japan Earthquake of July 12, 1993, by P.I. Yanev and C.R. Scawthorn, 12/23/93, (PB94-181500, A07, MF-A01).

NCEER-94-0001 "An Evaluation of Seismic Serviceability of Water Supply Networks with Application to the San Francisco Auxiliary Water Supply System," by I. Markov, Supervised by M. Grigoriu and T. O'Rourke, 1/21/94, (PB94-204013, A07, MF-A02).

NCEER-94-0002 "NCEER-Taisei Corporation Research Program on Sliding Seismic Isolation Systems for Bridges: Experimental and Analytical Study of Systems Consisting of Sliding Bearings, Rubber Restoring Force Devices and Fluid Dampers," Volumes I and II, by P. Tsopelas, S. Okamoto, M.C. Constantinou, D. Ozaki and S. Fujii, 2/4/94, (PB94-181740, A09, MF-A02 and PB94-181757, A12, MF-A03).

NCEER-94-0003 "A Markov Model for Local and Global Damage Indices in Seismic Analysis," by S. Rahman and M. Grigoriu, 2/18/94, (PB94-206000, A12, MF-A03).

NCEER-94-0004 "Proceedings from the NCEER Workshop on Seismic Response of Masonry Infills," edited by D.P. Abrams, 3/1/94, (PB94-180783, A07, MF-A02).

NCEER-94-0005 "The Northridge, California Earthquake of January 17, 1994: General Reconnaissance Report," edited by J.D. Goltz, 3/11/94, (PB94-193943, A10, MF-A03).

NCEER-94-0006 "Seismic Energy Based Fatigue Damage Analysis of Bridge Columns: Part I - Evaluation of Seismic Capacity," by G.A. Chang and J.B. Mander, 3/14/94, (PB94-219185, A11, MF-A03).

NCEER-94-0007 "Seismic Isolation of Multi-Story Frame Structures Using Spherical Sliding Isolation Systems," by T.M. Al-Hussaini, V.A. Zayas and M.C. Constantinou, 3/17/94, (PB94-193745, A09, MF-A02).

NCEER-94-0008 "The Northridge, California Earthquake of January 17, 1994: Performance of Highway Bridges," edited by I.G. Buckle, 3/24/94, (PB94-193851, A06, MF-A02).

NCEER-94-0009 "Proceedings of the Third U.S.-Japan Workshop on Earthquake Protective Systems for Bridges," edited by I.G. Buckle and I. Friedland, 3/31/94, (PB94-195815, A99, MF-A06).

NCEER-94-0010 "3D-BASIS-ME: Computer Program for Nonlinear Dynamic Analysis of Seismically Isolated Single and Multiple Structures and Liquid Storage Tanks," by P.C. Tsopelas, M.C. Constantinou and A.M. Reinhorn, 4/12/94, (PB94-204922, A09, MF-A02).

NCEER-94-0011 "The Northridge, California Earthquake of January 17, 1994: Performance of Gas Transmission Pipelines," by T.D. O'Rourke and M.C. Palmer, 5/16/94, (PB94-204989, A05, MF-A01).

NCEER-94-0012 "Feasibility Study of Replacement Procedures and Earthquake Performance Related to Gas Transmission Pipelines," by T.D. O'Rourke and M.C. Palmer, 5/25/94, (PB94-206638, A09, MF-A02).

NCEER-94-0013 "Seismic Energy Based Fatigue Damage Analysis of Bridge Columns: Part II - Evaluation of Seismic Demand," by G.A. Chang and J.B. Mander, 6/1/94, (PB95-18106, A08, MF-A02).

NCEER-94-0014 "NCEER-Taisei Corporation Research Program on Sliding Seismic Isolation Systems for Bridges: Experimental and Analytical Study of a System Consisting of Sliding Bearings and Fluid Restoring Force/Damping Devices," by P. Tsopelas and M.C. Constantinou, 6/13/94, (PB94-219144, A10, MF-A03).

NCEER-94-0015 "Generation of Hazard-Consistent Fragility Curves for Seismic Loss Estimation Studies," by H. Hwang and J-R. Huo, 6/14/94, (PB95-181996, A09, MF-A02).

NCEER-94-0016 "Seismic Study of Building Frames with Added Energy-Absorbing Devices," by W.S. Pong, C.S. Tsai and G.C. Lee, 6/20/94, (PB94-219136, A10, A03).

NCEER-94-0017 "Sliding Mode Control for Seismic-Excited Linear and Nonlinear Civil Engineering Structures," by J. Yang, J. Wu, A. Agrawal and Z. Li, 6/21/94, (PB95-138483, A06, MF-A02).

NCEER-94-0018 "3D-BASIS-TABS Version 2.0: Computer Program for Nonlinear Dynamic Analysis of Three Dimensional Base Isolated Structures," by A.M. Reinhorn, S. Nagarajaiah, M.C. Constantinou, P. Tsopelas and R. Li, 6/22/94, (PB95-182176, A08, MF-A02).

NCEER-94-0019 "Proceedings of the International Workshop on Civil Infrastructure Systems: Application of Intelligent Systems and Advanced Materials on Bridge Systems," Edited by G.C. Lee and K.C. Chang, 7/18/94, (PB95-252474, A20, MF-A04).

NCEER-94-0020 "Study of Seismic Isolation Systems for Computer Floors," by V. Lambrou and M.C. Constantinou, 7/19/94, (PB95-138533, A10, MF-A03).

NCEER-94-0021 "Proceedings of the U.S.-Italian Workshop on Guidelines for Seismic Evaluation and Rehabilitation of Unreinforced Masonry Buildings," Edited by D.P. Abrams and G.M. Calvi, 7/20/94, (PB95-138749, A13, MF-A03).

NCEER-94-0022 "NCEER-Taisei Corporation Research Program on Sliding Seismic Isolation Systems for Bridges: Experimental and Analytical Study of a System Consisting of Lubricated PTFE Sliding Bearings and Mild Steel Dampers," by P. Tsopelas and M.C. Constantinou, 7/22/94, (PB95-182184, A08, MF-A02).

NCEER-94-0023 “Development of Reliability-Based Design Criteria for Buildings Under Seismic Load,” by Y.K. Wen, H. Hwang and M. Shinozuka, 8/1/94, (PB95-211934, A08, MF-A02).

NCEER-94-0024 “Experimental Verification of Acceleration Feedback Control Strategies for an Active Tendon System,” by S.J. Dyke, B.F. Spencer, Jr., P. Quast, M.K. Sain, D.C. Kaspari, Jr. and T.T. Soong, 8/29/94, (PB95-212320, A05, MF-A01).

NCEER-94-0025 “Seismic Retrofitting Manual for Highway Bridges,” Edited by I.G. Buckle and I.F. Friedland, published by the Federal Highway Administration (PB95-212676, A15, MF-A03).

NCEER-94-0026 “Proceedings from the Fifth U.S.-Japan Workshop on Earthquake Resistant Design of Lifeline Facilities and Countermeasures Against Soil Liquefaction,” Edited by T.D. O’Rourke and M. Hamada, 11/7/94, (PB95-220802, A99, MF-E08).

NCEER-95-0001 "Experimental and Analytical Investigation of Seismic Retrofit of Structures with Supplemental Damping: Part 1 - Fluid Viscous Damping Devices," by A.M. Reinhorn, C. Li and M.C. Constantinou, 1/3/95, (PB95-266599, A09, MF-A02).

NCEER-95-0002 "Experimental and Analytical Study of Low-Cycle Fatigue Behavior of Semi-Rigid Top-And-Seat Angle Connections," by G. Pekcan, J.B. Mander and S.S. Chen, 1/5/95, (PB95-220042, A07, MF-A02).

NCEER-95-0003 "NCEER-ATC Joint Study on Fragility of Buildings," by T. Anagnos, C. Rojahn and A.S. Kiremidjian, 1/20/95, (PB95-220026, A06, MF-A02).

NCEER-95-0004 "Nonlinear Control Algorithms for Peak Response Reduction," by Z. Wu, T.T. Soong, V. Gattulli and R.C. Lin, 2/16/95, (PB95-220349, A05, MF-A01).

NCEER-95-0005 "Pipeline Replacement Feasibility Study: A Methodology for Minimizing Seismic and Corrosion Risks to Underground Natural Gas Pipelines," by R.T. Eguchi, H.A. Seligson and D.G. Honegger, 3/2/95, (PB95-252326, A06, MF-A02).

NCEER-95-0006 "Evaluation of Seismic Performance of an 11-Story Frame Building During the 1994 Northridge Earthquake," by F. Naeim, R. DiSulio, K. Benuska, A. Reinhorn and C. Li, to be published.

NCEER-95-0007 "Prioritization of Bridges for Seismic Retrofitting," by N. Basöz and A.S. Kiremidjian, 4/24/95, (PB95-252300, A08, MF-A02).

NCEER-95-0008 "Method for Developing Motion Damage Relationships for Reinforced Concrete Frames," by A. Singhal and A.S. Kiremidjian, 5/11/95, (PB95-266607, A06, MF-A02).

NCEER-95-0009 "Experimental and Analytical Investigation of Seismic Retrofit of Structures with Supplemental Damping: Part II - Friction Devices," by C. Li and A.M. Reinhorn, 7/6/95, (PB96-128087, A11, MF-A03).

NCEER-95-0010 "Experimental Performance and Analytical Study of a Non-Ductile Reinforced Concrete Frame Structure Retrofitted with Elastomeric Spring Dampers," by G. Pekcan, J.B. Mander and S.S. Chen, 7/14/95, (PB96-137161, A08, MF-A02).

NCEER-95-0011 "Development and Experimental Study of Semi-Active Fluid Damping Devices for Seismic Protection of Structures," by M.D. Symans and M.C. Constantinou, 8/3/95, (PB96-136940, A23, MF-A04).

NCEER-95-0012 "Real-Time Structural Parameter Modification (RSPM): Development of Innervated Structures," by Z. Liang, M. Tong and G.C. Lee, 4/11/95, (PB96-137153, A06, MF-A01).

NCEER-95-0013 "Experimental and Analytical Investigation of Seismic Retrofit of Structures with Supplemental Damping: Part III - Viscous Damping Walls," by A.M. Reinhorn and C. Li, 10/1/95, (PB96-176409, A11, MF-A03).

NCEER-95-0014 "Seismic Fragility Analysis of Equipment and Structures in a Memphis Electric Substation," by J-R. Huo and H.H.M. Hwang, 8/10/95, (PB96-128087, A09, MF-A02).

NCEER-95-0015 "The Hanshin-Awaji Earthquake of January 17, 1995: Performance of Lifelines," Edited by M. Shinozuka, 11/3/95, (PB96-176383, A15, MF-A03).

NCEER-95-0016 "Highway Culvert Performance During Earthquakes," by T.L. Youd and C.J. Beckman, available as NCEER-96-0015.

NCEER-95-0017 "The Hanshin-Awaji Earthquake of January 17, 1995: Performance of Highway Bridges," Edited by I.G. Buckle, 12/1/95, to be published.

NCEER-95-0018 "Modeling of Masonry Infill Panels for Structural Analysis," by A.M. Reinhorn, A. Madan, R.E. Valles, Y. Reichmann and J.B. Mander, 12/8/95, (PB97-110886, MF-A01, A06).

NCEER-95-0019 "Optimal Polynomial Control for Linear and Nonlinear Structures," by A.K. Agrawal and J.N. Yang, 12/11/95, (PB96-168737, A07, MF-A02).

NCEER-95-0020 "Retrofit of Non-Ductile Reinforced Concrete Frames Using Friction Dampers," by R.S. Rao, P. Gergely and R.N. White, 12/22/95, (PB97-133508, A10, MF-A02).

NCEER-95-0021 "Parametric Results for Seismic Response of Pile-Supported Bridge Bents," by G. Mylonakis, A. Nikolaou and G. Gazetas, 12/22/95, (PB97-100242, A12, MF-A03).

NCEER-95-0022 "Kinematic Bending Moments in Seismically Stressed Piles," by A. Nikolaou, G. Mylonakis and G. Gazetas, 12/23/95, (PB97-113914, MF-A03, A13).

NCEER-96-0001 "Dynamic Response of Unreinforced Masonry Buildings with Flexible Diaphragms," by A.C. Costley and D.P. Abrams," 10/10/96, (PB97-133573, MF-A03, A15).

NCEER-96-0002 "State of the Art Review: Foundations and Retaining Structures," by I. Po Lam, to be published.

NCEER-96-0003 "Ductility of Rectangular Reinforced Concrete Bridge Columns with Moderate Confinement," by N. Wehbe, M. Saiidi, D. Sanders and B. Douglas, 11/7/96, (PB97-133557, A06, MF-A02).

NCEER-96-0004 "Proceedings of the Long-Span Bridge Seismic Research Workshop," edited by I.G. Buckle and I.M. Friedland, to be published.

NCEER-96-0005 "Establish Representative Pier Types for Comprehensive Study: Eastern United States," by J. Kulicki and Z. Prucz, 5/28/96, (PB98-119217, A07, MF-A02).

NCEER-96-0006 "Establish Representative Pier Types for Comprehensive Study: Western United States," by R. Imbsen, R.A. Schamber and T.A. Osterkamp, 5/28/96, (PB98-118607, A07, MF-A02).

NCEER-96-0007 "Nonlinear Control Techniques for Dynamical Systems with Uncertain Parameters," by R.G. Ghanem and M.I. Bujakov, 5/27/96, (PB97-100259, A17, MF-A03).

NCEER-96-0008 "Seismic Evaluation of a 30-Year Old Non-Ductile Highway Bridge Pier and Its Retrofit," by J.B. Mander, B. Mahmoodzadegan, S. Bhadra and S.S. Chen, 5/31/96, (PB97-110902, MF-A03, A10).

NCEER-96-0009 "Seismic Performance of a Model Reinforced Concrete Bridge Pier Before and After Retrofit," by J.B. Mander, J.H. Kim and C.A. Ligozio, 5/31/96, (PB97-110910, MF-A02, A10).

NCEER-96-0010 "IDARC2D Version 4.0: A Computer Program for the Inelastic Damage Analysis of Buildings," by R.E. Valles, A.M. Reinhorn, S.K. Kunnath, C. Li and A. Madan, 6/3/96, (PB97-100234, A17, MF-A03).

NCEER-96-0011 "Estimation of the Economic Impact of Multiple Lifeline Disruption: Memphis Light, Gas and Water Division Case Study," by S.E. Chang, H.A. Seligson and R.T. Eguchi, 8/16/96, (PB97-133490, A11, MF-A03).

NCEER-96-0012 "Proceedings from the Sixth Japan-U.S. Workshop on Earthquake Resistant Design of Lifeline Facilities and Countermeasures Against Soil Liquefaction, Edited by M. Hamada and T. O'Rourke, 9/11/96, (PB97-133581, A99, MF-A06).

NCEER-96-0013 "Chemical Hazards, Mitigation and Preparedness in Areas of High Seismic Risk: A Methodology for Estimating the Risk of Post-Earthquake Hazardous Materials Release," by H.A. Seligson, R.T. Eguchi, K.J. Tierney and K. Richmond, 11/7/96, (PB97-133565, MF-A02, A08).

NCEER-96-0014 "Response of Steel Bridge Bearings to Reversed Cyclic Loading," by J.B. Mander, D-K. Kim, S.S. Chen and G.J. Premus, 11/13/96, (PB97-140735, A12, MF-A03).

NCEER-96-0015 "Highway Culvert Performance During Past Earthquakes," by T.L. Youd and C.J. Beckman, 11/25/96, (PB97-133532, A06, MF-A01).

NCEER-97-0001 "Evaluation, Prevention and Mitigation of Pounding Effects in Building Structures," by R.E. Valles and A.M. Reinhorn, 2/20/97, (PB97-159552, A14, MF-A03).

NCEER-97-0002 "Seismic Design Criteria for Bridges and Other Highway Structures," by C. Rojahn, R. Mayes, D.G. Anderson, J. Clark, J.H. Hom, R.V. Nutt and M.J. O'Rourke, 4/30/97, (PB97-194658, A06, MF-A03).

NCEER-97-0003 “Proceedings of the U.S.-Italian Workshop on Seismic Evaluation and Retrofit,” Edited by D.P. Abrams and G.M. Calvi, 3/19/97, (PB97-194666, A13, MF-A03).

NCEER-97-0004 "Investigation of Seismic Response of Buildings with Linear and Nonlinear Fluid Viscous Dampers," by A.A. Seleemah and M.C. Constantinou, 5/21/97, (PB98-109002, A15, MF-A03).

NCEER-97-0005 "Proceedings of the Workshop on Earthquake Engineering Frontiers in Transportation Facilities," edited by G.C. Lee and I.M. Friedland, 8/29/97, (PB98-128911, A25, MR-A04).

NCEER-97-0006 "Cumulative Seismic Damage of Reinforced Concrete Bridge Piers," by S.K. Kunnath, A. El-Bahy, A. Taylor and W. Stone, 9/2/97, (PB98-108814, A11, MF-A03).

NCEER-97-0007 "Structural Details to Accommodate Seismic Movements of Highway Bridges and Retaining Walls," by R.A. Imbsen, R.A. Schamber, E. Thorkildsen, A. Kartoum, B.T. Martin, T.N. Rosser and J.M. Kulicki, 9/3/97, (PB98-108996, A09, MF-A02).

NCEER-97-0008 "A Method for Earthquake Motion-Damage Relationships with Application to Reinforced Concrete Frames," by A. Singhal and A.S. Kiremidjian, 9/10/97, (PB98-108988, A13, MF-A03).

NCEER-97-0009 "Seismic Analysis and Design of Bridge Abutments Considering Sliding and Rotation," by K. Fishman and R. Richards, Jr., 9/15/97, (PB98-108897, A06, MF-A02).

NCEER-97-0010 "Proceedings of the FHWA/NCEER Workshop on the National Representation of Seismic Ground Motion for New and Existing Highway Facilities," edited by I.M. Friedland, M.S. Power and R.L. Mayes, 9/22/97, (PB98-128903, A21, MF-A04).

NCEER-97-0011 "Seismic Analysis for Design or Retrofit of Gravity Bridge Abutments," by K.L. Fishman, R. Richards, Jr. and R.C. Divito, 10/2/97, (PB98-128937, A08, MF-A02).

NCEER-97-0012 "Evaluation of Simplified Methods of Analysis for Yielding Structures," by P. Tsopelas, M.C. Constantinou, C.A. Kircher and A.S. Whittaker, 10/31/97, (PB98-128929, A10, MF-A03).

NCEER-97-0013 "Seismic Design of Bridge Columns Based on Control and Repairability of Damage," by C-T. Cheng and J.B. Mander, 12/8/97, (PB98-144249, A11, MF-A03).

NCEER-97-0014 "Seismic Resistance of Bridge Piers Based on Damage Avoidance Design," by J.B. Mander and C-T. Cheng, 12/10/97, (PB98-144223, A09, MF-A02).

NCEER-97-0015 “Seismic Response of Nominally Symmetric Systems with Strength Uncertainty,” by S. Balopoulou and M. Grigoriu, 12/23/97, (PB98-153422, A11, MF-A03).

NCEER-97-0016 “Evaluation of Seismic Retrofit Methods for Reinforced Concrete Bridge Columns,” by T.J. Wipf, F.W. Klaiber and F.M. Russo, 12/28/97, (PB98-144215, A12, MF-A03).

NCEER-97-0017 “Seismic Fragility of Existing Conventional Reinforced Concrete Highway Bridges,” by C.L. Mullen and A.S. Cakmak, 12/30/97, (PB98-153406, A08, MF-A02).

NCEER-97-0018 “Loss Asssessment of Memphis Buildings,” edited by D.P. Abrams and M. Shinozuka, 12/31/97, (PB98-144231, A13, MF-A03).

NCEER-97-0019 “Seismic Evaluation of Frames with Infill Walls Using Quasi-static Experiments,” by K.M. Mosalam, R.N. White and P. Gergely, 12/31/97, (PB98-153455, A07, MF-A02).

NCEER-97-0020 “Seismic Evaluation of Frames with Infill Walls Using Pseudo-dynamic Experiments,” by K.M. Mosalam, R.N. White and P. Gergely, 12/31/97, (PB98-153430, A07, MF-A02).

NCEER-97-0021 “Computational Strategies for Frames with Infill Walls: Discrete and Smeared Crack Analyses and Seismic Fragility,” by K.M. Mosalam, R.N. White and P. Gergely, 12/31/97, (PB98-153414, A10, MF-A02).

NCEER-97-0022 "Proceedings of the NCEER Workshop on Evaluation of Liquefaction Resistance of Soils," edited by T.L. Youd and I.M. Idriss, 12/31/97, (PB98-155617, A15, MF-A03).

MCEER-98-0001 "Extraction of Nonlinear Hysteretic Properties of Seismically Isolated Bridges from Quick-Release Field Tests," by Q. Chen, B.M. Douglas, E.M. Maragakis and I.G. Buckle, 5/26/98, (PB99-118838, A06, MF-A01).

MCEER-98-0002 "Methodologies for Evaluating the Importance of Highway Bridges," by A. Thomas, S. Eshenaur and J. Kulicki, 5/29/98, (PB99-118846, A10, MF-A02).

MCEER-98-0003 "Capacity Design of Bridge Piers and the Analysis of Overstrength," by J.B. Mander, A. Dutta and P. Goel, 6/1/98, (PB99-118853, A09, MF-A02).

MCEER-98-0004 "Evaluation of Bridge Damage Data from the Loma Prieta and Northridge, California Earthquakes," by N. Basoz and A. Kiremidjian, 6/2/98, (PB99-118861, A15, MF-A03).

MCEER-98-0005 "Screening Guide for Rapid Assessment of Liquefaction Hazard at Highway Bridge Sites," by T. L. Youd, 6/16/98, (PB99-118879, A06, not available on microfiche).

MCEER-98-0006 "Structural Steel and Steel/Concrete Interface Details for Bridges," by P. Ritchie, N. Kauhl and J. Kulicki, 7/13/98, (PB99-118945, A06, MF-A01).

MCEER-98-0007 "Capacity Design and Fatigue Analysis of Confined Concrete Columns," by A. Dutta and J.B. Mander, 7/14/98, (PB99-118960, A14, MF-A03).

MCEER-98-0008 "Proceedings of the Workshop on Performance Criteria for Telecommunication Services Under Earthquake Conditions," edited by A.J. Schiff, 7/15/98, (PB99-118952, A08, MF-A02).

MCEER-98-0009 "Fatigue Analysis of Unconfined Concrete Columns," by J.B. Mander, A. Dutta and J.H. Kim, 9/12/98, (PB99-123655, A10, MF-A02).

MCEER-98-0010 "Centrifuge Modeling of Cyclic Lateral Response of Pile-Cap Systems and Seat-Type Abutments in Dry Sands," by A.D. Gadre and R. Dobry, 10/2/98, (PB99-123606, A13, MF-A03).

MCEER-98-0011 "IDARC-BRIDGE: A Computational Platform for Seismic Damage Assessment of Bridge Structures," by A.M. Reinhorn, V. Simeonov, G. Mylonakis and Y. Reichman, 10/2/98, (PB99-162919, A15, MF-A03).

MCEER-98-0012 "Experimental Investigation of the Dynamic Response of Two Bridges Before and After Retrofitting with Elastomeric Bearings," by D.A. Wendichansky, S.S. Chen and J.B. Mander, 10/2/98, (PB99-162927, A15, MF-A03).

MCEER-98-0013 "Design Procedures for Hinge Restrainers and Hinge Sear Width for Multiple-Frame Bridges," by R. Des Roches and G.L. Fenves, 11/3/98, (PB99-140477, A13, MF-A03).

MCEER-98-0014 "Response Modification Factors for Seismically Isolated Bridges," by M.C. Constantinou and J.K. Quarshie, 11/3/98, (PB99-140485, A14, MF-A03).

MCEER-98-0015 "Proceedings of the U.S.-Italy Workshop on Seismic Protective Systems for Bridges," edited by I.M. Friedland and M.C. Constantinou, 11/3/98, (PB2000-101711, A22, MF-A04).

MCEER-98-0016 "Appropriate Seismic Reliability for Critical Equipment Systems: Recommendations Based on Regional Analysis of Financial and Life Loss," by K. Porter, C. Scawthorn, C. Taylor and N. Blais, 11/10/98, (PB99-157265, A08, MF-A02).

MCEER-98-0017 "Proceedings of the U.S. Japan Joint Seminar on Civil Infrastructure Systems Research," edited by M. Shinozuka and A. Rose, 11/12/98, (PB99-156713, A16, MF-A03).

MCEER-98-0018 "Modeling of Pile Footings and Drilled Shafts for Seismic Design," by I. PoLam, M. Kapuskar and D. Chaudhuri, 12/21/98, (PB99-157257, A09, MF-A02).

MCEER-99-0001 "Seismic Evaluation of a Masonry Infilled Reinforced Concrete Frame by Pseudodynamic Testing," by S.G. Buonopane and R.N. White, 2/16/99, (PB99-162851, A09, MF-A02).

MCEER-99-0002 "Response History Analysis of Structures with Seismic Isolation and Energy Dissipation Systems: Verification Examples for Program SAP2000," by J. Scheller and M.C. Constantinou, 2/22/99, (PB99-162869, A08, MF-A02).

MCEER-99-0003 "Experimental Study on the Seismic Design and Retrofit of Bridge Columns Including Axial Load Effects," by A. Dutta, T. Kokorina and J.B. Mander, 2/22/99, (PB99-162877, A09, MF-A02).

MCEER-99-0004 "Experimental Study of Bridge Elastomeric and Other Isolation and Energy Dissipation Systems with Emphasis on Uplift Prevention and High Velocity Near-source Seismic Excitation," by A. Kasalanati and M. C. Constantinou, 2/26/99, (PB99-162885, A12, MF-A03).

MCEER-99-0005 "Truss Modeling of Reinforced Concrete Shear-flexure Behavior," by J.H. Kim and J.B. Mander, 3/8/99, (PB99-163693, A12, MF-A03).

MCEER-99-0006 "Experimental Investigation and Computational Modeling of Seismic Response of a 1:4 Scale Model Steel Structure with a Load Balancing Supplemental Damping System," by G. Pekcan, J.B. Mander and S.S. Chen, 4/2/99, (PB99-162893, A11, MF-A03).

MCEER-99-0007 "Effect of Vertical Ground Motions on the Structural Response of Highway Bridges," by M.R. Button, C.J. Cronin and R.L. Mayes, 4/10/99, (PB2000-101411, A10, MF-A03).

MCEER-99-0008 "Seismic Reliability Assessment of Critical Facilities: A Handbook, Supporting Documentation, and Model Code Provisions," by G.S. Johnson, R.E. Sheppard, M.D. Quilici, S.J. Eder and C.R. Scawthorn, 4/12/99, (PB2000-101701, A18, MF-A04).

MCEER-99-0009 "Impact Assessment of Selected MCEER Highway Project Research on the Seismic Design of Highway Structures," by C. Rojahn, R. Mayes, D.G. Anderson, J.H. Clark, D'Appolonia Engineering, S. Gloyd and R.V. Nutt, 4/14/99, (PB99-162901, A10, MF-A02).

MCEER-99-0010 "Site Factors and Site Categories in Seismic Codes," by R. Dobry, R. Ramos and M.S. Power, 7/19/99, (PB2000-101705, A08, MF-A02).

MCEER-99-0011 "Restrainer Design Procedures for Multi-Span Simply-Supported Bridges," by M.J. Randall, M. Saiidi, E. Maragakis and T. Isakovic, 7/20/99, (PB2000-101702, A10, MF-A02).

MCEER-99-0012 "Property Modification Factors for Seismic Isolation Bearings," by M.C. Constantinou, P. Tsopelas, A. Kasalanati and E. Wolff, 7/20/99, (PB2000-103387, A11, MF-A03).

MCEER-99-0013 "Critical Seismic Issues for Existing Steel Bridges," by P. Ritchie, N. Kauhl and J. Kulicki, 7/20/99, (PB2000-101697, A09, MF-A02).

MCEER-99-0014 "Nonstructural Damage Database," by A. Kao, T.T. Soong and A. Vender, 7/24/99, (PB2000-101407, A06, MF-A01).

MCEER-99-0015 "Guide to Remedial Measures for Liquefaction Mitigation at Existing Highway Bridge Sites," by H.G. Cooke and J. K. Mitchell, 7/26/99, (PB2000-101703, A11, MF-A03).

MCEER-99-0016 "Proceedings of the MCEER Workshop on Ground Motion Methodologies for the Eastern United States," edited by N. Abrahamson and A. Becker, 8/11/99, (PB2000-103385, A07, MF-A02).

MCEER-99-0017 "Quindío, Colombia Earthquake of January 25, 1999: Reconnaissance Report," by A.P. Asfura and P.J. Flores, 10/4/99, (PB2000-106893, A06, MF-A01).

MCEER-99-0018 "Hysteretic Models for Cyclic Behavior of Deteriorating Inelastic Structures," by M.V. Sivaselvan and A.M. Reinhorn, 11/5/99, (PB2000-103386, A08, MF-A02).

MCEER-99-0019 "Proceedings of the 7th U.S.- Japan Workshop on Earthquake Resistant Design of Lifeline Facilities and Countermeasures Against Soil Liquefaction," edited by T.D. O'Rourke, J.P. Bardet and M. Hamada, 11/19/99, (PB2000-103354, A99, MF-A06).

MCEER-99-0020 "Development of Measurement Capability for Micro-Vibration Evaluations with Application to Chip Fabrication Facilities," by G.C. Lee, Z. Liang, J.W. Song, J.D. Shen and W.C. Liu, 12/1/99, (PB2000-105993, A08, MF-A02).

MCEER-99-0021 "Design and Retrofit Methodology for Building Structures with Supplemental Energy Dissipating Systems," by G. Pekcan, J.B. Mander and S.S. Chen, 12/31/99, (PB2000-105994, A11, MF-A03).

MCEER-00-0001 "The Marmara, Turkey Earthquake of August 17, 1999: Reconnaissance Report," edited by C. Scawthorn; with major contributions by M. Bruneau, R. Eguchi, T. Holzer, G. Johnson, J. Mander, J. Mitchell, W. Mitchell, A. Papageorgiou, C. Scaethorn, and G. Webb, 3/23/00, (PB2000-106200, A11, MF-A03).

MCEER-00-0002 "Proceedings of the MCEER Workshop for Seismic Hazard Mitigation of Health Care Facilities," edited by G.C. Lee, M. Ettouney, M. Grigoriu, J. Hauer and J. Nigg, 3/29/00, (PB2000-106892, A08, MF-A02).

MCEER-00-0003 "The Chi-Chi, Taiwan Earthquake of September 21, 1999: Reconnaissance Report," edited by G.C. Lee and C.H. Loh, with major contributions by G.C. Lee, M. Bruneau, I.G. Buckle, S.E. Chang, P.J. Flores, T.D. O'Rourke, M. Shinozuka, T.T. Soong, C-H. Loh, K-C. Chang, Z-J. Chen, J-S. Hwang, M-L. Lin, G-Y. Liu, K-C. Tsai, G.C. Yao and C-L. Yen, 4/30/00, (PB2001-100980, A10, MF-A02).

MCEER-00-0004 "Seismic Retrofit of End-Sway Frames of Steel Deck-Truss Bridges with a Supplemental Tendon System: Experimental and Analytical Investigation," by G. Pekcan, J.B. Mander and S.S. Chen, 7/1/00, (PB2001-100982, A10, MF-A02).

MCEER-00-0005 "Sliding Fragility of Unrestrained Equipment in Critical Facilities," by W.H. Chong and T.T. Soong, 7/5/00, (PB2001-100983, A08, MF-A02).

MCEER-00-0006 "Seismic Response of Reinforced Concrete Bridge Pier Walls in the Weak Direction," by N. Abo-Shadi, M. Saiidi and D. Sanders, 7/17/00, (PB2001-100981, A17, MF-A03).

MCEER-00-0007 "Low-Cycle Fatigue Behavior of Longitudinal Reinforcement in Reinforced Concrete Bridge Columns," by J. Brown and S.K. Kunnath, 7/23/00, (PB2001-104392, A08, MF-A02).

MCEER-00-0008 "Soil Structure Interaction of Bridges for Seismic Analysis," I. PoLam and H. Law, 9/25/00, (PB2001-105397, A08, MF-A02).

MCEER-00-0009 "Proceedings of the First MCEER Workshop on Mitigation of Earthquake Disaster by Advanced Technologies (MEDAT-1), edited by M. Shinozuka, D.J. Inman and T.D. O'Rourke, 11/10/00, (PB2001-105399, A14, MF-A03).

MCEER-00-0010 "Development and Evaluation of Simplified Procedures for Analysis and Design of Buildings with Passive Energy Dissipation Systems," by O.M. Ramirez, M.C. Constantinou, C.A. Kircher, A.S. Whittaker, M.W. Johnson, J.D. Gomez and C. Chrysostomou, 11/16/01, (PB2001-105523, A23, MF-A04).

MCEER-00-0011 "Dynamic Soil-Foundation-Structure Interaction Analyses of Large Caissons," by C-Y. Chang, C-M. Mok, Z-L. Wang, R. Settgast, F. Waggoner, M.A. Ketchum, H.M. Gonnermann and C-C. Chin, 12/30/00, (PB2001-104373, A07, MF-A02).

MCEER-00-0012 "Experimental Evaluation of Seismic Performance of Bridge Restrainers," by A.G. Vlassis, E.M. Maragakis and M. Saiid Saiidi, 12/30/00, (PB2001-104354, A09, MF-A02).

MCEER-00-0013 "Effect of Spatial Variation of Ground Motion on Highway Structures," by M. Shinozuka, V. Saxena and G. Deodatis, 12/31/00, (PB2001-108755, A13, MF-A03).

MCEER-00-0014 "A Risk-Based Methodology for Assessing the Seismic Performance of Highway Systems," by S.D. Werner, C.E. Taylor, J.E. Moore, II, J.S. Walton and S. Cho, 12/31/00, (PB2001-108756, A14, MF-A03).

MCEER-01-0001 “Experimental Investigation of P-Delta Effects to Collapse During Earthquakes,” by D. Vian and M. Bruneau, 6/25/01, (PB2002-100534, A17, MF-A03).

MCEER-01-0002 “Proceedings of the Second MCEER Workshop on Mitigation of Earthquake Disaster by Advanced Technologies (MEDAT-2),” edited by M. Bruneau and D.J. Inman, 7/23/01, (PB2002-100434, A16, MF-A03).

MCEER-01-0003 “Sensitivity Analysis of Dynamic Systems Subjected to Seismic Loads,” by C. Roth and M. Grigoriu, 9/18/01, (PB2003-100884, A12, MF-A03).

MCEER-01-0004 “Overcoming Obstacles to Implementing Earthquake Hazard Mitigation Policies: Stage 1 Report,” by D.J. Alesch and W.J. Petak, 12/17/01, (PB2002-107949, A07, MF-A02).

MCEER-01-0005 “Updating Real-Time Earthquake Loss Estimates: Methods, Problems and Insights,” by C.E. Taylor, S.E. Chang and R.T. Eguchi, 12/17/01, (PB2002-107948, A05, MF-A01).

MCEER-01-0006 “Experimental Investigation and Retrofit of Steel Pile Foundations and Pile Bents Under Cyclic Lateral Loadings,” by A. Shama, J. Mander, B. Blabac and S. Chen, 12/31/01, (PB2002-107950, A13, MF-A03).

MCEER-02-0001 “Assessment of Performance of Bolu Viaduct in the 1999 Duzce Earthquake in Turkey” by P.C. Roussis, M.C. Constantinou, M. Erdik, E. Durukal and M. Dicleli, 5/8/02, (PB2003-100883, A08, MF-A02).

MCEER-02-0002 “Seismic Behavior of Rail Counterweight Systems of Elevators in Buildings,” by M.P. Singh, Rildova and L.E. Suarez, 5/27/02. (PB2003-100882, A11, MF-A03).

MCEER-02-0003 “Development of Analysis and Design Procedures for Spread Footings,” by G. Mylonakis, G. Gazetas, S. Nikolaou and A. Chauncey, 10/02/02, (PB2004-101636, A13, MF-A03, CD-A13).

MCEER-02-0004 “Bare-Earth Algorithms for Use with SAR and LIDAR Digital Elevation Models,” by C.K. Huyck, R.T. Eguchi and B. Houshmand, 10/16/02, (PB2004-101637, A07, CD-A07).

MCEER-02-0005 “Review of Energy Dissipation of Compression Members in Concentrically Braced Frames,” by K.Lee and M. Bruneau, 10/18/02, (PB2004-101638, A10, CD-A10).

MCEER-03-0001 “Experimental Investigation of Light-Gauge Steel Plate Shear Walls for the Seismic Retrofit of Buildings” by J. Berman and M. Bruneau, 5/2/03, (PB2004-101622, A10, MF-A03, CD-A10).

MCEER-03-0002 “Statistical Analysis of Fragility Curves,” by M. Shinozuka, M.Q. Feng, H. Kim, T. Uzawa and T. Ueda, 6/16/03, (PB2004-101849, A09, CD-A09).

MCEER-03-0003 “Proceedings of the Eighth U.S.-Japan Workshop on Earthquake Resistant Design f Lifeline Facilities and Countermeasures Against Liquefaction,” edited by M. Hamada, J.P. Bardet and T.D. O’Rourke, 6/30/03, (PB2004-104386, A99, CD-A99).

MCEER-03-0004 “Proceedings of the PRC-US Workshop on Seismic Analysis and Design of Special Bridges,” edited by L.C. Fan and G.C. Lee, 7/15/03, (PB2004-104387, A14, CD-A14).

MCEER-03-0005 “Urban Disaster Recovery: A Framework and Simulation Model,” by S.B. Miles and S.E. Chang, 7/25/03, (PB2004-104388, A07, CD-A07).

MCEER-03-0006 “Behavior of Underground Piping Joints Due to Static and Dynamic Loading,” by R.D. Meis, M. Maragakis and R. Siddharthan, 11/17/03, (PB2005-102194, A13, MF-A03, CD-A00).

MCEER-03-0007 “Seismic Vulnerability of Timber Bridges and Timber Substructures,” by A.A. Shama, J.B. Mander, I.M. Friedland and D.R. Allicock, 12/15/03.

MCEER-04-0001 “Experimental Study of Seismic Isolation Systems with Emphasis on Secondary System Response and Verification of Accuracy of Dynamic Response History Analysis Methods,” by E. Wolff and M. Constantinou, 1/16/04 (PB2005-102195, A99, MF-E08, CD-A00).

MCEER-04-0002 "Tension, Compression and Cyclic Testing of Engineered Cementitious Composite Materials," by K. Kesner and S.L. Billington, 3/1/04, (PB2005-102196, A08, CD-A08).

MCEER-04-0003 "Cyclic Testing of Braces Laterally Restrained by Steel Studs to Enhance Performance During Earthquakes," by O.C. Celik, J.W. Berman and M. Bruneau, 3/16/04, (PB2005-102197, A13, MF-A03, CD-A00).

MCEER-04-0004 "Methodologies for Post Earthquake Building Damage Detection Using SAR and Optical Remote Sensing: Application to the August 17, 1999 Marmara, Turkey Earthquake," by C.K. Huyck, B.J. Adams, S. Cho, R.T. Eguchi, B. Mansouri and B. Houshmand, 6/15/04, (PB2005-104888, A10, CD-A00).

MCEER-04-0005 "Nonlinear Structural Analysis Towards Collapse Simulation: A Dynamical Systems Approach," by M.V. Sivaselvan and A.M. Reinhorn, 6/16/04, (PB2005-104889, A11, MF-A03, CD-A00).

MCEER-04-0006 "Proceedings of the Second PRC-US Workshop on Seismic Analysis and Design of Special Bridges," edited by G.C. Lee and L.C. Fan, 6/25/04, (PB2005-104890, A16, CD-A00).

MCEER-04-0007 "Seismic Vulnerability Evaluation of Axially Loaded Steel Built-up Laced Members," by K. Lee and M. Bruneau, 6/30/04, (PB2005-104891, A16, CD-A00).

MCEER-04-0008 "Evaluation of Accuracy of Simplified Methods of Analysis and Design of Buildings with Damping Systems for Near-Fault and for Soft-Soil Seismic Motions," by E.A. Pavlou and M.C. Constantinou, 8/16/04, (PB2005-104892, A08, MF-A02, CD-A00).

MCEER-04-0009 "Assessment of Geotechnical Issues in Acute Care Facilities in California," by M. Lew, T.D. O'Rourke, R. Dobry and M. Koch, 9/15/04, (PB2005-104893, A08, CD-A00).

MCEER-04-0010 "Scissor-Jack-Damper Energy Dissipation System," by A.N. Sigaher-Boyle and M.C. Constantinou, 12/1/04 (PB2005-108221).

MCEER-04-0011 "Seismic Retrofit of Bridge Steel Truss Piers Using a Controlled Rocking Approach," by M. Pollino and M. Bruneau, 12/20/04 (PB2006-105795).

MCEER-05-0001 "Experimental and Analytical Studies of Structures Seismically Isolated with an Uplift-Restraint Isolation System," by P.C. Roussis and M.C. Constantinou, 1/10/05 (PB2005-108222).

MCEER-05-0002 "A Versatile Experimentation Model for Study of Structures Near Collapse Applied to Seismic Evaluation of Irregular Structures," by D. Kusumastuti, A.M. Reinhorn and A. Rutenberg, 3/31/05 (PB2006-101523).

MCEER-05-0003 "Proceedings of the Third PRC-US Workshop on Seismic Analysis and Design of Special Bridges," edited by L.C. Fan and G.C. Lee, 4/20/05, (PB2006-105796).

MCEER-05-0004 "Approaches for the Seismic Retrofit of Braced Steel Bridge Piers and Proof-of-Concept Testing of an Eccentrically Braced Frame with Tubular Link," by J.W. Berman and M. Bruneau, 4/21/05 (PB2006-101524).

MCEER-05-0005 "Simulation of Strong Ground Motions for Seismic Fragility Evaluation of Nonstructural Components in Hospitals," by A. Wanitkorkul and A. Filiatrault, 5/26/05 (PB2006-500027).

MCEER-05-0006 "Seismic Safety in California Hospitals: Assessing an Attempt to Accelerate the Replacement or Seismic Retrofit of Older Hospital Facilities," by D.J. Alesch, L.A. Arendt and W.J. Petak, 6/6/05 (PB2006-105794).

MCEER-05-0007 "Development of Seismic Strengthening and Retrofit Strategies for Critical Facilities Using Engineered Cementitious Composite Materials," by K. Kesner and S.L. Billington, 8/29/05 (PB2006-111701).

MCEER-05-0008 "Experimental and Analytical Studies of Base Isolation Systems for Seismic Protection of Power Transformers," by N. Murota, M.Q. Feng and G-Y. Liu, 9/30/05 (PB2006-111702).

MCEER-05-0009 "3D-BASIS-ME-MB: Computer Program for Nonlinear Dynamic Analysis of Seismically Isolated Structures," by P.C. Tsopelas, P.C. Roussis, M.C. Constantinou, R. Buchanan and A.M. Reinhorn, 10/3/05 (PB2006-111703).

MCEER-05-0010 "Steel Plate Shear Walls for Seismic Design and Retrofit of Building Structures," by D. Vian and M. Bruneau, 12/15/05 (PB2006-111704).

MCEER-05-0011 "The Performance-Based Design Paradigm," by M.J. Astrella and A. Whittaker, 12/15/05 (PB2006-111705).

MCEER-06-0001 "Seismic Fragility of Suspended Ceiling Systems," H. Badillo-Almaraz, A.S. Whittaker, A.M. Reinhorn and G.P. Cimellaro, 2/4/06 (PB2006-111706).

MCEER-06-0002 "Multi-Dimensional Fragility of Structures," by G.P. Cimellaro, A.M. Reinhorn and M. Bruneau, 3/1/06 (PB2007-106974, A09, MF-A02, CD A00).

MCEER-06-0003 "Built-Up Shear Links as Energy Dissipators for Seismic Protection of Bridges," by P. Dusicka, A.M. Itani and I.G. Buckle, 3/15/06 (PB2006-111708).

MCEER-06-0004 "Analytical Investigation of the Structural Fuse Concept," by R.E. Vargas and M. Bruneau, 3/16/06 (PB2006-111709).

MCEER-06-0005 "Experimental Investigation of the Structural Fuse Concept," by R.E. Vargas and M. Bruneau, 3/17/06 (PB2006-111710).

MCEER-06-0006 "Further Development of Tubular Eccentrically Braced Frame Links for the Seismic Retrofit of Braced Steel Truss Bridge Piers," by J.W. Berman and M. Bruneau, 3/27/06 (PB2007-105147).

MCEER-06-0007 "REDARS Validation Report," by S. Cho, C.K. Huyck, S. Ghosh and R.T. Eguchi, 8/8/06 (PB2007-106983).

MCEER-06-0008 "Review of Current NDE Technologies for Post-Earthquake Assessment of Retrofitted Bridge Columns," by J.W. Song, Z. Liang and G.C. Lee, 8/21/06 06 (PB2007-106984).

MCEER-06-0009 "Liquefaction Remediation in Silty Soils Using Dynamic Compaction and Stone Columns," by S. Thevanayagam, G.R. Martin, R. Nashed, T. Shenthan, T. Kanagalingam and N. Ecemis, 8/28/06 06 (PB2007-106985).

MCEER-06-0010 "Conceptual Design and Experimental Investigation of Polymer Matrix Composite Infill Panels for Seismic Retrofitting," by W. Jung, M. Chiewanichakorn and A.J. Aref, 9/21/06 (PB2007-106986).

MCEER-06-0011 "A Study of the Coupled Horizontal-Vertical Behavior of Elastomeric and Lead-Rubber Seismic Isolation Bearings," by G.P. Warn and A.S. Whittaker, 9/22/06 (PB2007-108679).

MCEER-06-0012 "Proceedings of the Fourth PRC-US Workshop on Seismic Analysis and Design of Special Bridges: Advancing Bridge Technologies in Research, Design, Construction and Preservation," Edited by L.C. Fan, G.C. Lee and L. Ziang, 10/12/06.

MCEER-06-0013 "Cyclic Response and Low Cycle Fatigue Characteristics of Plate Steels," by P. Dusicka, A.M. Itani and I.G. Buckle, 11/1/06 06 (PB2007-106987).

MCEER-06-0014 "Proceedings of the Second US-Taiwan Bridge Engineering Workshop," edited by W.P. Yen, J. Shen, J-Y. Chen and M. Wang, 11/15/06.

MCEER-06-0015 "User Manual and Technical Documentation for the REDARS™ Import Wizard," by S. Cho, S. Ghosh, C.K. Huyck and S.D. Werner, 11/30/06.

MCEER-06-0016 "Hazard Mitigation Strategy and Monitoring Technologies for Urban and Infrastructure Public Buildings: Proceedings of the China-US Workshops," edited by X.Y. Zhou, A.L. Zhang, G.C. Lee and M. Tong, 12/12/06.

MCEER-07-0001 "Static and Kinetic Coefficients of Friction for Rigid Blocks," by C. Kafali, S. Fathali, M. Grigoriu and A.S. Whittaker, 3/20/07.

MCEER-07-0002 "Hazard Mitigation Investment Decision Making: Organizational Response to Legislative Mandate," by L.A. Arendt, D.J. Alesch and W.J. Petak, 4/9/07.

MCEER-07-0003 "Seismic Behavior of Bidirectional-Resistant Ductile End Diaphragms with Unbonded Braces in Straight or Skewed Steel Bridges," by O. Celik and M. Bruneau, 4/11/07.

MCEER-07-0004 "Modeling Pile Behavior in Large Pile Groups Under Lateral Loading," by A.M. Dodds and G.R. Martin, 4/16/07.

MCEER-07-0005 "Experimental Investigation of Blast Performance of Seismically Resistant Concrete-Filled Steel Tube Bridge Piers," by S. Fujikura, M. Bruneau and D. Lopez-Garcia, 4/20/07.

MCEER-07-0006 "Seismic Analysis of Conventional and Isolated Liquefied Natural Gas Tanks Using Mechanical Analogs," by I.P. Christovasilis and A.S. Whittaker, 5/1/07.

MCEER-07-0007 "Experimental Seismic Performance Evaluation of Isolation/Restraint Systems for Mechanical Equipment – Part 1: Heavy Equipment Study," by S. Fathali and A. Filiatrault, 6/6/07.

MCEER-07-0008 "Seismic Vulnerability of Timber Bridges and Timber Substructures," by A.A. Sharma, J.B. Mander, I.M. Friedland and D.R. Allicock, 6/7/07.

MCEER-07-0009 "Experimental and Analytical Study of the XY-Friction Pendulum (XY-FP) Bearing for Bridge Applications," by C.C. Marin-Artieda, A.S. Whittaker and M.C. Constantinou, 6/7/07.

MCEER-07-0010 "Proceedings of the PRC-US Earthquake Engineering Forum for Young Researchers," Edited by G.C. Lee and X.Z. Qi, 6/8/07.

MCEER-07-0011 "Design Recommendations for Perforated Steel Plate Shear Walls," by R. Purba and M. Bruneau, 6/18/07.

MCEER-07-0012 "Performance of Seismic Isolation Hardware Under Service and Seismic Loading," by M.C. Constantinou, A.S. Whittaker, Y. Kalpakidis, D.M. Fenz and G.P. Warn, 8/27/07.

MCEER-07-0013 "Experimental Evaluation of the Seismic Performance of Hospital Piping Subassemblies," by E.R. Goodwin, E. Maragakis and A.M. Itani, 9/4/07.

MCEER-07-0014 "A Simulation Model of Urban Disaster Recovery and Resilience: Implementation for the 1994 Northridge Earthquake," by S. Miles and S.E. Chang, 9/7/07.

MCEER-07-0015 "Statistical and Mechanistic Fragility Analysis of Concrete Bridges," by M. Shinozuka, S. Banerjee and S-H. Kim, 9/10/07.

MCEER-07-0016 "Three-Dimensional Modeling of Inelastic Buckling in Frame Structures," by M. Schachter and AM. Reinhorn, 9/13/07.

MCEER
EARTHQUAKE ENGINEERING TO EXTREME EVENTS
University at Buffalo, The State University of New York
Red Jacket Quadrangle ▪ Buffalo, New York 14261
Phone: (716) 645-3391 ▪ Fax: (716) 645-3399
E-mail: *mceer@buffalo.edu* ▪ WWW Site *http://mceer.buffalo.edu*
University at Buffalo *The State University of New York*

ISSN 1520-295X